Lawrence Berkeley Laboratory
UNIVERSITY OF CALIFORNIA

APPLIED SCIENCE DIVISION

Simulation of the Steady-state Transport of Radon from Soil into Houses with Basements Under Constant Negative Pressure

C. de Oliveira Loureiro
(Ph.D. Thesis)

May 1987

APPLIED SCIENCE DIVISION

Prepared for the U.S. Department of Energy under Contract DE-AC03-76SF00098

LBL-24378

SIMULATION OF THE STEADY-STATE TRANSPORT OF RADON FROM SOIL INTO HOUSES WITH BASEMENTS UNDER CONSTANT NEGATIVE PRESSURE

by
Celso de Oliveira Loureiro

A dissertation submitted in partial fulfillment
of the requirements for the degree of
Doctor of Philosophy
(Environmental Health Sciences)
in The University of Michigan
1987

Lawrence Berkeley Laboratory
University of California
Berkeley, CA 94720

ABSTRACT

SIMULATION OF THE STEADY-STATE TRANSPORT OF RADON FROM SOIL INTO HOUSES WITH BASEMENTS UNDER CONSTANT NEGATIVE PRESSURE

by
Celso de Oliveira Loureiro

CoChairs: James E. Martin, Linda M. Abriola

Normal conditions in a house can produce negative pressures as high as 20 Pa relative to the outside. This underpressure, which is a maximum at the base of the house (the basement, for instance), can induce a flow of soil gas into the house, through cracks or any other openings in the understructure of the building. Radon (Rn-222), which is produced in the soil and mixed in the soil gas, can then be transported into the house through a complex combination of molecular diffusion and forced convection. In many of the cases where high levels of indoor radon concentrations have been observed in houses, the soil gas has been concluded to be the main source.

A theoretical model was developed to simulate this phenomenon, under some specific assumptions. The model simulates: 1) the generation and decay of radon within the soil; 2) its transport throughout the soil due to diffusion and convection induced by the pressure disturbance applied at a crack in the basement; 3) its entrance into the house through the crack; and 4) the resultant indoor radon concentration. The most important assumptions adopted in the model were: 1) a steady-state condition; 2) a house with a basement; 3) a

geometrically well-defined crack at the wall-floor joint in the basement; and 4) a constant negative pressure applied at the crack in relation to the outside atmospheric pressure.

Two three-dimensional finite-difference computer programs were written to solve the mathematical equations of the model. The first program, called PRESSU, was used to calculate: 1) the pressure distribution within the soil as a result of the applied disturbance pressure at the crack; and 2) the resultant velocity distribution of the soil gas throughout the soil matrix. The second program, called MASTRA, was used to: 1) solve the radon mass-transport equation, and to calculate the concentration distribution of radon in the soil gas within the whole soil; and 2) to calculate the entry rate of radon through the crack into the basement, and the final indoor radon concentration.

A parametric sensitivity analysis performed on the model, revealed several features of the mechanisms involved in the transport of radon into the house. Then, based on the theoretical simulations, the influences of all important parameters on these radon transport mechanisms were described in detail. Results of the tests showed that the model performs consistently with physical expectations. Among all the parameters analyzed, it was concluded that the most important are: 1) k – the soil permeability; 2) the pressure differential from inside to outside; and 3) the radium (Ra-226) concentration in the soil particles. For $k \leq 1.0 \times 10^{-12}[m^2]$, the entry rate of radon into the house was dominated by diffusion, and consequently the resultant indoor radon concentration varied very slowly with soil permeability. For $k \geq 1.0 \times 10^{-12}[m^2]$, the convective transport of radon from the soil into the house predominated over diffusion, and the indoor radon concentration was found to be strongly dependent (almost linearly) on the soil permeability. These effects were observed for an applied delta pressure of $5.0[Pa]$. It is expected that a variation of the delta pressure would affect directly this turning point of $k = 1.0 \times 10^{-12}[m^2]$. The indoor radon concentration was found to be directly, though not linearly, related to the pressure differential. The concentration of Ra-226 in the soil particles had a direct linear effect on the indoor radon concentration.

For my wife Laura,

our son Rafael,

and the new one that is coming.

ACKNOWLEDGEMENTS

I would like to express my gratitude to the people who helped me during the execution of this work. In a especial way I want to thank the members of my doctoral committee who were always generous in sharing their time with me, and in giving me assistance whenever I needed. My sincere thanks go to Dr. Rich Sextro and the Indoor Air Quality Group at the Lawrence Berkeley Laboratory, for helping me in defining the topic of the dissertation, and for providing financial and technical support for the execution of the project. The trust, and the complete freedom that he offered me in the conduction of my research were very much appreciated. Also I want to thank Professor Linda Abriola, at the Department of Civil Engineering of The University of Michigan, for her invaluable advice, and the enormous help in the development of the mathematical model. With talent, and appropriate criticism she illuminated my way many times when I thought to be lost. I am very grateful to the faculty of the Department of Environmental and Industrial Health, especially to the Professors James Martin and Arnold Jacobson, for providing a working environment for me, in the labs of the Radiological Health Program. To them I also send my thanks for the general guidance in my researches, as well as for the sincere friendship and the productive intellectual atmosphere that I have enjoyed all these years of graduate studies in that program. I am also very grateful to Professor Perry Samson for letting me test the model, using his account, in the VAX-8600 computer of the Department of Oceanic and Atmospheric Sciences.

My graduate studies at The University of Michigan were made possible, initially with a scholarship from the *Còmissão Nacional de Energia Nuclear* – the Brazilian National Committee on Nuclear Energy –, and lately with: 1) a student research scholarship provided by

Consumers Power Company of Michigan; and, 2) a student research assistantship provided by the Indoor Environment Program, at Lawrence Berkeley Laboratory, supported by U.S. DOE through contract No. DE - AC03 - 76SF00098.

Many other people have helped me during this work, and although I could not mention them all, I would particularly like to thank: Rich Guimond and Tim Krohe, at the Office of Radiation Protection, Environmental Protection Agency, Washington, D.C., for the initial guidance in the subject of indoor radon, during a summer internship at the ORP; Bob Cornish, for his friendship and sincere interest in my work, and for the long hours discussing it, when he shared with me his broad scientific knowledge; Janis Michael, for her counselling with the text processor; my mother-in-law, Branca Mendes, for being with us at home, and offering her help, in the moments we needed it most; and the Brazilian community, as well as other friends in Ann Arbor, for their continuous encouragement and moral support.

In a very special way I would like to express my most sincere gratitude to my parents, Celso and Sylvia Loureiro, for their endless support of all kinds, and most especially for teaching me with the example of their lives, to have hope in the future and to endure in the search of my ideals.

Finally, I want to express my appreciation to my wife Laura, and our son Rafael. With their love, they made the years living in Ann Arbor, the most beautiful time of my life.

TABLE OF CONTENTS

LIST OF FIGURES

Figure

LIST OF TABLES

Table

LIST OF APPENDICES

Appendix

CHAPTER I

INTRODUCTION

Objective and Scope.

Normal operation of residential buildings generates small underpressure differences from inside to outside across the bottom of the building shell, inducing a flow of soil gas from the ground into the interior of the house, through cracks and other openings in the understructure in contact with the soil. Radon being produced in the soil is then carried along with the flow of soil gas into the house, in a complex diffusive-convective transport process. The building acts as a trap for radon, and depending on the radon entry rate, as well as on the air exchange rate, the indoor radon can reach elevated concentrations, typically one order of magnitude larger, but ranging far higher than the outdoor concentration.

Radon (Rn-222) is a radioactive noble gas, which decays in a sequence of short-lived decay products. When inhaled, these airborne short-lived radon progeny attach to the internal walls of the respiratory tract exposing the lung tissues to damaging alpha radiation. The importance of this problem comes from the fact that exposure to the radon-daughters has been associated with the induction of lung cancer in miners, mostly in the uranium mining industry.

The objective of this thesis is to formulate a mathematical model to simulate the problems of: 1) radon production and decay in the soil around the house; 2) radon transport through the soil; 3) radon entrance into the house through idealized openings in the understructure

of the house; 4) and the final indoor radon concentration, as a function of an applied steady-state negative pressure in the basement.

A three-dimensional numerical model based on a finite-difference approximation was developed to solve the problem. The numerical model was then implemented in a computer program separated in two parts: in the first module, the distribution of the disturbance pressure and the flow of soil gas throughout the soil were calculated based on the negative pressure applied at the basement floor inside the house; in the second module, the distribution of radon concentration in the soil was calculated by solving the convective-diffusive radon transport equation. The radon entry rate into the house and the final indoor radon concentration were also evaluated in the second module.

In this chapter I introduce the concepts associated with the problem of indoor radon, emphasizing its significance as a risk to the public health. My objective here is to characterize the proper dimension of the problem, and the level of knowledge about it, in order to justify the current interest in the subject, which resulted in the development of this thesis. I also describe here the evolution of the research in this area, and the statement of a hypothesis which underlies the execution of this work.

Next, in Chapter II, I review prior models which simulated the production and transport of radon in soil, with special interest on those models dealing with transport of radon from the soil into houses. Then I start describing the basics of my own model: the initial assumptions; the geometrical configuration; and the physical concept of the model.

The mathematical equations expressing the model are presented in Chapter III. Then, in Chapter IV, I describe the application of the finite-difference numerical method to solve the differential equations of the model. I also describe the computer programs written for the implementation of the numerical method.

Chapter V contains the procedure adopted for the adjustment and calibration of the computer model. After being adjusted the programs are then tested for their sensitivity to the variation of each isolated parameter, through the full length of the expected range of

variation. Based on theoretical simulations, the influences of all important parameters on the mechanisms of radon transport from soil into houses are described in detail.

An overview of the work developed in this dissertation, with the conclusions and recommendations for further studies, as well as for improvements of the models, are presented in Chapter VI.

Finally, a few observations at this point will be appropriate. First, it should be pointed out that the element under concern in this work is the radioisotope radon-222. Therefore, in this dissertation, unless otherwise indicated, I consider that the name *radon* means its isotope radon-222. Another observation is related to the the units adopted to represent radioactivity, and radon concentration in air. In representing the radioactivity, I have decided to use the unit *curie (Ci)*, or more specifically its 10^{-12} fraction *picocurie (pCi)*, instead of the SI unit *becquerel (Bq)*. The relation between these units is such that 1 Bq = 27 pCi, where one becquerel represents one radioactive disintegration per second. Also, in representing radon concentration in air, I have adopted the unit $[pCi/l]$, instead of the SI unit $[Bq/m^3]$. Note that 1 $[Bq/m^3] = 0.027$ $[pCi/l]$. The reason for adopting these units is because of the still large number of reports and papers using them, facilitating then the intercomparison of data.

Justification.

Situation of the Indoor Radon Problem.

In order to characterize the problem of indoor radon concentration in houses, it would be useful to start with a brief description of the origins of radon, its sources, its behavior in the environment, and the health impacts associated with it.

Uranium-238 is the parent of a natural radioactive decay family, whose elements are ubiquitously distributed in trace amounts all over the earth's crust. The principal members of the U-238 series are shown in Figure (1.1). If it were not for the various chemical, physical, biological and temporal processes occurring in the environment, and affecting differently

each element of the radioactive family, the whole series would always be in radioactive equilibrium, where the decay rate of any element is equal to the decay rate of its parent, and consequently equal to the decay rate of the first member, uranium-238. However, these several environmental processes affecting the radioactive family, act as selective mechanisms, separating the elements of the series in subgroups of elements sharing similar characteristics, and giving to these subgroups a distinct destiny and pathway through nature. Thus, although the secular radioactive equilibrium exists in a global sense, it is rarely observed in any relatively small sample of the earth's crust. The relative value of the decay rate of one particular element of the radioactive series, compared with the activity of its progeny, is a significant feature for the formation of subgroups within the family. For instance, a long-lived element with short-lived decay products, even when separated from the whole series by any environmental process, will persist together as a subgroup of the series in the environment.

An important subgroup of the uranium-238 radioactive decay family is the one formed by the isotope radium-226, and its short-lived decay products: radon-222; polonium-218; lead-214; bismuth-214; and polonium-214. The head of this subgroup, the element radium-226, reacts with materials in nature forming solid compounds slightly soluble in water, which makes it available for being separated from earlier members of the series by the action of aquifers, facilitating its distribution through nature. Concentrations of uranium and radium show generally an average radioactive equilibrium. However, large deviations from equilibrium are also observed due to differential selection in nature caused by different geochemical properties of uranium and radium compounds [My83]. Chemically, radium is one of the alkaline earth elements, similar to calcium and barium, and has a tendency to follow these elements in the environment [NC84a]. Since it is easily transported throughout the environment, radium-226 ended up widely distributed, in trace amounts, in all materials of the surface of the earth such as rocks, sand, soil, and water . In the United States, Ra-226 concentrations in typical surface soils have been reported in the range $1.08 \pm .54$ $[pCi/g]$ [Na85]. The average value of 1.0 $[pCi/g]$ has been proposed as a reference radium concentration in normal soil, a value which serves as a basis for comparison with other

Figure 1.1 — Uranium (U-238) radioactive decay series.

(Reference: Kocher, [Ko81])

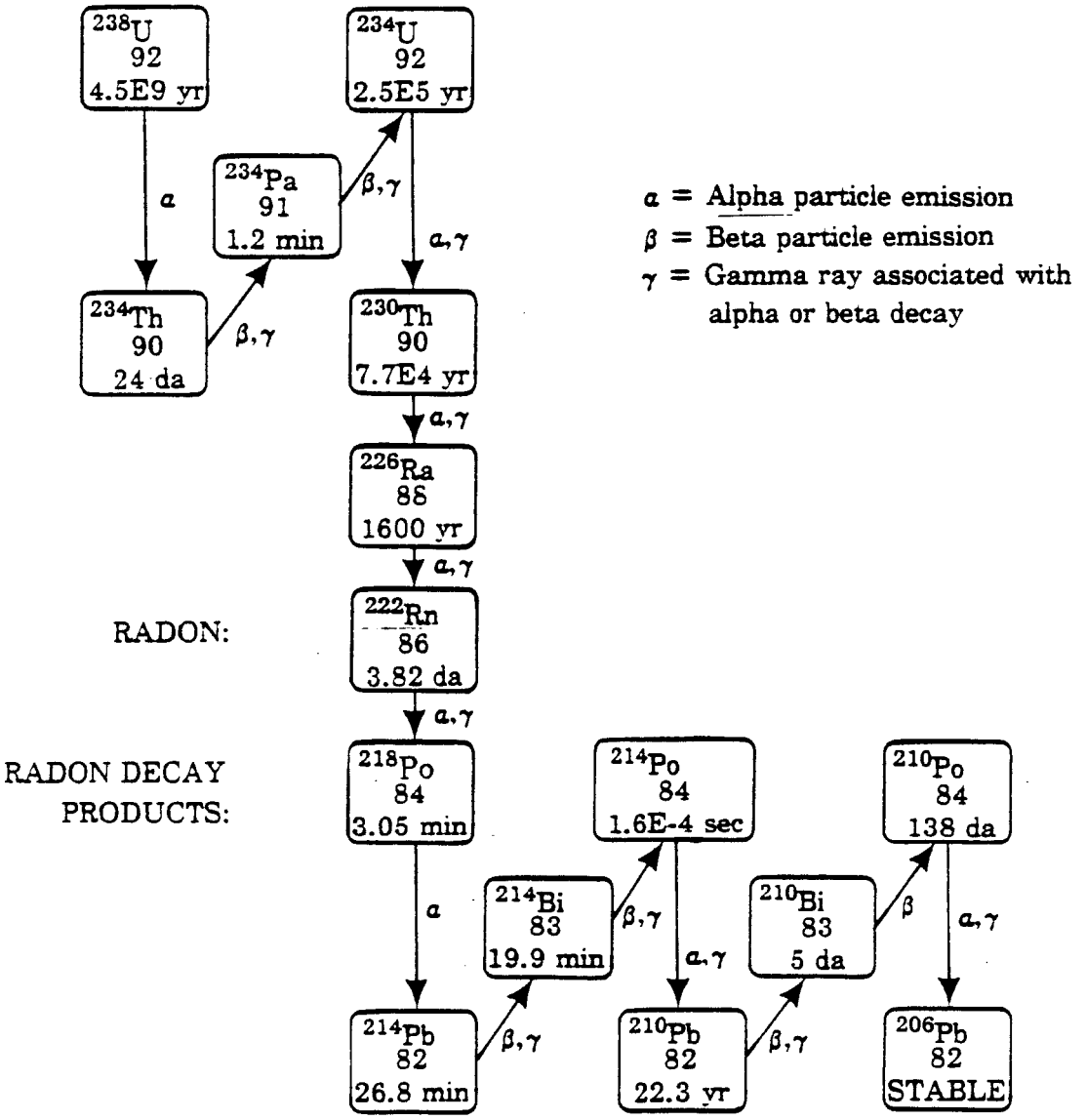

(Reference: Kocher, [Ko81])

materials [NC84b]. In granite rocks, and in soils near phosphate and uranium mining areas, and uranium mill tailings piles, the Ra-226 concentration is usually much higher.

Radium-226 has a relatively long half-life of 1600 years [Ko81], and because it is so widely spread on the surface of the earth, it constitutes a perennial source of its direct decay-product – the isotope radon-222 – the most important element of the whole radioactive series in relation to the associated environmental impacts.

Radon-222 is an inert, noble gas, which undergoes radioactive decay by alpha-emission, with a half-life of 3.82 days. [Ko81]. It is the only gaseous element at ordinary temperature (radon liquefies at -62 °C) [Ev69], of the entire uranium decay series. It presents, consequently, a unique ability to escape from its location of formation reaching the atmospheric air, and areas far from its origin. In typical soils, the radon diffusion length – the average distance traveled by the radon atoms diffusing in the soil, before decaying – is approximately of $1[m]$. The decay of an atom of radium-226 within the molecular structure of its chemical compound in the rock, soil particle or any other medium such as the surface coatings on soil grains, generates an atom of radon-222 which, being inert, does not react with either the remnants of the former radium compound, or with any other substance present in the medium. Consequently, the radon atom is ready to move away from its place of birth, as soon as it is formed. However, not all radon atoms formed within the solid structure where the radium compound is located (being a soil particle, or a solid rock), will be able to escape to the exterior of the solid medium, reaching the air surrounding it. Only a fraction of the total number of radon atoms generated inside the solid is able to make it to the outside. This portion, called the radon *emanating fraction*, is inversely related to the physical dimension of the medium, being very small for large solid blocks of rock, and reaching the top of the range in soils with small size particles such as in clays. Measurements of emanating fraction of radon-222 in soils have been reported elsewhere with a range of 0.05-0.7 , and a typical value of 0.2. [Na85].

Except for a small amount of radon liberated from the water bodies on the Earth's crust, surface soil is essentially the only source of radon-222 to the atmospheric air. [NC84a],

[Na85]. In the soil, the fraction of radon atoms that succeeds in escaping from the solid particles into the void space, gets mixed with the soil gas[1] present in the pore space. For a typical case of radium-226 concentration of 1.0 $[pCi/g]$; soil particle density of 2,650 $[Kg/m3]$; radon emanating fraction of 0.2; and soil porosity of 0.5; the resultant concentration of radon in the soil gas turns out to be about[2] 530 $[pCi/l]$. So, after being mixed with the soil gas, the radon atoms are then transported throughout the matrix of the soil pore space due to basically two distinct mechanisms: molecular diffusion, caused by variations of the radon atoms concentrations in space; and pressure-induced flow, caused by the presence of any disturbance pressure field eventually added to the hydrostatic pressure distribution in the soil. The value of the radon flux crossing the soil-air interface into the atmosphere depends on the strength of the source term in the soil, as well as on the strength of the transport mechanisms mentioned above. A representative value of 0.5 $[pCi/m^2s]$ for the emanation rate of radon in ordinary surface soils of the United States has been suggested elsewhere. [NC84b]. The soil gas escaping from the surface soil into the atmosphere, with a relatively high concentration of radon-222 (typically around 500 $[pCi/l]$), will then get mixed with the atmospheric air, and be diluted down to outdoor concentrations, typically around 0.1 $[pCi/l]$. [NC84b].

Radon-222 can also be introduced into the interior of buildings, where it becomes trapped and, depending on the strength of the source as well as on the air exchange rate of the house, it can reach elevated concentrations, much above the concentration outdoors. Sources of indoor radon are complex in nature, and depend not only on the concentration of radium (Ra-226) in materials inside and soils outside the building, but also on: 1) the physical characteristics of these materials, such as porosity, permeability, and moisture content; 2) the environmental factors such as wind, variations of atmospheric pressure, temperature, and precipitation; and, 3) on the structural and operational characteristics of the house. Figure (1.2) shows the various possible sources of indoor radon. The most important source, for the largest number of cases of high indoor radon (Rn-222) concentrations in single-family houses in the U.S., is the soil gas surrounding the building foundations. [Ne84a]. Radon in

[1] Soil gas is defined in Chapter II.

[2] This calculation was based on Eq.(3.14) - Chapter III.

the soil gas can penetrate into a house due to diffusion through the foundation structures in contact with the soil (basement walls, and floor slab), or through any cracks and other eventual openings in these structures. Also, radon in the soil gas can be brought into the house, through these same openings, due to a convective flow forced by small pressure differences created across the building shell as a result of the wind blowing against the external walls of the house (the wind effect), and the temperature differences between inside and outside the building (the stack effect), as well as the effect of any unbalanced mechanical ventilation (exhaust system) in the house. The possibility of a forced convective flow from the soil into the interior of the building, constitutes part of the hypothesis of this dissertation, as will be described later.

Other possible but not very significant sources of indoor radon are the building materials containing elevated concentrations of radium (Ra-226). Radon-222 generated within these materials can diffuse through, and emanate from, the material into the interior of the building. Some utilities in the house, such as water, can also constitute significant sources of indoor radon in some specific cases. Water supplies obtained from underground aquifers being in contact, deep in the ground, with radium-containing materials that emanate directly into the water may contain elevated concentrations of dissolved radon-222, which can be liberated from the water into the interior of the house during heating and agitation, such as in water heaters, showers and washing machines. Surface water supplies are usually low in dissolved radon, and do not contribute significantly to indoor radon level. The relative magnitude of all these radon sources depends on specific circumstances, where either one of them could predominate. However it has been widely recognized that, for most of the cases of houses with high indoor radon concentration in the United States, soil is the major source [Ne84a], [Br83], [NC84a], [NC84b], [Ak84], [Ea84].

Concentrations of indoor radon vary over a large range, of approximately two to three orders of magnitude. While typical concentrations in U.S. residences vary around 1.0 $[pCi/l]$, measurements of indoor radon in the range between 10 to several hundreds $[pCi/l]$ have been often reported in the literature, and concentrations greater than 1000 $[pCi/l]$ are not

Figure 1.2 — Representation of the various possible sources of indoor radon in homes.

(Adapted from a figure presented by Nero, [Ne86])

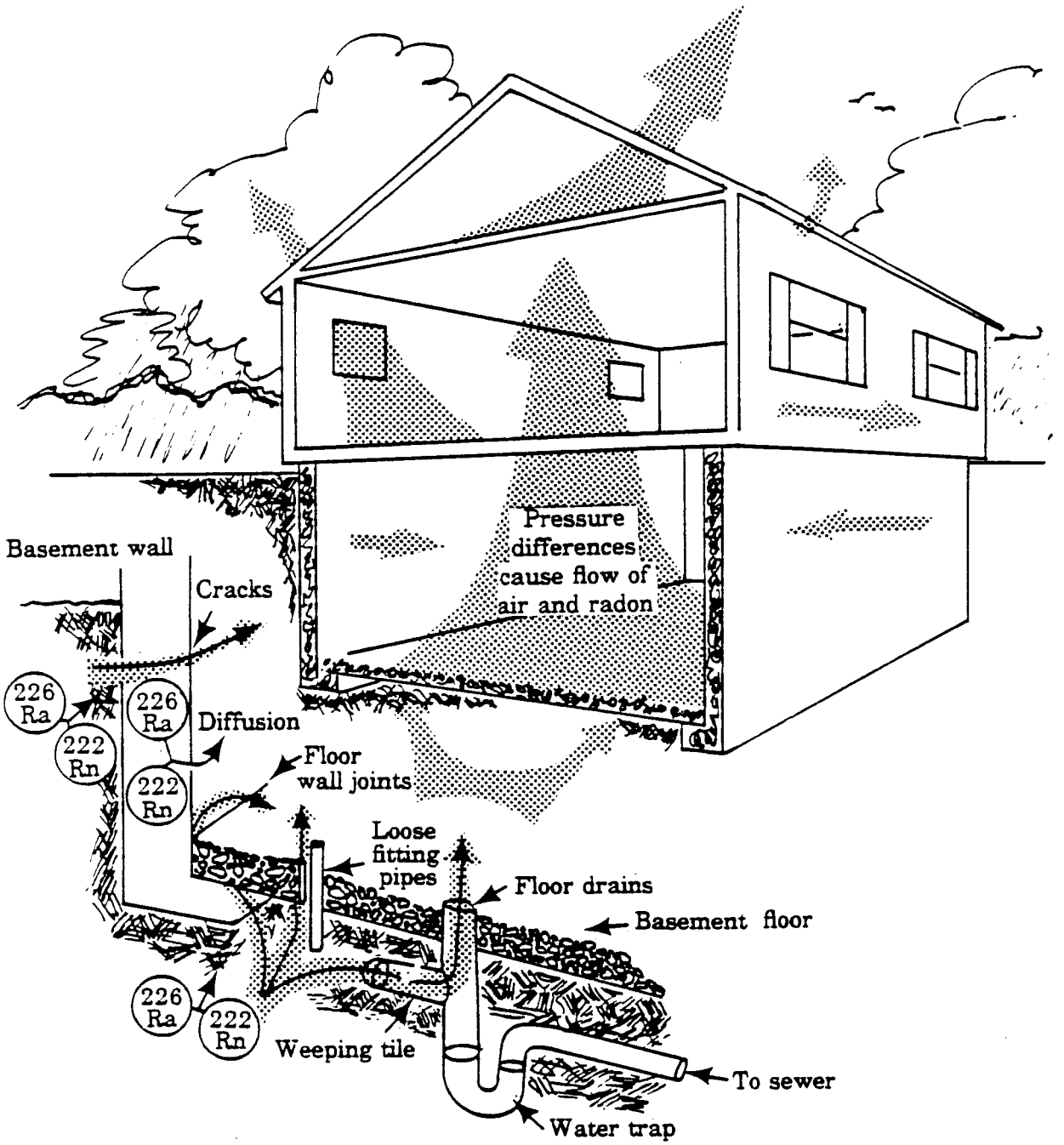

unknown. [Se87]. However, even with all the studies and measurement data on indoor radon available today, there is still a lack of clear and unequivocal characterization of the distribution of indoor radon concentration in the United States. In a statistical analysis of the available measurement data on indoor radon, collected in 22 locations representing 17 of the 48 contiguous states, Nero and a group of researchers at the Lawrence Berkeley Laboratory, developed a frequency distribution of radon (Rn-222) concentrations in single-family homes, which could be used as an approximation for the actual distribution [Ne84b]. Based on their conclusions, the distribution of annual-average concentration of indoor radon (Rn-222) in single-family homes in the U.S. could be characterized approximately by a geometrical mean of 0.9 ± 0.1 $[pCi/l]$, and a geometric standard deviation of 2.8 ± 0.2. They also concluded that the average annual indoor Rn-222 concentration would be in the vicinity of 1.5 $[pCi/l]$, and that 2%, or approximately one million U.S. homes, would have annual-average indoor Rn-222 concentrations exceeding 8 $[pCi/l]$. [Ne84b]. A study conducted in Sweden indicated that about 2 to 3%, or more than 30,000 Swedish houses, have indoor radon concentrations exceeding 10 $[pCi/l]$. [Ak84].

Another isotope of radon, thoron (Rn-220), is also generated in the soil, on the average, at the same rate as radon (Rn-222). Thoron is a member of another natural radioactive decay series headed by the element thorium (Th-232). Because of its short half-life, about 55 seconds, thoron has a short transport range in the soil, and consequently a lower entry rate into the houses as compared with the isotope radon (Rn-222), with a half-life of 3.82 days. Therefore, indoor concentrations of thoron are generally much lower than concentrations of radon (Rn-222). The focus of this dissertation is exclusively on the more abundant isotope, radon (Rn-222).

Up to this point I have described only the aspects related to radon (Rn-222), without mentioning its decay-products, which are, in fact, the major cause of concern as far as the radiological health impacts are concerned. So, in the sequence of the radioactivity decay series after radon-222, there are four radionuclides with half-lives shorter than 30 minutes, as shown in Fig.(1.1). These so called short-lived decay products of radon, or simply radon

daughters, or radon progeny, are solid metals represented by the elements: polonium (Po-218); lead (Pb-214); bismuth (Bi-214); and polonium (Po-214), with half-lives of 3.05 [min], 26.8 [min], 19.9 [min], and 163.7 [μs], respectively. [Ko81]. The two isotopes of polonium, Po-218 and Po-214, decay by alpha emission. Bismuth (Bi-214) and lead (Pb-214) decay by beta emission.

Because of the technical difficulties in measuring each short-lived radon daughter separately, and having realized that the airborne radiation dose to the human lung is predominantly attributable to the radon-daughters rather than to radon, a new unit was defined for use in the early uranium mining industry, that could represent the concentration of the radon daughters as a group, instead of each radionuclide isolated. The concept of the *Potential Alpha Energy Concentration*, (PAEC), measured in units of *working level*, (WL), was then defined and worded as: *One WL is any combination of the short-lived decay products of radon-222, in one liter of air, that will result in the ultimate emission by them of* 1.3×10^5 *MeV of alpha energy.* [Ev69]. Adoption of the numerical factor 1.3×10^5 MeV, comes from the fact that this number is equal to the total alpha-decay energy ultimately delivered from a mixture of the short-lived radon daughters, each one of them in radioactive equilibrium with 100 pCi of radon-222, after the decay of all the short-lived radon progeny, up to the last atom of polonium-214. In other words, it means that one liter of air with 100 pCi of radon-222, in complete radioactive equilibrium with its daughters, contains one WL. Yet, the definition of the working level is not restricted to equilibrium conditions, and applies to any combination of the radon progeny such that, say at 50% equilibrium, the same liter with 100 pCi of radon-222 contains 0.5 WL. An equilibrium factor could then be defined as the ratio of the radon daughter concentration in WL, to the radon-222 concentration in $[pCi/l]$, multiplied by the factor 100.

Besides the PAEC, expressing the concentration of the radon-daughters, another unit had to be defined to represent the cumulative occupational radiation exposure of the uranium mining workers to the radon daughters. For this purpose, the *Working Level Month* (WLM) was then defined as the product of the concentration in WL times the exposure duration

given in multiples of a 170-hour[3] occupational month. [NC84a]. It is important to note that the WLM unit expresses occupational exposure. In order to adopt this concept to represent exposure to the population in general, it needs to be modified appropriately to account for the different exposure time of individuals of the public, as well as for different breathing rate of distinct age groups of the population. A detailed description of the methodology used in evaluating doses to the population exposed to radon progeny was presented elsewhere. [NA84b].

The radon daughters are formed as free atoms in the air, but have high chemical reactivity, and a strong tendency to attach to all surfaces including the surfaces of airborne particles and droplets in the outdoor and indoor atmosphere, room walls, and lung tissue. Part of the radon daughters formed in air is readily removed due to attachment to the surfaces of objects nearby (plate-out). Consequently, because of plate-out, the airborne radon daughters are almost never in radioactive equilibrium with their parent radon-222. The age of the mass of air is also an important factor affecting the equilibrium, because it determines the time available for the radon progeny to grow. The degree of disequilibrium is usually larger indoors (more surfaces to plate-out, and because of the ventilation) than in outdoor environment. In residential buildings, the equilibrium factor is typically 0.5. Therefore, using this equilibrium factor, and the annual-average indoor radon concentration of 1.5 $[pCi/l]$ in single-family houses in the U.S., as mentioned above, the corresponding value for an annual-average indoor radon-daughter concentration would be about 0.0075 WL. An individual of the general population, living indoors 80% of the time, and with a breathing rate 75% of the breathing rate of a worker (typical assumptions in the literature [Hu83]), would receive in one year a total accumulated exposure to radon-daughters of about $0.0075 \times \left(\frac{365 \times 24}{170}\right) \times 0.75 \times 0.8 \approx 0.23$ WLM, resulting in a lifetime average exposure of $70 \times 0.23 \approx 16$ WLM (assuming a 70-year average life for the population).

When inhaled in the air, a fraction of the radon daughters, attached or unattached to air particles, will stick to the internal walls of the respiratory track, where they stay until they

[3] Here I note that there are differences in the literature regarding this time factor in the WLM definition. Evans, [Ev69], defined this unit of time as an average month consisting of $40 \times \frac{52}{12} \approx 173$ working hours. However, more recent papers have simplified the definition of a working month to 170 working hours. [Na84a], [IC81].

are cleared by movement of mucus, or disintegrated by radioactive decay. Since the half-lives of the radon daughters are relatively short compared with the time for the clearance process of the internal mucus of the respiratory track to take place, most of the radon daughters end up decaying, and consequently exposing the internal walls and tissues of the lungs with their damaging alpha-radiation. In this respect, because radon does not get trapped in the respiratory track, and because the amount of time that radon stays in the air inside the lungs between inhalation and exhalation (a few seconds) is very small relative to its half-life (3.82 days), its contribution to the internal dose to the respiratory track is very small when compared with the dose due to its progeny. Therefore, the radon daughters rather than radon itself, constitute the main source of radiation exposure to the population, and consequently represent the major health risk. In the context of the ultimate health impact, the radon gas can be considered as an environmental vector, or an intermediate vehicle, which transposes the risk from its potential stage represented by the radon sources in the soils, to its full realization represented by the exposure of radon-daughters to the respiratory track of the population in general.

The health risk associated with exposure to radon daughters is the induction of lung cancer –or, more specifically, bronchial cancer – due to the absorption of alpha radiation in the basal-cell layer of the upper respiratory track. It should be emphasized however, that there is no clear indication of the existence of this risk at low exposure levels, such as those comparable to the average level in the environment. All evidence of the risk comes from studies of occupational groups exposed to extremely high concentrations. Epidemiological studies performed in Europe and North America, on workers in underground uranium mining (and other mining industries) exposed to elevated concentrations of radon daughters, have demonstrated a correlation between the incidence of excess bronchogenic cancer and the accumulated dose received by the exposed group. [NAS80], [UN77], [NC84b].

In the early stages of operation of the uranium mining industries, the health risk associated with radon-daughters was not known, and no special consideration was given to the problem. Consequently, the working conditions in this respect were extremely adverse. For example,

the radon-daughter concentrations in the U.S. underground uranium mines before 1960, ranged generally from 10 to 100 or more WL, with an average cumulative exposure of the miners above 1,000 WLM, considerably in excess of the current occupational limit of 4 WLM per year. [NAS80].

The elevated incidence of bronchogenic cancer among these miners constitutes the principal basis for establishing the numerical cause-effect relationship between radon daughter exposure and lung cancer. However, a few problems arise in estimating the dose-response factors for miners, and also in extending the results to the general population. The first difficulty is the uncertainty in the miner data, especially in relation to the assessment of doses received by the exposed groups. Another difficulty arises in adopting a model to extrapolate the results obtained in a relatively homogeneous group of miners, exposed to elevated concentrations, to the general population, fundamentally heterogeneous in composition and habits, and exposed to environmental levels of radon daughters. Nevertheless, a few attempts have been made to estimate the risk of lung cancer in the population from exposure to radon daughters. The National Council on Radiation Protection and Measurements, estimated the lifetime lung cancer risk, averaged over age factors, under environmental conditions, per WLM per year as $9.1 \times 10^{-3} \left[\frac{\#\text{cases}}{\text{person.WLM/yr}}\right]$ [NC84b]. Based on this figure, and on the estimated average environmental exposure of 0.23 $[WLM/year]$, it is possible to estimate the lifetime environmental risk of lung cancer due to exposure to radon daughters as $0.0091 \times 0.23 = 0.0021$, or 0.2%. Assuming that the lung cancer cases induced in one generation are expressed uniformly over a 45 year period [NC84b], the above estimated risk would amount to about 10,000 lung cancer deaths per year in the U.S. population of 225 million people. In a review of this subject, Nero considered possible variations on the average background concentrations, and estimated a range from 1000 to 20,000 cases of lung cancer in the U.S. population caused by the exposure to radon daughters at environmental levels. [Ne83].

In order to establish a term of comparison, it should be mentioned that the lifetime lung cancer risk for non-smokers from natural causes, is approximately 1%. [NC84b]. Therefore,

according to the estimation above, the risk of lung cancer attributable to the exposure to radon daughters at the average environmental concentrations, is about one-fifth of the risk for non-smokers. Although it seems small when compared with the risk in the non-smoking population, the lifetime risk of 0.2% (10,000 deaths a year) is still very high compared with the estimated risks from other environmental pollutants. [Ne86]. Besides that, for the people living in those approximately one million **hot houses** mentioned above, where the annual-average indoor radon concentration is above 8 $[pCi/l]$, (more than five times the annual-average concentration), such exposures entail risks well above the risk for the non-smoking population, or even similar to the risk of the smoking population.

Formulation of the Hypothesis.

This dissertation is inserted into the broad research efforts taking place in the Indoor Environment Program, of the Applied Science Division of the Lawrence Berkeley Laboratory, for the characterization of the problem of indoor radon. The specific subject of my thesis is part of a theoretical approach that, together with some experiments being conducted parallel in the group, have the objective of explaining the mechanisms and the factors affecting the entrance of radon from the soil into the interior of residential buildings. In order to justify the formulation of the hypothesis underlying the execution of this work, it would be appropriate to describe some of the major findings of the group, and the evolution of the understanding of the problem.

Two areas of research were initially established in the Indoor Environmental Program to investigate the problem of high indoor radon concentration. The first one was oriented to the study of materials used in buildings construction, and their ability to produce and liberate radon into the interior of the house. At that time it was believed that sources of indoor radon in most of the cases, were mainly the diffusion from soils and building materials, and were of a stable and constant nature. The other area of research resulted from the concern that the practices being adopted for sealing and tightening homes for energy conservation could increase the concentration of indoor pollutants (including radon) to levels much higher than the ones experienced so far. Then, a program for measuring indoor

radon concentrations, ventilation rate, and some other environmental parameters in several locations in the U.S. was established with the objective of investigating the relationship between indoor radon concentrations and other parameters, especially the ventilation rate and the radon source strength. The main observations from this measurement program were that [Ne86]: 1) the indoor radon concentrations showed variations in a very large range; 2) the ventilation rate varied in a much smaller range than the indoor concentration; 3) and only a weak statistical correlation existed between indoor radon concentration and ventilation. These facts were surprising because it was strongly suspected that ventilation would have a profound effect on the indoor radon concentration, which should then be clearly apparent in a regression analysis of these variables. Therefore, the conclusion from this part of the project was that although the ventilation rate, in fact, affects inversely the concentration of indoor radon when the amount of radon in the indoor air is fixed, or when the entry rate of radon into the building is constant, the large variability found in the indoor radon concentration could not be explained by the smaller range observed in the ventilation rate measurements. Consequently, the source term, or the radon entry rate into the buildings should be varying as well, and most significantly, the variation of the radon entry rate, rather than the ventilation rate, should be the most important element to explain variability in indoor radon concentration.

On the other hand, results from the studies of the materials had shown that diffusion from the materials internally to the house could only explain the concentration at the low end of the observed distribution of indoor radon concentrations. In contrast, it was known that soil has the potential capacity of generating radon in quantity enough to produce high concentrations in homes. However, diffusion was supposed to be the fundamental mechanisms to promote escape of radon from soil into the house, but diffusion alone could not explain the high values in the indoor radon distribution.

Therefore, considering that the indoor radon source should be variable, and its variability the main factor affecting the indoor radon concentration, then if the soil is the only radon source with potential to produce enough radon to explain concentrations at the high end

of the distribution, but if the diffusion alone is not large enough to accomplish this, then another transport mechanism should be taking place in addition to diffusion in bringing radon from the soil into the house. Obtaining an answer for this problem became therefore the most important scientific task.

Parallel to these research activities, investigations from other groups in the Applied Science Division of LBL, on the ventilation and infiltration in homes had concluded that houses are ventilated mainly due to uncontrolled infiltrations of air coming from outside, entering the lower part of the building, and leaving back to the outside at the upper part of the house, passing through openings in the building shell such as floor-wall joints, loose fitting pipes, cracks, floor drain, windows and roof. This uncontrolled infiltration is caused by small pressure differences between indoor and outdoor, generated by two factors: the effect of the wind blowing against the external walls of the the house, and the effect of the difference in temperature between indoor and outdoor atmosphere (called stack effect), creating an internal upward flux of air from the bottom to the top of the house.

Based on these results and observations, the following hypothesis was then developed [Ne86]:

- Radon might enter houses from soil, not only by molecular diffusion, but mainly by a complex mechanism of diffusive-convective flow of soil gas from the ground into the interior of the building through openings in the building shell;
- The same forces responsible for the uncontrolled ventilation, causing the overall infiltration of air through the building shell, should also bring some soil gas from the ground into the house;
- These forces are small pressure differences of the order of a few pascals created between the indoor and outdoor environment by the wind speed and temperature differences.

In order to test this hypothesis, several experiments with corresponding theoretical studies, were designed emphasizing some aspects of the problem. One of these experiments was undertaken to measure the disturbance of the pressure field in the ground around houses. These alterations in the pressure field were expected from the hypothesis of pressure-driven diffusive-convective flow of soil gas from the soil into the house. In the experiment, per-

formed in a house in the Pacific Northwest, some probes were driven into the soil at distances up to 10 meters from homes. The objective was to see if the homes were drawing enough soil gas from the ground such that a depression on the pressure field in the soil could actually be detected. Also, tracer gases were injected at some probe points and monitored in others, with the objective of characterizing the pattern of the flow of the soil gas throughout the soil matrix toward the building. Approximate theoretical models were then proposed to calculate the pressure differences, air flow velocities and radon entry rates implied by this hypothesis. [Na86], [Ne86], [Mo86].

The long range objective of the work reported here was to increase the understanding of the complex mechanisms transporting radon from soil into homes, and to use this understanding to interpret experimental results and guide new experiments, leading eventually to improved methods for controlling indoor radon concentrations.

Other investigators studying this problem have also reached similar conclusions and have proposed similar hypothesis. In a study of Swedish houses with elevated radon concentrations, Åkerblom and others, [Ak84], concluded that a convective flow of soil air into the house, forced by pressure differences from inside to outside, was the main source of indoor radon. However, no further possible explanations were suggested for the development of these underpressure differences in the house. In a program designed to reduce the indoor radon concentrations in Canadian homes, Eaton and Scott, [Ea84], proposed that the major cause of elevated indoor radon is the entry rate of soil-generated radon due to pressure driven flow of soil gas into the house. They also proposed the same theories of the stack and wind effects to explain the mechanisms to induce underpressure and to force soil gas from the ground into the houses. Remedial actions adopted in these houses, by sealing the joints and openings in the foundation structures, and by reducing the pressure differences between the house and the soil, have shown good results in reducing the indoor radon concentration.

CHAPTER II

BACKGROUND

Review of the Existing Radon Transport Models.

The element radon (Rn-222) was discovered in 1900 by Friedrich Ernst Dorn, a German chemist, and since then numerous papers have been published about it. A comprehensive review of this subject was performed by Tanner in 1964, and supplemented in 1979. [Ta64], [Ta79]. Also, a good reference on the radon isotopes, their chemical and physical properties, as well as their behavior in nature was published by Serdyukova and Kapitanov in the Russian literature, in 1969, and translated to English in 1978. [Se78].

The interest in radon and its behavior in rocks and soil, especially on the radon transport processes below the earth's surface, was initially on the application in the prospecting and mining of uranium. With increasing concern for the possible occupational and environmental impacts caused by radon daughters in the uranium industry, research on radon was then directed toward explaining and controlling the high concentration of radon in uranium mines, and emanation of radon from uranium mill tailings, as well as in understanding the general behavior of radon in the environment.

Knowledge of the characteristics of porous media, and more specifically on the flow of substances through porous media, is of fundamental importance to understanding the processes involved in the generation and transport of radon in rocks and soils. DeWiest, [De69], edited a compilation of topics on flow through porous media, more related to groundwater hydrology, and Scheidegger, [Sc74], wrote a classic monograph on the physics of flow through

porous media. In a brief but careful review of this subject, Nazaroff and others [Na85] have described the important aspects of the general field of flow through porous media, relevant to the problem of generation and transport of radon in the soil.

The general transport equation of a particular substance in a porous medium containing a source, such as radon in soil, can be derived from the application of the principle of conservation of mass in an elementary volume of the medium, equating the total variation of mass within the volume, to the net balance of mass, with all sinks and sources being considered. The combination of the general transport equation representing the conservation of mass, with Darcy's law[1] relating flow with the spatial variable, constitutes then the basic approach for the development of models expressing transport mechanisms in soil, such as the molecular diffusion and the pressure-induced convective flow, in relation to physical properties of the soil as a porous medium. An adaptation of this basic approach for the formulation of a model for the transport of radon in the near surface of the soil containing a source, and in presence of a concentration gradient and a pressure gradient, was originally performed by Clements in his doctoral dissertation [Cl74a], which includes a substantive review of earlier works on the subject. The method and resultant equations of the model were also described by Clements and Wilkening in another paper [Cl74b]. In his work, Clements analyzed the effects of variation of atmospheric pressure on the flux of radon from ground surfaces.

Other mathematical models expressing the transport of radon in rocks and soils, for different applications, were described in the literature. Rogers and Nielson [Ro81] proposed a one-dimensional model to describe radon attenuation in multilayer cover materials over uranium tailings, where the molecular diffusion was the only transport mechanism considered. The objective was to develop a procedure for calculation of the thickness of cover in order to reduce the radon attenuation to a minimum specified. Boundary conditions were discussed, and a one-dimensional analytical solution was developed and applied in several cases. A one-dimensional computer program was written for the solution of a general case of a multilayer cover. Later in another paper, Rogers and others [Ro-83] recognized the existence of a natural convective flow of soil gas in the geosphere, which could result in a long term

[1] Darcy's law is presented in Chapter III and Appendix B.

radon transport through the uranium mill tailings cover significantly higher than the values predicted with a model using simple diffusion theory. A new version of their model was then formulated, with the addition of the convective term in the general transport equation. An analytical solution was developed for a one-dimensional, steady-state condition, with constant velocity. In another study, Bates and Edwards [Ba80], [Ed80], [Ba81], applied a convective-diffusive radon transport equation to model the time dependent flux of radon from the walls into the interior of underground uranium mines as a function of the pressure applied at the surfaces of the walls. One of the objectives was to simulate the effectiveness of overpressure ventilation on the radon concentration in the interior of mines. They also used their model to investigate the flux of radon through multilayer materials represented by the ore and the strengthened structure on the walls of the mine. The mathematical model was expressed in two versions: the first one in a two-dimensional cylindrically symmetric coordinate system [Ba80], [Ed80]; and the second in one-dimensional geometry [Ba81]. The model was solved with a finite difference numerical approximation in both versions.

The models expressing the transport of radon into houses and the resultant indoor radon concentration are still at the early stage of development, and are not very numerous. One of the first attempts to develop a mathematical model for this problem was performed by Collé et al. [Co81], in their review on radon transport through and exhalation from building materials. It was common belief, at the time, that the dominant source of indoor radon in houses under ordinary conditions was from diffusion from building materials, as well as diffusion and convective flow from the ground through the materials composing the understructure of the building in contact with the soil. Consequently the transport of radon from the ground into the house, in a pressure-induced flow through openings in the understructure of the building was not addressed in detail in Collé's work. However, a diffusive-convective radon transport model was proposed, and one-dimensional analytical solutions presented for different configurations of sources, time-dependency and boundary conditions, in a simplified geometry. In his review on the sources of indoor radon in houses, Bruno [Br83] proposed a descriptive model for the transport of radon into houses, and suggested that the infiltration of soil gas directly into a house is generally the main source of

indoor radon. He also suggested that the infiltration of soil gas into the houses is caused by the indoor heating (stack effect) and wind forces (wind effect). An important contribution to the subject of indoor radon modeling was given by Nazaroff and others [Na85], in their excellent review of the factors influencing soil as a source of indoor radon. The mathematical equations expressing the pressure-generating mechanisms (wind and stack effects), and the general radon transport from soil into houses were all proposed in a unified model. However, no solution of their model has yet been applied to a real or simulated situation – an undertaking that will be performed in this dissertation.

Analytical solutions of the equations for the transport of radon into houses through openings in the building shell are impossible, even for simple geometry. Consequently, the solutions must be achieved numerically, and attempts in this regard have just begun. [Sco82], [DS83], [Ea84], [DS85], [Mo86]. Scott and Eaton have modeled time variation of the pressure distribution in the soil around a house with basement, as well as the soil gas convective flow rates and indoor radon concentrations produced by those pressures, as a function of the wind speed and direction. In their first approach, [DS83], a two-dimensional model was developed, where the pressure distribution on the surface of the soil was linearized, and the resultant pressure distribution throughout the whole soil calculated in a steady-state finite-difference numerical approximation. Knowing the pressure distribution, the flow of soil gas through the soil and into the house through defined openings in the basement was then calculated using Darcy's law. A finite-element computer program was also developed for this configuration. [Ea84]. In another approach, [DS85], the pressure distribution on the surface of the soil was first simulated in a wind tunnel experiment with a reduced scale model of the house. Then, using the normalized results from the wind tunnel simulation and the actual weather measurement data, the pressure distribution throughout the soil, the flow of soil gas, the entry rate of radon into the house, and the final indoor radon concentration were calculated with a steady-state three-dimensional finite-element computer model. The input data were considered constant in each hour, and the program was run for each hourly interval for the total length of the weather data used. According to them, a single run of the program involved over 60 hours of computing time. These models neglected the diffusive

mechanism of radon transport in the soil, and considered only the convective component of the flux. Also, the use of the models was restricted to the simulation of houses with basements, and the pressure induced flow caused by the wind and temperature differences.

Mowris [Mo86] developed simplified analytical techniques to predict the radon entry rates in houses with basements or crawl spaces. In his approach, the flow of soil gas from the soil into the house is considered dependent upon basically two factors: the strength of the driving force, represented by the pressure difference from inside to outside of the house; and the resistance to soil gas flow offered by the soil and the openings in the building understructure. Mowris discussed the factors responsible for the underpressurization of buildings, and developed an analytical model expressing the strength of the driving force, or the total pressure difference in the house in relation to the temperature differences (stack effect pressure), the wind induced pressures, and to the pressures resulting from unbalanced mechanical ventilation. The resistance to soil gas flow through soil was modeled on a heat transfer analog, and the resistance to soil gas flow through basement gaps and cracks was modeled based on previous work by Jergling [Je81]. He also wrote a steady-state two-dimensional finite-difference computer program based on Darcy's Law and the continuity equation, to calculate the pressure distribution, and soil gas flow throughout the soil around the basement of a house. The numerical model was used for comparison with the predictions from the simplified analytical model. Mowris' model does not deal with the radon transport equation, and consequently does not answer the question of the radon concentration distribution in the soil. In his model, the radon entry rate into the house is calculated based on the assumption that the radon concentration is constant and equal to the level found deep in the soil. Therefore, since the radon concentration in the soil, at the soil-crack interface is always lower than the maximum concentration found deep in the ground, Mowris' model has the tendency of overestimating the radon entry rate, especially in extreme circumstances when: first, the underpressure difference in the basement is small, resulting in a small flow of soil gas, with a predominance of diffusion, and a consequent reduction of radon concentration at the crack interface; and second, the permeability of the soil is very high, resulting in an increase of flow of air from the atmosphere, diluting the

radon concentration at the air-crack interface.

As a starting point for the model developed in this dissertation, I assume a steady-state underpressure difference applied at the basement of a house. A gap formed by the concrete shrinkage is assumed to exist at the floor-wall joint in the basement.[2] Outside the basement, the soil is assumed to be formed first by an aggregate region followed by the block of undisturbed soil. The location of the gap, the size of the aggregate regions, and all the geometrical dimensions of the problem are well established. The floor-wall gap, which in this dissertation is called the *crack*,[3] constitutes the communicating channel between the interior of the basement and the soil outside. The model is then developed in two parts: in the first part, the pressure distribution and the soil gas flow is calculated throughout the whole soil block; in the second part, the convective-diffusive radon transport equation is solved in the domain of the soil block, with the calculation of the radon concentration distribution throughout the soil, the radon entry rate through the crack into the basement, and the final indoor radon concentration. The model was written for a three-dimensional configuration, using a finite-difference numerical approximation. To my best knowledge, this model is unique in its features, and constitutes an appropriate tool for the investigation of the factors affecting the radon distribution in the soil around a house, and the mechanisms responsible for the transport of radon from the soil into the house.

Initial Assumptions.

The model developed in this dissertation is based on single-family houses with poured concrete basement floor and walls, and with a simplified geometrical design with a rectangular horizontal cross-section. A gap is assumed to exist at the junction between the floor and the walls all along the perimeter of the basement, resulted either by design or from the natural shrinkage of the concrete slab of the basement floor. This gap, (here called a *crack*), is assumed to be the only opening in the understructure of the house, and conse-

[2] Also, this gap could be purposeful, i.e. some houses have a drainage crack system at the floor-wall interface for draining away any water.

[3] A distinction between a gap and a crack has been made elsewhere, [Mo86], as: 1) crack is due to mechanical cracking on the building shell, leaving an irregular surface inside the crack; 2) gap is due to purposeful construction techniques, leaving a relatively smooth surface inside the gap. However, in this dissertation I deal exclusively with the floor-wall gap, which I have called the crack.

quently the only communicating channel available for the soil gas to flow from the soil into the house. The soil is considered to be the only source of indoor radon. Outdoor airborne radon, and releases from indoor sources are not considered. Radon is assumed to penetrate into the house due to a diffusive-convective transport mechanism through the crack. Other mechanisms of radon entrance into the house, such as diffusion and flow of soil gas through the concrete of the basement (not through the crack) are not considered in the model. The house, although composed of the basement and the floor level, will be considered, for the matter of mixing of indoor radon, as a single chamber. In order to allow the simulation of the effects of spatial variations of the parameters affecting the radon entrance into the house, the model was conceived in a three-dimensional configuration. Other assumptions and simplifications will be described.

The first basic assumption in the model is the steady-state condition. It is clear though, that the problem of indoor radon is very dynamic in nature, being influenced by several environmental parameters which are variable with time, either on a random basis, or on a daily or annual cycle. Wind speed and direction change constantly in the atmospheric boundary layer following the variations of the turbulent eddies, in a random manner; temperature of the atmospheric air near the ground shows daily and seasonal cycles; atmospheric pressure, stability, and precipitation also show periodical and sporadic variations and occurrences; and human habits, and the operational features of a house are also intrinsically variable parameters. All these factors affect the sources and sinks of radon within the house, and consequently the steady-state assumption is not strictly valid. However, some modeling difficulties and, most important, the computing costs involved in a time-dependent computer program, especially in a large three-dimensional configuration, make a time-dependent model almost prohibitive. Therefore, for reasons of simplicity and reduction of computing costs, the steady-state condition is adopted in this model. Nevertheless, a few other points could also be mentioned to justify the steady-state assumption. The wind speed is, among all the pressure generating parameters, the one that shows the highest fluctuations and consequently is supposed to be most responsible for the short term variations of the radon entry rates into the houses. A study performed elsewhere and quoted by Nazaroff, [Na85], showed

that the variation of the wind speed could be generally characterized by two frequences: a high frequency representing the variations of short duration in the wind speed, with period in the order of 1 minute; and a low frequency with period of about 4 days. According to this, a typical wind speed would show fast fluctuations in the order of minutes, around an average value that would be sustained for longer periods of about 4 days. The question is how fast an induced disturbance pressure would propagate through the soil, and how fast the flow of the soil gas would react to this new established pressure distribution in the soil. Nazaroff [Na85] has addressed this problem, and calculated that the characteristic times for propagation of pressure disturbances in soil depend on the physical properties of the soil such as porosity and permeability, and can vary from few minutes in cases of sandy silt and gravel soil, to a few days in cases of clayey soil. Yet the transport velocities of the soil gas for typical pressure distribution in the soil, range from few $[cm/hour]$ for sandy and gravel soil, to less than 1 $[\mu m/day]$ in clayey soil. [Ea84]. Therefore, the propagation of the disturbance pressure in the soil can be regarded as taking place almost instantly compared to the reaction of the soil gas flow, and consequently to the transport of radon in the soil. With all this information it is possible to conclude that since a typical average wind power is sustained for periods of about 4 days, the assumption of steady-state condition is not an unreasonable one in cases of high permeability soils, where the induced disturbance pressure is completely propagated in a much shorter period. On the other hand, for very low permeability soils, the convective component of the radon transport mechanism becomes irrelevant compared with the diffusive component, which is not affected by the variability of the pressure generating mechanisms. Therefore, for these cases also, since the radon entry rate is mainly caused by molecular diffusion and almost invariable with time, the assumption of steady-state, although not a strictly valid one, might be adopted as well.

A constant negative pressure differential is assumed to exist at the bottom of the house, between the basement floor and the atmospheric air at the ground level outside. The atmospheric pressure at the ground level is assumed constant and undisturbed. In other words, the absolute pressure at the floor of the basement is assumed to be constant and equal to the sum of the atmospheric pressure, plus the weight of the air column formed by

the basement depth, minus the defined disturbance delta pressure. This defined disturbance delta pressure is assumed to be the net result of all pressure generating mechanisms acting on the house, such as the wind forces, temperature differences and unbalanced mechanical ventilation. It is not the purpose in this dissertation to discuss these pressure generating mechanisms in houses. For a general description of this subject the reader is directed to the papers of Nazaroff [Na85], and Mowris [Mo86]. The objective here is to model the spatial variation of the radon transport through the soil, and the entry rate into the house, based on a defined steady delta pressure, assumed to be localized at the basement floor of the house. The idea of symmetry is implicit in this assumption, and one important consideration should be addressed. This is related to the fact that the disturbance pressure field is not symmetrically distributed in the soil around the house, mainly because of the wind effect. Other pressure generating mechanisms such as the stack effect, or any unbalanced mechanical ventilation, are likely to induce symmetrical disturbance pressure distributions in the ground, but the effect of the wind power on the external walls of the house adds an unsymmetrical component to the distribution. Therefore, it should be recognized that the predictions of the model assuming a symmetrical disturbance pressure distribution around the house constitute an approximation of the actual situation.

The soil block around and underneath the understructure of the house is considered to be an unsaturated porous medium with no open channels and fractures, and to be formed of well defined regions of homogeneous and isotropic material. A region containing aggregate material soil is located immediately outside the house, between the basement walls and the undisturbed soil. Another aggregate region is defined underneath the basement floor slab. Within these regions, all soil parameters such as the porosity, permeability, soil particle density, concentration of radium (Ra-226), and radon emanation fraction are all considered constant and isotropic. However, these parameters are allowed to vary in different regions of the soil block.

The moisture content of the soil is a parameter of fundamental importance, affecting the soil permeability, the radon diffusivity constant, and the radon emanation fraction, as well

as the general transport of radon throughout the soil. However, because of the complexity involved in these interactions, the effect of the moisture content in the soil is not implicitly considered in the model. The way adopted for handling this issue was to develop the model leaving the moisture consideration aside, and then to consider the moisture content of the soil in a parameterized approach, during the selection of the values for the input parameters of the model. In other words, the choice of the input values for the parameters of soil permeability, diffusivity constant, and radon emanation fraction should be made initially for the dry soil, and then converted to the correspondent level of moisture content of the soil, according to some correction criteria. Nazaroff has discussed the effect of soil moisture on those parameters, and his results can be used as an approximated correction criteria. [Na85]. According to Nazaroff, in sandy soils the moisture content does not affect significantly the air permeability until the amount of moisture reaches the field capacity,[4] which for that particular kind of soil is in the range between 43 to 47% of water saturation. For levels of moisture beyond the field capacity, the air permeability of the soil decreases very rapidly down to zero at 100% moisture saturation. In clayey soils, on the other hand, the air permeability is more sensitive to the moisture content even at levels lower than the field capacity. [Na85]. The radon diffusion coefficient in soil is also strongly affected by the moisture content of the soil, in a way that could be described qualitatively by the following. For low levels of moisture content, the water is located mainly on the grain surfaces, and in small pores of the soil, leaving the large pores unobstructed. Since the radon diffusion in soils occurs mainly through the large pores, the diffusivity constant is only weakly affected by low levels of moisture content. However, as the moisture in the soil increases, the large pores become obstructed and the radon diffusion coefficient is then strongly reduced. In soils with 100% water saturation, the radon diffusion coefficient reaches values of up four orders of magnitude lower than the value at the dry soil. [Na85]. The effect of the soil moisture on the emanation fraction of radon from the soil particles into the soil pore space is rather peculiar: the presence of water around the soil particle enhances the amount of radon that, being produced in the soil particle, ends up in the soil pore space. The reason for

[4] The *field capacity* is defined as the amount of moisture remained in the soil after being completely saturated, and then left to rest for two days. It is expressed as a percentage of the soil pore space.

this phenomenon is, in simple terms, due to the fact that the water absorbs part of the recoil energy of the radon being emanated from the soil particle. This reduces the range of the radon atoms in the soil pore space, impeding many of them from reaching and penetrating back into the other neighbor soil particle, and consequently increasing the fraction of radon atoms that stay in the soil pore space. Thus, based on this qualitative information it is possible to reach some conclusions about the overall effect of moisture on the production and transport of radon in soils, which could be summarized as: 1) dry soils present the best condition for the radon transport, but the emanation fraction is greatly reduced, and consequently the total release of radon from the soil is not at its maximum; 2) in moist soils, the transport of radon is slightly reduced, but the radon emanation fraction is highly enhanced, a condition that allows the total production of radon to be at its maximum ; and 3) in wet soils, the emanation fraction is still high, but the diffusivity coefficient and the air permeability are greatly reduced, which also reduces the total release of radon from the soil. [Na85]. Therefore, when selecting the values for the input parameters for the model, the moisture content of the soil should be considered, and then the values of the soil permeability, radon diffusion coefficient, and the radon emanation fraction adjusted accordingly, based on the considerations above.

The soil gas is supposed to be formed by a mixture of air[5] and a very small molecular concentration of radon. No other gas or vapor is supposed to exist in the mixture. Considering the relatively small concentration of radon expected in the mixture, the density of the soil gas is assumed to be unaltered by mixing with radon. Also, it is expected that under the range of the applied pressure disturbance, as well as the range of the soil depth in the proposed configuration of the problem, the density of the soil gas does not change significantly. Consequently, the soil gas is considered incompressible. Moisture migration through the soil is neglected, and the flow of soil gas throughout the soil block is assumed to occur in a single gaseous phase.

[5] The volume fractions of the main components of dry atmospheric air are: 78.09% of nitrogen (N_2); 20.95% of oxygen (O_2); 0.93% of argon (Ar); and 0.03% of carbon dioxide (CO_2). [Ir81].

Geometrical Configuration of the Model.

The geometrical configuration of the model is shown in Figure (2.1). The soil block under consideration is represented as a parallelepiped of dimensions $2L_x$, $2L_y$, and L_z. The house is also considered a smaller parallelepiped of dimensions $2l_x$, $2l_y$, and $(l_z + h)$ partially embedded in the center and upper part of the soil block. The basement, represented by the part of the house embedded in the soil block has the dimensions $2l_x$, $2l_y$, and l_z. A region of aggregate soil material is located around the basement with thickness represented by $l_{x-aggr.}$, $l_{y-aggr.}$, and $l_{z-aggr.}$ in the x, y, and z directions respectively.

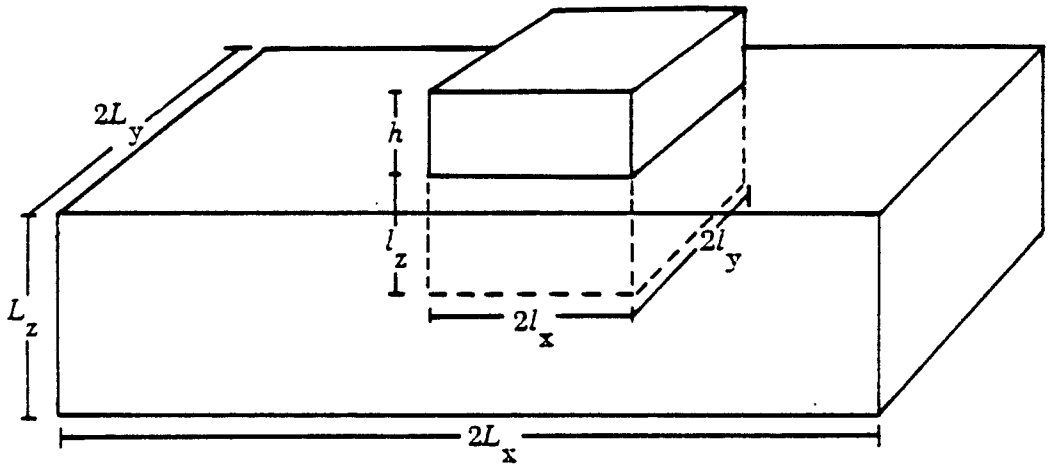

Figure 2.1 — Geometric configuration of the soil block with the house and basement.

In fact, due to the symmetry in the xy plane, the model will be developed in a reduced geometrical configuration represented by one quarter of the figure above, with the dimensions L_x, L_y, L_z and l_x, l_y, l_z for the soil block and the basement, respectively, as represented in Figure (2.2).

The entry route for soil gas into the basement is defined as the concrete shrinkage gap located at the wall-footer-floor joint along all the perimeter of the basement floor. Figure (2.3a) represents a vertical cross-section of the actual configuration at the gap, showing the

Figure 2.2 — View of a quarter of the soil block where the numerical solution for the model is developed.

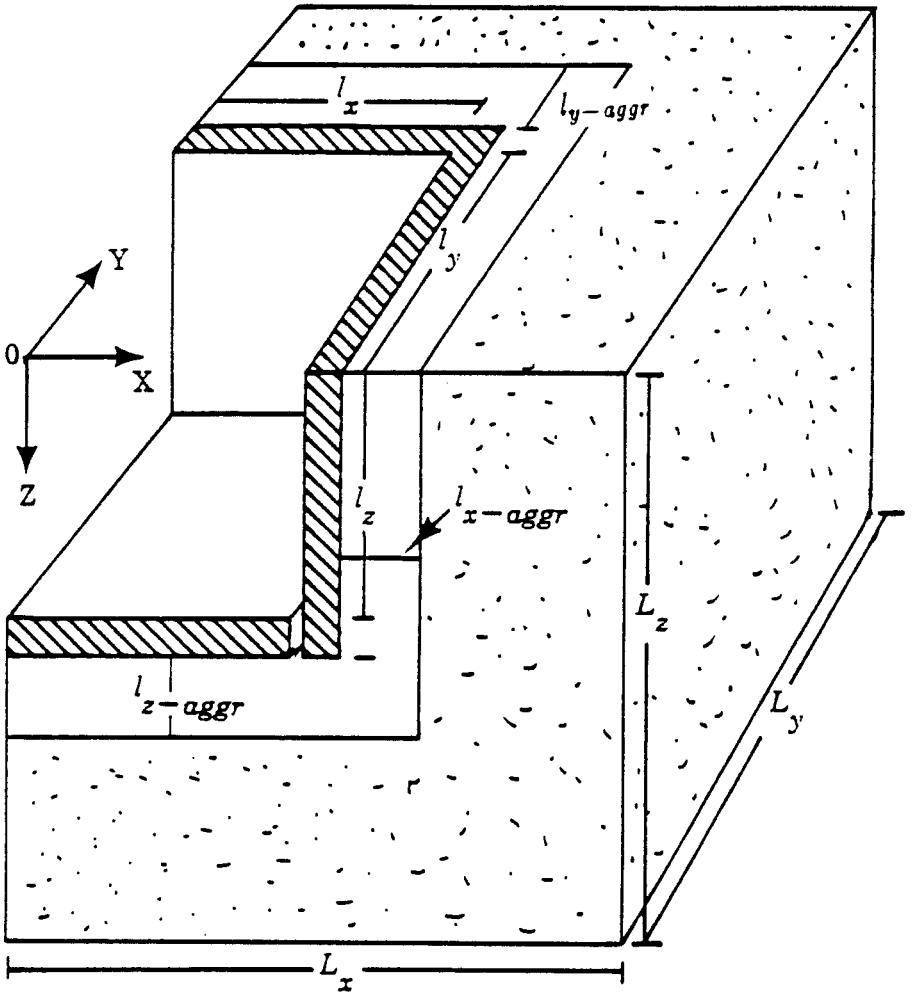

aggregate region, the wall, the footer, the floor slab, and the soil gas pathway through the gap. A simplification of this configuration is assumed in the model, as represented in Figure (2.3b). In this simplified geometry, the footer is not considered, and the crack is assumed to be located between the floor slab and the wall. Figure (2.3c) represents a vertical view of the basement floor, showing the extension of the crack all along the perimeter of the room.

Physical Description of the Model.

The important features of the model, and the interdependence among its elements, are

Figure 2.3 — Configuration of the crack in the basement.

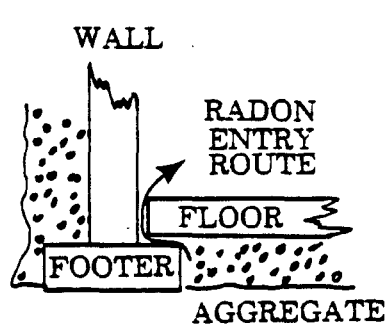

(A) Actual Configuration

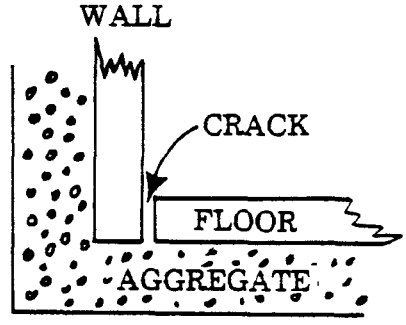

(B) Configuration assumed in the model

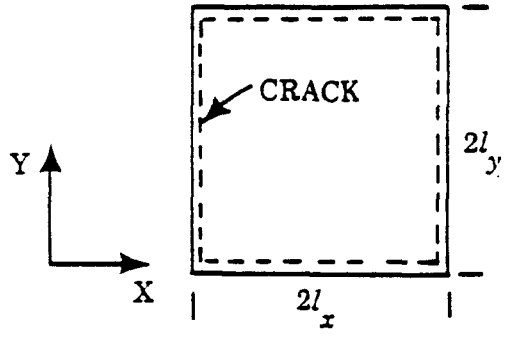

(C) Top view of the basement floor with the crack

shown in the flow-chart of Figure (2.4). The sequence of events starts with an steady negative pressure disturbance, ΔP, added to the absolute pressure in the basement, at the defined crack. This disturbance underpressure propagates through the soil, establishing a steady disturbance pressure distribution in addition to the hydrostatic pressure distribution in the soil. The new established disturbance pressure distribution then induces a steady non-uniform flow of soil gas throughout the soil matrix. Meanwhile, since the radon source is assumed to be homogeneously and isotropically distributed in the soil matrix, radon is being produced at a constant rate at any point in the soil pore space. The decay rate of radon at a point in the soil pore space is not constant, but depends on the radon concentration

at that point. Then, from the total interaction of these elements of the model – which is expressed by the radon mass transport equation – the distribution of radon concentration, as well as the total flux of radon throughout the soil block are established. The radon entry rate into the house is then given by the distribution of the total flux of radon through the soil. Finally, based on the radon entry rate into house, its geometric dimension, and its ventilation rate, the resultant indoor radon concentration is then established.

Figure 2.4 — General flow-chart representing the main elements of the radon transport model.

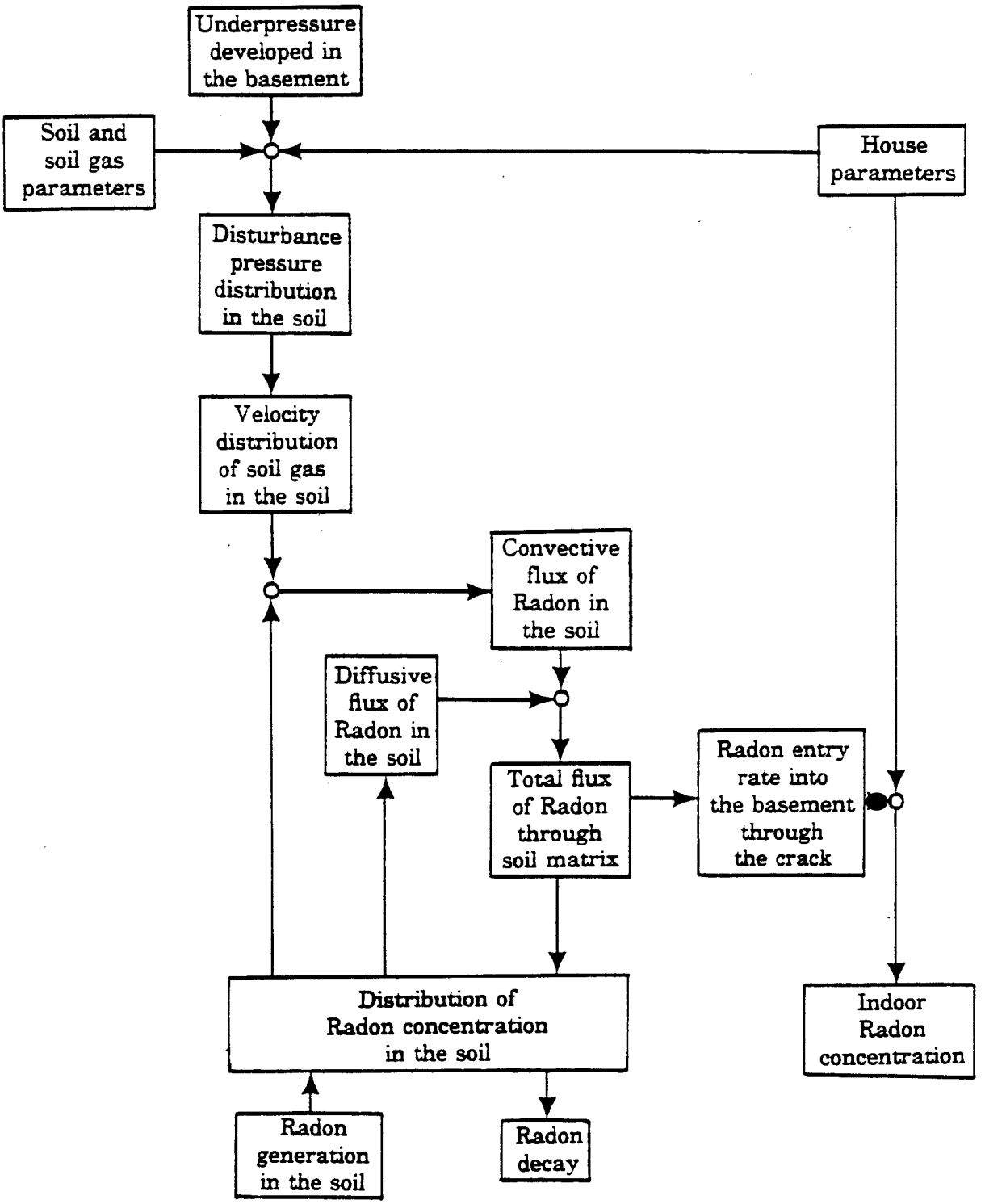

CHAPTER III

MATHEMATICAL FORMULATION OF THE MODEL

The objective in this chapter is to formulate the mathematical expressions of the problem, based on the proposed physical model as it was described in the last chapter.

First I derive the equation for the disturbance pressure field in the soil, with the definition of the boundary conditions. Then, I define the production rate of radon in the soil pore space, as well as the diffusive and convective components of the radon flux throughout the soil block. The equation for the radon concentration field in the soil, with the proposed boundary conditions, are presented next. Finally I formulate the expressions for calculating the entry rate of radon into the house, and the resultant indoor radon concentration.

In the last part of the chapter I present a dimensionless version of these expressions, in the same order that they were introduced, which will be used later in the development of the computer model.

Disturbance Pressure Distribution in the Soil.

The absolute pressure distribution in the soil is the result of the addition of two independent pressure components named the hydrostatic pressure distribution and another one here called the disturbance pressure distribution.

The hydrostatic pressure distribution results from the mass of air in equilibrium (at rest) within the soil, and is expressed by the fact that the vertical gradient of the hydrostatic pressure at any point is equal to the specific weight of the air at that point.

That means:

$$\frac{dP_H}{dz} = \rho g.$$

Integrating the expression above, gives:

$$P_H(z) = \rho g z + C_1. \tag{3.1}$$

At the surface of the soil, $z = 0$ and $P_H(0) = P_A$, or the atmospheric pressure. Therefore, the constant of integration C_1 can be written as:

$$|P_H(z)|_{z=0} = P_A = C_1,$$

and Eq.(3.1) becomes:

$$P_H(z) = P_A + \rho g z, \tag{3.2}$$

where,

$P_H(z) =$ Absolute hydrostatic pressure at depth z in the soil, in $[N/m^2]$;

$P_A =$ Atmospheric pressure (Absolute pressure at $z = 0$), in $[N/m^2]$;

$\rho =$ Soil gas density, in $[Kg/m^3]$;

$g =$ Acceleration due to gravity, in $[m/s^2]$;

$z =$ Depth in the soil, in $[m]$.

The so called disturbance pressure distribution in the soil is caused by the addition of a pressure disturbance at any point in the soil, which then propagates throughout the whole

soil block, and finally reaches a new equilibrium. This pressure distribution is independent of the hydrostatic pressure distribution and is added to this later one in such a way that the actual absolute pressure $P(x, y, z)$ at any point (x, y, z) in the soil is given by[1]:

$$P(x, y, z) = P_H(z) + p(x, y, z), \tag{3.3}$$

or,

$$P(x, y, z) = P_A + \rho g z + p(x, y, z), \tag{3.4}$$

where,

$P(x, y, z) =$ Resultant absolute pressure at the point (x, y, z) in the soil, in $[N/m^2]$;

$p(x, y, z) =$ Disturbance pressure added to the point (x, y, z) in the soil, in $[N/m^2]$.

In particular, at the soil surface, $z = 0$, and it is assumed that $P(x, y, z) = P_A$, so that from Eq.(3.4) :

$$p(x, y, 0) = 0. \tag{3.5}$$

In other words, at the soil surface the pressure disturbance is zero.

At the basement floor - $(z = l_z)$, see Fig.(2.2) - the pressure disturbance is by definition equal to the applied pressure differential , $-\Delta P$, and from Eq.(3.4) the absolute pressure at the basement floor can be expressed as: $P_B = P(x, y, l_z) = P_A + \rho g l_z - \Delta P$, for $0 \leq x \leq l_x$ and $0 \leq y \leq l_y$, or:

$$P_B = P_A + \rho g l_z - \Delta P, \tag{3.6}$$

where,

[1] Note that if the pressure disturbance distribution in the soil is zero, the mass of air is in equilibrium.

$P_B =$ Absolute pressure at the basement floor, in $[N/m^2]$;

$l_z =$ Depth of the basement floor, in $[m]$;

$\Delta P =$ Defined pressure distribution applied at the basement floor, in $[N/m^2]$.

Now I proceed with the derivation of the disturbance pressure field equation[2].

Since I have assumed that the soil gas is incompressible in the circumstances of this problem, the pressure field in the soil can be derived from the following two equations[3]: 1- Darcy's law for the velocity field; 2- Continuity equation.

Darcy's Law.

The general expression for the flow of gas through a porous medium is obtained from Darcy's Law.[4] In its differential form, Darcy's law states that the velocity of the soil gas flow at any point (x, y, z) within the soil matrix is proportional to the difference between the gradient of the absolute pressure in the soil and the specific weight of the soil gas. For isotropic soils, the differential form of Darcy's law can be expressed as (See Appendix B):

$$\vec{q} = -\left(\frac{k}{\mu}\right)\left(\vec{\nabla} P - \rho \vec{g}\right), \tag{3.7}$$

where,

$k =$ Soil permeability at the point (x, y, z) in the soil, in $[m^2]$;

$\mu =$ Soil gas dynamic viscosity, in $[Ns/m^2]$;

$\vec{q} =$ Soil-gas seepage velocity vector, (equal to the volume of soil gas flowing per unit of time, per unit of geometric cross-sectional area), in $[m/s]$;

---

[2] In the mathematical formulation that follows, I start all the derivation considering the absolute pressure distribution. However, since I am interested in the effects caused by the applied disturbance pressure, and since the disturbance pressure distribution is independent of the hydrostatic pressure distribution, I will end up with mathematical expressions dealing only with the disturbance pressure distribution.

[3] If I had assumed compressibility of the soil gas, then the model would have required a third equation (equation of state) for the derivation of the pressure field in the soil.

[4] Justification of the applicability of Darcy's law in this problem was presented elsewhere [Na85].

$P =$ Absolute pressure at the point (x, y, z) in the soil, in $[N/m^2]$;

$\vec{g} =$ Gravity acceleration vector[5], in $[m/s^2]$;

$\rho =$ Soil gas density, in $[Kg/m^3]$;

$\vec{\nabla} =$ Gradient operator.

Substituting the value of the absolute pressure from Eq.(3.4) into Darcy's expression, Eq.(3.7), yields:

$$\begin{aligned}\vec{q} &= -\left(\frac{k}{\mu}\right)\left[\vec{\nabla}(P_A + \rho g z + p) - \rho\vec{g}\right], \\ &= -\left(\frac{k}{\mu}\right)\left(\rho\vec{g} + \vec{\nabla}p - \rho\vec{g}\right).\end{aligned}$$

Therefore, the Darcy's differential expression for an isotropic soil can be expressed in terms of the disturbance pressure distribution only:

$$\vec{q} = -\left(\frac{k}{\mu}\right)\vec{\nabla}p. \tag{3.8}$$

Or in three-dimensional cartesian coordinates, such as:

$$u = -\left(\frac{k}{\mu}\right)\frac{\partial p}{\partial x}, \tag{3.9a}$$

$$v = -\left(\frac{k}{\mu}\right)\frac{\partial p}{\partial y}, \tag{3.9b}$$

$$w = -\left(\frac{k}{\mu}\right)\frac{\partial p}{\partial z}, \tag{3.9c}$$

where u, v, and w are the components of the seepage velocity vector $\vec{q}$, in the x, y, and z directions respectively.

Continuity Equation.

The continuity equation expresses the mass balance for the soil gas in the soil matrix, and can be written as (See Appendix A):

$$\frac{\partial(\epsilon\rho)}{\partial t} + \vec{\nabla} \cdot (\rho\vec{q}) = 0, \tag{3.10}$$

where,

ϵ = Soil porosity, [dimensionless];

$\vec{\nabla}\cdot$ = Divergence operator.

Since I have assumed a steady-state condition, the first term of Eq.(3.10) is zero, and the continuity equation then becomes:

$$\vec{\nabla} \cdot (\rho\vec{q}) = 0.$$

But since I have also assumed an incompressible flow regimen, the soil gas density is supposed to be invariable and the continuity equation can be finally expressed as:

$$\vec{\nabla} \cdot \vec{q} = 0. \tag{3.11}$$

Now, substituting the velocity vector $\vec{q}$ given from Darcy's expression, Eq.(3.8), into the continuity equation, Eq.(3.11) yields:

$$\vec{\nabla} \cdot \left[-\left(\frac{k}{\mu}\right) \vec{\nabla} p \right] = 0.$$

But since the soil gas dynamic viscosity is assumed to be constant, the equation above becomes:

$$\vec{\nabla} \cdot \left(k\vec{\nabla} p \right) = 0. \tag{3.12a}$$

Or, in three-dimensional cartesian coordinates, it is expressed as:

$$\frac{\partial}{\partial x}\left(k\frac{\partial p}{\partial x}\right)+\frac{\partial}{\partial y}\left(k\frac{\partial p}{\partial y}\right)+\frac{\partial}{\partial z}\left(k\frac{\partial p}{\partial z}\right)=0. \qquad (3.12b)$$

Equation above is a linear second order partial differential equation, and represents the disturbance pressure field distribution in the soil matrix[6].

Boundary Conditions for the Disturbance Pressure Distribution.

Figure (3.1) represents a quarter of the soil block. In this figure I define six distinct boundaries whose conditions must be specified in order to solve Eq.(3.12) for the disturbance pressure distribution in the soil. Table (3.1) summarizes the boundary conditions for each region of that configuration. A detailed description of the boundary condition imposed at the soil/crack interface is presented in Appendix E.

Soil-Gas Velocity Field in the Soil.

With the disturbance pressure field determined from Eq.(3.12) and boundary conditions, the velocity field[7] will be given directly from the differential form of Darcy's law, expressed in Eq.(3.8) and repeated here as:

$$\vec{q}=-\left(\frac{k}{\mu}\right)\vec{\nabla}p, \qquad (3.13a)$$

or,

---

[6] The permeability k is assumed to be constant within an specific region of the soil, but can take different values at other defined regions of the soil block. At the boundary between two regions of the soil with different permeabilities, the value of k should be calculated as a weighted average. (See Appendix H).

[7] Here I note again that I have considered the z-axis oriented downward. Consequently, the positive direction of the velocity component w is also downward.

Figure 3.1 — A quarter of the soil block, with the identification of the regions where the boundary conditions are imposed. (See Tables (3.1) and (3.2)).

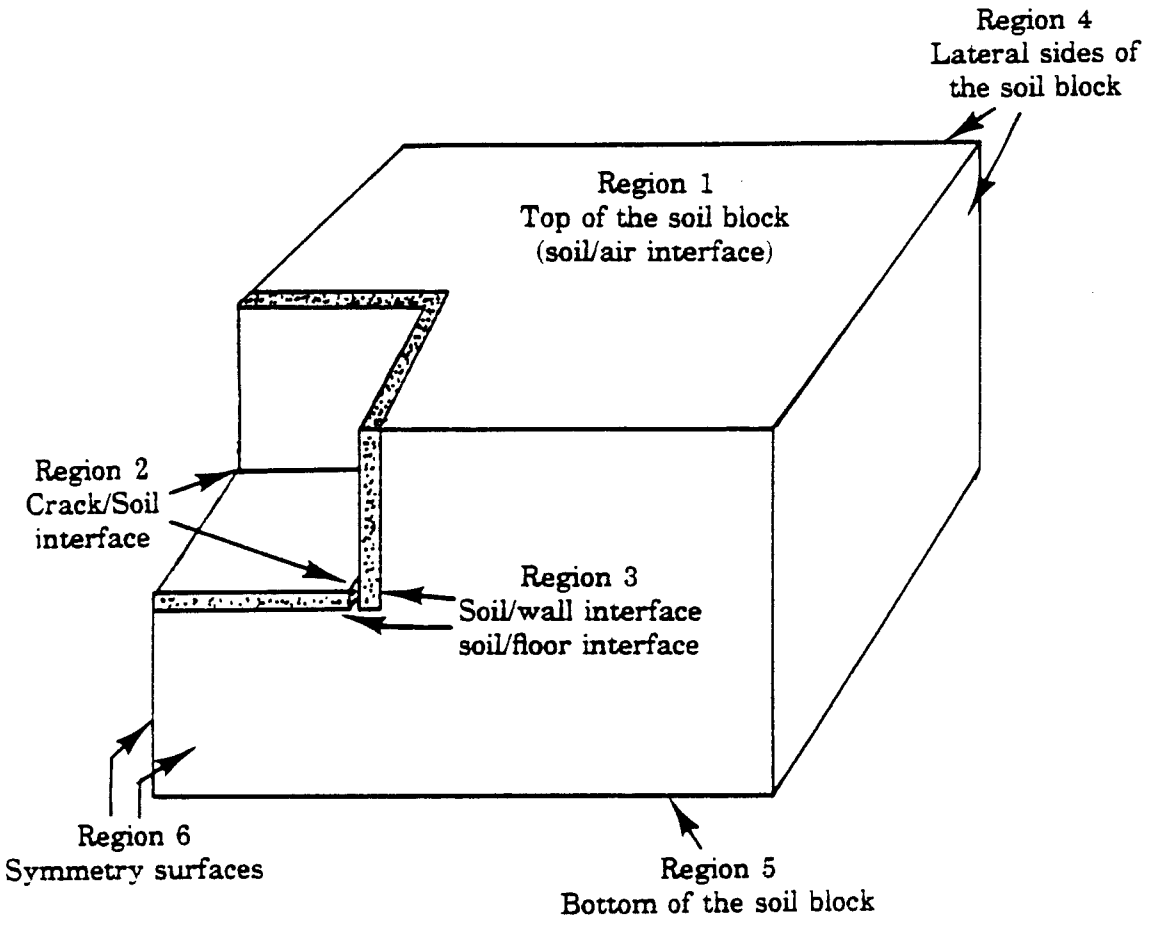

$$u = -\left(\frac{k}{\mu}\right)\frac{\partial p}{\partial x}, \tag{3.13b}$$

$$v = -\left(\frac{k}{\mu}\right)\frac{\partial p}{\partial y}, \tag{3.13c}$$

$$w = -\left(\frac{k}{\mu}\right)\frac{\partial p}{\partial z}. \tag{3.13d}$$

Table 3.1 — Boundary conditions for the solution of Eq.(3.12), the disturbance pressure field in the soil block.

Region[♯]	Description	Boundary Conditions
1	Top of the soil block. (Soil-air interface).	The disturbance pressure is zero at the top of the soil block. $(p_{(z=0)} = 0)$.
2	Interface between the defined crack and the soil underneath it.	Due to continuity, the disturbance pressure and the velocity of the soil gas at the interface must be continuous functions of distance, such that: $p_{(IN-)} = p_{(IN+)}$; $w_{(IN-)} = w_{(IN+)}$; as the points $(IN-)$ and $(IN+)$ get closer to the interface (IN). (See details in Appendix E).
3	Interface of the soil and the basement walls and floor, except at the region # 2.	No-flow boundary. Permeability of concrete (walls and floor) is much lower than the soil permeability. Then, from Eq.(3.9), the soil gas velocity perpendicular to these structures is assumed to be zero. $(\vec{q} = 0)$
4	Lateral sides[♭] of the soil block.	No-flow boundary. At sufficiently large distances from the crack (the center of pressure disturbance) the pressure will be practically invariable with distance. Therefore the gradient of the disturbance pressure, perpendicular to the external boundaries of the soil block, is assumed to be equal to zero. $(\vec{\nabla} p = 0)$.
5	Bottom[♭] of the soil block.	No-flow boundary. The same as in region # 4.
6	Planes of symmetry of the soil block. (External vertical surfaces that separate the quarter block from the whole soil block).	No-flow boundary. Due to symmetry, there should be no flow crossing these surfaces. Therefore, the disturbance pressure gradient, perpendicular to the planes of symmetry of the soil block is assumed to be equal to zero. $(\vec{\nabla} p = 0)$.

♯– The boundary regions of the soil block are defined in Fig.(3.1).

♭– To assume that at the boundaries 4 and 5, the perpendicular gradient of the disturbance pressure is zero, means that we consider the dimensions of the soil block to be sufficiently large.

Production Rate of Radon in the Soil Pore Space.

The production rate of radon into the soil pore space is proportional to: the concentration of Radium-226 in the soil; the soil density, and the radon emanating fraction. It is expressed as [Na85, pg.33]:

$$S = f\rho_s[Ra]\lambda_{Rn}\left(\frac{1-\epsilon}{\epsilon}\right), \tag{3.14}$$

where,

$S =$ Production rate of radon into the pore space, in $[Ci/m^3 s]$;

$f =$ Radon emanating fraction, [dimensionless];

$\rho_s =$ Density of the soil grains, in $[Kg/m^3]$;

$\lambda_{Rn} =$ Radon decay constant, in $[s^{-1}]$;

$[Ra] =$ Concentration of Ra-226 in the soil grains, in $[Ci/Kg]$.

Flux of Radon Throughout the Soil.

The vectorial flux[8] of radon through the soil matrix is made up of two components: the convective and diffusive flux.

The convective term represents the fact that atoms of radon are carried along with the bulk movement of soil gas through the soil matrix. It is expressed as:

$$\vec{J_C} = \vec{q}\rho\theta, \tag{3.15a}$$

or,

[8] Here I observe that the term Radon Flux is used in this dissertation as a synonym of the most general term Radon Flux Density, which is defined as the amount of radon crossing a unit area, per unit of time.

$$\vec{J}_C = \vec{q}C, \tag{3.15b}$$

where,

$\vec{J}_C =$ Convective component of the total radon bulk flux in the soil matrix, (equal to the amount of radon crossing a geometric area in the soil, per unit of time), in $[Ci/m^2 s]$;

$\vec{q} =$ Soil gas seepage velocity vector, (equal to the volume flow of soil gas per unit of time, per unit of geometrical cross-sectional area), in $[m/s]$;

$\rho =$ Density of the soil gas, in $[Kg/m^3]$;

$\theta =$ Ratio of radon activity to the mass of soil gas, (a relative mass concentration between radon and soil gas), in $[Ci/Kg]$;

$C =$ Radon concentration in the soil gas, in $[Ci/m^3]$.

The diffusive term of the radon flux is expressed by Fick's law for molecular diffusion in a porous medium, and represents the movement of the radon atoms through the soil pore space due to differences in the radon concentration. For an isotropic[9] soil the Fick's law is expressed as:

$$\vec{J}_D = -D\rho\vec{\nabla}\theta. \tag{3.16}$$

Since I have assumed the flow incompressible, and since the molecular concentration of radon in the soil gas is considered very small, the soil gas density is supposed to be constant and not affected by the presence of radon. So, the equation above can be written as[10]:

$$\vec{J}_D = -D\vec{\nabla}(\rho\theta) = -D\vec{\nabla}C, \tag{3.17}$$

---

[9] If the soil were considered as an anisotropic porous medium, Fick's law would have been expressed similarly to Eq.(3.16), except that the bulk diffusion coefficient of radon in soil would have been replaced by $\tilde{D}$ - the molecular diffusion tensor.

[10] Here I note some confusion in the literature regarding the concept and the use of the *bulk* and *effective* diffusion coefficients of radon in soil. This point was made clear first by Cullot [Cu76]. Nazaroff [Na85] has also clarified this subject significantly. According to Nazaroff, the bulk and effective diffusion coefficients of radon in soil are related by the soil porosity as: $D = \epsilon D_{eff}$.

where,

$\vec{J}_D =$ Diffusive component of the total radon bulk flux in the soil matrix, (equal to the amount of radon crossing a geometric area in the soil, per unit of time), in $[Ci/m^2 s]$;

$D =$ Bulk diffusion coefficient for the radon in the soil matrix, (equal to the ratio of the diffusive flux across a geometrical area to the gradient of the interstitial concentration of radon), in $[m^2/s]$.

An additional mass-transport phenomenon occurring simultaneously with molecular diffusion is the *mechanical dispersion*, in which the spreading of the tracer atoms (radon) occurs in the direction of the average flow of soil-gas, as well as in the transversal direction, caused by the variation of velocity (in magnitude and direction) at microscopic level around the soil particles. At the macroscopic level, the resulting effect (or the total spreading) caused by these two phenomena – molecular diffusion and mechanical dispersion – is usually called the *hydrodynamic dispersion* in the soil. Consequently, the spreading of the tracer (radon) throughout the soil should be represented by an expression similar to Fick's law where D is replaced by the hydrodynamic dispersion coefficient of radon in soil, D_h, which is equal to the sum of the molecular diffusion coefficient, D, plus the mechanical dispersion coefficient of radon in soil, D_m, [Be79]. The mechanical dispersion coefficient is directly related to the seepage velocity of soil gas in soil. Therefore, since the velocity of the gas in the configuration being studied, is expected to be very small all over the soil block, except at the regions very close to the soil-crack interface, the mechanical dispersion phenomenon is not expected to be significant, and consequently the hydrodynamic dispersion is reduced to the molecular diffusion.

Thus, for the soil-house configuration treated in this dissertation, it has been assumed that the transport of radon in soil is caused only by molecular diffusion of radon, and convection flow of soil-gas containing radon. The total radon bulk flux through the soil matrix is then the vectorial sum of its convective and diffusive components, and can be expressed as:

$$\vec{J} = \vec{J}_C + \vec{J}_D = \vec{q}C - D\vec{\nabla}C, \tag{3.18}$$

where,

$\vec{J} =$ Total radon bulk flux in the soil matrix, (equal to the amount of radon crossing a geometric area in the soil, per unit of time), in $[Ci/m^2 s]$.

Radon Concentration Field in the Soil.

Concentration of radon in the soil pore space is finally evaluated with the following general transport equation (See Appendix D):

$$\frac{\partial}{\partial t}(C\epsilon) = -\vec{\nabla} \cdot \vec{J} + S\epsilon - \lambda_{Rn} C\epsilon. \tag{3.19}$$

Substituting $\vec{J}$, from Eq.(3.18), into Eq.(3.19) yields:

$$\frac{\partial}{\partial t}(C\epsilon) = \vec{\nabla} \cdot \left(D\vec{\nabla} C\right) - \vec{\nabla} \cdot (\vec{q}C) + \epsilon\,(S - \lambda_{Rn} C)\,. \tag{3.20}$$

The equation above is the general transport equation for radon through the soil matrix. Here I note that the velocity field $\vec{q}$ has been already evaluated from Eq.(3.13), and it also satisfies the continuity equation:

$$\frac{\partial}{\partial t}(\epsilon\rho) + \vec{\nabla} \cdot (\rho\vec{q}) = 0.$$

At steady-state and incompressible flow conditions, these equations become:

- **Mass Balance** -

$$\vec{\nabla} \cdot \left(D\vec{\nabla} C\right) - \vec{\nabla} \cdot (\vec{q}C) + \epsilon\,(S - \lambda_{Rn} C) = 0, \tag{3.21}$$

- **Continuity** -

$$\vec{\nabla} \cdot \vec{q} = 0, \tag{3.22}$$

which can also be written in their three-dimensional form as:

$$\begin{aligned}
&\frac{\partial}{\partial x}\left(D\frac{\partial C}{\partial x}\right) - \frac{\partial}{\partial x}(uC) + \\
&\frac{\partial}{\partial y}\left(D\frac{\partial C}{\partial y}\right) - \frac{\partial}{\partial y}(vC) + \\
&\frac{\partial}{\partial z}\left(D\frac{\partial C}{\partial z}\right) - \frac{\partial}{\partial z}(wC) + \epsilon(S - \lambda_{Rn}C) = 0,
\end{aligned} \tag{3.23}$$

and,

$$\frac{\partial u}{\partial x} + \frac{\partial v}{\partial y} + \frac{\partial w}{\partial z} + = 0. \tag{3.24}$$

Boundary Conditions for the Solution of the Radon-Transport Equation.

Considering the same configuration represented in Figure (3.1), the boundary conditions for the mass-balance equation are summarized in the following Table (3.2). Since the concentration of radon in the atmospheric air (typical values of $0.1[pCi/l]$ - [NC84a]) is much smaller than the radon concentration in soil gas (typical values larger than $500[pCi/l]$ - see Chapter I), and since it is expected that the flow of air at the soil-air interface, caused by the disturbance pressure, occurs in the direction from the air into the ground, then it is assumed that, as a boundary condition, the concentration of radon at the soil-air interface (region #1) is equal to zero. A detailed discussion on the boundary condition imposed on the soil/crack interface (region # 2) is presented in Appendix F.

Table 3.2 — Boundary conditions for the solution of Eqs.(3.21) and (3.22), the radon concentration field in the soil block.

Region[♯]	Description	Boundary Conditions
1	Top of the soil block. (Soil-air interface).	The radon concentration is zero at the top of the soil block. ($C_{(z=0)} = 0$).
2	Interface between the defined crack and the soil underneath it.	Due to continuity, the radon concentration and the radon flux at the soil-crack interface must be both a continuous function of distance, such that: $C_{(IN-)} = C_{(IN+)}$; $J_{(IN-)} = J_{(IN+)}$; as the points $(IN-)$ and $(IN+)$ get closer to the interface (IN). (See details in Appendix F).
3	Interface of the soil and the basement walls and floor, except at the region # 2.	No-flow boundary. At the walls and floor, the permeability and diffusivity constants are much smaller than those at the soil. Consequently, from Eqs. (3.8) and (3.18), the flux J perpendicular to these boundaries is assumed to be zero. ($J = 0$).
4	Lateral sides[♭] of the soil block.	No-flow boundary. At sufficiently large distances from the crack the disturbance pressure field and the radon concentration field are considered to be invariable in the direction perpendicular to these surfaces. Consequently, from Eqs. (3.8) and (3.18), the flux J, perpendicular to the surface is assumed to be zero. ($J = 0$)
5	Bottom[♭] of the soil block.	No-flow boundary. The same as in region # 4.
6	Planes of symmetry of the soil block. (External vertical surfaces that separate the quarter block from the whole soil block).	No-flow boundary. Due to symmetry, there should be no flow crossing these surfaces. Therefore, the flux of radon trough the planes of symmetry of the soil block is assumed to be zero. ($J = 0$).

♯– The boundary regions of the soil block are defined in Fig.(3.1).

♭– To assume that at the boundaries 4 and 5, the perpendicular gradient of both the disturbance pressure and the radon concentration are zero, means that we consider the dimensions of the soil block to be sufficiently large.

Entry Rate of Radon into the House.

The total entry rate of radon into one quarter of the house will be given by the product of the flux of radon at the exit of the crack into the house, and the average cross-sectional area of the crack in a quarter of the house. It can be expressed as:

$$R_{total} = J_{EX} \cdot A_{crack}, \tag{3.25}$$

where,

R_{total} = Total radon entry rate into a quarter of the house, in $[Ci/s]$;

J_{EX} = Flux of radon at the exit of the crack, into the house, in $[Ci/m^2.s]$;

A_{crack} = Average cross-sectional area of the crack, in a quarter of the house, in $[m^2]$.

Indoor Radon Concentration.

The indoor radon concentration will be calculated based on a mass balance within the house, represented by the following differential equation:[11]

$$\frac{\partial C_{indoor}}{\partial t} = \frac{4R_{total}}{V} - (\lambda_{Rn} + \lambda_V)\, C_{indoor} + \lambda_V\, C_{outdoor}, \tag{3.26}$$

where,

C_{indoor} = Indoor radon concentration, in $[Ci/m^3]$;

$C_{outdoor}$ = Outdoor radon concentration, in $[Ci/m^3]$;

V = Total volume of the house, in $[m^3]$;

λ_V = Air exchange rate (ventilation rate), in $[s^{-1}]$.

[11] For the sake of completeness, the outdoor radon concentration is also considered in the formulation of Eq.(3.26). However, since the contribution of outdoor radon to indoor radon concentration is usually small (less than 10%), the source of radon from outdoor air will be neglected in the application of the model.

Then, at steady-state the indoor radon concentration will be expressed as:

$$C_{indoor} = \frac{\frac{4R_{total}}{V} + \lambda_V C_{outdoor}}{(\lambda_{Rn} + \lambda_V)}. \tag{3.27}$$

Dimensionless Transformation of the Mathematical Expressions.

It will be useful for later computations to transform the mathematical equations of the model into a dimensionless form. In order to do this, all variables will be multiplied by the appropriate combinations of the following defined characteristic parameters[12]:

$\Delta P =$ Characteristic disturbance pressure, in $[N/m^2]$;

$\frac{1}{\lambda_{Rn}} =$ Characteristic time, in $[s]$;

$L_{ch} =$ Characteristic length, in $[m]$;

$D_{ch} =$ Characteristic bulk diffusion coefficient, in $[m^2/s]$;

$U_{ch} =$ Characteristic velocity of the soil gas, in $[m/s]$;

$k_{ch} =$ Characteristic permeability, in $[m^2]$;

$S_{ch} =$ Characteristic production rate of radon in the soil pore space, in $[Ci/m^3 s]$.

The objective here is to make each variable dimensionless. The equations will be transformed separately, with the dimensionless variables represented by a superscripted asterisk.

Definition of the Dimensionless Variables.

The following characteristic parameters and dimensionless variables are defined:

[12] The value of the characteristic parameters D_{ch}, k_{ch}, and S_{ch} will be selected as those of the most common material in the soil block.

– Characteristic length –

$$L_{ch} = \sqrt{\frac{D_{ch}}{\lambda_{Rn}}}, \tag{3.28}$$

– Characteristic velocity –

$$U_{ch} = \sqrt{D_{ch}\lambda_{Rn}}, \tag{3.29}$$

– Dimensionless seepage velocity vector –

$$\vec{q}^{*} = \frac{\vec{q}}{U_{ch}}, \tag{3.30}$$

– Dimensionless disturbance pressure –

$$p^{*} = \frac{p}{\Delta P}, \tag{3.31}$$

– Dimensionless source term –

$$S^{*} = \frac{S}{S_{ch}}, \tag{3.32}$$

– Dimensionless radon concentration in the soil pore space –

$$C^{*} = \frac{C}{S_{ch}/\lambda_{Rn}} = \frac{C}{C_{ch}}, \tag{3.33}$$

– Dimensionless coordinates –

$$x^{*},\ y^{*},\ z^{*} = \frac{x}{L_{ch}},\ \frac{y}{L_{ch}},\ \frac{z}{L_{ch}}, \tag{3.34}$$

– Dimensionless permeability –

$$k^{*} = \frac{k}{k_{ch}}, \tag{3.35}$$

– Dimensionless diffusion coefficient of radon in soil –

$$D^* = \frac{D}{D_{ch}}, \tag{3.36}$$

– Dimensionless gradient operator –

$$\vec{\nabla}^* = L_{ch}\vec{\nabla}. \tag{3.37}$$

Dimensionless Form of the Disturbance Pressure Field.

Substituting these dimensionless variables into the disturbance field equation, as expressed by Eq.(3.12a), yields:

$$\frac{\vec{\nabla}^*}{L_{ch}} \cdot \left[k^* k_{ch} \frac{\vec{\nabla}^*}{L_{ch}} \left(p^* \Delta P \right) \right] = 0. \tag{3.38}$$

But, since ΔP, k_{ch}, and L_{ch} are constant, the equation above becomes[13]:

$$\vec{\nabla}^* \cdot \left(k^* \vec{\nabla}^* p^* \right) = 0, \tag{3.39a}$$

or, in three-dimensional cartesian coordinates,

$$\frac{\partial}{\partial x^*} \left(k^* \frac{\partial p^*}{\partial x^*} \right) + \frac{\partial}{\partial y^*} \left(k^* \frac{\partial p^*}{\partial y^*} \right) + \frac{\partial}{\partial z^*} \left(k^* \frac{\partial p^*}{\partial z^*} \right) = 0. \tag{3.39b}$$

[13] The dimensionless permeability k^* is constant in a region of the soil block, but can change from one region to another.

Dimensionless Form of the Soil Gas Velocity Field.

The velocity field equation given by Darcy's expression, Eq.(3.8):

$$\vec{q} = -\left(\frac{k}{\mu}\right)\vec{\nabla}p,$$

can be written in terms of the dimensionless variables as it follows:

$$U_{ch}\vec{q}^{*} = -\left(\frac{k^{*}k_{ch}}{\mu}\right)\frac{\vec{\nabla}^{*}(\Delta P p^{*})}{L_{ch}} = -\left(\frac{k_{ch}}{\mu}\right)\left(\frac{\Delta P}{L_{ch}}\right)k^{*}\vec{\nabla}^{*}p^{*},$$

or,

$$\vec{q}^{*} = -\left(\frac{k_{ch}}{\mu}\right)\left(\frac{\Delta P}{L_{ch}U_{ch}}\right)k^{*}\vec{\nabla}^{*}p^{*}.$$

But from Eqs. (3.28) and (3.29), $L_{ch}U_{ch} = D_{ch}$. Then, the equation above becomes:

$$\vec{q}^{*} = -\left(\frac{k_{ch}}{\mu}\right)\left(\frac{\Delta P}{D_{ch}}\right)k^{*}\vec{\nabla}^{*}p^{*},$$

or,

$$\vec{q}^{*} = -K_S k^{*}\vec{\nabla}^{*}p^{*}, \tag{3.40a}$$

which, in three-dimensional cartesian coordinates is expressed as:

$$u^{*} = -K_S k^{*}\frac{\partial p^{*}}{\partial x^{*}}, \tag{3.40b}$$

$$v^{*} = -K_S k^{*}\frac{\partial p^{*}}{\partial y^{*}}, \tag{3.40c}$$

$$w^{*} = -K_S k^{*}\frac{\partial p^{*}}{\partial z^{*}}, \tag{3.40d}$$

where K_S is the dimensionless group:

$$K_S = \frac{k_{ch}\Delta P}{\mu D_{ch}}. \tag{3.40e}$$

Dimensionless Form of the Total Radon Flux in the Soil Matrix.

The total flux given by Eq.(3.18), $\vec{J} = \vec{q}C - D\vec{\nabla}C$, can be written in dimensionless form as follows:

$$\begin{aligned}\vec{J} &= U_{ch}\vec{q}\frac{S_{ch}}{\lambda_{Rn}}C^* - D_{ch}D^*\frac{\vec{\nabla}^*}{L_{ch}}\left(\frac{S_{ch}}{\lambda_{Rn}}C^*\right), \\ &= \left(\frac{U_{ch}S_{ch}}{\lambda_{Rn}}\right)\vec{q}^*\,C^* - \left(\frac{D_{ch}S_{ch}}{L_{ch}\lambda_{Rn}}\right)D^*\vec{\nabla}^*C^*.\end{aligned}$$

Dividing both terms of the equation above by $S_{ch}L_{ch}$ yields:

$$\frac{\vec{J}}{L_{ch}S_{ch}} = \left(\frac{U_{ch}}{L_{ch}\lambda_{Rn}}\right)\vec{q}^*\,C^* - \left(\frac{D_{ch}}{L_{ch}^2\lambda_{Rn}}\right)D^*\vec{\nabla}^*C^*.$$

But using Eqs. (3.28) and (3.29) it can be shown that the coefficients $U_{ch}/(L_{ch}\lambda_{Rn})$, and $D_{ch}/(L_{ch}^2\lambda_{Rn})$, which appear in the equation above, are equal to one. Therefore, the dimensionless form of the total radon flux can be expressed as:

$$\vec{J}^* = \frac{\vec{J}}{L_{ch}S_{ch}} = \vec{q}^*\,C^* - D^*\vec{\nabla}^*C^*, \tag{3.41a}$$

or,

$$\vec{J} = (L_{ch}S_{ch})\left(\vec{q}^*\,C^* - D^*\vec{\nabla}^*C^*\right). \tag{3.41b}$$

Dimensionless Form of the Radon Transport Equation.

The radon transport equation:

$$\vec{\nabla} \cdot \left(D \vec{\nabla} C \right) - \vec{\nabla} \cdot (\vec{q} C) + \epsilon \left(S - \lambda_{Rn} C \right) = 0,$$

can be written in terms of the dimensionless variables as it follows:

$$\frac{\vec{\nabla}^*}{L_{ch}} \cdot \left[\frac{D_{ch} D^*}{L_{ch}} \left(\frac{S_{ch}}{\lambda_{Rn}} C^* \right) \right] - \frac{\vec{\nabla}^*}{L_{ch}} \cdot \left(U_{ch} \vec{q} \frac{S_{ch}}{\lambda_{Rn}} C^* \right) + \epsilon \left(S^* S_{ch} - S_{ch} C^* \right) = 0,$$

or,

$$\left(\frac{D_{ch}}{L_{ch}^2 \lambda_{Rn}} \right) \vec{\nabla}^* \cdot \left(D^* \vec{\nabla}^* C^* \right) - \left(\frac{U_{ch}}{L_{ch} \lambda_{Rn}} \right) \vec{\nabla}^* \cdot \left(\vec{q}^* C^* \right) + \epsilon \left(S^* - C^* \right) = 0.$$

The dimensionless groups in the equation above are equal to one, according to the definitions of Eqs. (3.28) and (3.29). Therefore, it can be simplified as:

$$\vec{\nabla}^* \cdot \left(D^* \vec{\nabla}^* C^* \right) - \vec{\nabla}^* \cdot \left(\vec{q}^* C^* \right) + \epsilon \left(S^* - C^* \right) = 0. \tag{3.42}$$

The dimensionless version of the continuity equation can be expressed as:

$$\frac{\vec{\nabla}^* \cdot U_{ch} \vec{q}^*}{L_{ch}} = 0,$$

or,

$$\vec{\nabla}^* \cdot \vec{q}^* = 0. \tag{3.43}$$

Dimensionless Form of the Radon Entry Rate into the House.

The radon entry rate equation, $R_{total} = J_{EX} \cdot A_{crack}$, Eq.(3.25), can be written in terms of the dimensionless variables as it follows.

From Eq.(3.41a), the dimensionless form of the radon flux at the exit of the crack, into the house, J_{EX}, can be expressed as:

$$J_{EX}^{\sim} = \frac{J_{EX}}{L_{ch} S_{ch}}. \tag{3.44}$$

Also, the dimensionless form of the cross-sectional area A_{crack} can be expressed as:

$$A_{crack}^{\sim} = \frac{A_{crack}}{L_{ch}^2}. \tag{3.45}$$

Therefore, substituting these values into the equation for R, yields:

$$R_{total} = \left(S_{ch} L_{ch}^3\right) J_{EX}^{\sim} A_{crack}^{\sim}. \tag{3.46}$$

Now, dividing both terms by the characteristic radon entry rate, $S_{ch} L_{ch}^3$, the equation above becomes:

$$R_{total}^{\sim} = \frac{R_{total}}{R_{ch}} = \frac{R_{total}}{S_{ch} L_{ch}^3} = J_{EX}^{\sim} A_{crack}^{\sim}. \tag{3.47}$$

CHAPTER IV

DEVELOPMENT OF THE COMPUTER MODEL

The objective of this chapter is to define a method of solution for the differential equations of the proposed model, and also to describe the computer codes in which this method was implemented.

The equations representing the disturbance pressure field the soil gas velocity field, and the radon concentration field in the soil block are all three-dimensional linear partial differential equations which, together with the imposed boundary conditions can not be solved analytically. Consequently, a solution by a numerical method becomes mandatory.

Solution for the disturbance pressure, and the radon concentration fields, both second order, linear, partial differential equations, will be achieved using the Patankar-Spalding numerical technique [Pa80], called *Discretization Method*, which is basically a control-volume approach to the finite difference method. In this technique, the domain of the variable under control is first fully divided in non-overlapping spaces called control-volumes. A node, or a grid point, is defined at the center of each control-volume. All together, these nodes form a grid filling the whole calculation domain, with a control-volume surrounding each grid point. The idea here is that the value of the dependent variable, over the whole space of the control-volume can be represented by the value at the grid point located in its center.

The differential equation is then integrated over each control-volume individually. Piecewise interpolation functions expressing the spatial profile of the dependent variable between grid points, are defined in order to evaluate the integral properly. The result of this is a set

of algebraic equations (discretization equations), one for each grid point, expressing the value of the dependent variable, as a function of the values at a group of neighbor points. Consequently, for a grid mesh composed of N grid nodes, the continuous domain of the differential equation is transformed in a set of N algebraic discretization equations which can now be solved by one of the appropriate methods of linear algebra.

The main advantage of the control-volume approach in deriving the discretization equations is that it guarantees the conservation of the physical quantities in question, such as the mass in the case of the radon transport equation, over any group of control-volumes and, consequently, over the whole calculation domain. Such feature is independent of the grid mesh size, and even a coarse grid mesh solution would present an exact integral balance.[Pa80, pg.30].

Solution of the other differential equation of the model, the soil gas velocity field – a first order, linear, partial differential equation – will be obtained after the solution for the pressure field by a simple numerical derivative of the pressure distribution throughout the soil block.

Numerical Solution (Discretization Formulation).

Before starting the derivation of the algebraic equations representing the differential equations of the model, it is necessary to define the coordinate system as well as the grid notation with which the model is developed.

System of Coordinates.

Because of the symmetry in this problem, only one quarter of the soil block will be considered for the calculations. The origin of coordinates is located at the center of the top soil surface,

Figure 4.1 — Location of the coordinate system in the soil block.

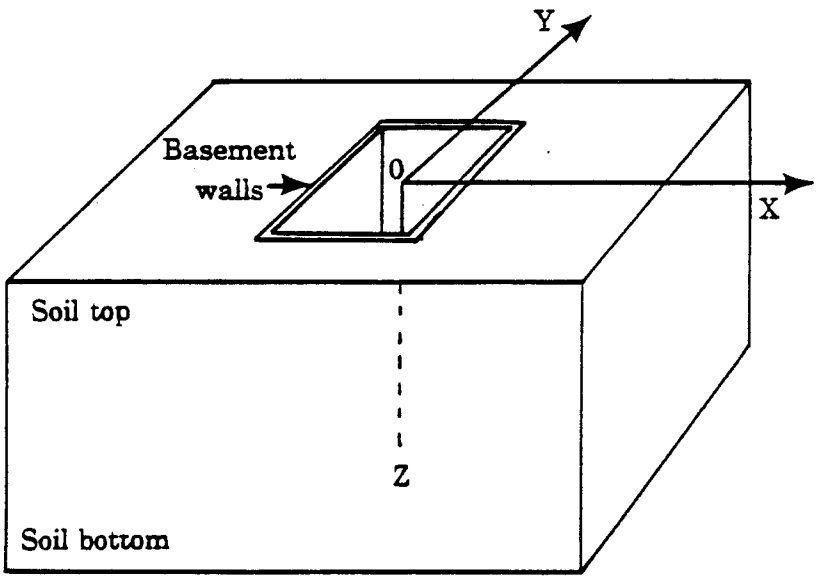

which corresponds to the center of the basement ceilings, as shown in Figure (4.1). The quarter of the soil block, with the system of coordinates, where the numerical model will be developed, is represented in Figure (4.2). The vertical axis of the coordinate system is assumed to have its positive direction oriented downward.

Grid Notation.

The objective here is to describe the computational grid in its general terms. Further specifications about the grid mesh will be presented later with the description of the control-volume locations and grid generation.

The soil block is assumed to be cut by several parallel planes in all three directions. The intersections of these planes form the control-volumes which constitute the basic units of the discretization method to applied here. The sizes of these control-volumes are not constant,

Figure 4.2 — A quarter of the soil block, with the defined coordinate system for the three-dimensional model.

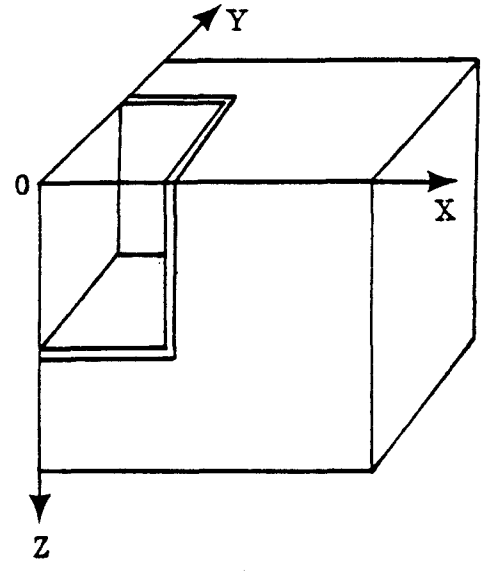

but vary depending on the level of details, or the degree of variation we expect to find in each specific region of the soil.

The common face between any two adjacent control-volumes is denominated the *interface*. A node is assumed to be located at the center of each control-volume, such that a line connecting any two adjacent nodes will intersect the interface at its geometrical center.[1] Figure (4.3) shows a generic node P, with its neighbors at all three directions, represented with the following notation:

E	-	East node	(x-direction);
W	-	West node	(x-direction);
N	-	North node	(y-direction);
S	-	South node	(y-direction);
T	-	Top node	(z-direction);
B	-	Bottom node	(z-direction).

In order to represent the control-volumes and the grid mesh the following general notation

[1] It should be emphasized that each node is located at the center of its respective control-volume, but the interfaces of the control-volumes are not necessarily located halfway between opposite nodes.

Figure 4.3 — Grid cluster showing a generic node P, with all its neighbors E, W, N, S, B, and T.

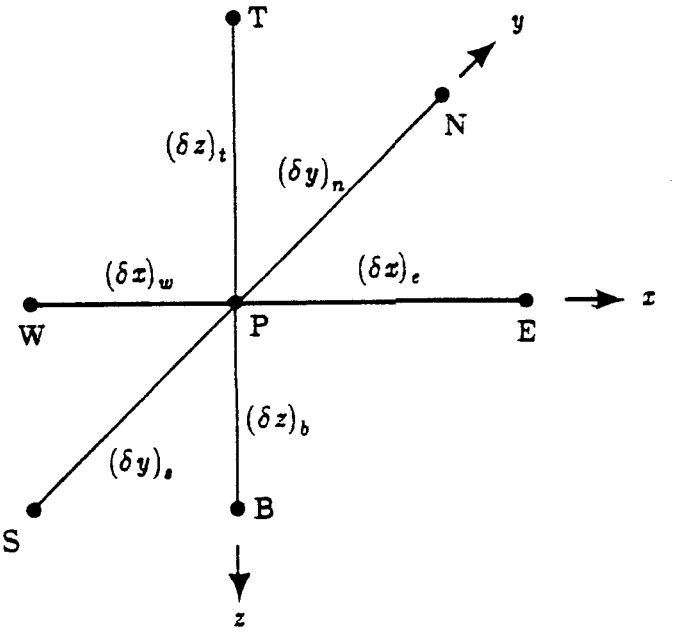

is also adopted:

Upper case letters	: Represent the nodes in the grid;
Lower case letters	: Represent the control volume interfaces;
Δx, Δy, Δz	: Represent the control volume dimensions;
δx, δy, δz	: Represent the distances between nodes.

Note that since the nodes are located at the geometrical center of its respective control-volume, then the dimensionless distance between any two adjacent nodes is equal to the arithmetic mean of the dimensionless sizes of these control-volumes in that specific direction. and can be expressed as:

$$(\delta x)^*_e = \frac{\Delta x^*_P + \Delta x^*_E}{2}, \tag{4.1a}$$

$$(\delta x)^*_w = \frac{\Delta x^*_W + \Delta x^*_P}{2}, \tag{4.1b}$$

$$(\delta y)^*_n = \frac{\Delta y^*_P + \Delta y^*_N}{2}, \tag{4.1c}$$

$$(\delta y)_s^* = \frac{\Delta y^*_S + \Delta y^*_P}{2}, \tag{4.1d}$$

$$(\delta z)_b^* = \frac{\Delta z^*_P + \Delta z^*_B}{2}, \tag{4.1e}$$

$$(\delta z)_t^* = \frac{\Delta z^*_T + \Delta z^*_P}{2}. \tag{4.1f}$$

Discretization Equation for the Disturbance Pressure Field.

The dimensionless version of the equation for the disturbance pressure field was already derived,(Eq.(3.39)), and is repeated here as:

$$\vec{\nabla}^* \cdot \left(k^* \vec{\nabla}^* p^* \right) = 0, \tag{4.2a}$$

or,

$$\frac{\partial}{\partial x^*}\left(k^* \frac{\partial p^*}{\partial x^*} \right) + \frac{\partial}{\partial y^*}\left(k^* \frac{\partial p^*}{\partial y^*} \right) + \frac{\partial}{\partial z^*}\left(k^* \frac{\partial p^*}{\partial z^*} \right) = 0. \tag{4.2b}$$

According to the discretization method, this differential equation will be integrated over the whole control-volume, and then transformed to a system of algebraic equations relating the value of p^*_P, at the node P, to the values at the neighboring nodes p^*_E, p^*_W, p^*_N, p^*_S, p^*_B, and p^*_T. These algebraic equations, here called ***discretization equations***, will take the following form:

$$a_P p^*_P = a_E p^*_E + a_W p^*_W + a_N p^*_N + a_S p^*_S + a_B p^*_B + a_T p^*_T, \tag{4.3}$$

where a_P, a_E, a_W, a_N, a_S, a_B, and a_T are the discretization coefficients, which will be defined later in Eq.(4.9).

Figure (4.4) shows a generic node P, its neighbors, and the control-volume. Here, for simplicity of representation and with no lack of generalization, only two dimensions are

Figure 4.4 — A generic control-volume (here represented with only two dimensions) where the discretization method is applied.

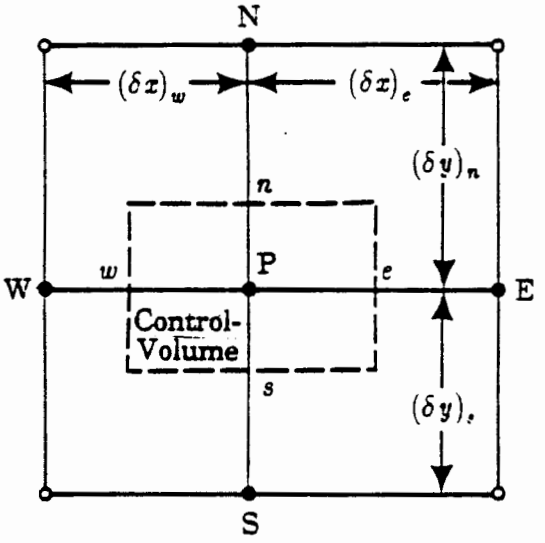

represented.

Thus, integrating Eq.(4.2b) over the whole control-volume yields:

$$\int_t^b \int_s^n \int_w^e \frac{\partial}{\partial x^*}\left(k^* \frac{\partial p^*}{\partial x^*}\right) dx^* dy^* dz^* +$$

$$\int_w^e \int_t^b \int_s^n \frac{\partial}{\partial y^*}\left(k^* \frac{\partial p^*}{\partial y^*}\right) dy^* dz^* dx^* +$$

$$\int_s^n \int_w^e \int_t^b \frac{\partial}{\partial z^*}\left(k^* \frac{\partial p^*}{\partial z^*}\right) dz^* dx^* dy^* = 0,$$

or,

$$\int_t^b \int_s^n \left[\left(k^* \frac{\partial p^*}{\partial x^*}\right)_e - \left(k^* \frac{\partial p^*}{\partial x^*}\right)_w\right] dy^* dz^* +$$

$$\int_w^e \int_t^b \left[\left(k^* \frac{\partial p^*}{\partial y^*}\right)_n - \left(k^* \frac{\partial p^*}{\partial y^*}\right)_s\right] dz^* dx^* + \qquad (4.4).$$

$$\int_s^n \int_w^e \left[\left(k^* \frac{\partial p^*}{\partial z^*}\right)_b - \left(k^* \frac{\partial p^*}{\partial z^*}\right)_t\right] dx^* dy^* = 0$$

At this point, in order to continue with the derivation above, it is necessary to find an

approximation for the terms $k^{\star}\vec{\nabla}^{\star}p^{\star}$ evaluated at the interfaces e, w, n, s, b, and t of the control-volume. For doing so, I assume that the terms $k^{\star}\vec{\nabla}^{\star}p^{\star}$, evaluated at each interface, prevail over the entire interface of the control-volume. I also assume that the function $p^{\star}$ is piecewise continuous and linear between nodes, and can be approximated as:

$$\left(k^{\star}\frac{\partial p^{\star}}{\partial x^{\star}}\right)_{e} = k_{e}^{\star}\left[\frac{p_{E}^{\star}-p_{P}^{\star}}{(\delta x)_{e}^{\star}}\right], \tag{4.5a}$$

$$\left(k^{\star}\frac{\partial p^{\star}}{\partial x^{\star}}\right)_{w} = k_{w}^{\star}\left[\frac{p_{P}^{\star}-p_{W}^{\star}}{(\delta x)_{w}^{\star}}\right], \tag{4.5b}$$

$$\left(k^{\star}\frac{\partial p^{\star}}{\partial y^{\star}}\right)_{n} = k_{n}^{\star}\left[\frac{p_{N}^{\star}-p_{P}^{\star}}{(\delta y)_{n}^{\star}}\right], \tag{4.5c}$$

$$\left(k^{\star}\frac{\partial p^{\star}}{\partial y^{\star}}\right)_{s} = k_{s}^{\star}\left[\frac{p_{P}^{\star}-p_{S}^{\star}}{(\delta y)_{s}^{\star}}\right], \tag{4.5d}$$

$$\left(k^{\star}\frac{\partial p^{\star}}{\partial z^{\star}}\right)_{b} = k_{b}^{\star}\left[\frac{p_{B}^{\star}-p_{P}^{\star}}{(\delta z)_{b}^{\star}}\right], \tag{4.5f}$$

$$\left(k^{\star}\frac{\partial p^{\star}}{\partial z^{\star}}\right)_{t} = k_{t}^{\star}\left[\frac{p_{P}^{\star}-p_{T}^{\star}}{(\delta z)_{t}^{\star}}\right]. \tag{4.5g}$$

In the expressions above, the permeability $k^{\star}$ must be evaluated at the interface of the control volume. It was assumed that the soil permeability is constant and isotropic within each defined region of the soil block. Furthermore, because of the way in which the control-volumes are located within the soil block, matching the boundaries of those defined regions, the soil permeability is also assumed to be constant within any control-volume. However, a discontinuity in the value of permeability may exist in the interfaces between two distinct regions of the soil block. In order to deal with this problem, it is proposed that the permeability at the control-volume interfaces can be approximated by the weighted average of the values of $k^{\star}$ at the opposite nodes (see Appendix H), such as[2]:

$$k_{e}^{\star} = \frac{k_{P}^{\star}k_{E}^{\star}}{\left(\frac{\Delta x_{P}^{\star}k_{E}^{\star}+\Delta x_{E}^{\star}k_{P}^{\star}}{\Delta x_{P}^{\star}+\Delta x_{E}^{\star}}\right)}, \tag{4.6a}$$

$$k_{w}^{\star} = \frac{k_{W}^{\star}k_{P}^{\star}}{\left(\frac{\Delta x_{W}^{\star}k_{P}^{\star}+\Delta x_{P}^{\star}k_{W}^{\star}}{\Delta x_{W}^{\star}+\Delta x_{P}^{\star}}\right)}, \tag{4.6b}$$

[2] This approximation is shown to conserve mass in Appendix H.

$$k_n^* = \frac{k_P^* k_N^*}{\left(\frac{\Delta y_P^* k_N^* + \Delta y_N^* k_P^*}{\Delta y_P^* + \Delta y_N^*}\right)}, \tag{4.6c}$$

$$k_s^* = \frac{k_S^* k_P^*}{\left(\frac{\Delta y_S^* k_P^* + \Delta y_P^* k_S^*}{\Delta y_S^* + \Delta y_P^*}\right)}, \tag{4.6d}$$

$$k_b^* = \frac{k_P^* k_B^*}{\left(\frac{\Delta z_P^* k_B^* + \Delta z_B^* k_P^*}{\Delta z_P^* + \Delta z_B^*}\right)}, \tag{4.6e}$$

$$k_t^* = \frac{k_T^* k_P^*}{\left(\frac{\Delta z_T^* k_P^* + \Delta z_P^* k_T^*}{\Delta z_T^* + \Delta z_P^*}\right)}. \tag{4.6f}$$

Now, with these assumptions, the substitution of Eq.(4.5) into Eq.(4.4) yields:

$$\int_t^b \int_s^n \left\{ k_e^* \left[\frac{p_E^* - p_P^*}{(\delta x)_e^*} \right] - k_w^* \left[\frac{p_P^* - p_W^*}{(\delta x)_w^*} \right] \right\} dy^* dz^* +$$
$$\int_w^e \int_t^b \left\{ k_n^* \left[\frac{p_N^* - p_P^*}{(\delta y)_n^*} \right] - k_s^* \left[\frac{p_P^* - p_S^*}{(\delta y)_s^*} \right] \right\} dz^* dx^* +$$
$$\int_t^b \int_s^n \left\{ k_b^* \left[\frac{p_B^* - p_P^*}{(\delta z)_b^*} \right] - k_t^* \left[\frac{p_P^* - p_T^*}{(\delta z)_t^*} \right] \right\} dx^* dy^* = 0,$$

or,

$$\left\{ k_e^* \left[\frac{p_E^* - p_P^*}{(\delta x)_e^*} \right] - k_w^* \left[\frac{p_P^* - p_W^*}{(\delta x)_w^*} \right] \right\} \Delta y^* \Delta z^* +$$
$$\left\{ k_n^* \left[\frac{p_N^* - p_P^*}{(\delta y)_n^*} \right] - k_s^* \left[\frac{p_P^* - p_S^*}{(\delta y)_s^*} \right] \right\} \Delta z^* \Delta x^* + \tag{4.7}$$
$$\left\{ k_b^* \left[\frac{p_B^* - p_P^*}{(\delta z)_b^*} \right] - k_t^* \left[\frac{p_P^* - p_T^*}{(\delta z)_t^*} \right] \right\} \Delta x^* \Delta y^* = 0,$$

which can then be written in the following algebraic discretization equation:

$$a_P p_P^* = a_E p_E^* + a_W p_W^* + a_N p_N^* + a_S p_S^* + a_B p_B^* + a_T p_T^*, \tag{4.8}$$

where,

$$a_E = k_e^* \left[\frac{\Delta y^* \Delta z^*}{(\delta x)_e^*} \right], \tag{4.9a}$$

$$a_W = k_w^* \left[\frac{\Delta y^* \Delta z^*}{(\delta x)_w^*} \right], \tag{4.9b}$$

$$a_N = k_n^* \left[\frac{\Delta z^* \Delta x^*}{(\delta y)_n^*} \right], \tag{4.9c}$$

$$a_S = k_s^* \left[\frac{\Delta z^* \Delta x^*}{(\delta y)_s^*} \right], \tag{4.9d}$$

$$a_B = k_b^* \left[\frac{\Delta x^* \Delta y^*}{(\delta z)_b^*} \right], \tag{4.9e}$$

$$a_T = k_t^* \left[\frac{\Delta x^* \Delta y^*}{(\delta z)_t^*} \right], \tag{4.9f}$$

and,

$$a_P = a_E + a_W + a_N + a_S + a_B + a_T. \tag{4.9g}$$

Soil-Gas Velocity Field.

Solution of the algebraic system of the discretization equations for the disturbance pressure field will result in the value of the disturbance pressure p^* for each node of the soil block. Then, the next step is to calculate the soil gas velocity field for the same set of nodes, which will be done using Darcy's equation. Here however I make an important observation. The components of the velocity vector will be calculated in a displaced, or *staggered*, grid. (See [Pa80]). In this staggered grid, the velocity components are calculated not at the nodes but at points that lie on the faces of the control-volume. For instance, the x-direction velocity components, u_e^* and u_w^*, are calculated at the interfaces e and w, respectively. This approach will be useful later on for the calculation of the diffusion-convection equation (the radon concentration field).

Assuming a piecewise linear variation of the disturbance pressure between the nodes, the dimensionless velocity components at the interfaces are obtained from Eq.(3.40), and expressed as:

$$u_e^* = -K_S k_e^* \left[\frac{p_E^* - p_P^*}{(\delta x)_e^*} \right], \tag{4.10a}$$

$$u_w^* = -K_S k_w^* \left[\frac{p_P^* - p_W^*}{(\delta x)_w^*} \right], \tag{4.10b}$$

$$v_n^* = -K_S k_n^* \left[\frac{p_N^* - p_P^*}{(\delta y)_n^*} \right], \tag{4.10c}$$

$$v_s^* = -K_S k_s^* \left[\frac{p_P^* - p_S^*}{(\delta y)_s^*} \right], \tag{4.10d}$$

$$w_b^* = -K_S k_b^* \left[\frac{p_B^* - p_P^*}{(\delta z)_b^*} \right], \tag{4.10e}$$

$$w_t^* = -K_S k_t^* \left[\frac{p_P^* - p_T^*}{(\delta z)_t^*} \right]. \tag{4.10f}$$

Discretization Equation for the Radon Concentration Field.

The concentration field of radon in the soil is given by the mass balance equation which, in its three-dimensional dimensionless form, Eq.(3.42), can be separated respectively into the diffusive, convective and source-sink terms, and expressed as:

$$\left[\frac{\partial}{\partial x^*} \left(D^* \frac{\partial C^*}{\partial x^*} \right) + \frac{\partial}{\partial y^*} \left(D^* \frac{\partial C^*}{\partial y^*} \right) + \frac{\partial}{\partial z^*} \left(D^* \frac{\partial C^*}{\partial z^*} \right) \right] - \left[\frac{\partial}{\partial x^*} \left(u^* C^* \right) + \frac{\partial}{\partial y^*} \left(v^* C^* \right) + \frac{\partial}{\partial z^*} \left(w^* C^* \right) \right] + \epsilon \left(S^* - C^* \right) = 0. \tag{4.11}$$

Also, the soil-gas velocity must satisfy the continuity equation[3]:

[3] Note that the continuity equation was already satisfied with the solution of the pressure field. However, for the convenience of the method, it is used again here for the derivation of the discretization equation of the radon mass transport equation in the soil.

$$\frac{\partial u^*}{\partial x^*} + \frac{\partial v^*}{\partial y^*} + \frac{\partial w^*}{\partial z^*} = 0. \tag{4.12}$$

These two coupled equations will be transformed in a system of algebraic discretization equations, similar to the one found for the pressure field, Eq.(4.8), relating the value of C_P^*, at the node P, to the values at the neighboring nodes C_E^*, C_W^*, C_N^*, C_S^*, C_B^*, and C_T^*, such as[4]:

$$a_P C_P^* = a_E C_E^* + a_W C_W^* + a_N C_N^* + a_S C_S^* + a_B C_B^* + a_T C_T^* + b. \tag{4.13}$$

Rewriting the mass-balance equation, Eq.(4.11), with the dimensionless convective and diffusive fluxes grouped together yields:

$$\frac{\partial J_x^*}{\partial x^*} + \frac{\partial J_y^*}{\partial y^*} + \frac{\partial J_z^*}{\partial z^*} = \epsilon (S^* - C^*), \tag{4.14}$$

where[5],

$$J_x^* = u^* C^* - D^* \frac{\partial C^*}{\partial x^*}, \tag{4.15a}$$

$$J_y^* = v^* C^* - D^* \frac{\partial C^*}{\partial y^*}, \tag{4.15b}$$

$$J_z^* = w^* C^* - D^* \frac{\partial C^*}{\partial z^*}. \tag{4.15c}$$

Now, integrating Eq.(4.14) over the entire control volume (see Fig.(4.4)), yields:

$$\begin{aligned} &\int_t^b \int_s^n \int_w^e \frac{\partial J_x^*}{\partial x^*} dx^* dy^* dz^* + \\ &\int_w^e \int_t^b \int_s^n \frac{\partial J_y^*}{\partial y^*} dy^* dz^* dx^* + \\ &\int_s^n \int_w^e \int_t^b \frac{\partial J_z^*}{\partial z^*} dz^* dx^* dy^* = \int_t^b \int_s^n \int_w^e \epsilon (S^* - C^*) dx^* dy^* dz^*. \end{aligned} \tag{4.16}$$

---

[4] A general description, with an analysis, of the discretization equations of this form was presented originally by Patankar, [Pa80]. In this chapter I present only the basic steps of their derivation, to support a practical application. A detailed derivation, applicable to this specific problem, is shown in Appendix I.

[5] Note that u^*, v^*, and z^* denote the dimensionless velocity components of the seepage velocity vector $\vec{q}^*$ in the x, y, and w directions respectively.

At this point it is necessary to make some assumptions regarding the profile of the flux J^* and the source-plus-sink term $\epsilon(S^* - C^*)$ over the control-volume. Therefore I assume that: (1) the value of the flux J^* at any interface is constant (prevails) over the entire face; (2) the value of the source-and-sink term at the node P prevails over the entire control-volume. With these assumptions, Eq.(4.16) becomes:

$$\left[(J_x^*)_e - (J_x^*)_w\right]\Delta y^*\Delta z^* +$$

$$\left[(J_y^*)_n - (J_y^*)_s\right]\Delta z^*\Delta x^* +$$

$$\left[(J_z^*)_b - (J_z^*)_t\right]\Delta x^*\Delta y^* = \epsilon(S^* - C^*)_P(\Delta x^*\Delta y^*\Delta z^*)_P,$$

or,

$$(J_e^* - J_w^*) + (J_n^* - J_s^*) + (J_b^* - J_t^*) = \epsilon(S^* - C^*)_P(\Delta x^*\Delta y^*\Delta z^*)_P, \qquad (4.17)$$

where,

$$J_e^* = (J_x^*)_e(\Delta y^*\Delta z^*)_P, \qquad (4.18a)$$

$$J_w^* = (J_x^*)_w(\Delta y^*\Delta z^*)_P, \qquad (4.18b)$$

$$J_n^* = (J_y^*)_n(\Delta z^*\Delta x^*)_P, \qquad (4.18c)$$

$$J_s^* = (J_y^*)_s(\Delta z^*\Delta x^*)_P, \qquad (4.18d)$$

$$J_b^* = (J_z^*)_b(\Delta x^*\Delta y^*)_P, \qquad (4.18e)$$

$$J_t^* = (J_z^*)_t(\Delta x^*\Delta y^*)_P. \qquad (4.18f)$$

Similarly, integrating the continuity equation, Eq.(4.12), over the entire control volume, yields:

$$(u_e^* - u_w^*)(\Delta y^*\Delta z^*)_P + (v_n^* - v_s^*)(\Delta z^*\Delta x^*)_P + (w_b^* - w_t^*)(\Delta x^*\Delta y^*)_P = 0,$$

or,

$$(F_e^* - F_w^*) + (F_n^* - F_s^*) + (F_b^* - F_t^*) = 0. \tag{4.19}$$

where F_i^* is the dimensionless flow rate defined at the generic interface i of the control-volume, and expressed as:

$$F_e^* = u_e^*(\Delta y^* \Delta z^*)_P, \tag{4.20a}$$

$$F_w^* = u_w^*(\Delta y^* \Delta z^*)_P, \tag{4.20b}$$

$$F_n^* = u_n^*(\Delta z^* \Delta x^*)_P, \tag{4.20c}$$

$$F_s^* = u_s^*(\Delta z^* \Delta x^*)_P, \tag{4.20d}$$

$$F_b^* = u_b^*(\Delta x^* \Delta y^*)_P, \tag{4.20e}$$

$$F_t^* = u_t^*(\Delta x^* \Delta y^*)_P. \tag{4.20f}$$

Now, multiplying Eq.(4.19) by C_P^*, (the value of the radon concentration at the node P), and subtracting it from Eq.(4.17), yields:

$$\begin{aligned} &(J_e^* - F_e^* C_P^*) - (J_w^* - F_w^* C_P^*) + \\ &(J_n^* - F_n^* C_P^*) - (J_s^* - F_s^* C_P^*) + \\ &(J_b^* - F_b^* C_P^*) - (J_t^* - F_t^* C_P^*) = \epsilon\,(S_P^* - C_P^*)\,(\Delta x^* \Delta y^* \Delta z^*)_P\,. \end{aligned} \tag{4.21}$$

With the assumption of uniformity over the control-volume face, it is possible to demonstrate that (see Appendix I):

$$J_e^* - F_e^* C_P^* = a_E\,(C_P^* - C_E^*)\,, \tag{4.22a}$$

$$J_w^* - F_w^* C_P^* = a_W\,(C_W^* - C_P^*)\,, \tag{4.22a}$$

$$J_n^* - F_n^* C_P^* = a_N\,(C_P^* - C_N^*)\,, \tag{4.22a}$$

$$J_s^* - F_s^* C_P^* = a_S\,(C_S^* - C_P^*)\,, \tag{4.22a}$$

$$J_b^* - F_b^* C_P^* = a_B \left(C_P^* - C_B^* \right), \tag{4.22a}$$

$$J_t^* - F_t^* C_P^* = a_T \left(C_T^* - C_P^* \right). \tag{4.22a}$$

Then, substituting Eq.(4.22) into Eq.(4.21) yields:

$$\begin{aligned} &\left(a_E + a_W + a_N + a_S + a_B + a_T + \epsilon \Delta x^* \Delta y^* \Delta z^*\right)_P C_P^* = \\ &= a_E C_E^* + a_W C_W^* + a_N C_N^* + a_S C_S^* + a_B C_B^* + a_T C_T^* + \left(\epsilon S^* \Delta x^* \Delta y^* \Delta z^*\right)_P. \end{aligned} \tag{4.23}$$

Finally, the discretization equation for the mass balance equation can then be written in the standard format as:

$$a_P C_P^* = a_E C_E^* + a_W C_W^* + a_N C_N^* + a_S C_S^* + a_B C_B^* + a_T C_T^* + b, \tag{4.24}$$

where the coefficients a_E, a_W, a_N, a_S, a_B, a_T, and the constant term b are expressed as[6]:

$$a_E = G_e^* \mathcal{A}\left(|P_e|\right) + \left[\left[-F_e^*, 0\right]\right], \tag{4.25a}$$

$$a_W = G_w^* \mathcal{A}\left(|P_w|\right) + \left[\left[+F_w^*, 0\right]\right], \tag{4.25b}$$

$$a_N = G_n^* \mathcal{A}\left(|P_n|\right) + \left[\left[-F_n^*, 0\right]\right], \tag{4.25c}$$

$$a_S = G_s^* \mathcal{A}\left(|P_s|\right) + \left[\left[+F_s^*, 0\right]\right], \tag{4.25d}$$

$$a_B = G_b^* \mathcal{A}\left(|P_b|\right) + \left[\left[-F_b^*, 0\right]\right], \tag{4.25e}$$

$$a_T = G_t^* \mathcal{A}\left(|P_t|\right) + \left[\left[+F_t^*, 0\right]\right], \tag{4.25f}$$

$$a_P = a_E + a_W + a_N + a_S + a_B + a_T + \left(\epsilon \Delta x^* \Delta y^* \Delta z^*\right)_P, \tag{4.25g}$$

$$b = \left(\epsilon S^* \Delta x^* \Delta y^* \Delta z^*\right)_P, \tag{5.25h}$$

[6] The symbol $\left[\left[\ \right]\right]$ denotes the largest value of the quantities within it.

and where the dimensionless flow rate F^*, and conductance G^*, as defined at the interfaces e, w, n, s, b, t are expressed respectively as:

$$F_e^* = u_e^* (\Delta y^* \Delta z^*)_P \,, \tag{4.26a}$$

$$F_w^* = u_w^* (\Delta y^* \Delta z^*)_P \,, \tag{4.26b}$$

$$F_n^* = u_n^* (\Delta z^* \Delta x^*)_P \,, \tag{4.26c}$$

$$F_s^* = u_s^* (\Delta z^* \Delta x^*)_P \,, \tag{4.26d}$$

$$F_b^* = u_b^* (\Delta x^* \Delta y^*)_P \,, \tag{4.26e}$$

$$F_t^* = u_t^* (\Delta x^* \Delta y^*)_P \,, \tag{4.26f}$$

and,

$$G_e^* = \frac{D_e^*}{(\delta x)_e^*} (\Delta y^* \Delta z^*)_P \,, \tag{4.27a}$$

$$G_w^* = \frac{D_w^*}{(\delta x)_w^*} (\Delta y^* \Delta z^*)_P \,, \tag{4.27b}$$

$$G_n^* = \frac{D_n^*}{(\delta y)_n^*} (\Delta z^* \Delta x^*)_P \,, \tag{4.27c}$$

$$G_s^* = \frac{D_s^*}{(\delta y)_s^*} (\Delta z^* \Delta x^*)_P \,, \tag{4.27d}$$

$$G_b^* = \frac{D_b^*}{(\delta z)_b^*} (\Delta x^* \Delta y^*)_P \,, \tag{4.27e}$$

$$G_t^* = \frac{D_t^*}{(\delta z)_t^*} (\Delta x^* \Delta y^*)_P \,, \tag{4.27f}$$

and where the Peclet numbers P, as defined at the interfaces are expressed as:

$$P_e = \frac{F_e^*}{G_e^*} = \left(\frac{u^*}{D^*} \right)_e (\delta x)_e^*, \tag{4.28a}$$

$$P_w = \frac{F_w^*}{G_w^*} = \left(\frac{u^*}{D^*} \right)_w (\delta x)_w^*, \tag{4.28b}$$

$$P_n = \frac{F_n^*}{G_n^*} = \left(\frac{u^*}{D^*} \right)_n (\delta y)_n^*, \tag{4.28c}$$

$$P_s = \frac{F_s^*}{G_s^*} = \left(\frac{u^*}{D^*}\right)_s (\delta y)_s^*, \tag{4.28d}$$

$$P_b = \frac{F_b^*}{G_b^*} = \left(\frac{u^*}{D^*}\right)_b (\delta z)_b^*, \tag{4.28e}$$

$$P_t = \frac{F_t^*}{G_t^*} = \left(\frac{u^*}{D^*}\right)_t (\delta z)_t^*, \tag{4.28f}$$

and where $\mathcal{A}(|P_i|)$ is the selected interpolation function, (dependent on the Peclet number P_i), used for the evaluation of the flux J_i at a generic interface i. The form of the interpolation function to be used in the Eq.(4.25) depends on the scheme selected to interpolate the flux at the control volume interfaces. A detailed description of several different discretization schemes, with an analysis of their applicability in this problem is presented in Appendix I. Among the schemes analyzed, the so called *power law* scheme has been recommended the best formulation [Pa80], in which the interpolation function is expressed as:

$$\mathcal{A}(|P|) = \left[\left[0, (1 - 0.1\,|P|)^5\right]\right]. \tag{4.29}$$

Location of the Control-Volumes (Grid Generation).

The practice adopted here for locating the grid nodes is first to draw the control-volume boundaries, and then to place a grid point (the node) at the geometric center of each control-volume. The attractiveness of this scheme is that it facilitates the handling of the discontinuities in the boundaries of the calculation domain. In this sense, the control-volume faces are located in such a way that they fill completely the continuous boundary, with no discontinuity occurring within a control-volume face. The locations of the grid nodes follow as a consequence.

The physical discontinuities in the soil block are determined by the presence of the basement within the soil, the crack in the basement floor, as well as by the soil aggregate regions surrounding the basement, and are dependent on the direction being considered. In the x

Figure 4.5 — Soil block with the number of control volumes within each segment in all three dimensions.

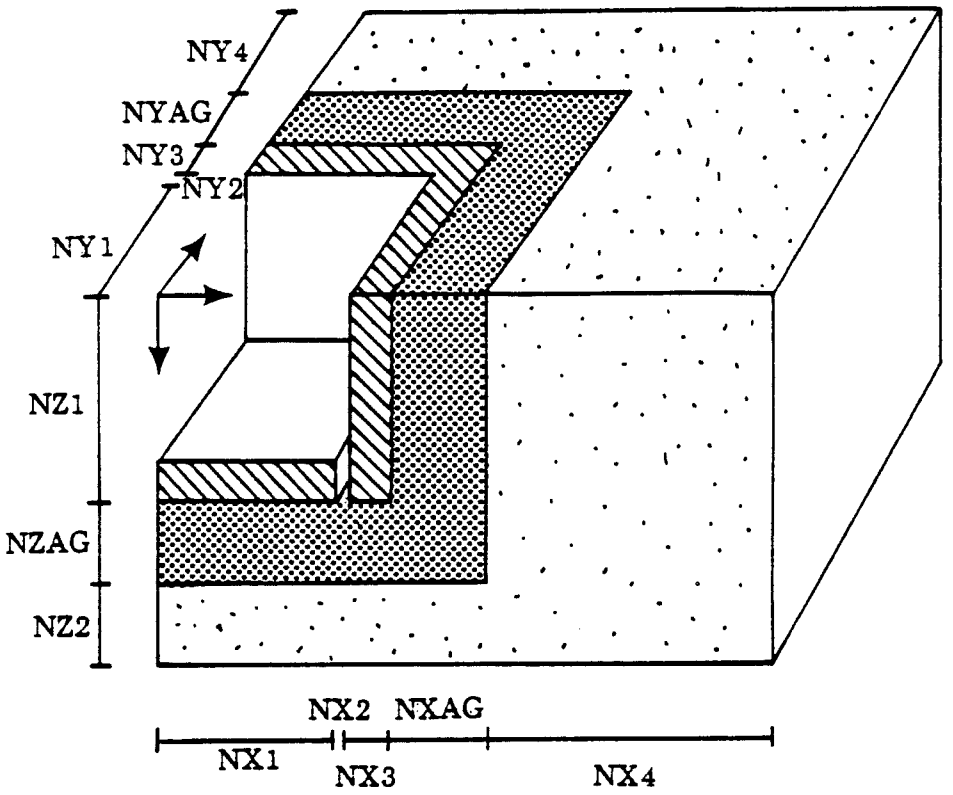

or y directions, five continuous regions may be identified: (1) from the center of the block, to the beginning of the crack; (2) the crack itself; (3) the vertical wall of the basement; (4) the aggregate region in the soil; (5) from the aggregate region, to the end of the block . In the vertical direction, three regions are defined within the soil block: (1) the upper region, above the basement; (2) the aggregate region under the region; (3) and the lower region, from the aggregate to the end of the soil block.

Figure (4.5) shows the soil block with the specified regions, and the number of control-volume faces at each defined continuous segment of the calculation domain in all directions. Thus, the number of C.V. faces in the x-direction are:

N_x1 = # of faces under the basement floor;

N_x2 = # of faces under the crack ;

N_x3 = # of faces under the wall ;

N_xAG = # of faces within the soil aggregate region;

N_x4 = # of faces in the soil, out of the aggregate region .

Similarly to the x-direction, the number of C.V. faces in the y-direction are: N_y1, N_y2, N_y3, N_yAG, and N_y4.

Finally, in the z-direction, the number of C.V faces are:

N_z1 # of faces in the upper region of the soil block;

N_z2 # of faces in the lower region of the soil block;

N_zAG # of faces within the soil aggregate region.

The location of each control-volume is identified by its position order i, j, k in the x, y, and z directions respectively. Specification of the control-volume dimensions is then made using three vectors: $CV_x(i)$, $CV_y(j)$, and $CV_z(k)$.

The sizes of the control-volumes within each defined segment of the soil block are not equally distributed. Because of the difference in scale among the defined regions of the block, and also because the variables being studied (pressure, radon concentration) are expected to have larger variations at some specific locations (closer to the crack, for instance), the sizes of the control-volume faces under each segment are not equally distributed. The idea here is to increase the number of nodes, reducing the grid mesh, in the region close to the crack under the basement where large variations in the dependent variable are expected to occur. Furthermore, although neither the disturbance pressure nor the radon concentration in the soil gas is expected to vary significantly near the external boundaries of the soil block, the grid mesh will also be reduced there in order to handle the boundary conditions. The concern here is that the conditions imposed on the external boundaries of the soil block are of the second type, where the value of the derivative of the dependent variable, rather than its specific value, is given at the boundaries. Therefore, in order to improve the approximation of the numerical derivative, the grid mesh should also be reduced at the external boundaries.

In order to achieve these purposes, the grid mesh will be made finer at the extremities of

each segment, increasing progressively toward to the center of the segment, following the equation of a circle. The algorithm used to calculate the size of all control-volumes, based on the equation of a circle, is described in Appendix G.

It should be noted here that the actual distribution of the mesh grid can be changed at each run of the program. In Chapter V, during the adjustment of the computer program, attempts will be made in order to verify how sensitive the computer programs are to variations of the grid mesh, and also to determine the best grid configuration, considering the performance of the programs and the computer costs involved. An example of a possible grid configuration [7] is presented in Figures (4.6) and (4.7) which show the distribution of the control-volumes in a vertical cross-section of the soil block, both in a whole frame, and also in an expanded area underneath the crack. Figure (4.8) shows the same grid, but on a horizontal cross-section of the soil block.

General Description of the Entire Computer Program.

The computer model implementing the numerical method described above was designed as an interactive code composed of two coupled main programs named PRESSU and MASTRA, which are run separately. Figure (4.9) shows a block diagram of the whole code.

The program PRESSU must be run first, because it gives the initial configuration of the case being modeled. PRESSU specifies the geometrical parameters of the model; generates the control-volumes and the computational grid within the calculation domain of the block; calculates the pressure distribution, as well as the velocity distribution of the soil gas, throughout the whole soil block; and stores the produced data in seven permanent files, (PARAM, CVX, CVY, CVZ, XVELO, YVELO, and ZVELO), which constitute the link with the program MASTRA.

[7] In fact, the grid mesh presented here is already the one which resulted from the adjustment of the computer programs, as discussed in Chapter V.

Figure 4.6 — Two-dimensional view of the control-volumes on a vertical cross-section of the soil block

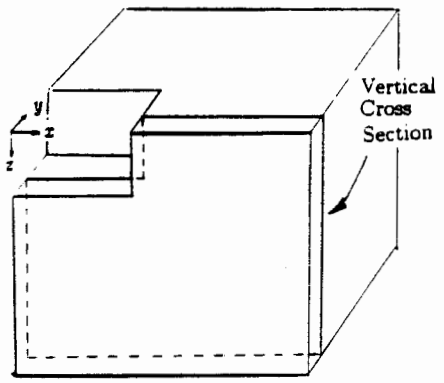

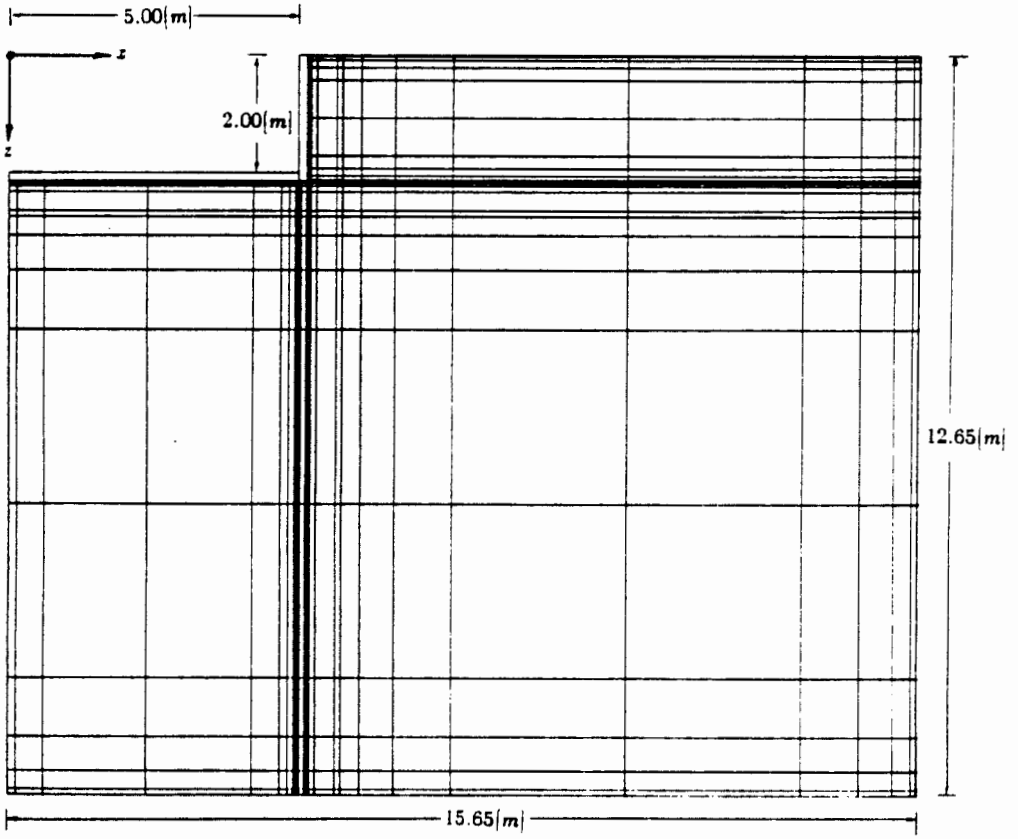

Figure 4.7 — Expanded view of the control-volumes under the soil-crack interface, on a vertical cross-section of the soil block.

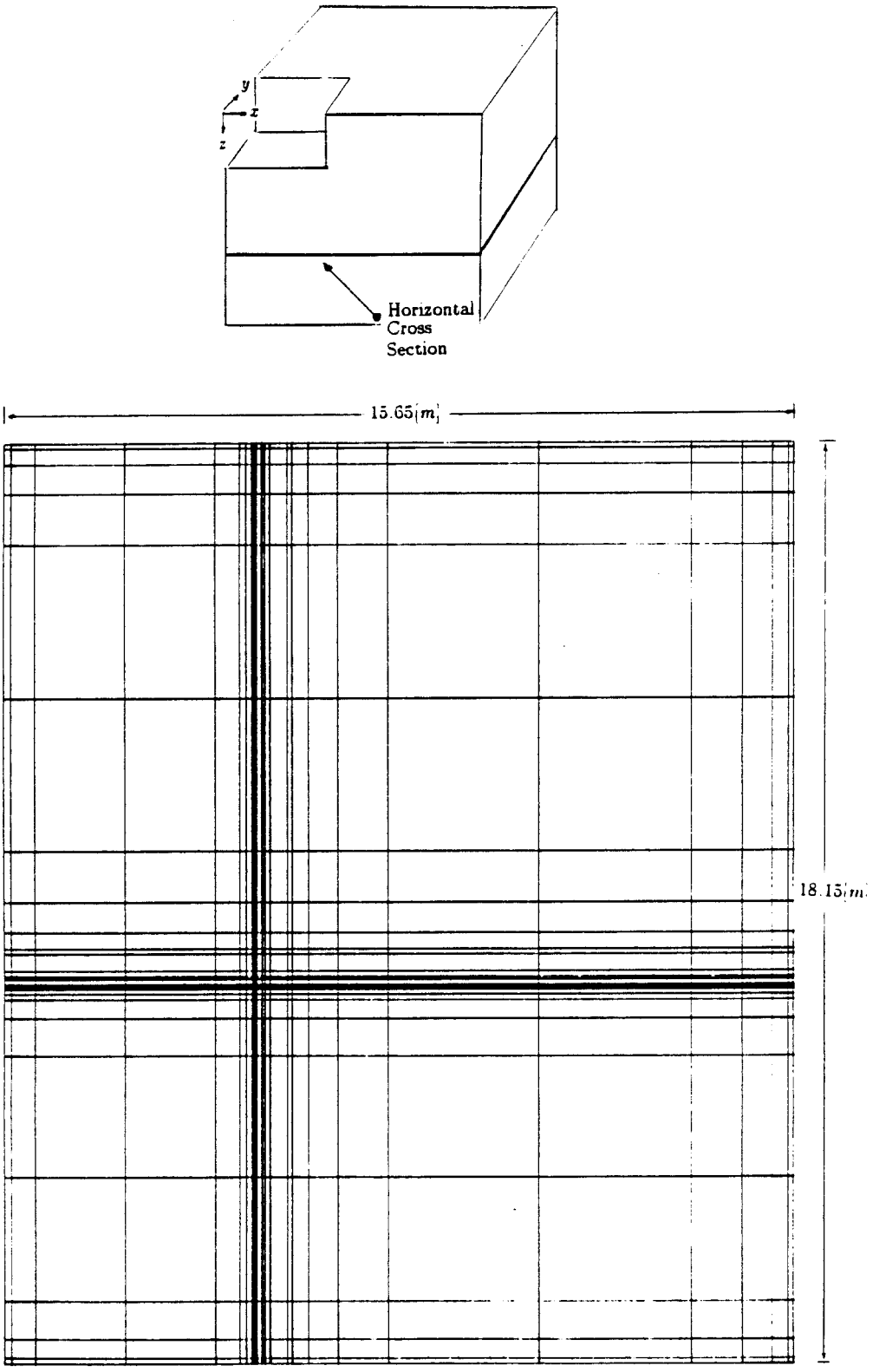

Figure 4.8 — Two-dimensional view of the control-volumes on a horizontal cross-section of the soil block

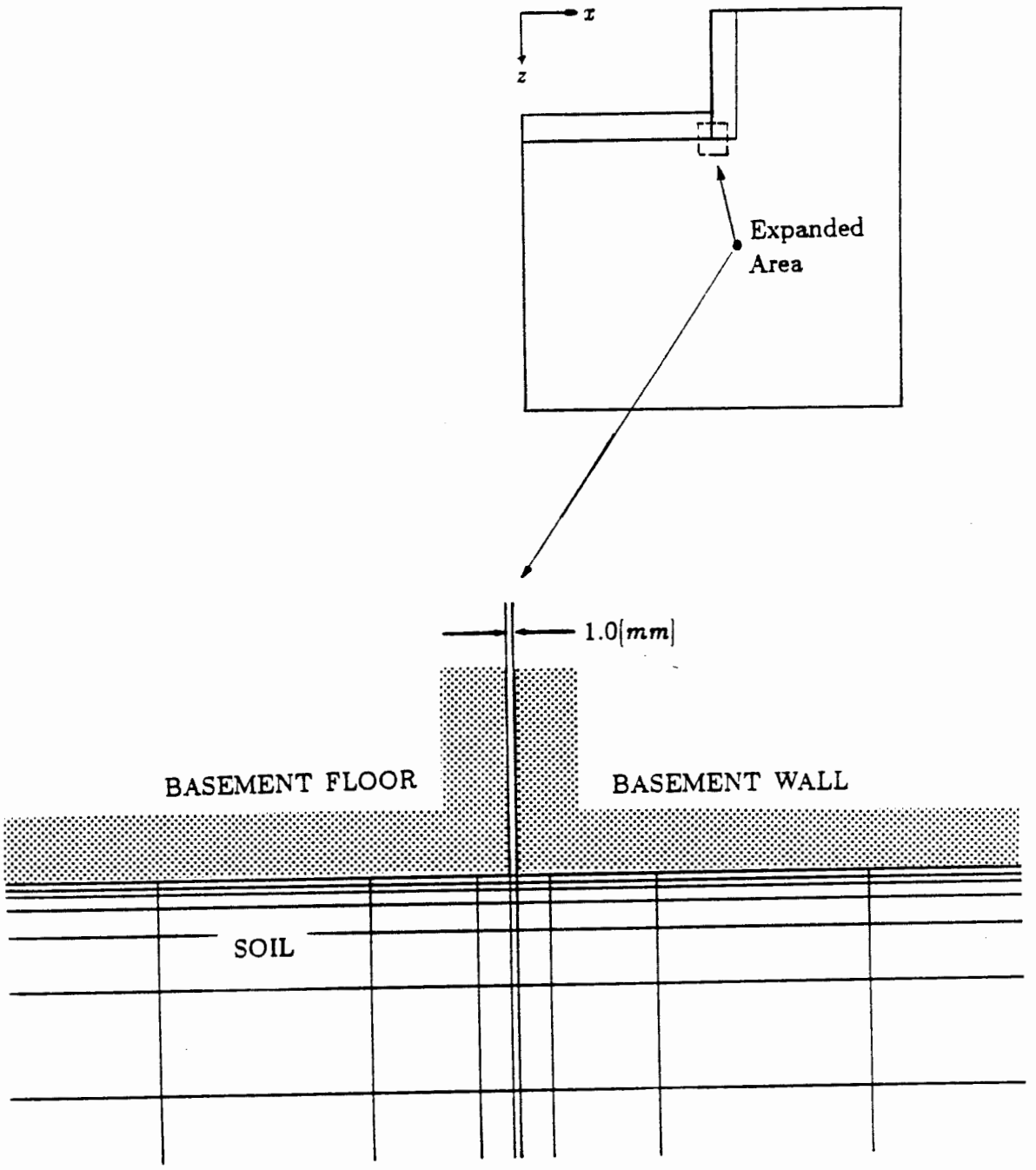

Figure 4.9 — Block diagram of the complete computer model.

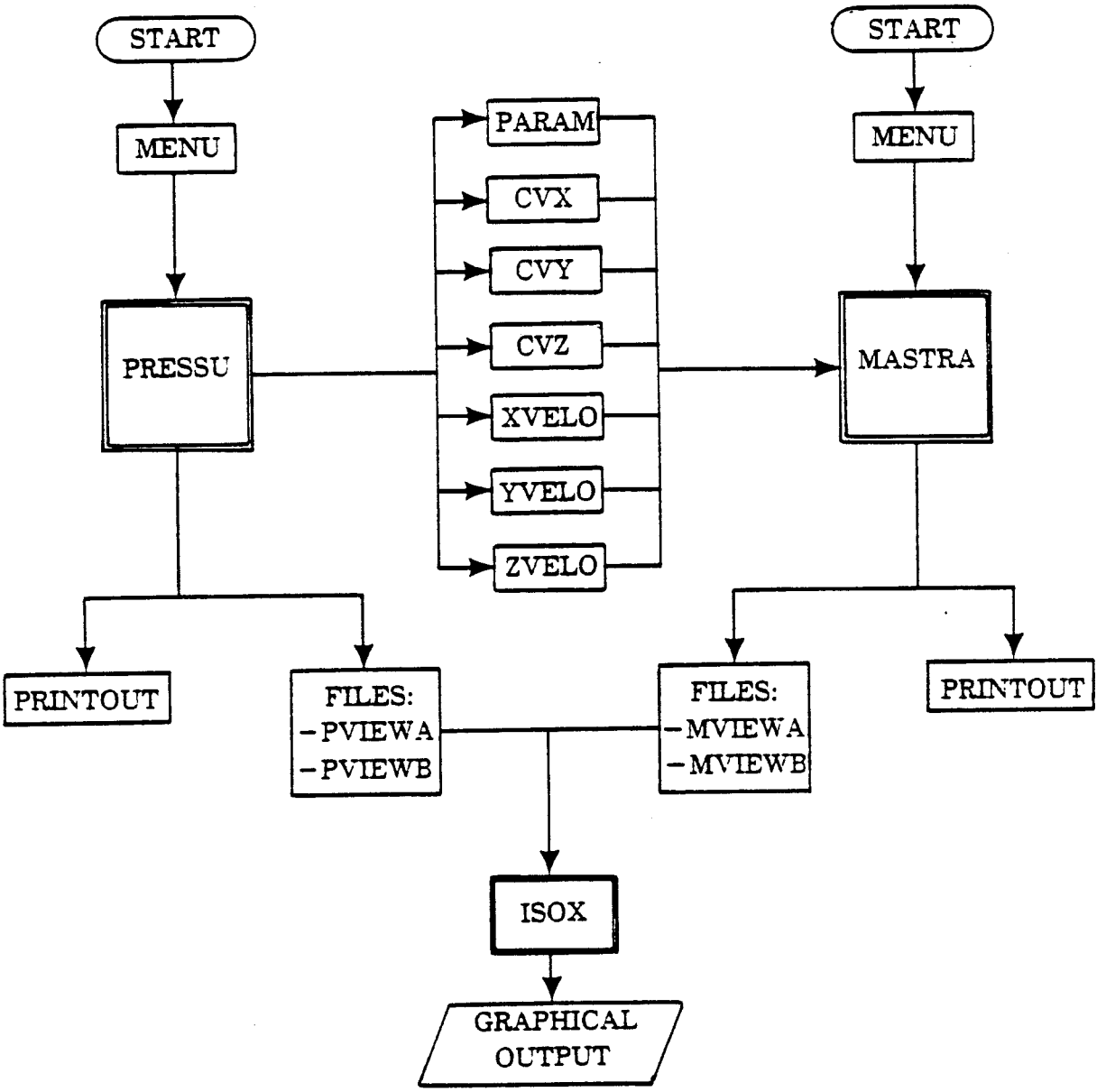

MASTRA then uses these data and, together with its own menu-selected input parameters, it calculates the distribution of radon concentration in the soil gas throughout the soil block. It also calculates the radon flow through the crack and into the basement, with the resultant indoor concentration.

Both programs are menu-oriented, allowing the control of the input and output at each run. A set of default values for the parameters, representing a typical case, is internally defined in the code.

The output of these programs constitutes a printout and four permanent files which can be used later for graphic generation purposes. The printout reproduces all the input parameters, and shows the calculated variables at specified vertical, or horizontal, layers of the soil block.

In the output permanent files, both programs store the calculated values of the variables at two specified vertical cross sections of the soil block. For instance, PRESSU stores in the file PVIEWA the pressure distribution in the first defined cross section of the soil block. The same data are stored in the file PVIEWB, but now being framed in a smaller region around the crack in the basement. So, the former file allows a graphical representation of a cross sectional view of the whole block, while the later one allows a closer view of the cross section near the crack. The files PVIEWC and PVIEWD are recorded in a similar way, representing the pressure distribution in the second defined cross-sectional view of the block. Similarly, MASTRA stores in the files MVIEWA, MVIEWB, MVIEWC, and MVIEWD the radon concentration distribution in two specified cross-sectional views of the block.

The data in these view files can then be used to generate a graphical representation of the modeled variable distribution in vertical sections of the block. A program named ISOX, developed elsewhere at The University of Michigan [Be85], and adapted for a personal computer environment was used for this purpose. ISOX reads the data in those files, and plots the isolines for the specified values of the variable, showing then its distribution

throughout the whole cross section of the block.

The computer code, including PRESSU and MASTRA, was written in FORTRAN 77 (see list in Appendix L), and was run in the Amdahl-5860 computer of the Michigan Terminal System, and in the VAX-8600 computer of the Atmospheric and Oceanic Sciences Department of the Engineering School, at The University of Michigan. ISOX was used in an IBM-XT personal computer.

Algorithm Used in PRESSU for the Solution of the Disturbance Pressure Field.

The velocity of the soil gas within the soil, close to the soil-crack interface, w_{soil}, was evaluated in Appendix E. Its dimensionless form, given in Eq.(E.12), is repeated here as:

$$\tilde{w}_{soil} = -K_S \left(\frac{2\tilde{k}}{\Delta \tilde{z}} \right) (\tilde{p}_P - \tilde{p}_{IN}) , \tag{4.30}$$

where,

$\tilde{p}_P =$ dimensionless disturbance pressure at the first control-volume underneath the crack;

$\tilde{p}_{IN} =$ dimensionless disturbance pressure at the soil crack interface;

$\Delta \tilde{z} =$ dimensionless size, in the z-direction, of the first control-volume underneath the crack;

$\tilde{k} =$ permeability of the soil at the first control-volume underneath the crack;

$K_S =$ dimensionless constant, defined by Eq.(E.12b).

Also, the velocity of the soil gas within the crack, w_{crack}, was evaluated in Appendix E. Its dimensionless form, given by Eq.(E.11), is repeated here as:

$$\tilde{w}_{crack} = -K_C (1 + \tilde{p}_{in}) , \tag{4.31}$$

where,

$K_C =$ dimensionless constant, defined by Eq.(E.11b).

According to the boundary conditions imposed on the soil-crack interface, the values of the disturbance pressure and the soil-gas velocity at the points in the soil close to the soil-crack interface should converge to the respective values of pressure and velocity at a point within the crack, as these points get closer and closer to the soil-crack interface. In other words, w^*_{crack} and w^*_{soil}, as calculated above, should converge to the same finite value. This condition constitute the basic approach of the iterative method adopted in PRESSU for the solution of the disturbance pressure equation in the soil block.

Therefore, in order to implement the boundary conditions, as expressed in Table (3.1), and solve the pressure field equation, PRESSU uses the following iterative algorithm:

Step # 1 - Initial assumption about the disturbance pressure distribution within the soil block.

Initially, the disturbance pressure distribution is arbitrarily assumed to be zero at all points within the soil block. Furthermore, the initial disturbance pressure distribution at the soil crack interface, p^*_{IN}, is assumed to be such that it makes $w^*_{soil} = w^*_{crack}$, for $p^*_P = 0$. Thus, from the equations above, the initial values of p^*_{IN} are expressed as:

$$p^*_{IN} = -\frac{K_C}{K_C + K_S\left(\frac{2k^*}{\Delta z^*}\right)}. \tag{4.32}$$

Step # 2 - Calculation of a *new* disturbance pressure at all control-volumes in the soil block, including p^*_P, the dimensionless disturbance pressure at the control-volumes underneath the crack.

The conditions imposed on all boundaries of the soil block, for the solution of the pressure field equation, are the following:

- At the top surface:

- First order boundary condition;
- The disturbance pressure is assumed to be equal to zero (invariable);

- At the soil-crack interface:
  - First order boundary condition;
  - At each iteration, the disturbance pressure at the crack interface, $\check{p}_{IN}$, is assumed to be known, either from the initial assumptions, or from the last iteration;
  - Note that the disturbance pressure at the crack interface varies at each iteration, but is expected to converge to a finite value as the number of iterations increase;
- At the basement walls and floor, and all other external surfaces of the soil block:
  - Second type boundary condition;
  - The gradient of the disturbance pressure perpendicular to these surfaces is equal to zero, (invariable).

A description of the general algorithm, used in this part of the program for calculating the pressure distribution throughout the soil block will be presented later in the items: 1) general algorithm for handling the calculation in the numerical grid; and 2) description of the program PRESSU.

Step # 3 - Calculation of a $\check{w}_{soil}$ and $\check{w}_{crack}$, based on Equations (4.30) and (4.31), respectively.

Step # 4 - Comparison[8] of $\check{w}_{soil}$ with $\check{w}_{crack}$.

If $\check{w}_{soil}$ is close to $\check{w}_{crack}$, within a tolerance limit, then the iteration routine is over, and PRESSU goes to step # 7. If not, PRESSU continues the iteration routine, moving to step # 5.

Step # 5 - Calculation of the **new** value of $\check{p}_{IN}$ - the disturbance pressure distribution at the soil-crack interface.

[8] PRESSU also adopts another convergence criteria, based on the maximum variation of the disturbance pressure at any node of the grid. According to this, the iterative routine is also finished when the maximum variation of the pressure at any node in the grid becomes lower than an established tolerance limit.

The new values of p^*_{IN} are calculated using the most recently calculated values of p^*_P, in such a way that it makes $w^*_{soil} = w^*_{crack}$. Thus, from Equations (4.30) and (4.31), p^*_{IN} can be expressed as:

$$p^*_{IN} = \frac{-K_C + K_C\left(\frac{2k^*}{\Delta z^*}\right) p^*_P}{-K_C + K_C\left(\frac{2k^*}{\Delta z^*}\right)}. \tag{4.33}$$

Step # 6 - Repeat steps #2 to #4.

Step # 7 - Output.

Algorithm Used in MASTRA for the Solution of the Radon Concentration Field.

In order to deal with the boundary conditions established at the crack interface, which were described in Appendix F, MASTRA uses the following iterative algorithm.

Step # 1 - Selection of an arbitrary initial distribution of the dimensionless radon concentration within the soil block.

Initially, the values of the radon concentration inside the soil block are made to vary exponentially, from zero at the top of the soil block, to its maximum value at the bottom of the block. The initial values of the radon concentration at the soil-crack interface are assumed to be zero.

Step # 2 - Calculation of a **new** radon concentration at all the control-volumes within the soil block, including C^*_P, the dimensionless radon concentration at the control-volumes underneath the crack.

The conditions imposed on all boundaries of the soil block, for solving the radon transport equation within it, are the following:

- At the top surface:

  - First order boundary condition;
  - The radon concentration at the top surface is assumed to be zero (invariable);
- At the soil-crack interface:
  - First order boundary condition;
  - At each iteration, the radon concentration at the crack interface, C^*_{IN}, is assumed to be known, either from the initial assumptions, or from the last iteration;
  - Note that the radon concentration at the crack interface varies at each iteration, but is expected to converge to a finite value as the number of iterations increase;
- At the basement walls and floor, and all other external surfaces of the soil block:
  - Second type boundary condition;
  - The gradient of the radon concentration (the radon flux), perpendicular to these surfaces is equal to zero, (invariable).

Step # 3 – Calculation of J^*_{soil}, the dimensionless radon flux from the soil through the crack interface, and J^*_{crack}, the radon flux through the crack interface, but calculated within the crack.

The fluxes J^*_{soil} and J^*_{crack} were calculated in Appendix F. They are also expressed here as:

$$J^*_{soil} = \left(w^* + \frac{2D^*}{\Delta z^*} \right) C^*_{IN} - \left(\frac{2d^*}{\Delta z^*} \right) C^*_P, \tag{4.34}$$

and,

$$J^*_{crack} = M C^*_{IN}, \tag{4.35}$$

where,

$C^*_{IN} =$ dimensionless radon concentration at the soil-crack interface;

$C^*_P =$ dimensionless radon concentration at the first control-volume underneath the crack;

$M =$ dimensionless constant defined in Eq.(F.43c);

$w^* =$ dimensionless velocity of the soil gas through the crack;

$D^* =$ dimensionless radon diffusivity coefficient in the control-volumes underneath the crack;

$\Delta z^* =$ dimensionless size, in the z-direction, of the control-volumes underneath the crack.

Step # 4 - Comparison [9] of J^*_{soil} with J^*_{crack}.

If J^*_{soil} is close to J^*_{crack}, within a tolerance limit, then the iteration routine is over, and MASTRA goes to step # 7. If not, MASTRA continues the iteration routine, moving to step # 5.

Step # 5 - Calculation of the **new** value of C^*_{IN} - the radon concentration distribution at the soil-crack interface.

The new values of C^*_{IN} are calculated using the most recently calculated values of C^*_P, in such a way that it makes $J^*_{soil} = J^*_{crack}$. Thus, from Equations (4.34) and (4.35), C^*_{IN} can be expressed as:

$$C^*_{IN} = \frac{\left(\frac{2D^*}{\Delta z^*}\right) C^*_P}{\left(\frac{2D^*}{\Delta z^*}\right) + w^* - M}. \tag{4.36}$$

Step # 6 - Repeat steps #2 to #4.

Step # 7 - Output.

General Algorithm for Handling the Calculation in the Numerical Grid.

The whole three-dimensional configuration of the model's calculation domain can be considered as formed by several two-dimensional layers of control-volumes in both vertical

[9] MASTRA also adopts another convergence criteria, based on the maximum variation of the radon concentration at any node of the grid. According to this, the iterative routine is also finished when the maximum variation of the radon concentration at any node in the grid becomes lower than an established tolerance limit.

and horizontal cross-sections of the block. Furthermore, each one of these two-dimensional layers is formed with lines of control-volumes. The nodes located in the center of the control-volumes form the grid. It is assumed that the value of the variable (disturbance pressure or radon concentration) within a control-volume is represented by the respective value at the node. Therefore, the objective is to calculate the values of the variables at these nodes. In order to do so, the three-dimensional grid of the model is calculated one layer at a time, until all layers of the grid are considered. At each layer, the calculation is performed one line at a time, and the procedure is repeated until all lines of the layer are visited.

The iterative method adopted here for the solution of the algebraic discretization equations at any layer of the grid can be called a *mixed-direction-line-by-line* method. In this method, at some specific layer, each grid line is solved separately using a tridiagonal matrix routine, based on the Thomas algorithm. [An84]. The whole layer is then solved by solving all grid lines of opposite directions on the layer, in an alternating-direction sequence. For example, when calculating a horizontal layer of the grid, we first select a grid line (say, in the y-direction). Then, assuming that the values of the variable at all the neighbor nodes (in the x and z-directions) are known from the latest calculation, we solve the system of equations representing the nodes along the selected line, using the tridiagonal matrix routine. Following this, we select the grid line in the opposite direction (x-direction) and do the same thing again. This procedure is repeated until all grid lines in both opposite directions of the layer have been calculated. This mixed direction iteration method was tested in a simplified problem of heat transfer in a two-dimensional surface of rectangular shape, with constant temperatures at the borders. The results compared very well with the analytical solution.

In order to implement this iterative procedure, the soil block has been divided into three regions: 1) the middle layers, formed by the first five horizontal layers of control-volumes located right underneath the basement floor; 2) the upper region, located above the middle layers; 3) and the lower region, located below the middle layers.

Because of the boundary conditions imposed at the soil-crack interface, the first middle layer

under the basement floor constitutes the most critical one for the solution of the algebraic discretization equations in the whole grid. Consequently, both PRESSU and MASTRA start the iterative process at this first middle layer. There, the procedure is initiated by selecting the grid lines located under the crack, and then marching in the direction of the external boundaries of the soil block. So, starting from the crack, the routine first goes to the north and east directions. Then, starting again under the crack, the routine marches toward to the west and south, covering in this way the whole layer. The idea implicit in this approach is that since the crack constitutes the center for the disturbance in the system, any sweep sequence should start at the crack, or as close as possible to it, making possible in this way to transmit the useful information from the crack into the soil block domain. The other four middle layers are calculated using the same procedure, except that the nodes in these layers do not have the conditions imposed from the crack.

After the calculation of the middle layers, the iterative routine is turned to the calculation of the vertical layers of the soil block, starting with those layers close to the crack lines, and moving away toward to the external boundaries of the soil block. The purpose of alternating vertical with horizontal layers is to improve the transmission, to the whole soil block, of the information given by the first kind boundary condition at the top of the block.

When the calculation of all vertical layers is finished, the iterative routine returns to the calculation of the horizontal layers of the upper and lower regions of the soil block. In the lower region, the procedure for calculating the lines is the same one adopted in the middle layers. In the upper region, the iterative procedure is slightly modified. There, the procedure starts with the calculation of the grid line close to the basement (in either direction), and then, alternating the x and y-directions, it marches to the external boundaries of the soil block.

Therefore, the iterative procedure adopted in PRESSU and MASTRA for solving the discretization equations at the numerical grid, can be summarized as:

Step # 1 - Solution at the five middle layers;

Step # 2 - Solution at the vertical layers;

Step # 3 - Solution at the horizontal layers of the lower region;

Step # 4 - Solution at the horizontal layers of the upper region;

Description of the Program PRESSU.

The main program PRESSU was divided in sixteen steps which will be described next. A listing of the program, as well as the subroutines, are presented in Appendix L.

Steps # 1 & 2 - Initial statements, and definition of the input parameters. The subroutine PMENU is called to handle the menu of input parameters to PRESSU.

Step # 3 - Calculation of some of the constants used in the dimensionless expressions. These constants were defined in Chapter 3.

Step # 4 - Calculation of the dimensionless sizes of all control-volumes in the soil block. The sizes of the control-volume faces are distributed in each segment, following an equation of a circle, as described in Appendix G. The sizes of the C.V. in the directions x, y, and z are stored in the vectors CVX(i), CVY(j), and CVZ(k), respectively.

Step # 5 - Calculation of the dimensionless permeability for all control-volumes in the soil block. These values are stored in the array PERM(i, j, k). Four distinct regions are defined in the soil block, with the following assigned permeabilities [10]:

PERMX = Permeability of the x-direction aggregate region;

PERMY = Permeability of the Y-direction aggregate region;

PERMZ = Permeability of the Z-direction aggregate region;

[10] Values of PERM(i, j, k) inside the house are made equal to zero.

PERM1 = Permeability of the rest of the soil block.

Step # 6 – Calculation of the dimensionless coefficients a_E, a_W, a_N, a_S, a_B, a_T, and a_P used in the discretization of the disturbance pressure field, as defined by Eq.(4.9). One set of these coefficients is assigned for each node of the grid, and stored in the arrays: AE(i,j,k); AW(i,j,k); AN(i,j,k); AS(i,j,k); AB(i,j,k); AT(i,j,k); and AP(i,j,k). Inside the house, all coefficients are made equal to zero. In order to help establishing the boundary conditions at the external surfaces and the bottom of the soil block, the coefficients perpendicular to those surfaces are also made equal to zero.[11]

Step # 7 – Initialization of the disturbance pressure distribution in the soil. These values are stored in the array PRES(i,j,k). The array PRESA(i,j,k) also stores the values of pressure, and is used in the convergence test. Initially, all values of the arrays PRES(i,j,k) and PRESA(i,j,k) within the complete block are assigned zero (including their extremities). The values at the extremities of these arrays are meant to be the pressure at the interfaces of the control-volumes forming the external boundaries of the soil block. All other values of the array PRES(i,j,k) represent the disturbance pressure at the respective node.

Step # 8 – Initialization of the disturbance pressure at the soil crack interface. The initial value of pressure at the crack interface such that it makes $w^*soil = w^*_{crack}$. It is given by Eq.(4.32).

Step # 9 – Solution of the disturbance pressure equation, first in the five horizontal middle layers, and then in all vertical layers of the soil block.
Solution of each layer will be achieved iteratively, in an alternating line-by-line sequence.

In calculating a line in the middle layer, the subroutine XDIR, or YDIR (depending if it is an x or y-line), is called to group the nodes of the line in a system of equation with the coefficients in a tridiagonal matrix form. Then, either subroutine calls the subroutine TRIDIM, which uses a tridiagonal method (Thomas algorithm – [An84]) to solve the line.

[11] This constitutes a redundant procedure for implementing the boundary conditions at those surfaces, because the gradient of the pressure perpendicular to those boundaries is also made equal to zero, as described in step # 9.

A complete sweeping of the middle layer is performed with both x and y-lines in an alternate sequence. After each line is calculated in the subroutine XDIR, or YDIR, the boundary conditions at the extremities of the line are up-to-dated, by making the value of the pressure the same in the last two control-volumes, at both ends of the line.

The vertical layers are calculated first in the bulk of the soil block, starting with the layers close to the wall of the basement and, alternating in the x and y-directions, moving toward to the external surfaces of the block. Then the vertical layers under the basement are calculated, starting with the layers close to the crack and, alternating in the x and y-directions, moving toward to the center of the block. In these vertical layers, only the z-lines are calculated. Thus, for each z-line the subroutine ZDIR is called to group the nodes of the line in a tridiagonal system. Then the subroutine TRIDIM is called to solve the line.

Step # 10 – Solution of the disturbance pressure equation in the horizontal layers of the lower region, and then in the upper region of the soil block.
These horizontal layers are calculated with a procedure similar to the one used for the middle layers, using the subroutines XDIR, YDIR, and TRIDIM.
At the end of this step, the arrays representing the velocity of the soil gas through the crack interface, WCRACK(i,j) and WSOIL(i,j), are calculated using the most recently calculated values of the array PRES(i,j,k).

Step # 11 – Test the convergence of PRESSU.
PRESSU finds the maximum difference of pressure occurring at any node in the soil block, since the last iteration. It also finds the maximum difference of soil gas velocity occurring at the soil-crack interface, since the last iteration. Then the convergence test is applied to check if these maximum differences in pressure and in velocity are below some established tolerance limit. If the results of the test show that the calculations have, either converged to the specified tolerance, or reached the maximum number of iterations, then PRESSU proceeds to step # 12, to calculate the velocity field of the soil gas throughout the soil block. If the convergence test fails, the program calculates the new pressure distribution at

the soil-crack interface, based on Eq.(4.33), and then returns to step # 9, starting a new iteration.

Step # 12 - Calculation of the three components of the soil gas velocity vector in the soil matrix.

In order to save computer memory, the three components of the soil gas velocity vector will be stored in the following arrays: AE(i,j,k), in the x-direction; AN(i,j,k), in the y-direction; and AB(i,j,k), in the z-direction. In MASTRA, these velocity components will be named XFLOW(i,j,k), YFLOW(i,j,k), and ZFLOW(i,j,k), respectively. These components are calculated in a displaced grid, which means that they are not represented at the nodes, but at the interface between two nodes.

Step # 13 - Transference of some parameters, and calculated variables, to fixed files, which will be used for coupling with MASTRA.

Steps# 14, 15, and 16 - Output, format statements, and list of variables.

The output of PRESSU is performed by calling the subroutine PREOUT.

Description of the Program MASTRA.

The main program MASTRA was divided in sixteen steps which will be described next. A listing of the program, as well as the subroutines, are presented in Appendix L.

Steps # 1 & 2 - Initial statements and definitions.

Step # 3 - Coupling with program PRESSU.

Data produced by PRESSU, and stored in fixed files are read in by MASTRA. Also, the subroutine MMENU is called to handle the menu of input parameters to MASTRA.

Step # 4 - Calculation of the parameters used in the dimensionless expressions of the program.

Step # 5 - Calculation of the dimensionless radon diffusion coefficient in soil, the dimensionless radon source term, and the soil porosity at each control-volume in the soil block. The following four regions are defined within the soil block: x-aggregate; y-aggregate; z-aggregate; and the bulk of soil beyond the aggregate regions. Each region will be assigned with its own dimensionless values of soil porosity, radon diffusivity, and radon source term, stored in the arrays: DIFFUS(i,j,k); POROSI(i,j,k); and SOURCE(i,j,k), respectively. Values inside the house are made equal to zero.

Step # 6 - Calculation of the dimensionless flow rate arrays.
The flow rates are calculated for the three directions x, y, and z separately, and are dependent on the components of the soil gas velocity. Consequently, the components of the flow rates are calculated at the interfaces of the control volumes, rather than at its center (or nodes).

Step # 7 - Calculation of the dimensionless coefficients a_E, a_W, a_N, a_S, a_B, a_T, and a_P used in the discretization of the radon concentration field, as defined by Eq.(4.25). One set of these coefficients is assigned for each node of the grid, and stored in the arrays: AE(i,j,k); AW(i,j,k); AN(i,j,k); AS(i,j,k); AB(i,j,k); AT(i,j,k); and AP(i,j,k). Inside the house, all coefficients are made equal to zero. In order to help establishing the boundary conditions at the external surfaces and the bottom of the soil block, the coefficients perpendicular to those surfaces are made equal to zero.[12]

Step # 8 - Initialization of the radon concentration distribution in the soil.
The dimensionless values of the radon concentration in the soil are stored in the array CONCEN(i,j,k). The array COTEST(i,j,k) contains the calculated values of the radon concentration from the last iteration (it will be used in the convergence test). Initially, the values of these arrays inside the soil block, are made to vary exponentially, from zero at the top of the block, to its maximum value at the bottom of the block. Within the house, and at the top of the soil block, the arrays CONCEN(i,j,k) and COTEST(i,j,k) are always

[12] This constitutes a redundant procedure for implementing the boundary conditions at those surfaces, because the gradient of the radon concentration, as well as the velocity of the soil gas perpendicular to those boundaries are also made equal to zero.

equal to zero. Initially, the concentration at the soil-crack interface is made equal to zero.

Step # 9 – Calculation of the radon distribution in the soil.

Calculations start with the middle layers. Each line in the middle layer is calculated in MASTRA by calling the subroutine XLINE or YLINE, which organizes the coefficients for that specific line, and calls the subroutine TRIDIM to solve it.

Then, MASTRA proceeds to calculate the vertical layers. At each vertical layer, the lines at the z-direction are calculated by the subroutines, ZLINE and TRIDIM.

Following this, MASTRA calculates the horizontal layers of the lower region, and the upper region of the soil block, using a procedure similar to the one used in the middle layers.

At the end of this step, the boundary conditions at the lateral and bottom of the soil block are adjusted, by making the concentration gradient perpendicular to those surfaces equal to zero.

Also, the dimensionless radon fluxes at the soil-crack interface – FCRACK and FSOIL – are calculated based on the Equations (4.34) and (4.35), and using the new calculated values of radon concentration stored in the array CONCEN(i, j, k).

Step # 10 – Test the convergence of MASTRA.

MASTRA finds the maximum difference of radon concentration occurring at any node in the soil block, since the last iteration. It also finds the maximum difference of radon flow occurring at the soil-crack interface, since the last iteration. Then the convergence test is applied to check if these maximum differences in radon concentration and in radon flux are below some established tolerance limit. If the results of the test show that the calculations have, either converged to the specified tolerance, or reached the maximum number of iterations, then MASTRA proceeds to step # 11, to calculate the radon entry rate into the house. If the convergence test fails, the program calculates the new radon concentration at the soil-crack interface, based on Eq.(4.36), and then returns to step # 9, starting a new iteration cycle.

Step # 11 – Calculate the radon entry rate into the house.

The total radon entry rate into the house is given by the sum of the entry rate through the interface of all control-volumes under the crack, as expressed in Appendix J, Eq.(J.10). Both the convective and the diffusive components of the radon entry rate are considered.

Step # 12 – Calculate the indoor radon concentration.

The indoor radon concentration is calculated based on the derivation presented in Appendix J, and expressed in Eq.(J.11).

Step # 13 – Calculate the radon flux to the atmosphere.

The radon flux to the atmosphere, at the top of the soil block, is calculated based on the derivation presented in Appendix K, and expressed in Eq.(K.7).

Steps # 14, 15, and 16 – Output, format statements, and list of variables.

The subroutine MASOUT is called to produce the output from MASTRA.

CHAPTER V

ANALYSIS OF THE MODEL

This chapter has two goals: first, to adjust the computer model so that it behaves according to what is expected; second, after adjusting the program, to test its sensitivity to the variation of every important parameter of the model. The ultimate purpose of these efforts is to obtain a better knowledge of the operational limits of the model, and better confidence in its performance.

Adjustment of the Computer Codes.

The computer programs are expected to perform in such a way that their results converge to the solution of the algebraic discretization equations representing the differential equations of the model. In writing the code, a few parameters, and functions were used for controlling its operation, in order to assure that: 1) the numerical method is applied correctly; 2) the boundary conditions are satisfied; 3) the iterative process of the code converges to the solution of the algebraic discretization equations; 4) and finally that the solution of the discretization equations approximate the solution of the original differential equations of the model. These, so called here, operational parameters are not considered variables of the model in the sense that they are not related to the problem of radon transport in the soil and into the house. However, these parameters have a direct effect on the performance of the code, controlling in different aspects the execution of the programs. The adjustment of the computer code consists then in identifying and setting up the appropriate values of all operational parameters of the program. It is important to note however that, in general,

there are no unique values for the adjustment parameters, and the selection of a particular value will be based on a compromise of factors underlying the convergence of the program, and the computer cost involved.

The important operational parameters that must be optimized in the programs PRESSU and MASTRA are the following:

1. Maximum number of iterations in the iterative process of the programs;
2. Definition of the grid – Number of control-volumes in the calculation domain of the soil block;
3. Size of the soil block;
4. Value of the turbulent diffusion coefficient of radon in the air of the basement – here called the enhanced radon diffusion coefficient, as defined in Appendix F;
5. Interpolation function used in the discretization of the radon transport equation of the model.

After being adjusted, these parameters will be incorporated as default in the programs PRESSU and MASTRA, and will be used during the next phase of the sensitivity analysis of the codes.

In the flow-chart of Fig. (5.1) I propose a procedure for adjusting the computer programs. It starts with the selection of the values for all the parameters of the model representing a typical configuration. The initial values of the operational parameters are selected arbitrarily, based on reasonable judgement. Then the sequence of tests starts, and at the end of each test, the appropriate value of the parameter is selected and adopted as default.

Values of the Model's Parameters for a Typical Case.

In Table (5.1) I present the values adopted for all input parameters of the model constituting a basic case under which the adjustment of the computer programs will be performed. Note that, in this table, I have also included an initial estimation of the operational parameters, which will be changed later during the execution of the adjustment tests that follow.

Figure 5.1 — Procedure for adjustment of the computer programs.

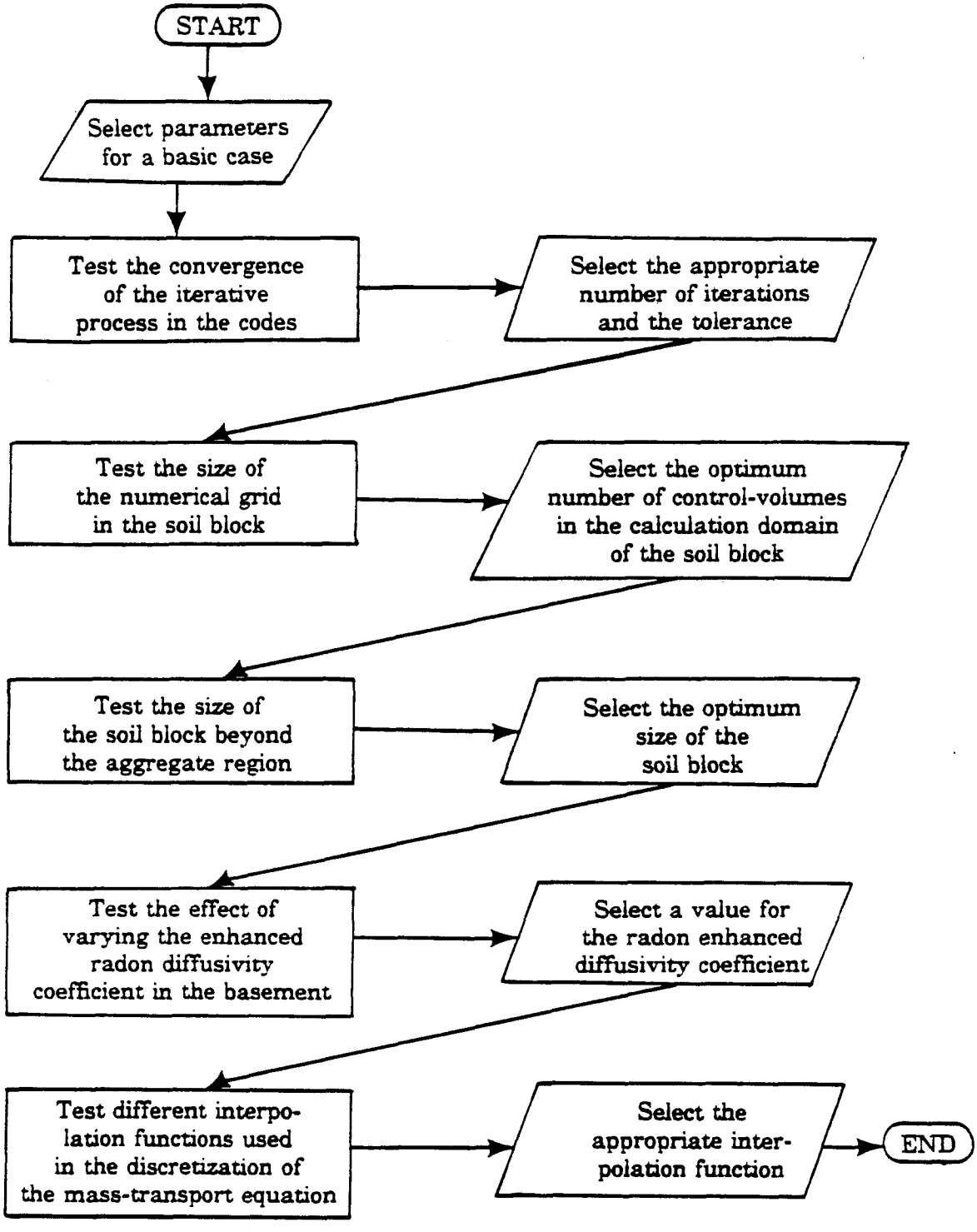

Table 5.1 — Input parameters for the basic case used in the adjustment of the computer programs.

Parameter	Value	Unit	Remark
Delta pressure	5	Pa	
Air exchange rate	1.39×10^{-4}	s^{-1}	
Enhanced radon diffus. coef.	1.2×10^{-3}	m^2s^{-1}	Defined in Apdx.F
Soil permeability	1.0×10^{-12}	m^2	The aggregate
Bulk radon dif.coef. in soil	1.0×10^{-6}	m^2s^{-1}	regions are
Ra-226 conc. in soil part.	1.0×10^{-9}	$Ci.Kg^{-1}$	defined with
Soil porosity	0.5	-	the same
Radon emanating fraction	0.2	-	parameters
Soil particles density	2.65×10^{3}	$Kg.m^{-3}$	of the soil.
House dimensions:			See Fig.(2.1)
Basement area	$5\times5=25$	m^2	
Basement height	2	m	
Height of the house	3	m	
Width of the crack	1.0×10^{-3}	m	
Size of the soil block	9.5	m	See Fig.(2.2)
Aggregate in the x-direction	0.5	m	
Aggregate in the y-direction	0.5	m	
Aggregate in the z-direction	0.5	m	
Definition of the grid:			Number of nodes
N_x1, N_x2, N_x3, N_x4, N_xAG	10, 1, 4, 8, 4	-	under each block
N_y1, N_y2, N_y3, N_y4, N_yAG	10, 1, 4, 8, 4	-	segment.
N_z1, N_z2, N_zAG	10, 8, 4	-	See Fig.(4.5).

Convergence Test of the Computer Programs.

As it was described in Chapter IV, one algebraic discretization equation, representing either the disturbance pressure or the radon concentration in the soil gas, was derived for each node of the grid in the three-dimensional calculation domain of the soil block. All together, these algebraic equations form a very large system whose solution by direct methods of linear algebra becomes impractical. An iterative method[1] was then adopted for solving the system. In this algorithm, at each iteration, the system is reduced to the equations representing only one line of grid nodes in the calculation domain, which is then solved using a tri-diagonal method based on the Thomas algorithm, [An84]. The values of the function at all the nodes in the block, except at those being calculated in the line, are assumed to be known either from the initial arbitrary assignment, or from the calculation of the previous iteration. After all nodes of the grid are calculated, a new iteration cycle then begins, and the process is repeated indefinitely until either; 1) the maximum allowed number of iterations are performed; or 2) the maximum change occurring at any node of the grid in the soil block becomes lower than the adopted tolerance limit; or 3) the maximum change of the variable representing the boundary conditions at the soil-crack interface becomes lower than the adopted tolerance limit. It is expected that the process converges, leading to a fixed (a finite) value of the function at all nodes of the grid. It is also expected that the values at which the computer programs converge represent the solution of the algebraic discretization equations.

Therefore, the concept of convergence as applied here, is related to the expectation that the programs converge to a finite value, and this is what is going to be determined in this present test. It is assumed that if the programs were written correctly,[2] with the proper implementation of the numerical method, and if the calculations of the computer programs converge to finite values of both the distribution of the variable in the soil, as well as the boundary conditions at the soil-crack interface, then these finite values should also

---

[1] This iterative algorithm was defined in Chapter IV, item: general algorithm for handling the calculation in the numerical grid.

[2] It should be noted here that the subroutine TRIDIM - the routine that solves the lines of the grid using the Thomas algorithm - was tested in a simplified problem of heat flow in a one-dimensional bar, as well as in a two-dimensional surface, and the results compared very well with the analytical solution.

represent the solution of the algebraic discretization equations of the numerical model. This assumption could also be described with the following mathematical argument. Suppose that: 1) A is the matrix of the discretization coefficients of all grid nodes in the calculation domain; 2) X is the matrix of the values of the function at all grid nodes; and 3) B is the matrix of the source-sink terms and boundary conditions. Then, the whole system of algebraic discretization equations could be represented by the matrix equation $AX = B$. Note that A is invariable, but X and B vary at each iteration. Now, consider two consecutive iterations $i-1$ and i, where the system of equations is expressed as $AX_{i-1} = B_{i-1}$ and $AX_i = B_i$, respectively. Then subtracting one from the other, yields $A(X_i - X_{i-1}) = B_i - B_{i-1}$, or $A\Delta X_i = \Delta B_i$. Therefore, if in the iterative routine of the computer program, both ΔX_i and ΔB_i converge to zero as the number of iterations increases, then it is possible to conclude that: 1) the solution matrix X and the source-sink and boundary conditions matrix B are both converging to a finite value; 2) the variation of the residual $\Delta R_i = A\Delta X_i - \Delta B_i$ is converging to zero, and consequently the residual $R = AX - B$ is converging to a finite value; and 3) the iterative routine is evaluating the system of equations $AX = B$ correctly.

In order to test the convergence of the computer programs I let them run with a large number of iterations, and a very low tolerance limit. Then, the variations of the values of some selected indicators at each iteration, as compared with the values in the previous iteration, were plotted as a function of the iteration number. The indicators selected for testing the program PRESSU were the maximum variation of the disturbance pressure at any point in the soil block, and the maximum variation of the soil gas velocity occurring at any point at the soil-crack interface. For the program MASTRA the indicators of convergence were the maximum variation of radon concentration at any point in the whole soil block, and the maximum variation of the radon flux at any point at the soil-crack interface.

The results of the convergence test for the program PRESSU representing, at each iteration, the maximum variation of: 1) the pressure at some critical point in the soil block; 2) the soil gas velocity at some point at the soil-crack interface, are shown in Fig.(5.2), parts A and B respectively. It should be noted that both the pressure and the soil gas velocity

differences were expressed in their dimensionless units. Since what is important in this test is to consider the relative variation of these variables as the program proceeds in its iterative cycle, the use of the dimensionless units is perfectly acceptable. So, in Fig.(5.2) it is possible to observe that the pressure and soil gas velocity distributions calculated by PRESSU changed very rapidly during the first one hundred iterations, when the program then leveled off, approaching asymptotically the condition of negligible variation from one iteration to the next one. After the 200th iteration the maximum variation of pressure was lower than 5.0×10^{-5}, and the maximum variation of the soil gas velocity was lower than 1.5×10^{-3}. This suggests that, in fact, the iterative procedure in PRESSU converges to a finite result, leading to the actual solution of the algebraic discretization equation of the model. From the results shown in Fig.(5.2), I have adopted the number 200 as the maximum allowed number of iterations in the program PRESSU.

Fig.(5.3) shows the results of the convergence test for the program MASTRA, where the maximum variation of the radon concentration in soil, and the maximum variation of the radon flux through the crack are plotted against the iteration number. Dimensionless units are again used here. Comparing Fig(5.3) with Fig.(5.2) we can see that the program MASTRA converges much faster than PRESSU. This result should be expected since the velocity distribution of the soil gas throughout the soil block, which is used as an input parameter to the convective-diffusive radon transport equation in MASTRA, was already calculated in PRESSU. According to Fig.(5.3), the iterative process in MASTRA reached a plateau after the 80th iteration. Maximum variations of radon concentration in the soil, and radon flux at the soil-crack interface after the 100th iteration were lower than 1.5×10^{-6}, and 2.0×10^{-3} respectively. Based on these results I have adopted a maximum number of iterations in MASTRA of 100.

Therefore, it is possible to conclude from this test that the iterative procedure of both programs converges to a finite value, with the convergence of MASTRA being faster than in PRESSU.

Figure 5.2 — Convergence of the program PRESSU.

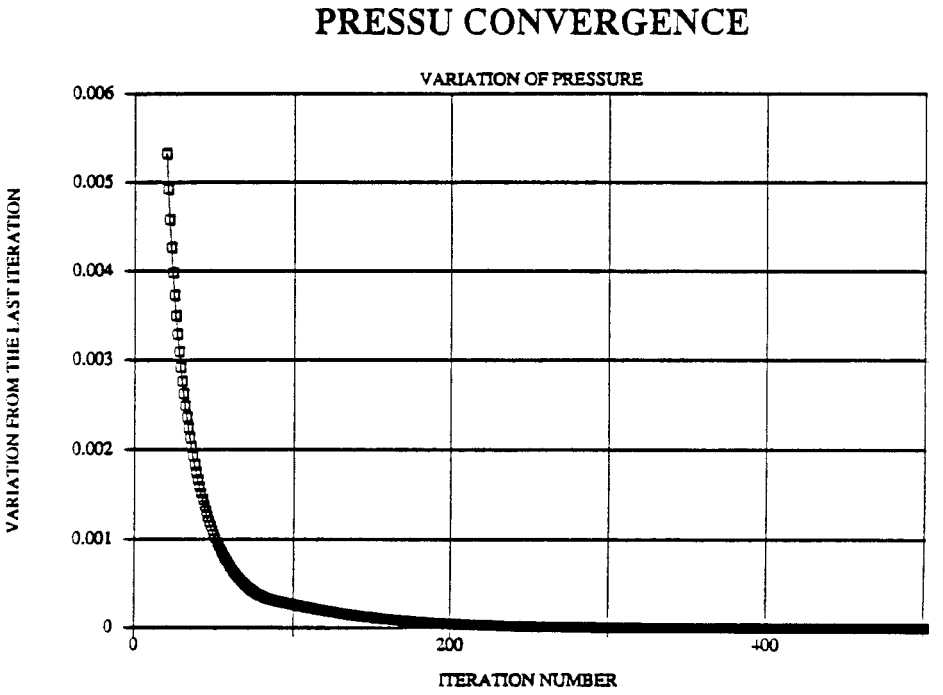

(A) - Maximum variation of disturbance pressure at a node within the soil block, for each iteration of PRESSU. (Pressure given in dimensionless units).

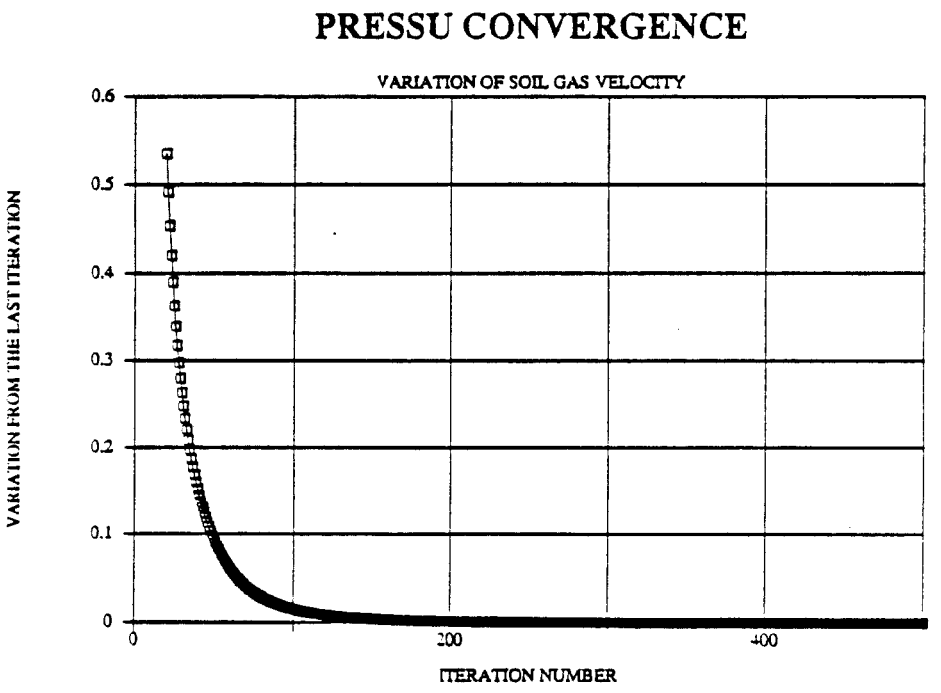

(B) - Maximum variation of the soil gas velocity at a node at the soil-crack interface, for each iteration of PRESSU. (Velocity given in dimensionless units.)

Figure 5.3 — Convergence of the program MASTRA.

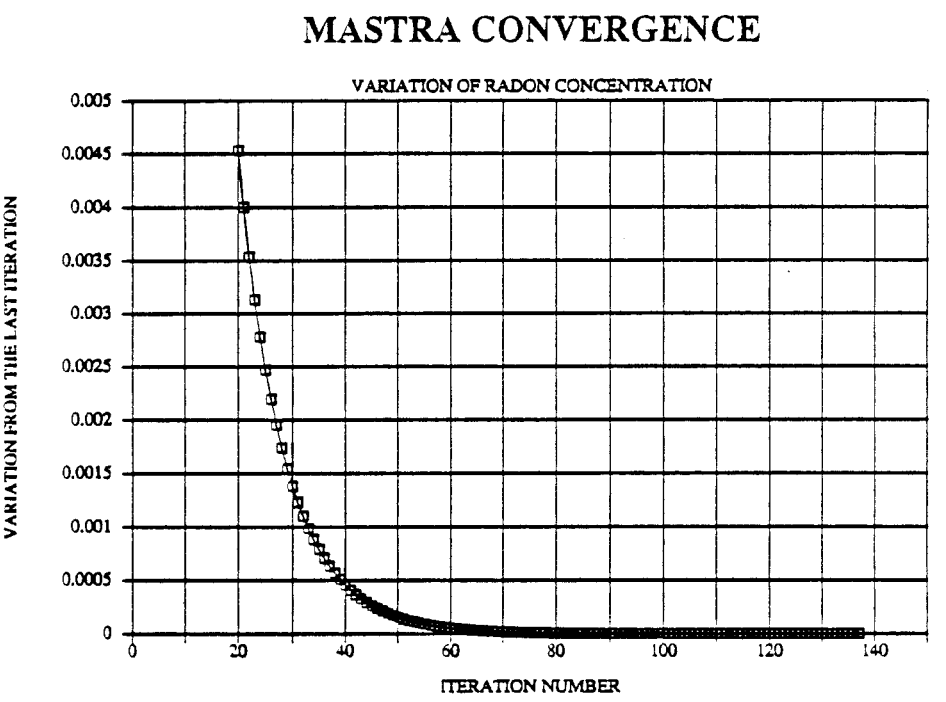

(A) - Maximum variation of the radon concentration at a node within the soil block, for each iteration of MASTRA. (Radon concentration given in dimensionless units).

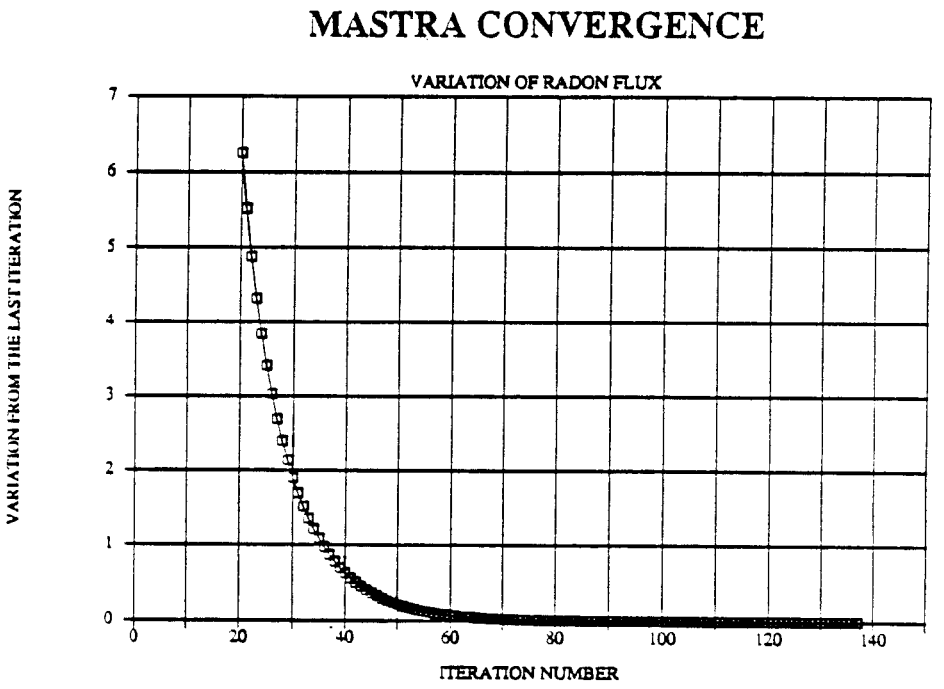

(B) - Maximum variation of the radon flux at a node at the soil-crack interface, for each iteration of MASTRA. (Radon flux given in dimensionless units.)

Test of the Size of the Numerical Grid.

The objective here is to test the effect that the size of the numerical grid has on the output of the programs PRESSU and MASTRA. It is expected that, in reducing the grid size, the discretization error of the numerical method is also reduced and consequently the solution of the algebraic discretization equations approximates the actual solution of the differential equations of the model. The ideal situation would be to have a very fine grid in order to reduce the discretization error to a minimum. However, the memory size available in the computer, as well as the CPU time involved, impose a practical limitation for the size of the numerical grid.

Thus, in order to test how the computer model responds to variations in the grid size, I have compared five cases with numerical grids of increasing size. In Table (5.2) I describe for each example case, the number of nodes assigned for the defined segments of the soil block, at the x, y, and z directions. Reference to the notation of these defined segments of the soil block is presented in Fig.(4.5) of the last chapter. The total number of nodes assigned for each run of the programs ranged from $2,535$ in the first case, to $24,389$ in the last one. Numerical grids larger than this last one could not be employed because of the computer memory available.[3]

The results of this test will be compared by observing two indicators: 1) the average velocity of the soil gas at the soil-crack interface; b) the average flux of radon at the same location. The calculated averages in both cases were weighted to the sizes of the respective control-volumes at each node. Table (5.3) shows the results. Since we are interested in observing relative variations of the indicator variables, dimensionless units were used.

Fig.(5.4) shows: in part (A), the variation of the average soil gas velocity at the crack interface; and in part (B), the variation of the average flux of radon at the same location, for each defined case of grid size. Although the number of cases is small, and the size of

[3] The use of PRESSU and MASTRA , with a numerical grid of 25,000 nodes requires an allocation of about 5.5 megabytes of computer virtual memory. The computers in which these programs were run (Amdahl-5860, and VAX-8600), did not accepted a run of the programs with a grid size larger than about 25,000 nodes.

Table 5.2 — Distribution of control-volumes in the calculation domain of the soil block, for five different cases which will be used for testing the size of the numerical grid.

Segments of the soil block*	Example Case #				
	1	2	3	4	5
	Number of control-volumes				
In the x–direction:					
N_x1	4	6	6	8	10
N_x2	1	1	1	1	1
N_x3	2	4	4	4	4
N_x4	4	6	6	8	10
N_xAG	2	2	4	4	4
Total in the x–direction	13	19	21	25	29
In the y–direction:					
N_y1	4	6	6	8	10
N_y2	1	1	1	1	1
N_y3	2	4	4	4	4
N_y4	4	6	6	8	10
N_yAG	2	2	4	4	4
Total in the y–direction	13	19	21	25	29
In the z–direction:					
N_z1	4	6	6	8	10
N_z2	4	6	6	8	10
N_zAG	2	2	4	4	4
(Extra nodes)	5	5	5	5	5
Total in the y–direction	15	19	21	25	29
Total Number	2,535	6,859	9,261	15,625	24,389

* – For the appropriate notation, and location of these segments in the soil block, see Fig.(4.5).
– Note that the physical dimensions remain the same.

Table 5.3 — Test of the size of the numerical grid.

Case #	Average Soil-Gas Velocity at the Soil-Crack Interface. [Dimensionless]	Average Radon Flux at the Soil-Crack Interface. [Dimensionless]
1	−39.61	−42.83
2	−48.09	−49.90
3	−50.33	−51.64
4	−51.27	−52.56
5	−51.65	−52.91

the largest grid is still relatively modest, it is possible to observe some asymptotic tendency on both curves, which suggests that the predictions of the computer model are converging to a finite result, which should be the actual solution of the differential equations of the model. Because of the limitation imposed by the available computer memory, we are forced to adopt the grid configuration represented in the case #5 as the default grid for the next applications of the model, and to consider the predictions under this circumstance as the best practicable approximation to the solution of the original differential equations.

Test of the Size of the Soil Block.

The objective of this test is to evaluate how the size of the soil block affects the output of the computer models, and then to select the most appropriate size to be used as a default value in subsequent simulations.

As it was described in Chapter III, the boundary condition of no flow[4] imposed on the external surfaces, and the bottom, of the soil block requires that those surfaces be located far away from the crack - the center of disturbance for the system. So, considering only the aspect of enforcing the boundary conditions on those surfaces, it would be advisable to make the soil block as large as possible. However, since the size of the numerical grid is limited by the available computer memory, then the increase in the block size implies

[4] The boundary conditions were listed in Tables (3.1) and (3.2).

Figure 5.4 — Effect of the numerical grid size on the performance of PRESSU and MASTRA.

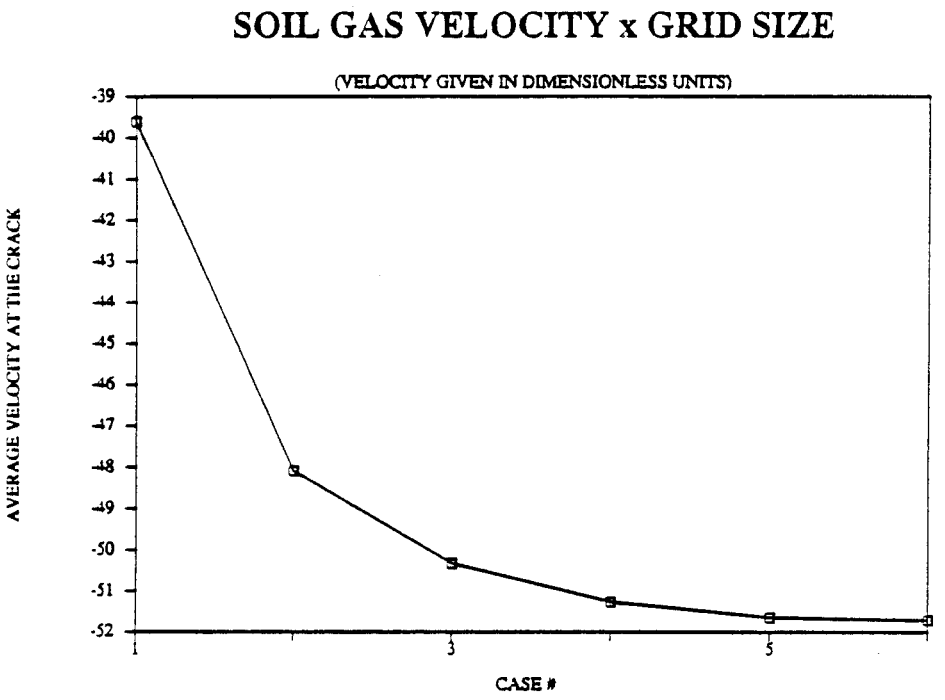

(A) - Variation of the average soil gas velocity at the soil-crack interface, for different sizes of the numerical grid. (See Table (5.3)).

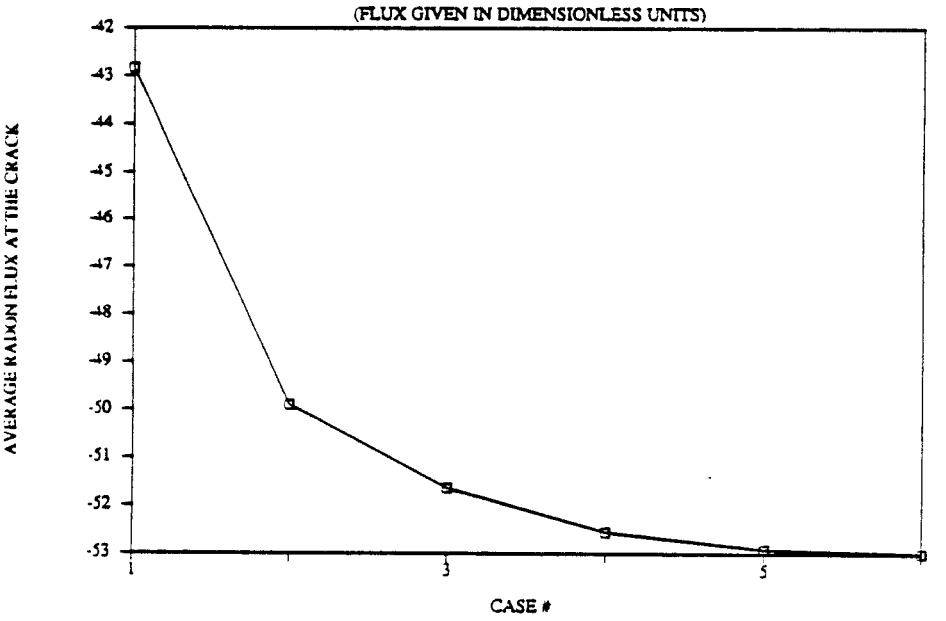

(B) - Variation of the average radon flux at the soil-crack interface, for different sizes of the numerical grid. (See Table (5.3)).

an increase of the control-volume sizes, resulting in a coarser grid, and consequently in a larger discretization error of the numerical calculation. Therefore, the selection of a size for the soil block is determined by a compromise between the enforcement of the boundary conditions on the external surfaces of the soil block, and the approximation of the numerical method.

In order to perform this test, I have run six cases where the thickness of the soil layer beyond the aggregate regions around the basement varied from 1 to 25 meters. As indicators I have observed the same variables used in the last test. They are: 1) the average velocity of the soil gas; and 2) the average flux of radon at the soil-crack interface. The results of this test are grouped in Table (5.4), and plotted in Fig.(5.5). As we can see, for small sizes of the soil block - lower than $10[m]$ - the boundary condition is not well justified and consequently the performance of the computer model, as measured by the soil gas velocity and the radon flux at the soil-crack interface, is clearly altered by variations in the thickness of the soil layer. Between the range of 10 to 25 $[m]$ of soil thickness, only a very small effect could be observed on those variables, which indicates that the increase in the grid coarseness within this range, and in that particular region of the soil block, is not significantly affecting the output of the program.

Table 5.4 — Test of the size of the soil block.

Thickness of the Soil Layer $[m]$	**Average Soil-Gas Velocity at the Soil-Crack Interface [Dimensionless]**	**Average Radon Flux at the Soil-Crack Interface [Dimensionless]**
1	−45.21	−47.49
5	−51.12	−52.50
10	−51:72	−52.99
15	−51.79	−53.05
20	−51.78	−53.04
25	−51.76	−53.01

Based on these results I have adopted a thickness of $10[m]$ as the default value for the soil block, which represents the beginning of the plateau shown in Fig.(5.5). The starting point of the plateau should satisfy the boundary conditions imposed on the external surfaces of the block easily well, and at the same time should provide, for a fixed grid size, the lowest grid spacing within the soil block.

Test of the Enhanced Radon Diffusivity Coefficient in the Air of the Basement.

The solution of the radon transport equation in the soil block requires the definition of not only the boundary conditions described in Table (3.2), but also the specification of the boundary conditions imposed on the radon concentration and on the radon flux at the exit of the crack, or more specifically at the interface between the crack and the basement.

As an approach for dealing with this problem I have proposed, in Appendix F, a configuration in which the radon diffusion coefficient in the basement, because of the turbulent mixture of air inside the house, is much larger than the radon diffusion coefficient in the air inside the crack. This newly adopted parameter in the model was then called the enhanced radon diffusion coefficient in air - D_o'. The idea here is that the transport of radon inside the basement should be totally dominated by the turbulent mixing of air, and completely independent of the velocity of the soil leaving the crack into the basement. The problem now is how to specify a value for this parameter. Since no specific reference to the subject has been found in the literature I have considered the enhanced radon diffusion coefficient in the air as another operational parameter of the computer model which should then be adjusted to represent as close as possible the idealized configuration. As described above the idealized configuration consists of a house with well mixed air such that the turbulent diffusion dominates the transport of radon in the air inside the basement. So, the criterion for adjusting the model for this particular parameter is to select the minimum value that makes the turbulent diffusion in the air the dominant transport mechanism.

Thus, the purpose of this test is to observe the effect on the performance of the model as we adopt different values for the enhanced radon diffusion coefficient. Also, it is expected

Figure 5.5 — Effect of the size of the soil block on the performance of PRESSU and MASTRA.

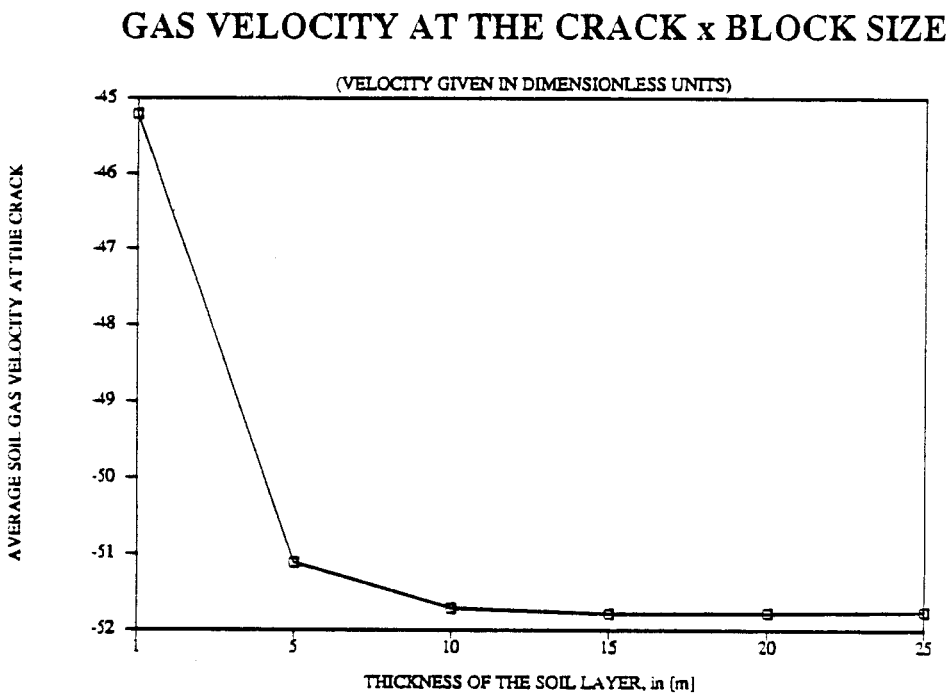

(A) - Variation of the average soil gas velocity at the soil-crack interface, for different thickness of the soil layer around the house. (See Table (5.4)).

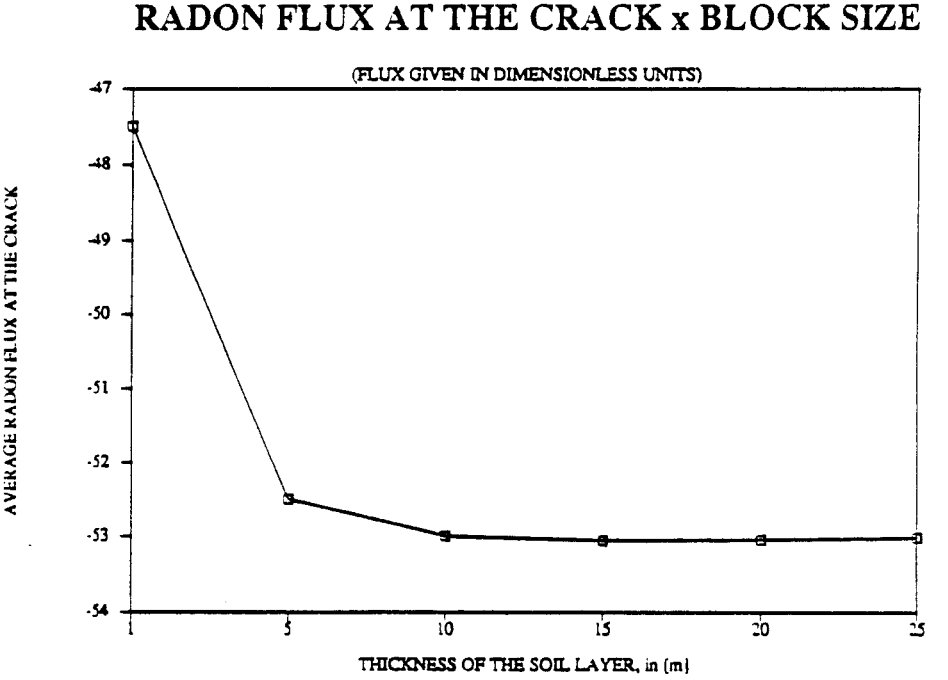

(B) - Variation of the average radon flux at the soil-crack interface, for different thickness of the soil layer around the house. (See Table (5.4)).

Table 5.5 — Test of the enhanced radon diffusivity coefficient.

Case #	Enhanced Radon Diffusivity Coef. $[m^2 s^{-1}]$	Average Radon Flux at the Crack Interface [Dimensionless]	Average Radon Conc. at the Crack Interface [Dimensionless]
1	1.2×10^{-5}	−48.97	0.9435
2	1.2×10^{-4}	−49.57	0.9405
3	1.2×10^{-3}	−51.72	0.9217
4	1.2×10^{-2}	−60.46	0.8807
5	1.2×10^{-1}	−66.33	0.8485
6	1.2×10^{0}	−68.96	0.8340
7	1.2×10^{1}	−69.90	0.8289
8	1.2×10^{2}	−70.21	0.8272
9	1.2×10^{3}	−70.31	0.8266
10	1.2×10^{4}	−70.34	0.8259

that at the end of the test, a value of this parameter will be selected to best represent the condition of well mixed air in the basement of the house.

In order to perform this test I have run 10 cases with the values of the enhanced radon diffusion coefficient starting with the value of radon diffusion coefficient in air, $(1.2\times10^{-5}[m^2/s])$, and spanning a range of ten orders of magnitude, from 1.2×10^{-5} to $1.2\times10^{4}[m^2/s]$. As indicators I have selected the average radon flux, and the average radon concentration in soil gas at the soil-crack interface. The results of the test are grouped in Table (5.5) and plotted in Fig.(5.6). Note that, since the selected range of D_o' is so large, this parameter was plotted in a logarithmic scale. The other variables were plotted with their dimensionless units, in a linear scale.

As we can see in Fig.(5.6), the change of the enhanced radon diffusion coefficient clearly affects the performance of the model, up the the point where D_o' is between 1.2×10^{0} to $1.2\times10^{1}[m^2/s]$, where the predictions from the model start leveling off. Values of D_o' above this level have very little effect on the model's predictions. These results then suggest that a figure around $1.2[m^2/s]$ would be the minimum value of the enhanced radon diffusion

coefficient characterizing a configuration of turbulent mixing of the air inside the house. Therefore, I have adopted the value for the enhanced radon diffusion coefficient as $1.2[m^2/s]$, which is five orders of magnitude larger than the radon diffusion coefficient in air.

Measurements of vertical turbulent diffusion coefficients in the atmosphere have been published in the literature, and could be used here for comparison with the results obtained above. Servant [Se66] measured the vertical profile of radon concentration in the lower atmosphere, between 0 and 100 meters, and calculated the mean coefficient of vertical turbulent diffusion of radon in this layer of the atmosphere. According to his results, the coefficient varied from 10^{-2} to $10^{2}[m^2/s]$, depending on the stability of the lower atmosphere. Stable conditions showed coefficients in the first half of the range, with the other half being observed in unstable conditions. Values of coefficients below $10^{-1}[m^2/s]$ were observed only during extremely stable atmospheric conditions.

Although there are clear differences between the radon transport mechanisms in the lower atmosphere, and in the indoor air, it would still be reasonable to assume that the radon diffusion coefficient in the air of a house with well mixed air indoors would be within the range of typical vertical turbulent diffusion coefficients, measured in the atmosphere at different stability conditions. Therefore, the adoption of a value for D_o' equal to $1.2[m^2/s]$, which is right in the middle of the range of vertical turbulent diffusion coefficient in the atmosphere as reported by Servant, would be justifiable. It should be emphasized though, that the selection of a value of the enhanced radon diffusion coefficient, D_o', equal to $1.2[m^2/s]$ reflects the intention of characterizing the house as a well mixed chamber, as far as the indoor air condition is concerned. In modeling other configurations of poorer mixing conditions of the indoor air, a lower value of D_o' should be used for the adjustment of the computer programs.

Test of the Interpolation Function.

The numerical method adopted in this thesis for transforming the radon transport differential equation into its correspondent algebraic system of discretization equations used a defined interpolation function to interpolate the value of the variable – radon concentration

Figure 5.6 — Effect of the enhanced radon diffusion coefficient on the performance of the computer model.

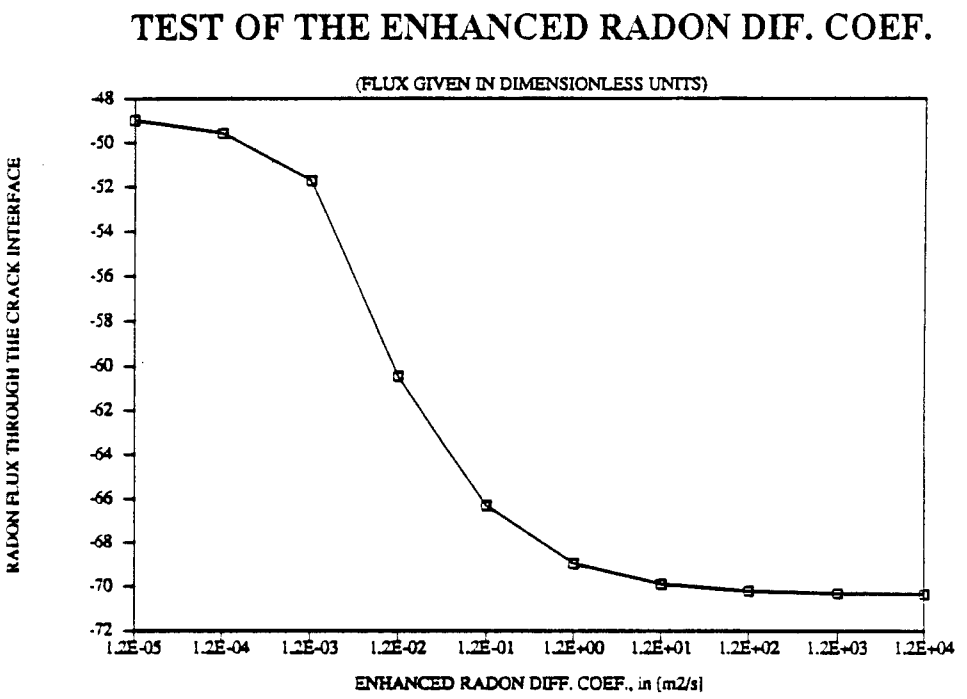

(A) - Variation of the average radon flux at the soil-crack interface, as a function of the enhanced radon diffusion coefficient. (See Table (5.5)).

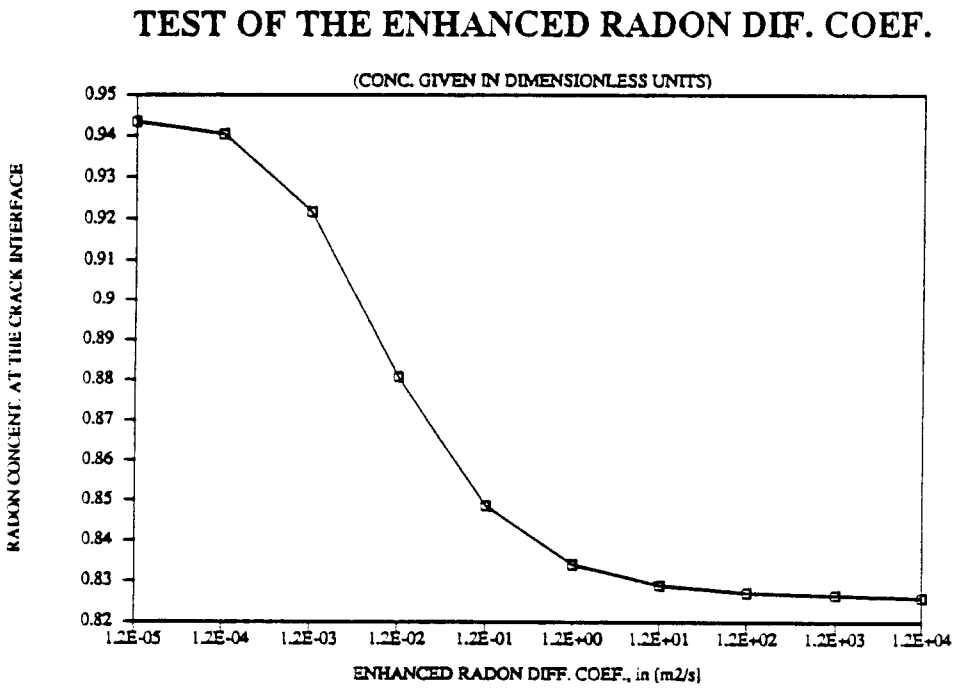

(B) - Variation of the radon concentration at the soil-crack interface, as a function of the enhanced radon diffusion coefficient. (See Table (5.5)).

in soil gas - at the interface of consecutive control-volumes in the soil block. The whole method was described in detail in Appendix I. Several different interpolation schemes were then suggested as possible alternatives to be used in the discretization method, including: central difference; upwind; hybrid; and the power law scheme.[5]

So, the purpose of this test is to investigate how the choice of a particular discretization function, among those already suggested, would affect the performance of the computer program. Note that since the radon transport equation is solved in MASTRA, the changes of the interpolation function will affect only that particular program. Thus, in order to perform this test, MASTRA was run with different interpolation functions, and the results grouped in Table (5.6). The indicators were, again, the average radon flux and the radon concentration at the soil-crack interface. As we can see, there was no significant variation on the model's predictions, which means that, for this particular configuration of soil and house parameters, the choice among those proposed interpolation schemes does not affect the performance of the computer program. However, for other soil-house configurations, especially for cases of high soil permeability, or high disturbance pressures, where the flow of soil gas through the soil and the crack is higher, the choice of the interpolation function is still expected to affect the model's prediction. Yet, the investigation of the effect of the interpolation function was not extended to those cases. In the original derivation of the discretization method, Patankar [Pa80] recommended the power law function as the best formulation for the interpolation scheme. Therefore, even though I have not observed any significant difference in the results when using the other alternatives, the power law function will be adopted as the default interpolation scheme in MASTRA.

Sensitivity Analysis of the Computer Model.

After the codes have been adjusted, making sure that: 1) the iterative process converges; 2) the soil block size is the minimum value in which the boundary conditions are still valid; 3) the grid mesh size is the optimum value; 4) and that the enhanced radon diffusion coefficient and the interpolation functions are selected appropriately, we proceed with the

[5] See Table (I.1) where the interpolation functions relative to these schemes are defined.

Table 5.6 — Test of the interpolation function.

Interpolation Function	Average Radon Flux at the Soil-Crack Interface [Dimensionless]	Average Radon Concentration at the Soil-Crack Interface [Dimensionless]
Central Difference	−52.99	0.9217
Upwind	−52.98	0.9213
Hybrid	−52.99	0.9217
Power Law	−52.99	0.9217

sensitivity analysis. The objective now is to verify how sensitive the model is to variations introduced to each one of its input parameters, individually, when all other parameters are kept constant. In doing so, we expect to get a better knowledge of the behavior of the model.

The parameters forming the base case which underlies the execution of the sensitivity analysis are presented in Table (5.7). The following variables were selected for the sensitivity analysis:

- Size of the house;
- Disturbance pressure applied in the basement;
- Size of the crack;
- Permeability of the soil.

These variables influence the distribution, in the soil block, of the disturbance pressure and the soil gas velocity , as well as the radon concentration, and consequently will affect the output of both programs PRESSU and MASTRA. Besides the variables listed above, there are others that will affect only the radon concentration distribution in the soil (MASTRA output), and should also be included in the sensitivity analysis. They are the following:

- Bulk diffusion coefficient of radon in soil;
- Soil porosity.

A list of these parameters, with typical values and expected range of variability is presented

Table 5.7 — Input parameters for the basic case, used in the sensitivity analysis of the computer programs.

Parameter	Value	Unit	Remark
Air exchange rate	1.39×10^{-4}	s^{-1}	
Enhanced radon diffusivity coef.	1.2	m^2s^{-1}	
Iteration Procedure :			
Maximum Iteration in PRESSU	200	-	
Maximum Iteration in MASTRA	100	-	
House dimensions:			See Fig.(2.1)
Basement area	$10\times15=150$	m^2	
Basement height	2	m	
Height of the house	3	m	
Size of the soil block	10.0	m	See Fig.(2.2)
Basement area	0.5	m	
Basement height	0.5	m	
Height of the house	0.5	m	
Definition of the grid:			Number of nodes
N_x1, N_x2, N_x3, N_x4, N_xAG	10, 1, 4, 8, 4	-	under each block
N_y1, N_y2, N_y3, N_y4, N_yAG	12, 1, 4, 8, 4	-	segment.
N_z1, N_z2, N_zAG	10, 8, 4	-	See Fig.(4.5).

in Table (5.8). Thus, in the sequence of tests that follows, each one of these parameters is assigned a typical value as listed in Table (5.8). Then each parameter is varied within its expected range, and the predictions of the computer model are analyzed.

Sensitivity Analysis of the Computer Model - Size of the House.

Variations with the size of the house could affect the model's predictions in a few aspects. First, because of the limitation related to the available computer memory, I have established

Table 5.8 — Range and typical values of the parameters used in the sensitivity analysis of the computer programs.

Parameter	Typical Value	Range	Unit	Reference
Delta Pressure	5	0 – 20	Pa	[Ea84]
Width of the Crack	1×10^{-3}	$(0.5 - 10.0)\times10^{-3}$	m	Author's Assumption
Soil Permeability	1×10^{-12}	$10^{-14} - 10^{-10}$	m^2	[Na85]
Bulk Diff. Coeff. of Radon in Soil	1×10^{-6}	$(0.5 - 5.0)\times10^{-6}$	m^2s^{-1}	[Na85]
Soil Porosity	0.5	0.4 – 0.6 0.43 – 0.54	– –	[Na85] [Sc74]
Ra-226 Concent. in Soil Particles	1×10^{-9}	$(0.2 - 4.0)\times10^{-9}$	$CiKg^{-1}$	[Na85]
Radon Emanating Fraction	0.2	0.05 – 0.7	–	[Na85]
Soil Particle Density	2.65×10^{3}	$(2.6 - 2.8)\times10^{3}$	Kgm^{-3}	[Na85]

a fixed numerical grid and, consequently, any variation in the house size or any physical dimension of the calculation domain will alter the grid spacing and the discretization error of the numerical method. Also, altering the size of the house, especially the area of the basement, will affect the amount of radon entering the house, and at the same time will affect the total volume in the house available for diluting the entering radon. Therefore, the indoor radon concentration will also be affected.

So, the purpose of this test is to verify how sensitive the computer model is to variations in the house size, more specifically to the variations in the basement area. The program was run four times with the basement area varying from 25 to 150$[m^2]$. The results representing

Table 5.9 — Sensitivity analysis of the computer programs - Variation of the basement area.

Basement Dimensions $[m \times m]$	Basement Area $[m^2]$	Average Radon Flux at the Crack Interface $[pCi.m^{-2}.s^{-1}]$	Average Radon Concent. at the Crack Interface [Dimensionless]	Indoor Radon Concent. $[pCi.l^{-1}]$
5×5	25	-52.94	0.8340	5.99×10^{-2}
7×7	49	-52.85	0.8350	4.27×10^{-2}
8×14	112	-52.69	0.8356	2.93×10^{-2}
10×15	150	-52.65	0.8356	2.48×10^{-2}

the average flux of radon and the radon concentration in soil gas at the crack interface, as well as the indoor radon concentration are grouped in Table (5.9), indicating that neither the radon flux nor the radon concentration at the crack interface has been affected significantly in these four cases. The whole range of the radon flux variation was lower than 0.6%, and the total variation of the radon concentration at the soil-crack interface was lower than 0.2%. Therefore, we can conclude that the variation of the basement area in the range observed, and the resultant variation of the grid spacing, does not affect the overall performance of the computer model in the soil block.

On the other hand, the final indoor radon concentration was reduced with the increase of the basement area, as expected. Since the width of the crack was kept constant, the increase in the basement area increases linearly the amount of radon entering the house. However, the volume for diluting the radon inside the house increases with the area of the basement. As a result, the increase of the basement area by a certain factor causes a decrease of the indoor radon concentration by the square root of that specific factor. The model's predictions confirm this. In the extreme cases, the basement area varied from 25 to $150[m^2]$, a six-fold increase. Correspondently, the indoor radon concentration decreased from 5.99×10^{-2} to $2.48 \times 10^{-2}[pCi/l]$, which is approximately a $\sqrt{6}$ decrease.

Sensitivity Analysis of the Computer Model – Variation of the disturbance pressure.

The shape of the spatial distribution of the disturbance pressure throughout the soil block, in a steady-state condition, is not affected by the value of the negative disturbance pressure applied at the basement. Yet, the absolute value of the pressure gradient at any point within the soil changes linearly with the applied disturbance pressure. Consequently, the seepage velocity of the soil gas through the soil will also changes linearly with the applied disturbance pressure according to Darcy's law, as expressed in Eq.(3.8). The increase of the soil gas velocity in the soil, which is directed toward to the crack, will bring a soil gas richer in radon from deeper in the soil block closer to the crack, increasing the radon concentration and at the same time reducing the radon concentration gradient at the soil-crack interface. The result, then, is an increase in the convective component of the radon flux through the crack, and a decrease of the diffusive component, with a net increase in the total flux of radon through the crack.

The objective of this test is to verify how the model responds to these effects as the applied negative disturbance pressure is varied within its expected range of variability. The test was performed running the programs five times with the applied disturbance pressure varying from practically zero (-1.0×10^{-6}) to $-20[Pa]$. The observed variables were: the average soil gas velocity; the average radon concentration in soil gas; and the average radon flux at the soil-crack interface; as well as the indoor radon concentration. The results are grouped in Table (5.10), and plotted in Figs. (5.7) and (5.8).

As we can see in Fig.(5.7), the average velocity of the soil gas at the soil-crack interface was negligible for a very small pressure, and increased linearly with the increase of the applied disturbance pressure, as expected. Also, the radon concentration at the crack interface responded positively to the increase of the delta pressure, showing a tendency to level off as the pressure reached its upper end of the range. In reality, the variation of the radon concentration in the soil gas at the soil-crack interface is expected to increase with the applied pressure up to a certain point where the contribution from poorer radon soil gas from regions of the soil closer to the top surface would tend to increase, causing the

Table 5.10 — Sensitivity analysis of the computer programs – Variation of the disturbance delta pressure.

Disturbance Delta Pressure $[Pa]$	Average Velocity of the Soil Gas at the Crack $[m.s^{-1}]$	Average Radon Concentration at the Crack [Dimensionless]	Average Flux of Radon at the Crack $[pCi.m^{-2}.s^{-1}]$	Indoor Radon Concent. $[pCi.l^{-1}]$
-1×10^{-6}	-1.00×10^{-11}	0.7597	-30.71	1.45×10^{-2}
-1	-1.47×10^{-5}	0.7768	-34.53	1.63×10^{-2}
-5	-7.36×10^{-5}	0.8356	-52.65	2.48×10^{-2}
-10	-1.47×10^{-4}	0.8868	-80.91	3.82×10^{-2}
-20	-2.94×10^{-4}	0.9310	-148.32	7.00×10^{-2}

dilution of radon concentration at the crack interface. However, the range of the disturbance pressure analyzed here, together with the value of soil permeability assumed in this test, was not enough to show this effect in this test. In the next test, with the variation of the soil permeability in a large range, this effect will be clearly demonstrated.

In Chapter III, the total bulk flux of radon throughout the soil matrix was described as being composed of two terms: the convective component, equal to the product of the seepage velocity of the soil gas times the concentration of radon in the soil gas; and the diffusive component, equal to the negative product of the bulk diffusion coefficient of radon in the soil matrix times the gradient of the radon concentration in the soil gas. Thus, multiplying the first two columns of Table (5.10) we can calculate the average convective flux, which subtracted from the average total flux in column 3, will give us the average diffusive component of the radon flux at the soil crack interface. Then, plotting these flux components together, we can observe the variation of the average radon flux, and its components, as a function of the applied disturbance pressure. (See Fig.(5.8)).

With no applied disturbance pressure, the velocity of the soil gas is zero and the flux of radon is reduced to its diffusive component. Then, progressively, as the the pressure in-

Figure 5.7 — Sensitivity analysis of the numerical model - Variation of the applied disturbance pressure. (Part 1).

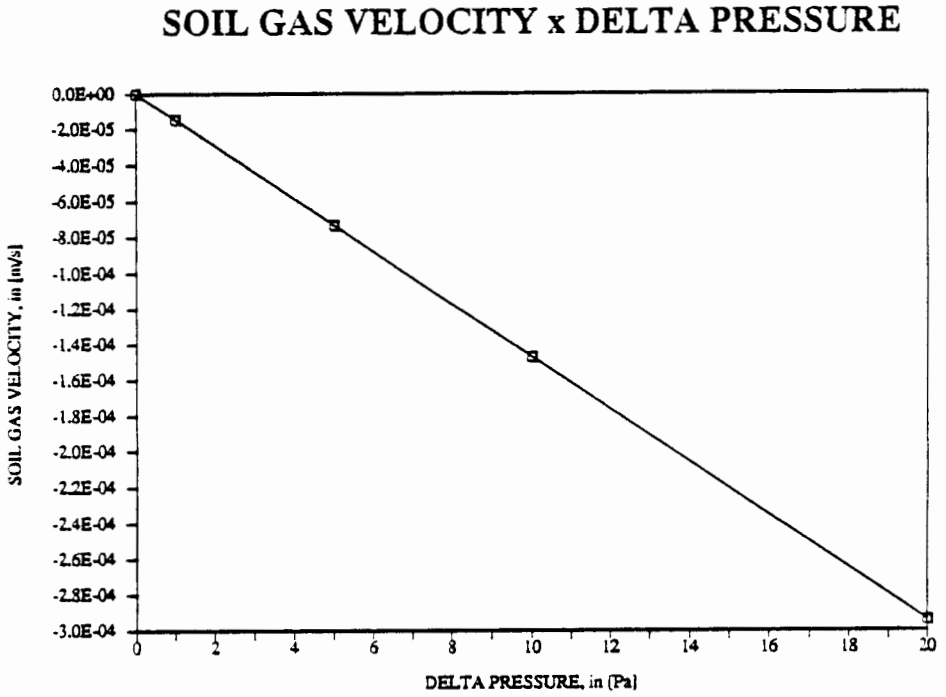

(A) - Average soil gas velocity at the soil-crack interface as a function of the applied disturbance pressure.

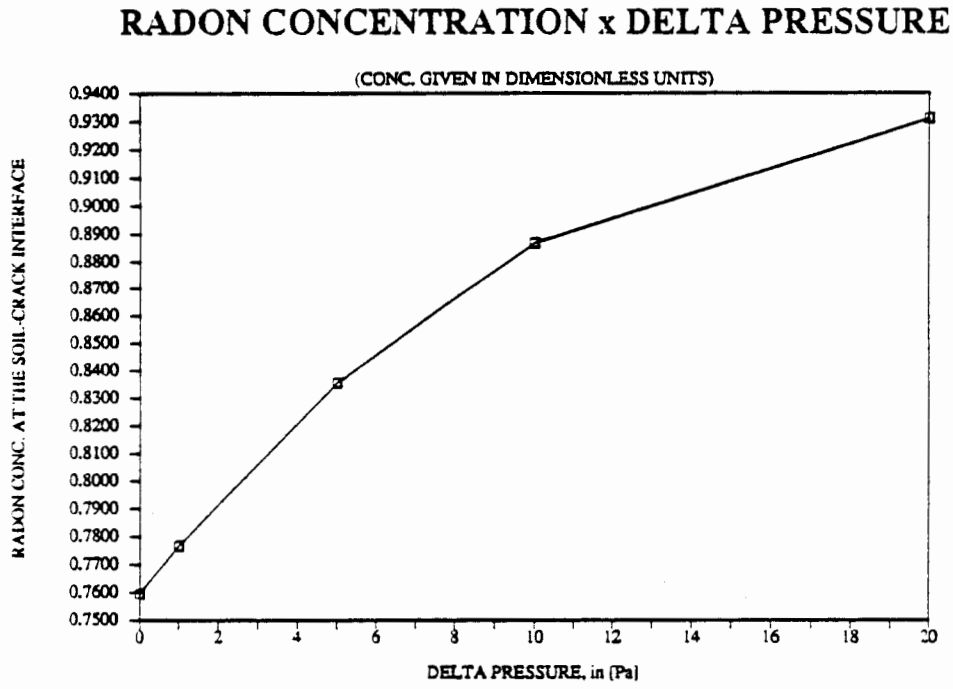

(B) - Average radon concentration in soil gas at the soil-crack interface as a function of the applied disturbance pressure.

Figure 5.8 — Sensitivity analysis of the numerical model - Variation of the applied disturbance pressure. (Part 2).

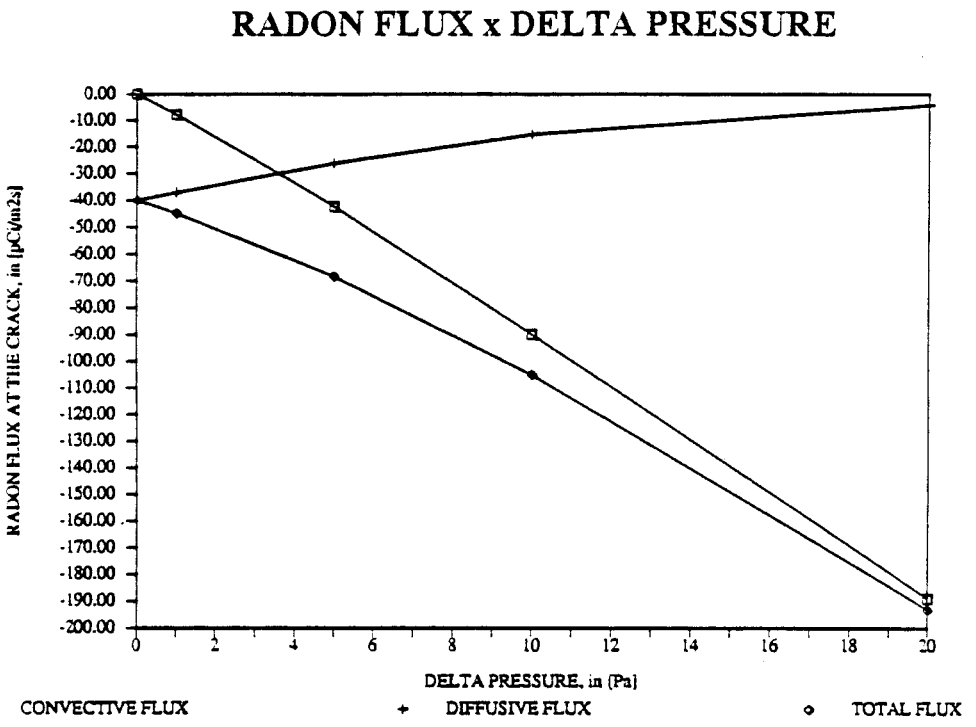

(A) - Diffusive and convective components of the average radon flux at the soil-crack interface as a function of the applied disturbance pressure.

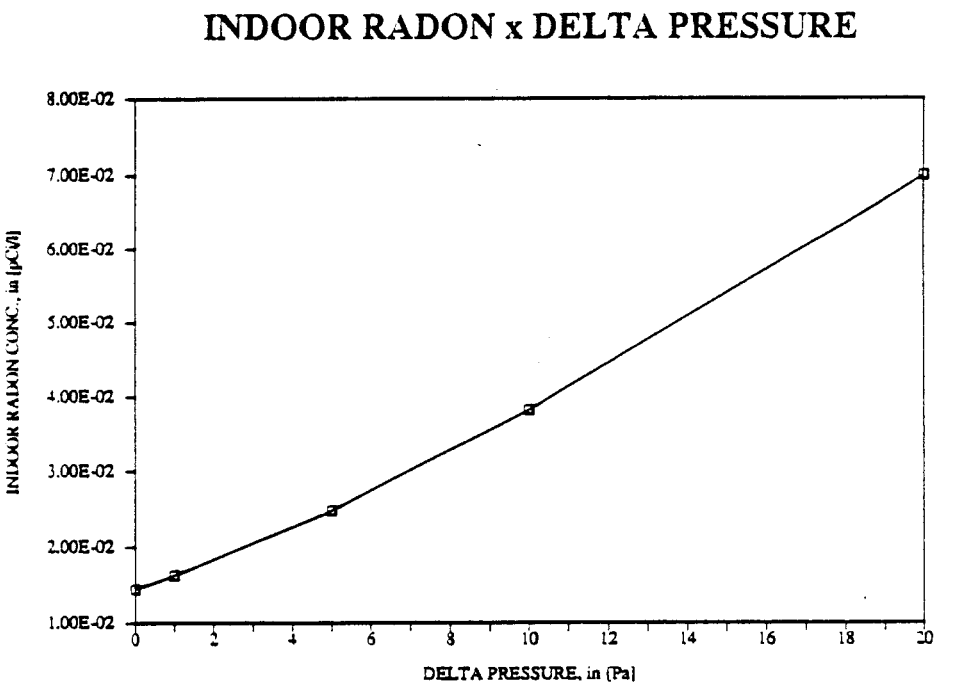

(B) - Indoor radon concentration as a function of the applied disturbance pressure.

creases the diffusive component of the flux decreases slowly while the convective component increases very rapidly (almost linearly with the pressure) and becomes, in the middle of the disturbance pressure range, the dominant component of the total flux. Therefore, for this particular configuration of soil permeability ($1.0\times10^{-12}[m^2]$), and radon bulk diffusion coefficient ($1.0\times10^{-6}[m^2/s]$), the flux of radon through the crack is dominated by the convective component, for applied disturbance pressures above $4[Pa]$. Note that for a configuration of soil with larger permeability, and approximately unchanged radon diffusion, the same pressure range would have caused a larger soil gas velocity variation and consequently the convective component of the radon flux would have dominated the total flux at an applied disturbance pressure lower than $4[Pa]$. The reversed effect should also be expected, that is, with a lower soil permeability, the convective component would only predominate, if ever, at pressures well above $4[Pa]$. More of these effects will be shown with the test of the soil permeability.

The indoor radon concentration, as we can see in Fig.(5.8B), also responded positively to the applied disturbance pressure, although not linearly. With the present value of the soil permeability, ($1.0\times10^{-12}[m^2]$), an increase of the delta pressure from almost zero to $-20[Pa]$, caused the indoor radon concentration to increase from 1.45×10^{-2} to $7.0\times10^{-2}[pCi/l]$, about a 4.8-fold increase. With a higher soil permeability, the same increase in delta pressure, would have caused a higher increase in the convective flow of radon into the house, and consequently the indoor radon concentration would have increased by a factor higher than 4.8. The inverse of this effect should also be expected.

Sensitivity Analysis of the Computer Model – Variation of the soil permeability and the crack width.

The flow of soil gas throughout the soil and into the crack is basically dependent on the distribution of the disturbance pressure in the soil and crack, and on the resistance that the soil and crack offer to the transport of the soil gas. The total resistance to the flow of soil gas from the soil into the house can be considered as a sum of two terms – the soil resistance and the crack resistance – which are, both, functions of the geometrical configuration of the

house and the physical properties of the medium. The crack resistance to the soil gas flow increases with the the depth of the crack as well as with the dynamic viscosity of the air, and decreases with the width of the crack. On the other hand, the resistance of the soil increases with the depth of the basement and the viscosity of the soil gas, and decreases with the width of the crack and the permeability of the soil. The crack width then affects in the same direction but with different degree, both terms of the resistance. However, because of its large range of variability – five or more orders of magnitude – the soil permeability is the most important parameter affecting the resistance of the soil to the flow of soil gas, and consequently to the whole transport of radon from the soil into the house.

Therefore, the purpose of this test now is to verify how sensitive the model is to variations in the resistance for the flow of the soil gas through the soil and into the houses. More specifically, I will test the response of the model to variations of the crack width and soil permeability, which are the most variable parameters affecting the resistance to flow of soil gas. In order to perform the test, four different crack widths were selected – 0.5, 1.0, 5.0, and 10.0$[mm]$ – and, for each one of them, the computer model was run six times, covering the range of variability of soil permeability, from 1.0×10^{-14} to $1.0\times10^{-9}[m^2]$. As indicators I have selected : 1) the total resistance to soil gas flow; 2) the average pressure at the soil-crack interface; 3) the average velocity of the soil gas at the soil-crack interface; 4) the average radon concentration in soil gas at the soil-crack interface; 5) the average flux of radon at the soil-crack interface; and 6) the indoor radon concentration. The results were grouped in Table (5.11). Note that the disturbance pressure and the radon concentration in the soil gas are given in dimensionless units. The reason for this is that since these variables have been normalized in the range between 0 and 1, it becomes easier to interpret the results in their dimensionless forms. In order to obtain the actual unit, the disturbance pressure and the radon concentration in soil gas have to be multiplied by their characteristic values of $5[Pa]$ and $530[pCi/l]$, respectively.

The results of this test will be analyzed from two distinct perspectives: first, I will consider the variation of the crack width and its effects on the model's predictions for different

Table 5.11 — Sensitivity analysis of the computer programs - Variation of the soil permeability and crack width.

Model's Predictions	Soil Permeability $[m^2]$	Crack Width $[mm]$			
		0.5	1.0	5.0	10.0
Net Resistance	1×10^{-14}	1.54×10^{8}	1.36×10^{8}	1.09×10^{8}	1.00×10^{8}
to the flow	1×10^{-13}	1.54×10^{7}	1.36×10^{7}	1.09×10^{7}	1.00×10^{7}
of the Soil Gas	1×10^{-12}	1.55×10^{6}	1.36×10^{6}	1.09×10^{6}	1.00×10^{6}
into the House.	1×10^{-11}	1.59×10^{5}	1.37×10^{5}	1.09×10^{5}	1.00×10^{5}
	1×10^{-10}	2.06×10^{4}	1.42×10^{4}	1.09×10^{4}	1.00×10^{4}
$[Pa.s.m^{-3}]$	1×10^{-9}	6.73×10^{3}	2.00×10^{3}	1.09×10^{3}	1.00×10^{3}
Disturbance	1×10^{-14}	-0.999	-0.999	-0.999	-0.999
Pressure	1×10^{-13}	-0.999	-0.999	-0.999	-0.999
at the Crack	1×10^{-12}	-0.997	-0.999	-0.999	-0.999
Interface.	1×10^{-11}	-0.967	-0.995	-0.999	-0.999
	1×10^{-10}	-0.748	-0.954	-0.999	-0.999
[Dimensionless]	1×10^{-9}	-0.229	-0.677	-0.995	-0.999
Average	1×10^{-14}	-1.30×10^{-6}	-7.36×10^{-7}	-1.84×10^{-7}	-1.00×10^{-7}
Velocity	1×10^{-13}	-1.30×10^{-5}	-7.36×10^{-6}	-1.84×10^{-6}	-1.00×10^{-6}
of the Soil Gas	1×10^{-12}	-1.29×10^{-4}	-7.36×10^{-5}	-1.84×10^{-5}	-1.00×10^{-5}
at the Crack	1×10^{-11}	-1.26×10^{-3}	-7.32×10^{-4}	-1.84×10^{-4}	-1.00×10^{-4}
Interface.	1×10^{-10}	-9.72×10^{-3}	-7.03×10^{-3}	-1.83×10^{-3}	-1.00×10^{-3}
$[m.s^{-1}]$	1×10^{-9}	-2.97×10^{-2}	-4.99×10^{-2}	-1.83×10^{-2}	-1.00×10^{-2}
Average	1×10^{-14}	-3.39×10^{1}	-3.09×10^{1}	-1.96×10^{1}	-1.40×10^{1}
Radon Flux	1×10^{-13}	-3.69×10^{1}	-3.26×10^{1}	-2.00×10^{1}	-1.43×10^{1}
at the Crack	1×10^{-12}	-7.59×10^{1}	-5.27×10^{1}	-2.43×10^{1}	-1.65×10^{1}
Interface.	1×10^{-11}	-6.26×10^{2}	-3.64×10^{2}	-9.00×10^{1}	-4.78×10^{1}
	1×10^{-10}	-4.53×10^{3}	-3.16×10^{3}	-8.00×10^{2}	-4.32×10^{2}
$[pCi.m^{-2}.s^{-1}]$	1×10^{-9}	-1.21×10^{4}	-1.54×10^{4}	-4.76×10^{3}	-2.54×10^{3}
Average Radon	1×10^{-14}	0.830	0.761	0.485	0.349
Concentration	1×10^{-13}	0.839	0.768	0.490	0.352
at the Crack	1×10^{-12}	0.903	0.836	0.534	0.382
Interface.	1×10^{-11}	0.940	0.938	0.841	0.660
	1×10^{-10}	0.879	0.850	0.822	0.814
[Dimensionless]	1×10^{-9}	0.765	0.584	0.492	0.479
Indoor	1×10^{-14}	7.98×10^{-3}	1.46×10^{-2}	4.62×10^{-2}	6.65×10^{-2}
Radon	1×10^{-13}	8.70×10^{-3}	1.54×10^{-2}	4.72×10^{-2}	6.75×10^{-2}
Concentration	1×10^{-12}	1.79×10^{-2}	2.48×10^{-2}	5.73×10^{-2}	7.77×10^{-2}
	1×10^{-11}	1.48×10^{-1}	1.72×10^{-1}	2.12×10^{-1}	2.25×10^{-1}
	1×10^{-10}	1.07×10^{0}	1.49×10^{0}	1.89×10^{0}	2.04×10^{0}
$[pCi.l^{-1}]$	1×10^{-9}	2.85×10^{0}	7.29×10^{0}	$1.12\times10^{+1}$	$1.20\times10^{+1}$

values of soil permeabilities; then, the emphasis will be placed on the variation of the soil permeability and the resultant effects at different crack widths.

As a starting point for this test I show in Fig.(5.9) how the model predicts the variations of the net resistance to soil gas flow as a function of the crack width (Part A), and soil permeability (Part B). As we can see, the predicted net resistance to soil gas flow varies inversely with both the crack width and soil permeability. In part A of Fig.(5.9), we can observe that for low soil permeability ($k \leq 1.0\times10^{-11}[m^2]$), the net resistance to the soil gas flow varied with the crack width following a similar pattern. For these cases, a variation of the crack width from 0.5 to 10.0$[mm]$ caused a decrease of the net resistance to soil gas flow by a factor of 1.55 approximately. But for the cases with high soil permeabilities ($k \geq 1.0\times10^{-10}[m^2]$), the curves deviated from the general pattern, showing a stronger variation in the range of the crack width between 0.5 and 5.00$[mm]$. In this crack width range the net resistance to the flow of soil gas was reduced by a factor of 1.89 for the soil permeability of $1.0\times10^{-10}[m^2]$, and by a factor of 6.17, for the case of the highest soil permeability considered, ($k = 1.0\times10^{-9}[m^2]$). In the crack width range from 5.0 to 10.0$[mm]$, the curves showed the same basic pattern.

These same features can be observed from another perspective, in part B of Fig.(5.9). There, for crack widths larger than 5.0$[mm]$, the net resistance to the soil gas flow varied inversely to the soil permeability in the whole range from 1.0×10^{-14} to $1.0\times10^{-9}[m^2]$. For crack widths lower than 5.0$[mm]$, the variation of the net resistance to the soil gas flow was also inversely proportional to the soil permeability, but now only in the range of soil permeabilities up to $1.0\times10^{-11}[m^2]$. Beyond this point, the curves deviated from the original pattern, suggesting a decreasing dependency on the soil permeability.

These results are consistent with the idea that the net resistance to soil gas flow is composed of a sum of two components: R_{soil}, the soil resistance; and R_{crack}, the crack resistance. The crack width affects both terms, but has a stronger effect on R_{crack} than on R_{soil}. The soil permeability affects only R_{soil}. Then, for very low permeabilities, R_{soil} is the dominant term of the net resistance, and the variation of the crack width will affect the net resistance in a

relatively small range. But for large permeabilities, R_{soil} is comparable with, or even smaller than, R_{crack} and consequently, the variations of the crack width will affect the net resistance in a larger range than in the cases before.

Continuing with the test, the model will be observed in relation to its prediction of the pressure distribution in the soil block, depending on the variations of the soil permeability and crack width. In Fig.(5.10) I have plotted the average pressure at the crack interface, as a function of the crack width and soil permeability. Note that the disturbance pressure distribution was normalized to the $(-1, 0)$ interval, where -1 is the pressure at the basement, and 0 is the pressure at the ground level outside. Consequently the pressure at the crack interface is numerically equal to the total pressure drop across the soil block.

Thus, as we can see in Table (5.11) and Fig.(5.10), for very small soil permeabilities ($k \leq 1.0\times10^{-12}[m^2]$), the average pressure at the soil-crack interface is very close to -1, and shows the tendency to get even closer to -1 as the crack width is increased. In other words, the pressure drop across the basement floor is very small compared with the pressure drop within the soil block, and tends to be even smaller as the crack width is increased within the range considered. What happens here is that the total resistance of the crack-soil configuration, in these ranges of soil permeability and crack width, is completely dominated by the value of its soil component, and consequently the pressure drop occurs almost totally within the soil block. Furthermore, increases in the crack width will cause a decrease to both the crack and soil components, and therefore to the net resistance to the soil gas flow. Now, since the applied disturbance pressure is constant, the total flow of soil gas will then increase inversely proportional to the decrease of the net resistance. But, for the same increase of the crack width, the decrease of the crack resistance is faster than the decrease of the total resistance and therefore the pressure drop across the crack length, which is equal to the product of the crack resistance times the flow of the soil gas, will decrease with the increase of the crack width.

Now, for large soil permeabilities ($k \geq 1.0\times10^{-11}[m^2]$), the crack resistance for the crack width in the range considered, can be of the same size, or even larger, than the soil resistance.

Figure 5.9 — Net resistance to the flow of soil gas as a function of the soil permeability and crack width.

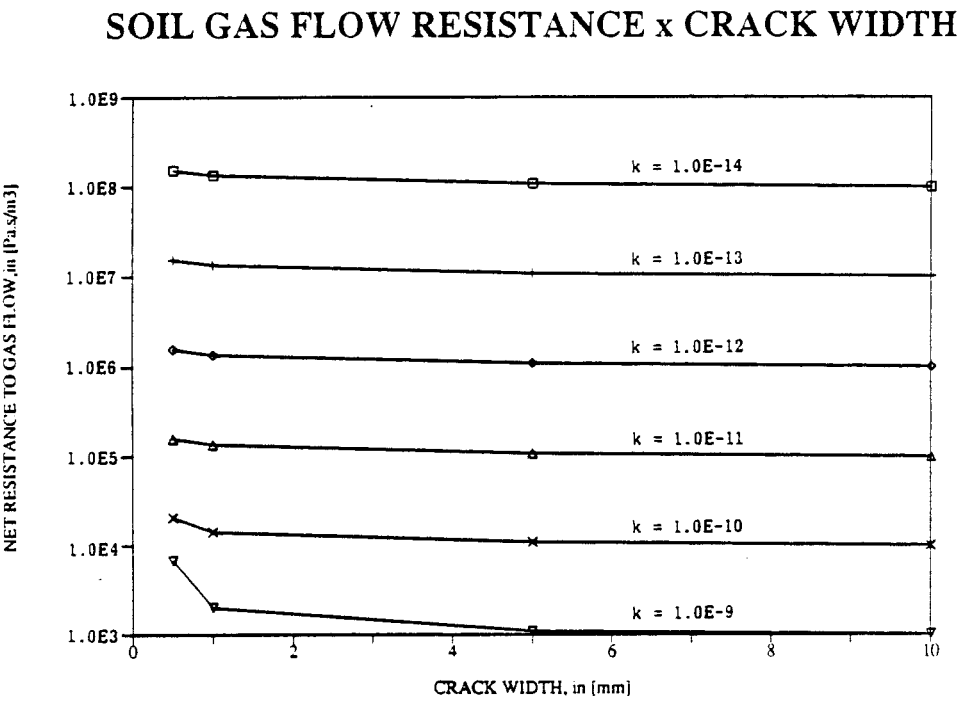

(A) – Net resistance to the flow of soil gas as a function of the crack width, for different values of the soil permeability.

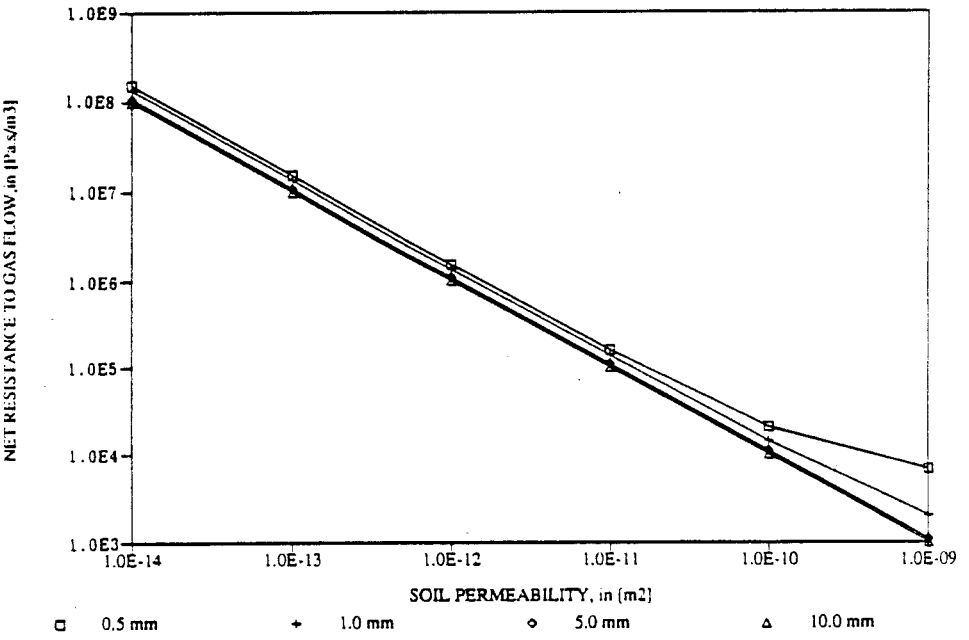

(B) – Net resistance to the flow of soil gas as a function of the soil permeability, for different values of the crack width.

Figure 5.10 — Average pressure at the soil-crack interface as a function of the crack width, for different soil permeabilities.

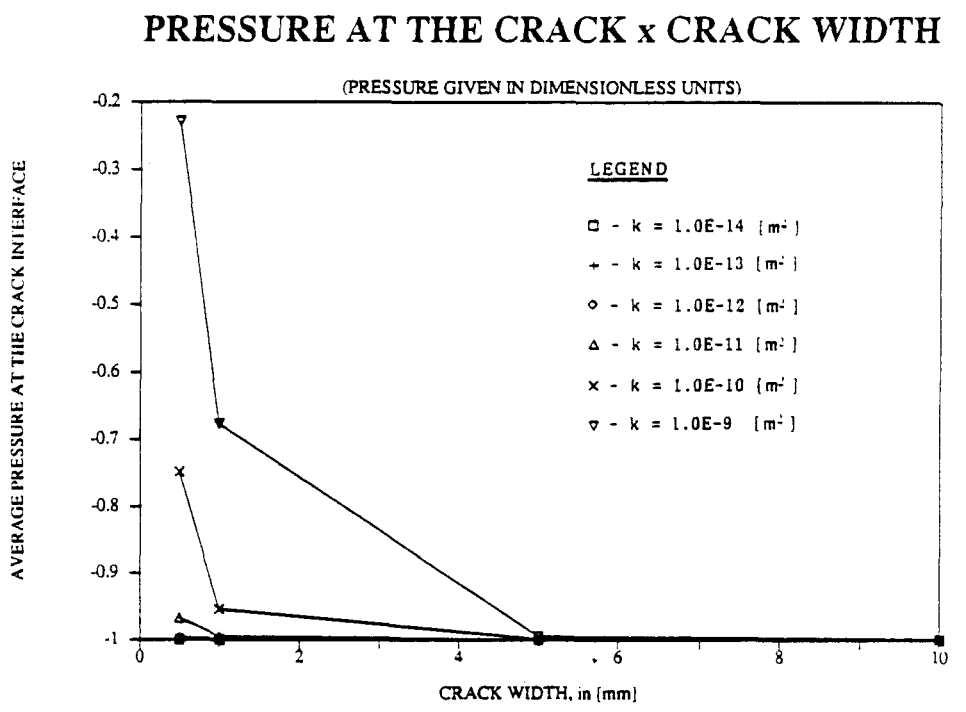

Therefore, the pressure drop across the basement floor can be comparable to the pressure drop within the soil block. Based on Fig.(5.10) we can say that in the present configuration of the house, where the basement is $2[m]$ below the ground, and the basement floor is $0.15[m]$ thick, a crack in the basement with a width larger than $5.0[mm]$ will cause a pressure drop lower than .5%, even for the soil with the highest permeability of $1.0\times10^{-9}[m^2]$. For crack widths between 1 and $5[mm]$, the pressure drop across the basement floor will be lower than 35%, even in the extreme value of soil permeability. And finally, crack widths between 0.5 and $1.0[mm]$, would cause pressure drops in the range of: 75% to 35%, for soil permeability of $1.0\times10^{-9}[m^2]$; 25% to 5% for soil permeability of $1.0\times10^{-10}[m^2]$; and from 5% to lower than 0.5%, for soil permeability of $1.0\times10^{-11}[m^2]$. It should be noted here that other house configuration would have affected the results above in such a way that, an increase in the basement depth would have increased the soil resistance, increasing the pressure drop in the soil. Also, an increase in the thickness of the basement floor would have increased the crack resistance and consequently the pressure drop across the basement floor.

The effect of crack width and soil permeability on the distribution of the disturbance pressure can also be analyzed by observing the disturbance pressure distribution at specified cross sections of the soil block. Thus, in Figures (5.11) to (5.18) I have plotted the disturbance pressure distribution in vertical cross-sections of the soil block, for different values of crack widths and soil permeabilities. These vertical cross-sections correspond to a vertical cut in the $x - z$ plane of the soil block, right at the first layer of control-volumes in the $y-$direction. The isolines in those figures correspond to the points with the same disturbance pressure.

So, the sequence of four figures, from Fig.(5.11) to Fig.(5.14), represents the disturbance pressure distribution in a soil with a very low permeability of $1.0\times10^{-14}[m^2]$, for different crack widths of 0.5, 1.0, 5.0, and $10.0[m^2]$ respectively. As we can see, the pressure profile in the soil is affected by the size of the crack width such that, as the crack width increases, the pressure isolines are moved far away from the crack – the center of disturbance of the system – and deeper into the soil block. This agrees with the discussion about Fig.(5.10), where it was shown that the pressure at the crack interface, or the pressure drop across the soil block, increased with the crack width. Therefore, a larger pressure drop within the soil block would result in the movement of the pressure isolines to points more distant from the crack, which is exactly the prediction in Figs.(5.11) to (5.14).

Now, the next sequence of four figures, from Fig.(5.15) to (5.18), represents the pressure profile in a soil with a higher permeability of $1.0\times10^{-10}[m^2]$, but with the same cases of crack widths. Here again, we can observe the same, or even more pronounced effect of expansion of the pressure isolines as the crack widths are increased. However, other details can also be observed if we compare the profiles for the same crack width, but different permeabilities. So, a comparison of Fig.(5.11) with Fig.(5.15) will show that for a small crack width of $0.5[mm]$ (or a large crack resistance to soil gas flow), an increase of soil permeability from 1.0×10^{-14} to $1.0\times10^{-10}[m^2]$ caused a contraction of the pressure isolines moving them closer to the crack. And this is because the increase in the soil permeability caused an increase in the total flow of soil gas, and since the crack resistance at a crack of

this size is comparable with the soil resistance for the soil permeability at the higher end ($1.0\times10^{-10}[m^2]$), the pressure drop across the crack also increased, reducing the pressure drop within the soil block. Then, with a lower pressure drop across the soil block, a new pressure distribution is established with the pressure isolines closer to the crack. The same effect, although not so much evident, can be observed comparing Fig.(5.12) and Fig.(5.16), representing the crack width of $1.0[mm]$, and the same soil permeabilities above. Now, for crack widths of 5.0 or $10.0[mm]$, the crack resistance to flow of soil gas is so small that the change in the total flow of soil gas resulted from changing the soil permeability from 1.0×10^{-14} to $1.0\times10^{-10}[m^2]$ does not alter significantly the pressure drop across the crack, and consequently the pressure profile throughout the soil block is unaffected by changes in the soil permeability. This effect can be observed clearly by comparing Fig.(5.13) with Fig.(5.17), for crack width of $5.0[mm]$, and Fig(5.14) with Fig.(5.18), for crack width of $10.0[mm]$, where the pressure profiles are almost identical.

From the analysis of the variation of the disturbance pressure distribution as a function of the crack width and soil permeability, within the ranges considered, we can conclude that:

- About the average pressure at the soil-crack interface -
  1) In soil with low permeability, ($k \leq 1.0\times10^{-12}[m^2]$), the pressure drop occurs almost entirely within the soil block. The pressure drop across the basement floor decreases with increased crack width;
  2) In soil with high permeability ($k \geq 1.0\times10^{-12}[m^2]$), the pressure drop occurs almost entirely within the soil block, for crack widths larger than $5.0[mm]$, and is distributed between the crack and the soil block, for crack widths lower than $5.0[mm]$;
- About the disturbance pressure distribution throughout the soil block -
  1) The pressure distribution within the soil is affected by the size of the crack, showing an expansion of the pressure isolines as the crack width is increased. This effect occurs at either high or low permeability of the soil;
  2) For crack widths larger than $5.0[mm]$ the pressure distribution within the soil is unchanged with the soil permeability;
  3) For crack widths smaller than $5.0[mm]$ the pressure distribution in the soil changes

with the soil permeability in such a way that an increase in the soil permeability results in a contraction of the pressure isolines to points closer to the crack.

Having seen how the model responds in relation to the distribution of disturbance pressure, I will now focus attention on the model's prediction about the soil gas velocity, radon concentration in the soil gas, and radon flux, as the crack width and the soil permeability are changed.

Thus, using the data from Table (5.11), the average velocity of soil gas as well as the radon flux through the soil-crack interface, as a function of the crack width and the soil permeability, were plotted in Fig.(5.19). In part A of that figure we can see that the soil gas velocity decreased with the crack width in a similar pattern for all values of soil permeability, except for the highest one, ($k = 1.0\times10^{-9}[m^2]$). The velocity of the soil gas through the crack is given by the quotient of the total flow of soil gas through the crack, to the cross sectional area of the crack. Therefore, the variation of the soil gas velocity with the crack width depends on how those two variables –the soil gas flow and the crack area – are affected separately by the crack width. For low soil permeabilities, we have seen that the soil resistance to soil gas flow shows a relatively small variation with the crack width. For instance, for soil permeabilities below $1.0\times10^{-11}[m^2]$, a variation of the crack width by a factor of 2, from 0.5 to $1.0[mm]$, reduces the net resistance to soil gas flow by a factor of 1.13, approximately. (See Table (5.11)). Consequently the total soil gas flow also increases by the same factor. Therefore, since the crack area was increased by a factor of 2, then the soil gas velocity was reduced by a factor of $1.13 \div 2 = 0.57$. But now, for high permeabilities and small crack widths, the net resistance to soil gas flow shows a stronger dependency on the crack width.[6] For example, in a case with the soil permeability equal to $1.0\times10^{-9}[m^2]$, an increase of the crack width from 0.5 to $1.0[mm]$ reduced the net resistance to soil gas flow by a factor of 3.37. Consequently in this case, instead of decreasing with the crack width, the velocity of the soil gas was increased by a factor of $3.37 \div 2 = 1.68$. This explains why, in Fig.(5.19), the curves representing the soil gas velocity for high soil permeabilities, and small crack widths, deviate from the general pattern of inverse dependency on the crack

[6] See Table (5.11) and Fig.(5.9).

Figure 5.11 — Disturbance pressure distribution in a vertical section of the soil block, with soil permeability equal to $1.0\times10^{-14}[m^2]$, and crack width equal to $0.5[mm]$.

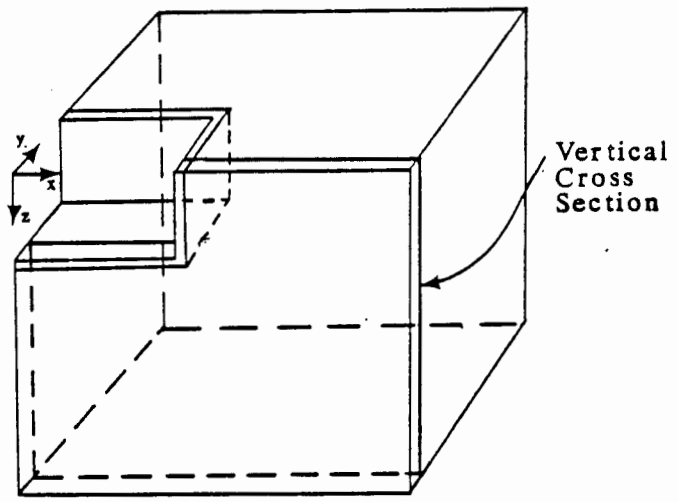

Location of the vertical cross-section in the soil block.

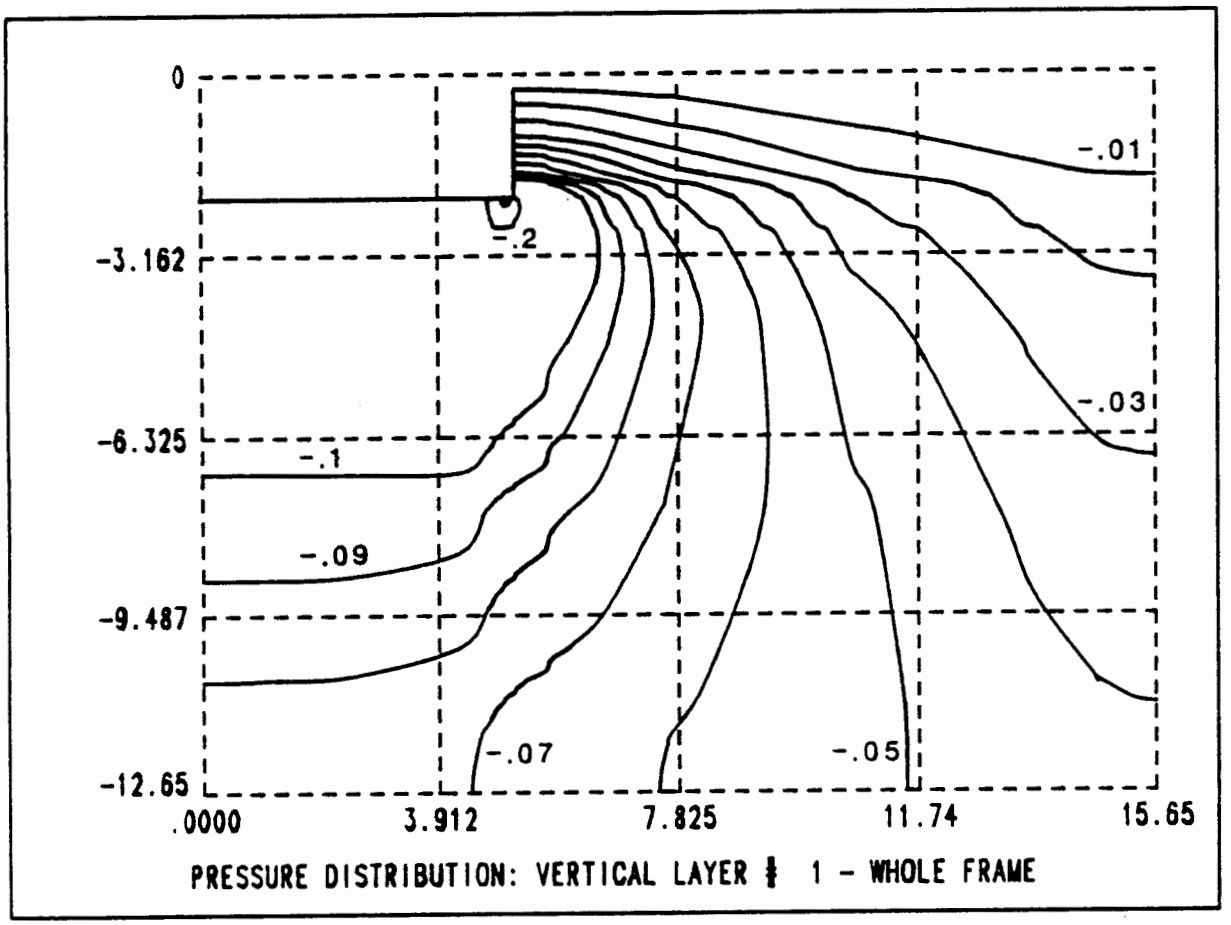

The disturbance pressure is normalized within the interval $(-1, 0)$.

Figure 5.12 — Disturbance pressure distribution in a vertical section of the soil block, with soil permeability equal to $1.0\times10^{-14}[m^2]$, and crack width equal to $1.0[mm]$.

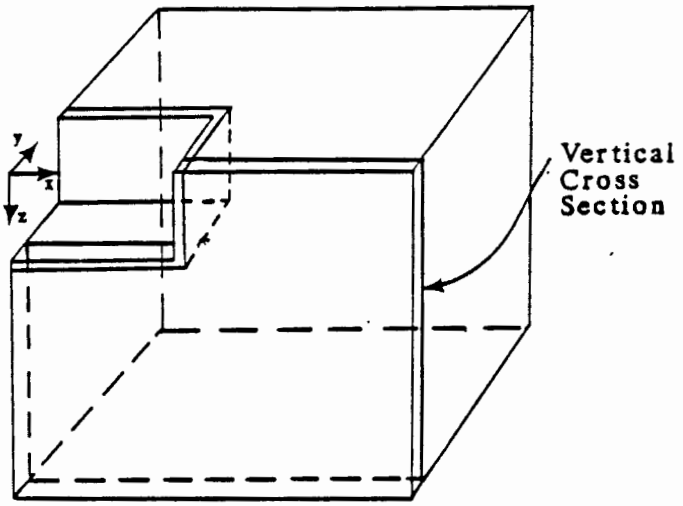

Location of the vertical cross-section in the soil block.

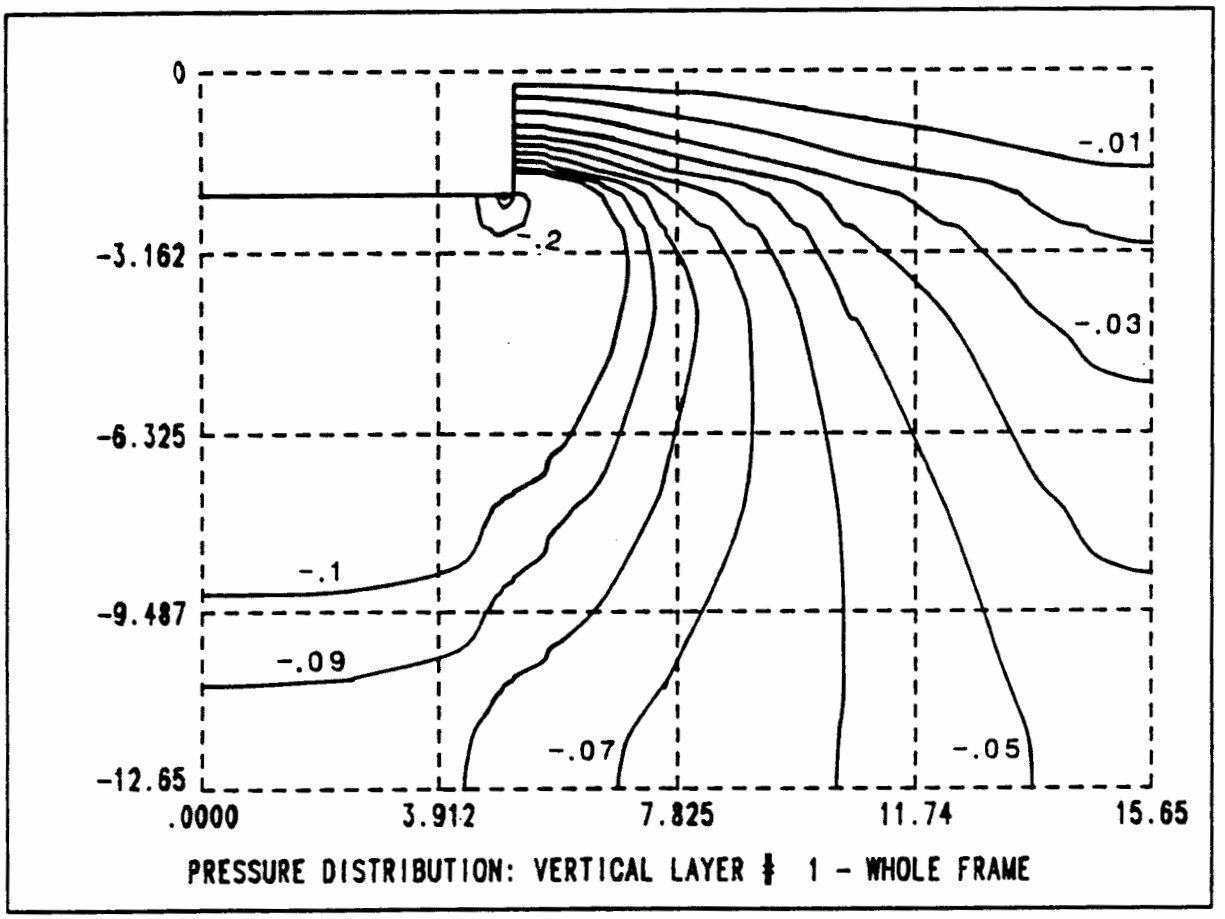

The disturbance pressure is normalized within the interval $(-1, 0)$.

Figure 5.13 — Disturbance pressure distribution in a vertical section of the soil block, with soil permeability equal to $1.0\times10^{-14}[m^2]$, and crack width equal to $5.0[mm]$.

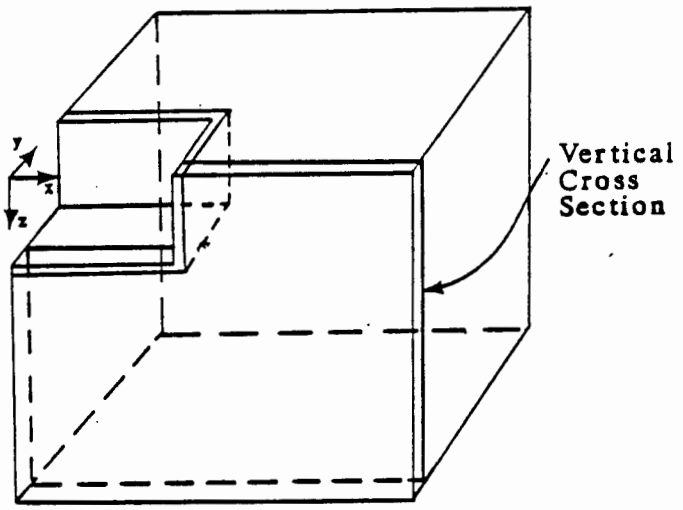

Location of the vertical cross-section in the soil block.

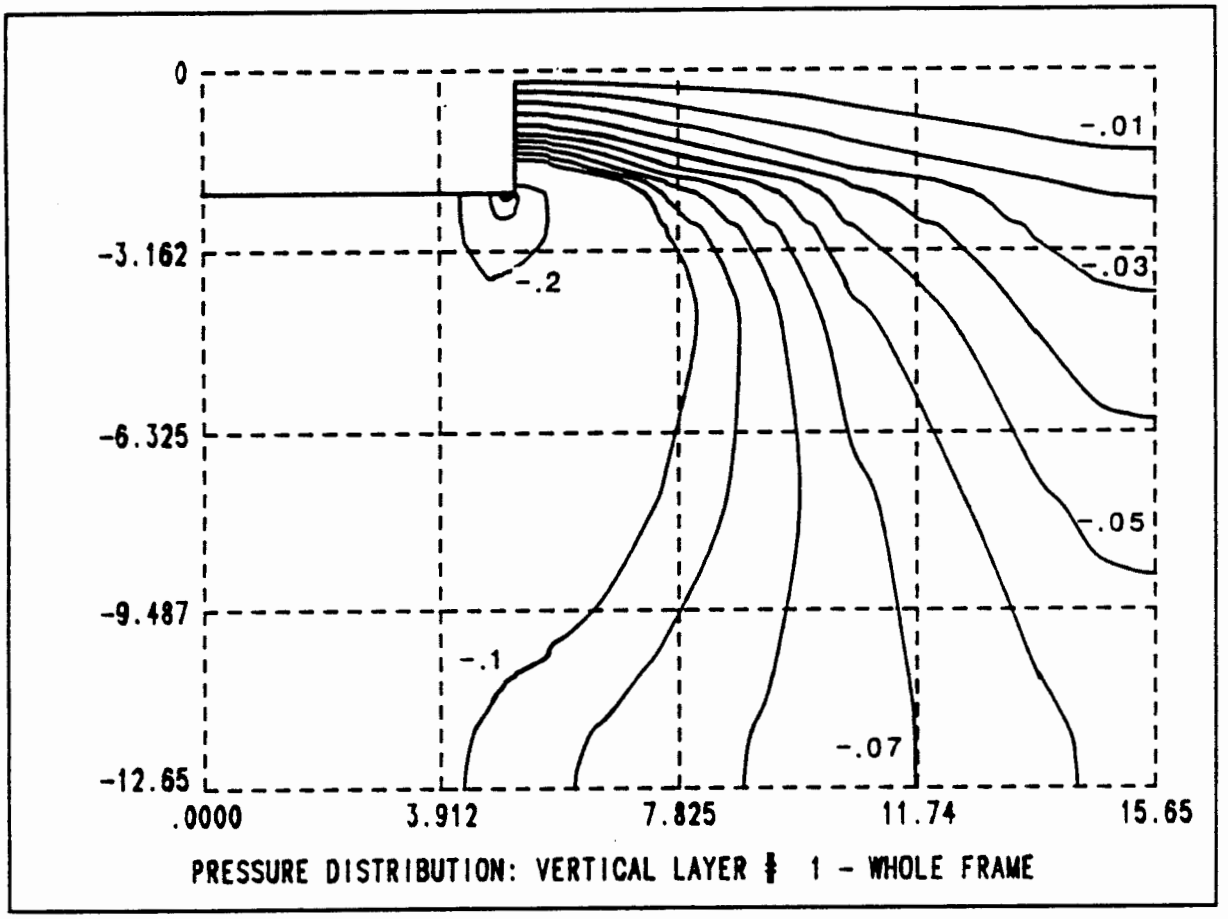

The disturbance pressure is normalized within the interval $(-1, 0)$.

Figure 5.14 — Disturbance pressure distribution in a vertical section of the soil block, with soil permeability equal to $1.0\times10^{-14}[m^2]$, and crack width equal to $10.0[mm]$.

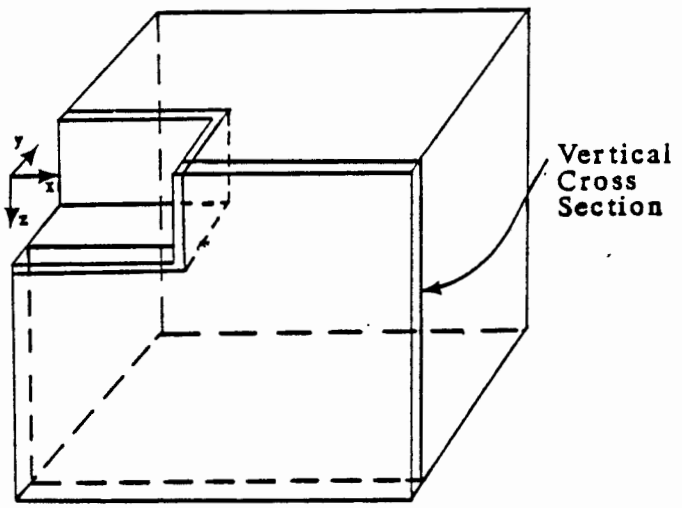

Location of the vertical cross-section in the soil block.

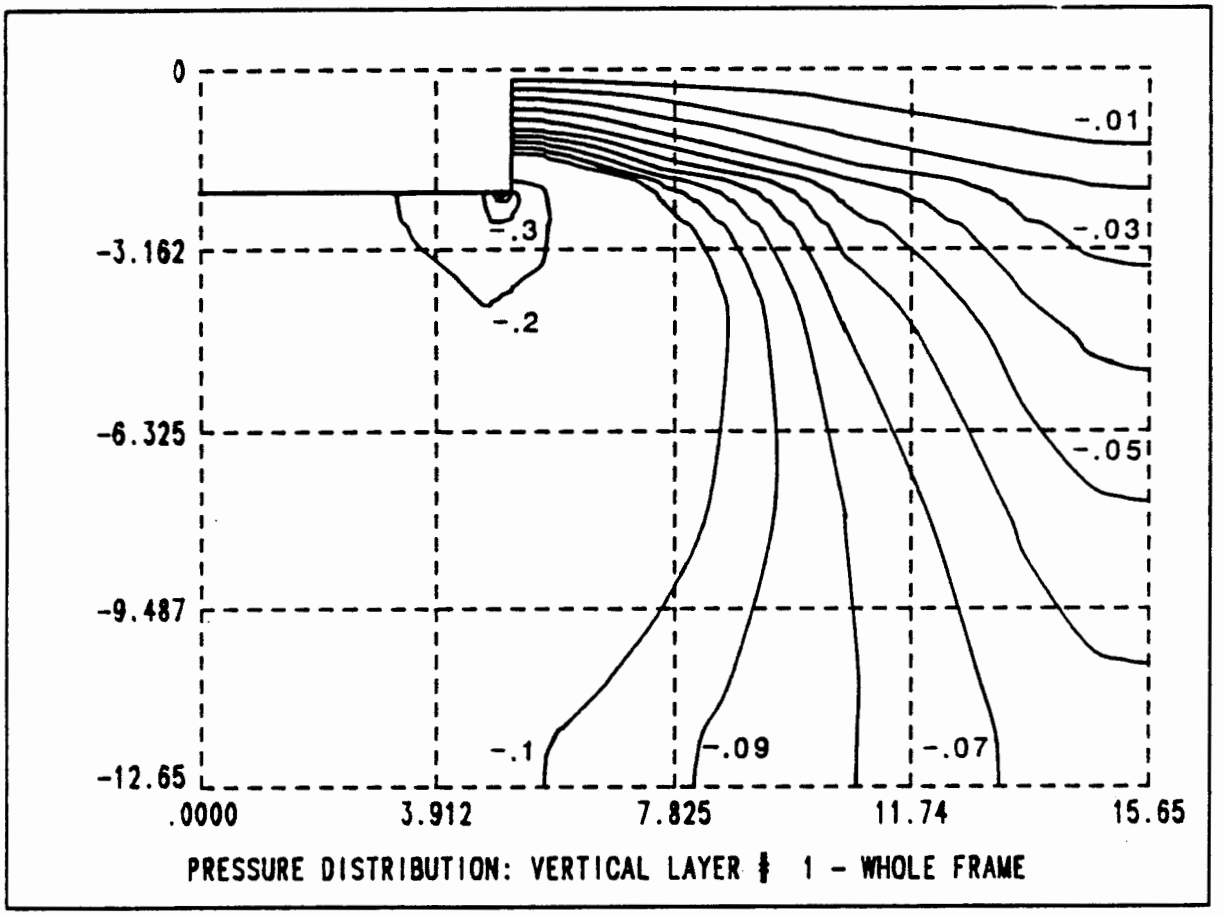

The disturbance pressure is normalized within the interval $(-1, 0)$.

Figure 5.15 — Disturbance pressure distribution in a vertical section of the soil block, with soil permeability equal to $1.0\times10^{-10}[m^2]$, and crack width equal to $0.5[mm]$.

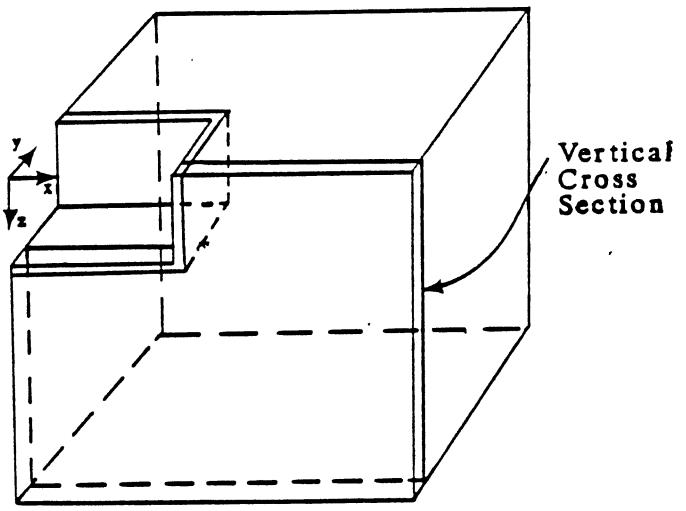

Location of the vertical cross-section in the soil block.

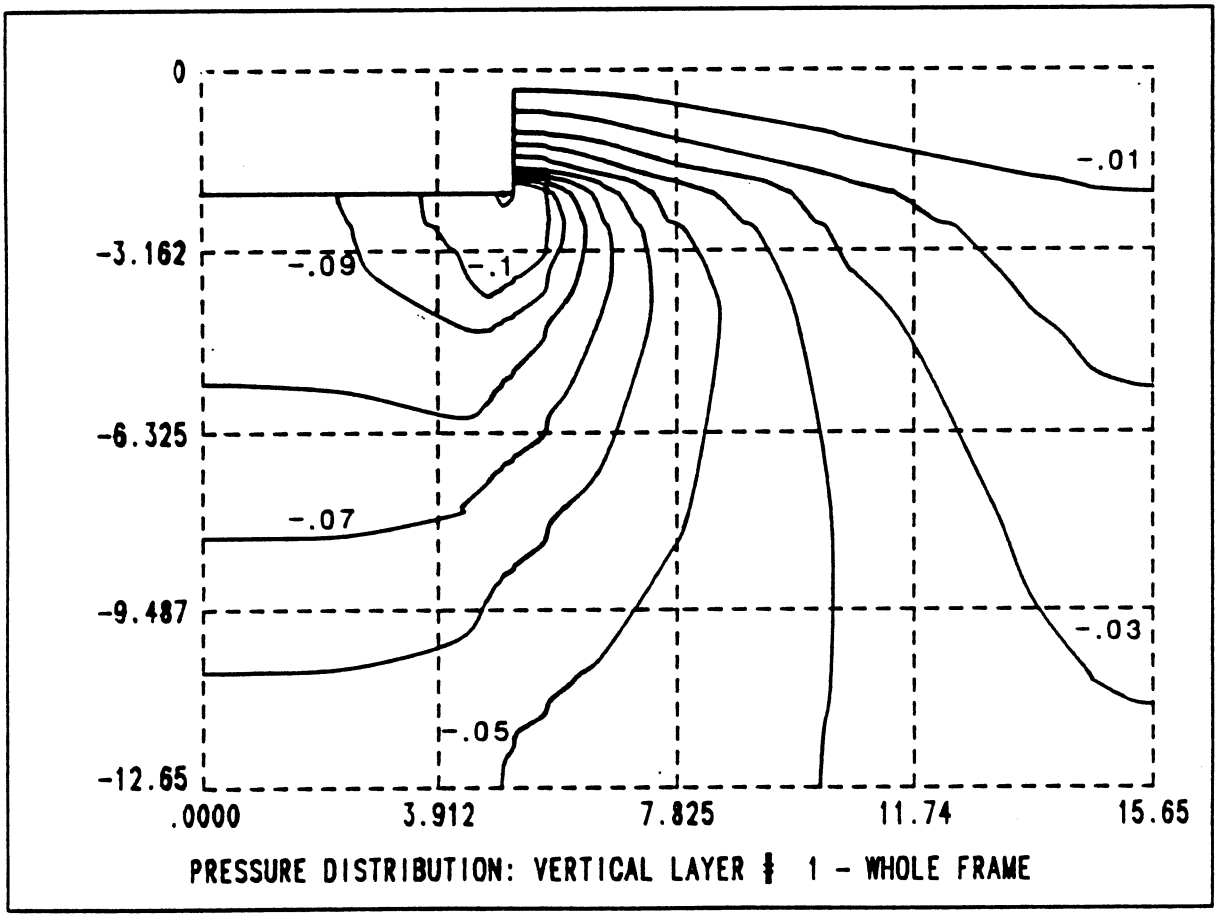

The disturbance pressure is normalized within the interval $(-1, 0)$.

Figure 5.16 — Disturbance pressure distribution in a vertical section of the soil block, with soil permeability equal to $1.0\times10^{-10}[m^2]$, and crack width equal to $1.0[mm]$.

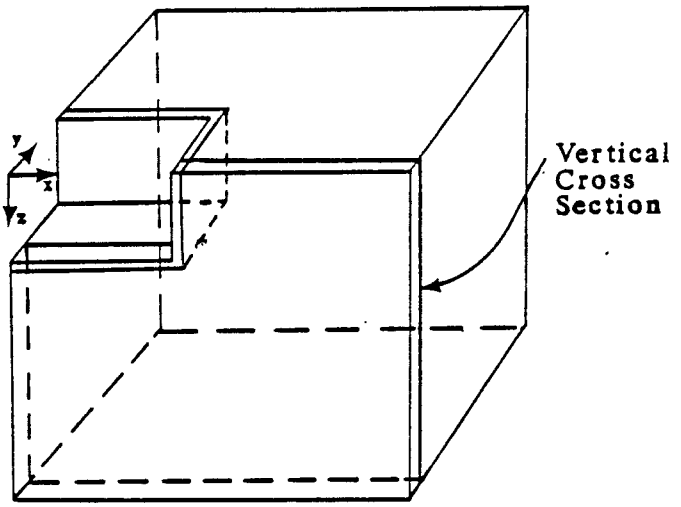

Location of the vertical cross-section in the soil block.

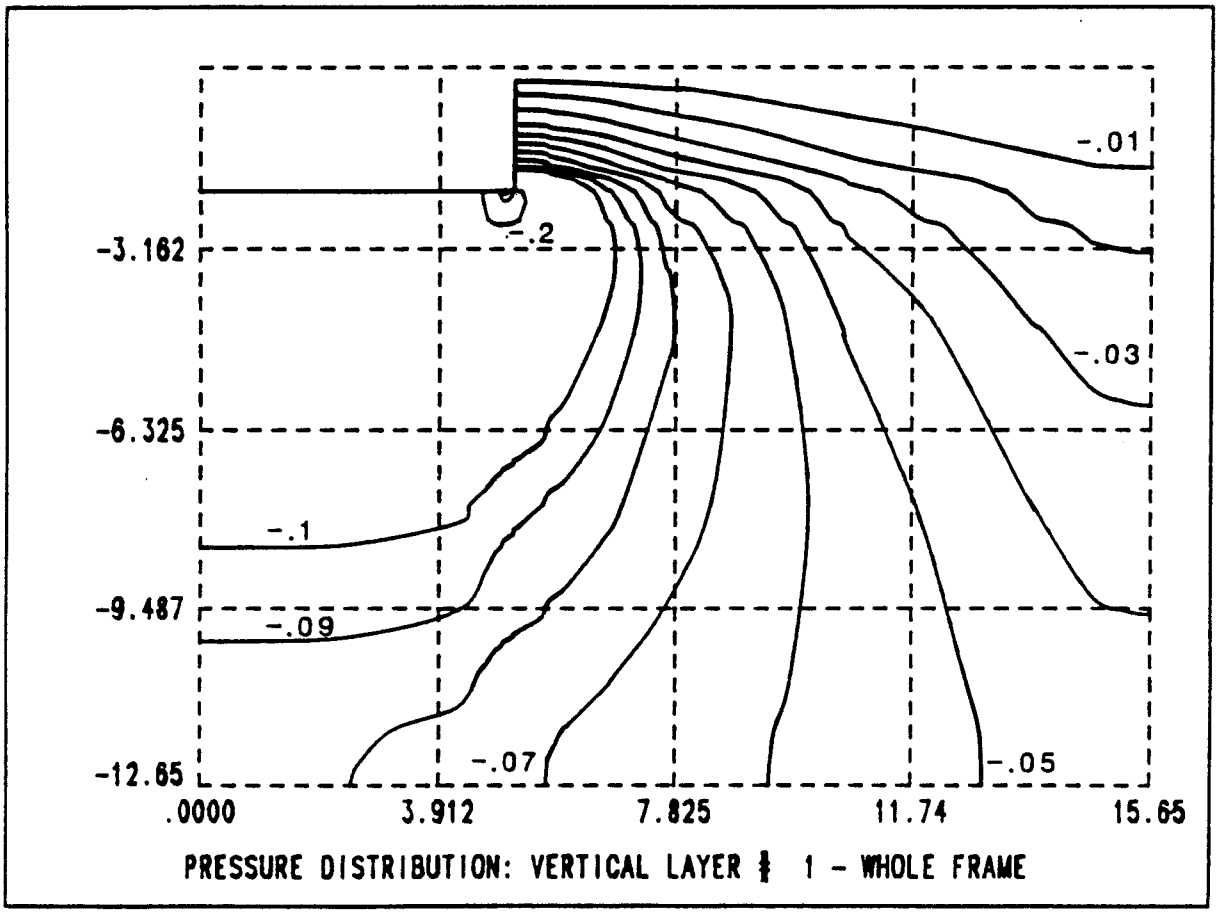

The disturbance pressure is normalized within the interval $(-1, 0)$.

Figure 5.17 — Disturbance pressure distribution in a vertical section of the soil block, with soil permeability equal to $1.0\times10^{-10}[m^2]$, and crack width equal to $5.0[mm]$.

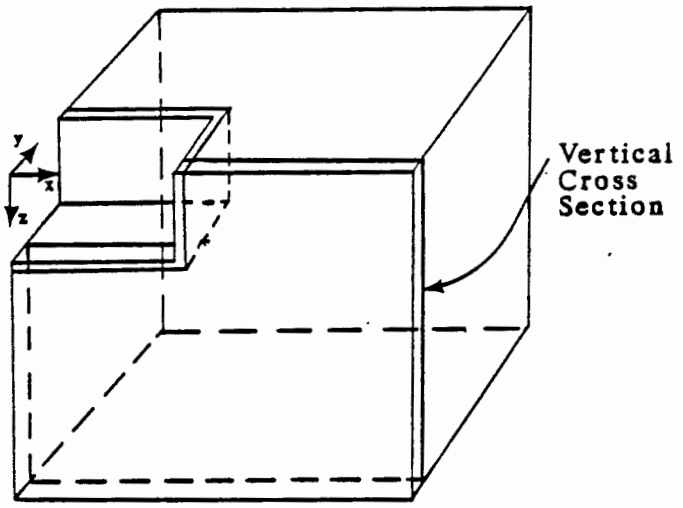

Location of the vertical cross-section in the soil block.

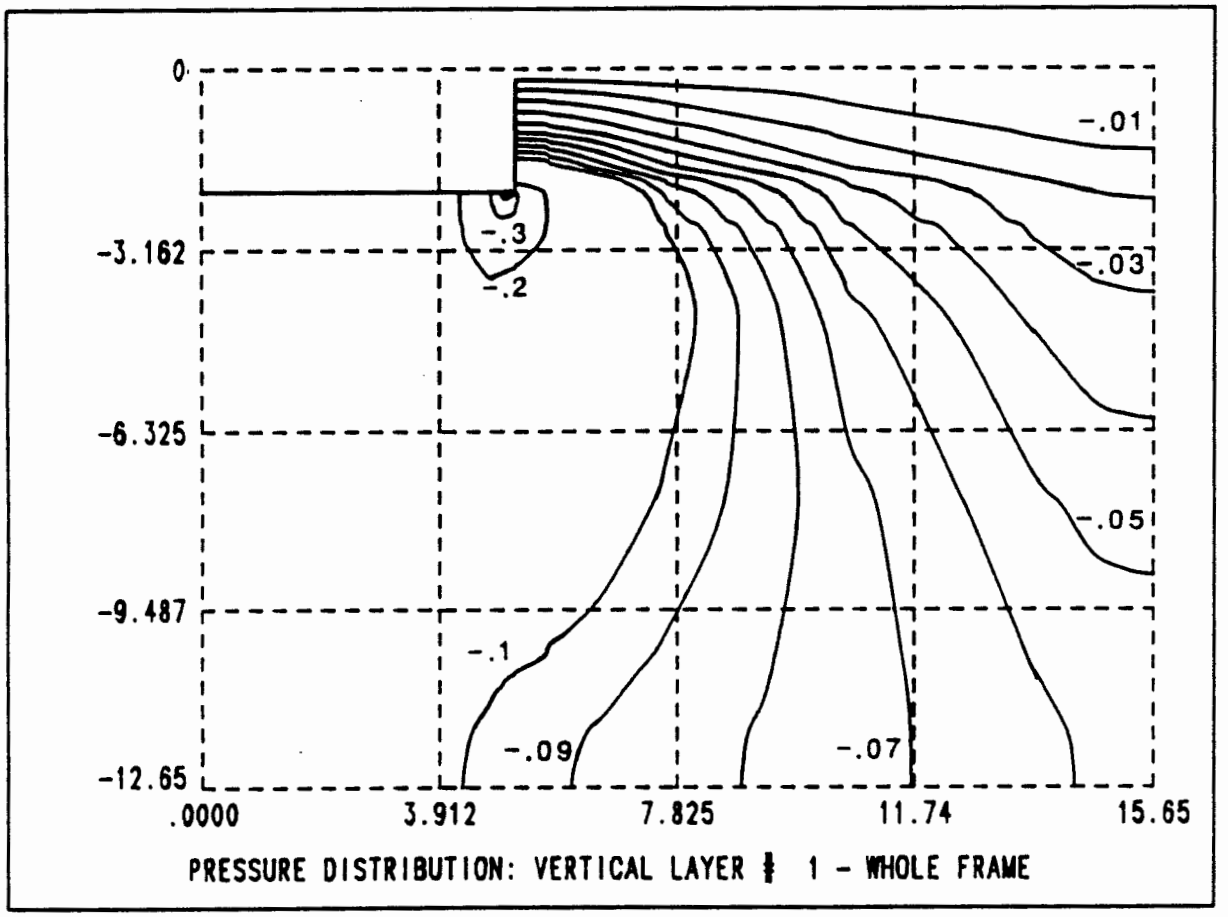

The disturbance pressure is normalized within the interval $(-1, 0)$.

Figure 5.18 — Disturbance pressure distribution in a vertical section of the soil block, with soil permeability equal to $1.0\times10^{-10}[m^2]$, and crack width equal to $10.0[mm]$.

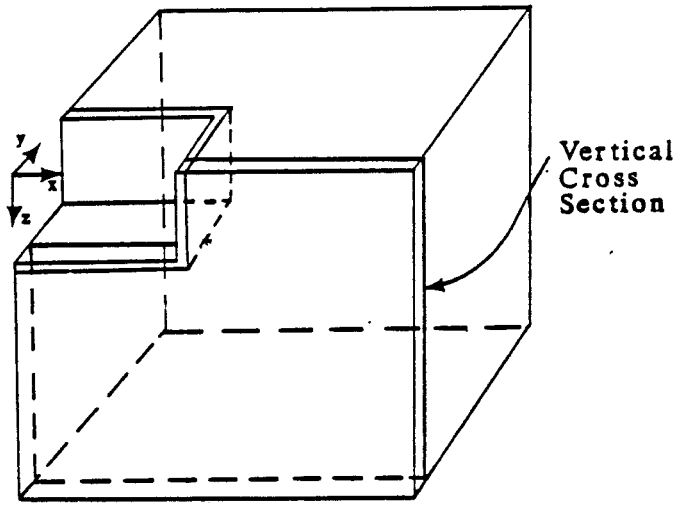

Location of the vertical cross-section in the soil block.

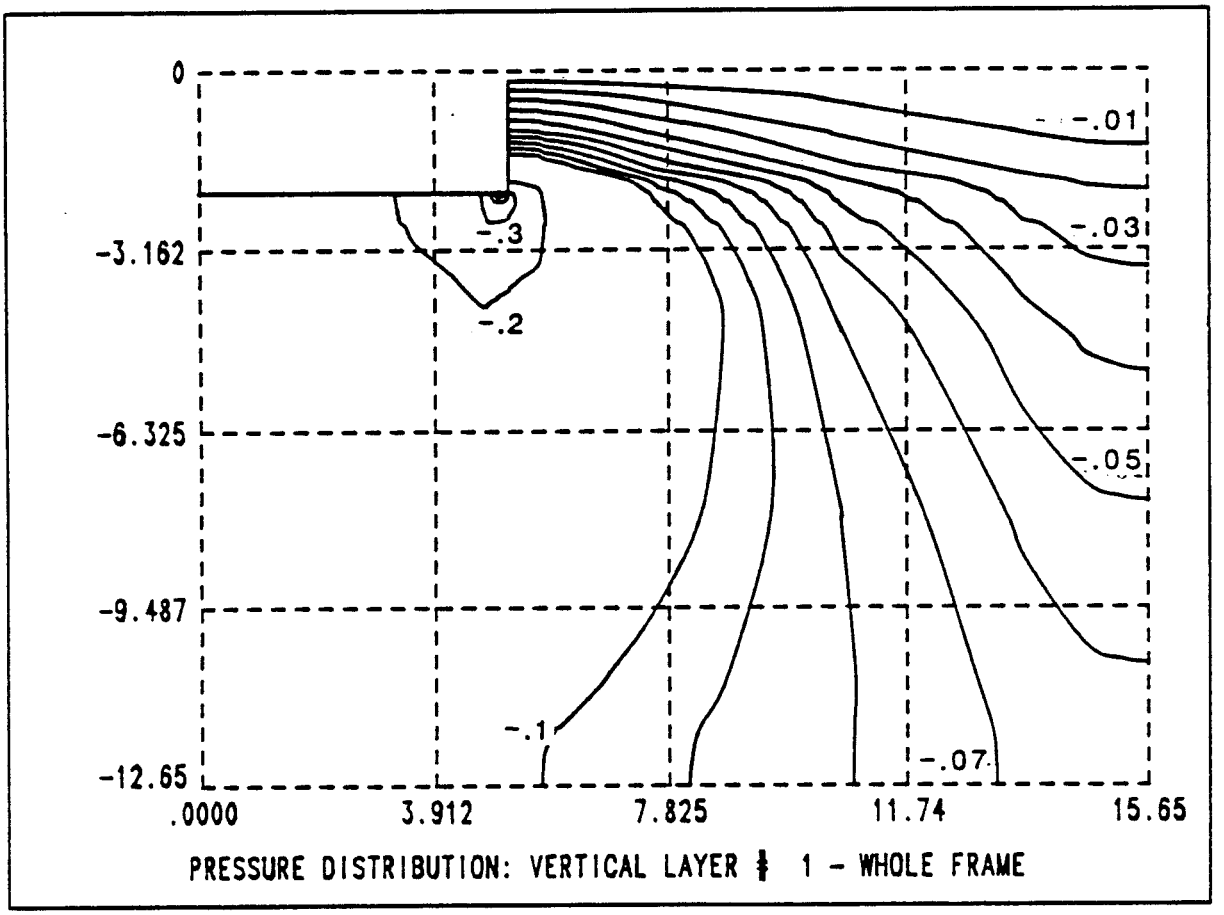

The disturbance pressure is normalized within the interval $(-1, 0)$.

width.

The variation of the total radon flux at the soil-crack interface, as a function of the crack width, for several soil permeabilities, is shown in part B of Fig.(5.19). The reason I have kept the graphs of the soil gas velocity and the radon flux in the same figure is to help in comparing these variables. Here it should be remembered that the total radon flux is composed of two components – the diffusive and the convective flux. So, in Fig.(5.19) we can see that, for high soil permeability ($k \geq 1.0\times10^{-11}[m^2]$), the soil gas velocity is high and the convective component of the radon flux predominates. Consequently, the behavior of the total radon flux with the crack width follows the same pattern shown by the soil gas velocity. However, for soil permeabilities below $1.0\times10^{-12}[m^2]$ the soil gas velocity is small, and the convective component of the radon flux becomes of the same order of magnitude, or even smaller than the diffusive component. Thus, for these cases, the total radon flux approaches a minimum value due to its diffusive component.

In order to provide another perspective to the interpretation of the relations described above, it would be useful to see how, in the model's predictions, the soil gas velocity and the radon flux vary with the soil permeability. So, in Fig.(5.20) and Fig.(5.21) I have plotted the variation of the soil gas velocity and the total radon flux, respectively, as a function of the soil permeability, for different values of the crack width. In each figure I have used both linear and logarithmic scales, which I think will help emphasizing some aspects of those curves. So, in Fig.(5.20) we can see that for large crack width ($\geq 5.00[mm]$), the variation of soil gas velocity is linear with the soil permeability, within the whole range considered, (1.0×10^{-14} to $1.0\times10^{-9}[m^2]$). But for small crack width, ($\leq 1.0[mm]$), the soil gas velocity varies linearly with the soil permeability only in a smaller range, from 1.0×10^{-14} to $1.0\times10^{-11}[m^2]$. Beyond that, the curves deviate from the straight line, indicating a less strong relationship than the linear one.

Now, in Fig.(5.21) we can see that, differently from the velocity of the soil gas, the radon flux does not vary linearly with the soil permeability. And the reason for that is because of the extra complexity in the composition of the total flux caused by its diffusive component.

Figure 5.19 — Soil gas velocity and radon flux as a function of the crack width, for different values of soil permeability.

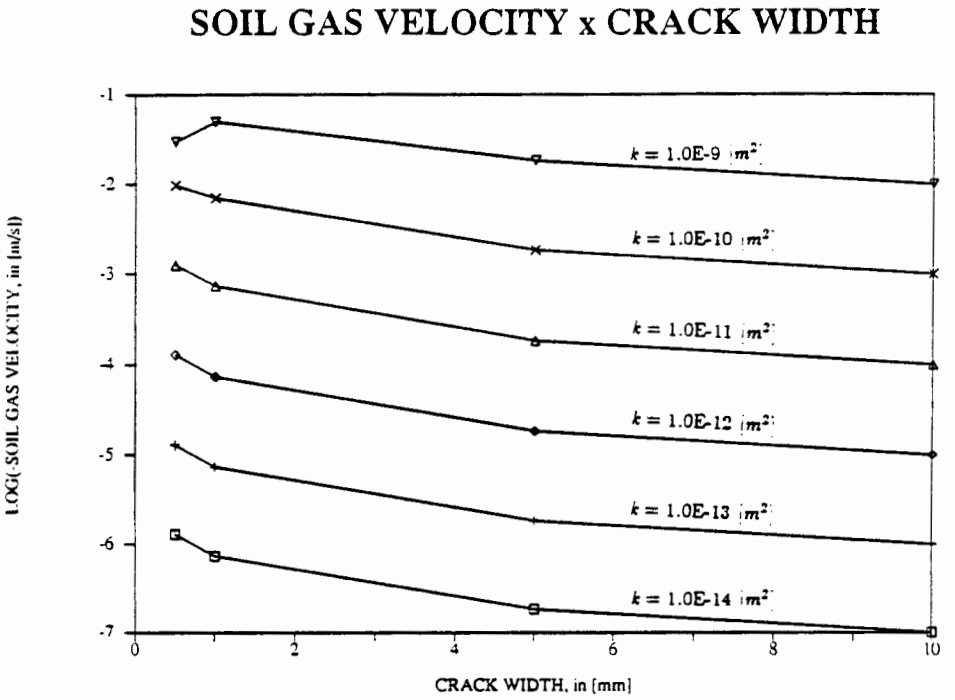

(A) - Average soil gas velocity at the soil-crack interface, as a function of the crack width, for different soil permeabilities.

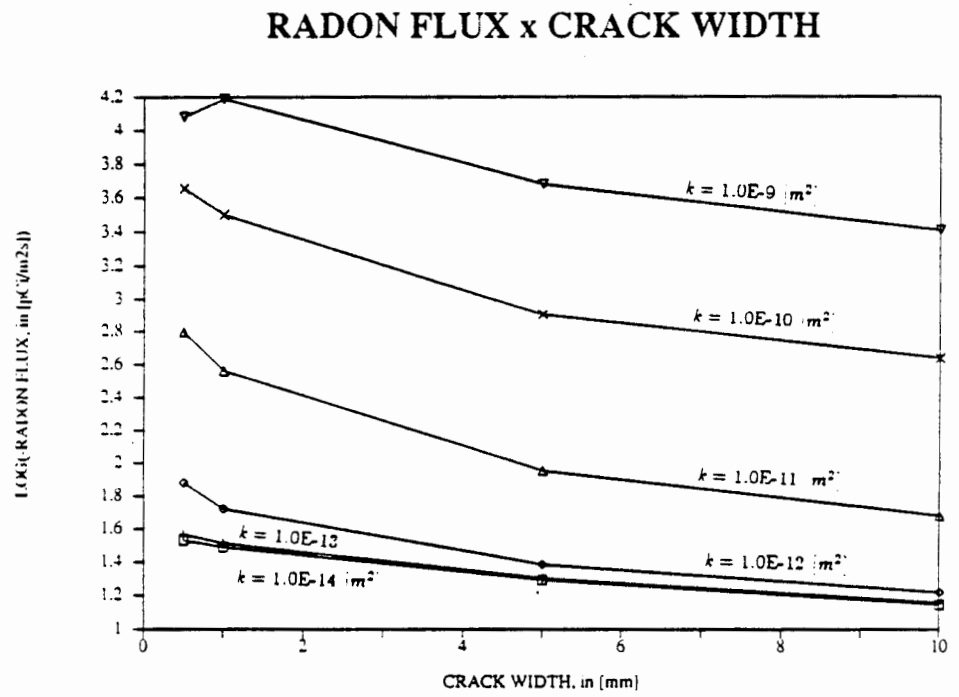

(B) - Average flux of radon through the soil-crack interface as a function of the crack width, for different soil permeabilities.

Figure 5.20 — Average soil gas velocity at the soil-crack interface, as a function of the soil permeability, for different values of crack width.

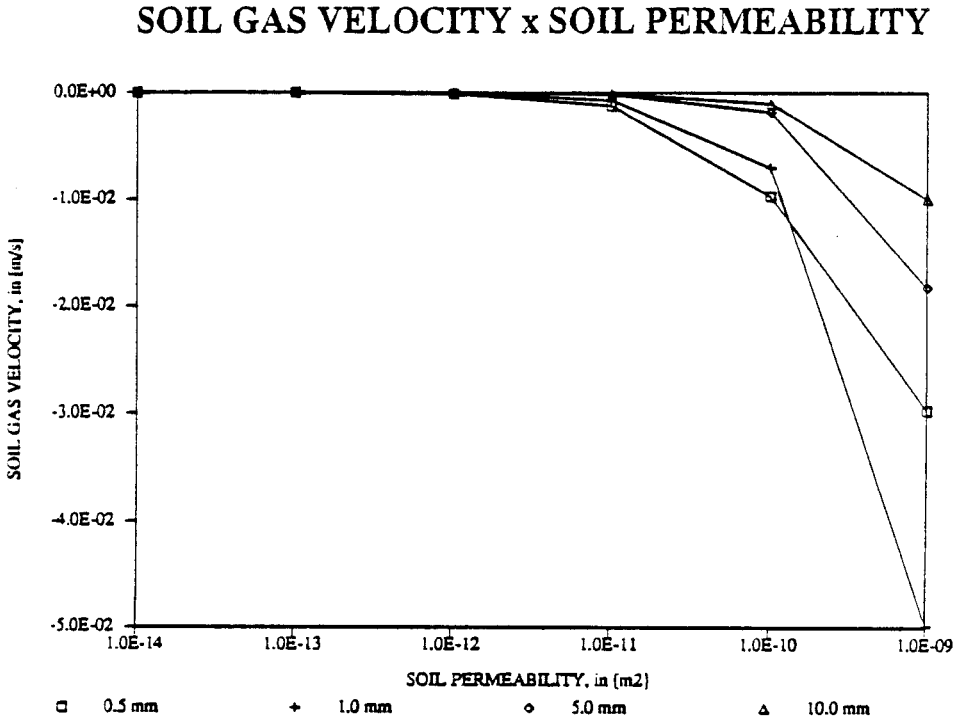

(A) - Version with the soil gas velocity in a linear scale.

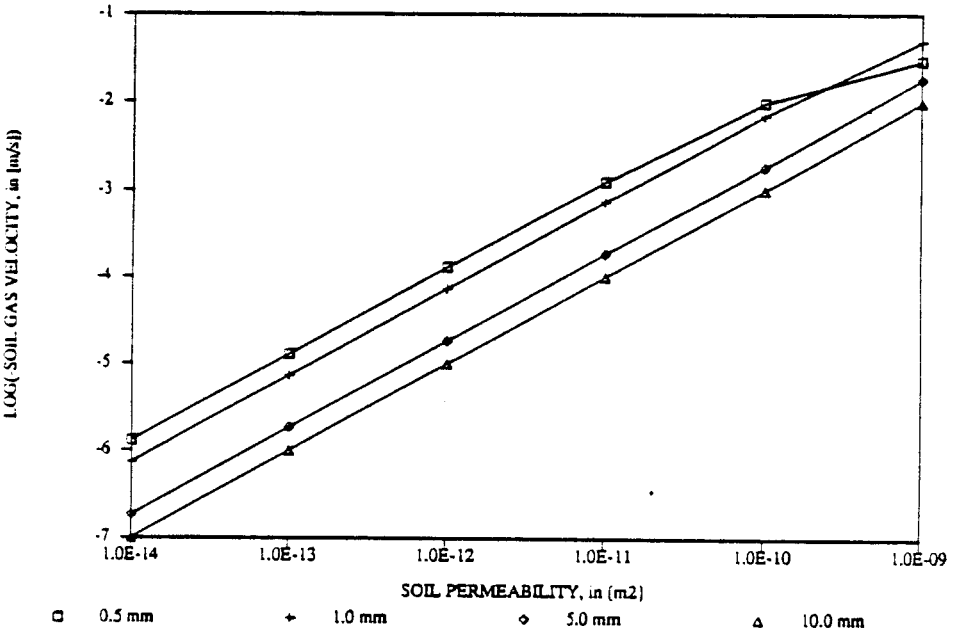

(B) - Version with the soil gas velocity in a logarithmic scale.

Figure 5.21 — Average flux of radon at the soil-crack interface, as a function of the soil permeability, for different values of crack width.

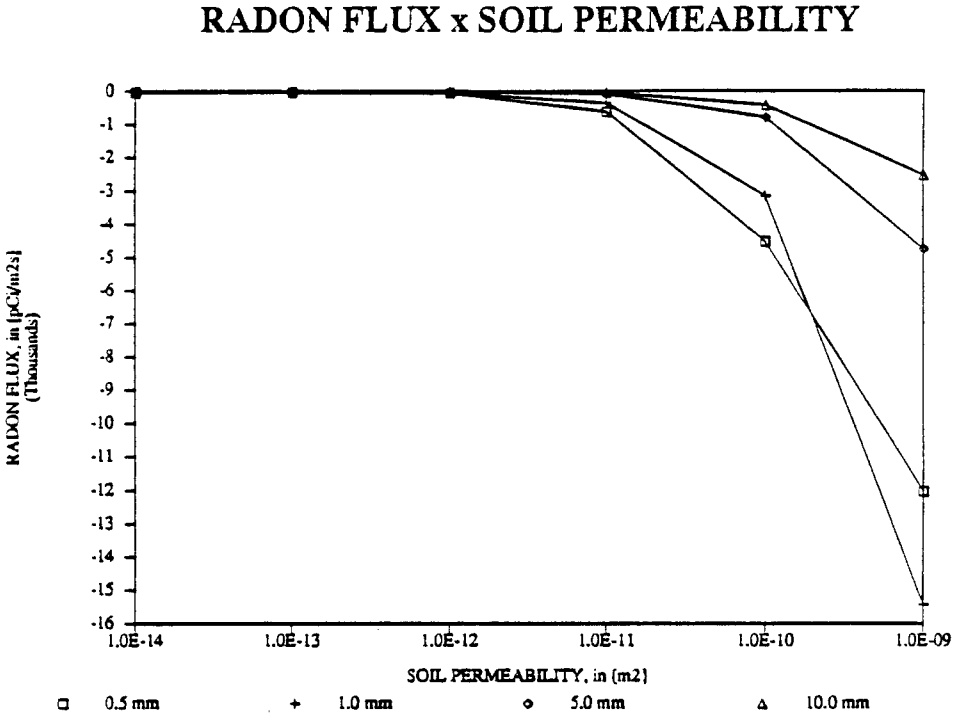

(A) - Version with the radon flux in a linear scale.

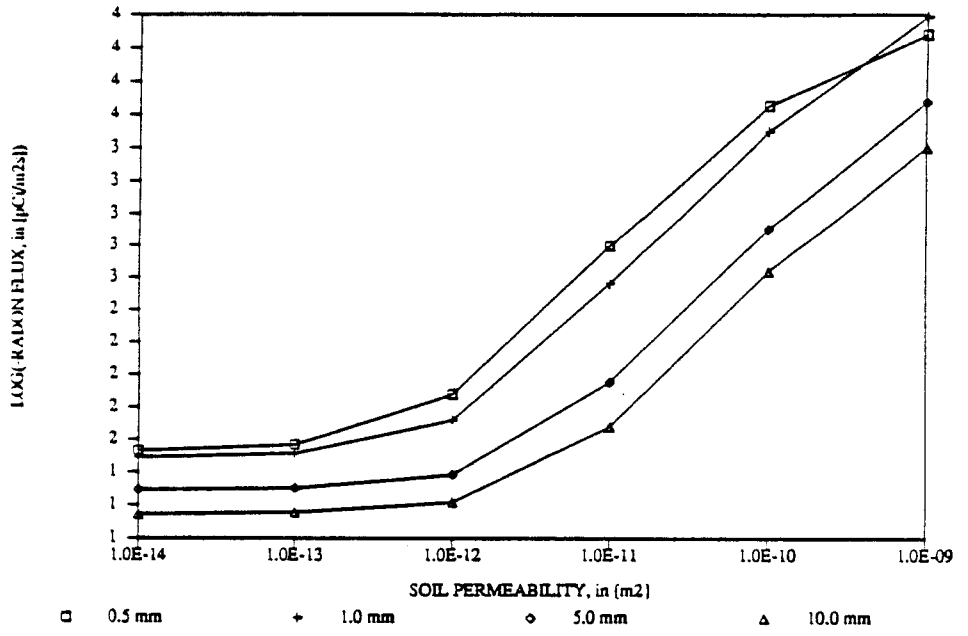

(B) - Version with the radon flux in a logarithmic scale.

Besides this, even the convective component of the radon flux, which is given by the product of the soil gas velocity times the radon concentration in the soil gas, at the soil-crack interface, is not linearly dependent on the soil permeability, because the radon concentration in the soil gas is also affected by the soil permeability and crack width, as we will see later. So, in Fig.(5.21), for soil permeability below $1.0\times10^{-12}[m^2]$ the diffusive component of the radon flux predominates, and the total radon flux becomes almost invariable with the soil permeability. Then, for soil permeabilities above $1.0\times10^{-12}[m^2]$ the convective component of the radon flux predominates and the total radon flux varies almost linearly with the soil permeability. The variation is not actually linear because, as we will see in the next figure, the concentration of radon in the soil gas at the crack interface does not vary linearly with the soil permeability.

In Fig.(5.22) I have plotted the radon concentration in the soil at the soil-crack interface as a function of the soil permeability and crack width. There we note that for soil permeabilities below $1.0\times10^{-12}[m^2]$ the radon concentration varies slowly with the soil permeability, and depends more on the crack width. Then, as the soil permeability increases above $1.0\times10^{-12}[m^2]$, the radon concentration increases up to a maximum and starts to decrease very rapidly. The location of these peaks of radon concentration depends of the crack width, but according to the model's predictions they occur with soil permeabilities between 1.0×10^{-11} and $1.0\times10^{-10}[m^2]$. The reason for these peaks is that, for the soil permeability below $1.0\times10^{-12}[m^2]$, the soil gas velocity is small and the radon transport occurs mainly by diffusion, and consequently the radon concentration is almost invariable with the soil permeability. But as the soil permeability increases above $1.0\times10^{-12}[m^2]$ the convection component of the radon flux assumes the predominant role in the radon transport process, bringing radon-richer soil gas from deeper in the soil and, consequently, increasing the radon concentration at the soil-crack interface. However, as the velocity of the soil gas through the crack interface increases with the soil permeability, not only the radon-rich soil gas from deep in the soil, but also the poor-radon air from the atmosphere and the upper part of the soil block are brought to the crack channel, resulting then in the dilution of the radon concentration in the soil gas at the soil-crack interface. It should be noted that the dilution

Figure 5.22 — Average radon concentration in the soil gas at the soil-crack interface, as a function of the soil permeability, for different values of the crack width.

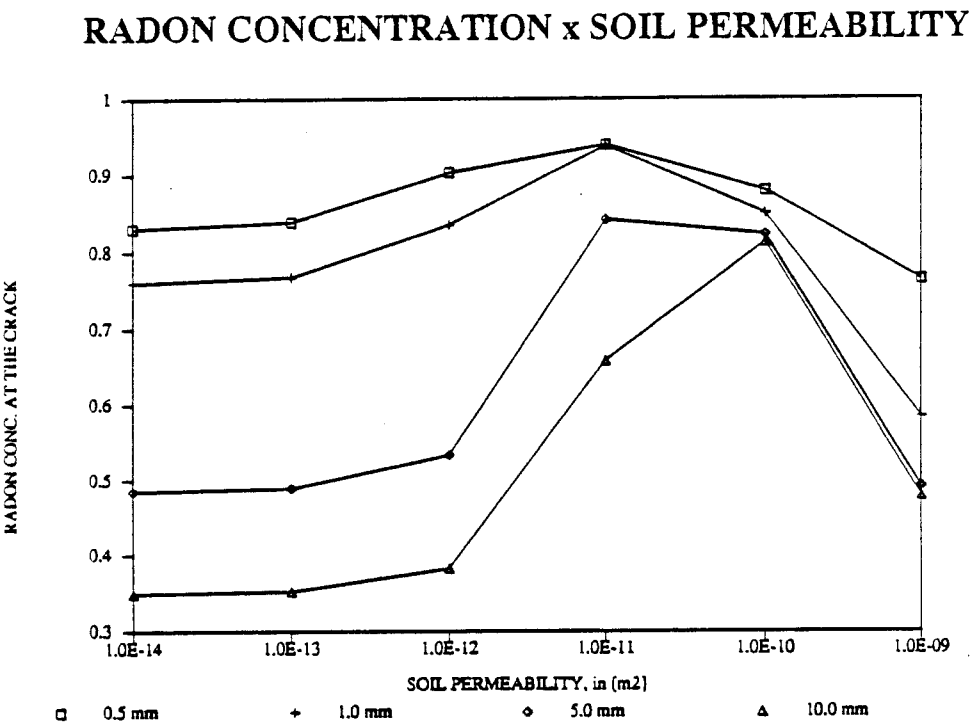

effect can also be affected by the depth of the basement, as well as by the location of the crack in the understructure of the house. Further insights on this dilution effect will be given next, with the vertical profiles of the radon concentration in soil gas within the soil block.

In order to show the dependency of the soil gas radon concentration, on the soil permeability, I have added a sequence of six figures, from Fig.(5.23) to Fig.(5.28), representing the profile of radon concentration in a vertical cross-section of the soil block, for different cases of soil permeability. The crack width was kept constant, and equal to $5.0[mm]$. The contour lines represent the points in the soil block with the same radon concentration, which is given in dimensionless units, normalized within the interval $(0, 1)$. Note that, to get the actual value of the radon concentration, its normalized result should be multiplied by its characteristic

value, $530[pCi.l^{-1}]$.

Thus, we can see in Figs. (5.23), (5.24), and (5.25) that, for low permeabilities ($k \leq 1.0\times10^{-12}[m^2]$), the profile of radon concentration is very little affected by the variation of soil permeability. However, for larger soil permeabilities, as shown in Figs. (5.26), (5.27), and (5.28), the distribution of radon concentration is clearly affected by the soil permeability. For example, comparing Fig.(5.26) with Fig.(5.27) we see that, increasing the soil permeability from 1.0×10^{-11} to $1.0\times10^{-10}[m^2]$, the contour lines of radon concentration in the upper part of the soil block, close to the house, are moved deeper into the soil, reflecting the dilution effect caused by the larger amount of poor radon air being transported from the atmosphere and the upper part of the soil. On the other hand, the contour lines under the basement are moved closer to the location of the crack, as a consequence of the richer radon soil gas being transported from deeper in the soil. Now, with a further increase in the soil permeability to $1.0\times10^{-9}[m^2]$, as shown in Fig.(5.28), the flow of soil gas increases even more making the dilution effect more evident.

Finally, the variation of the indoor radon concentration with the soil permeability and crack width was plotted in Fig.(5.29). There we can see that the indoor radon concentration is an increasing function of both the soil permeability and crack width. For soil permeability below $1.0\times10^{-12}[m^2]$, since the radon flux is mainly due to its diffusive component, the indoor radon concentration varies very slowly with the soil permeability. But for soil permeability above $1.0\times10^{-12}[m^2]$, the variation is strongly dependent on the soil permeability, with an almost linear relationship.

Sensitivity Analysis of the Computer Model – Bulk Diffusivity Coefficient of Radon in Soil.

In the absence of any disturbance pressure in the soil, the distribution of radon concentration with depth increases exponentially from a small value at the soil-air interface,[7] to its maximum finite value at infinite depth in the soil. The rate at which the concentration of radon changes with depth is determined by its *diffusion length* in the soil, which is defined

[7] As a boundary condition, the radon concentration at the soil-air interface was considered equal to zero. (See Table (3.2)).

Figure 5.23 — Distribution of radon concentration in soil gas, in a vertical cross-section of the soil block, with soil permeability equal to $1.0\times10^{-14}[m^2]$, and crack width equal to $5.0[mm]$.

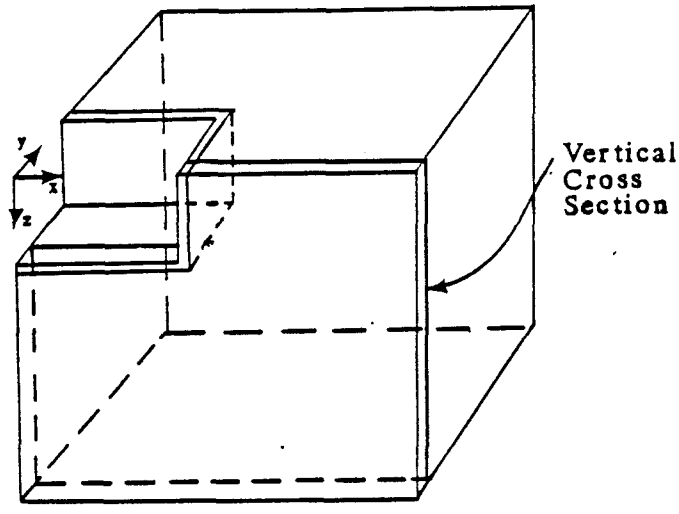

Location of the vertical cross-section in the soil block.

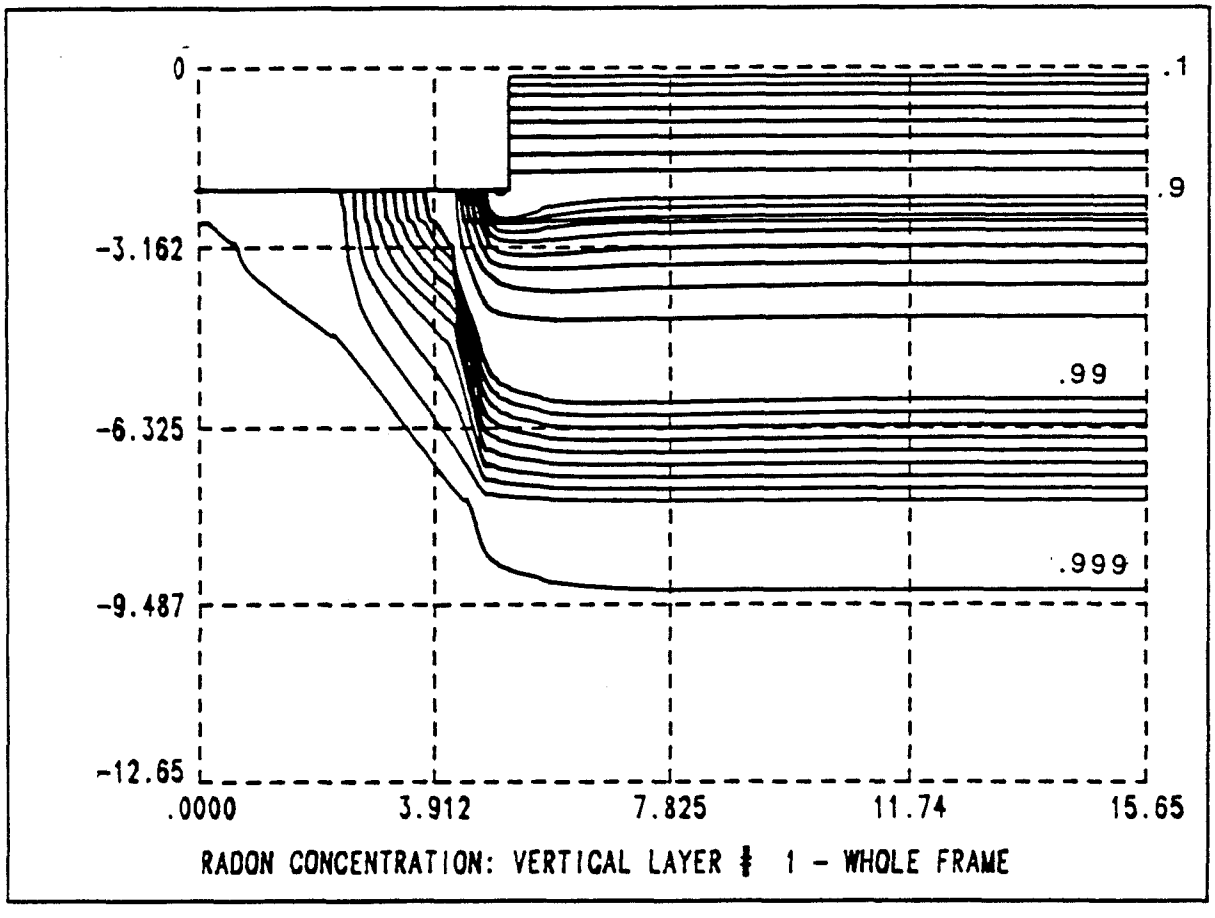

The radon concentration is normalized within the interval $(0, 1)$.

Figure 5.24 — Distribution of radon concentration in soil gas, in a vertical cross-section of the soil block, with soil permeability equal to $1.0\times10^{-13}[m^2]$, and crack width equal to $5.0[mm]$.

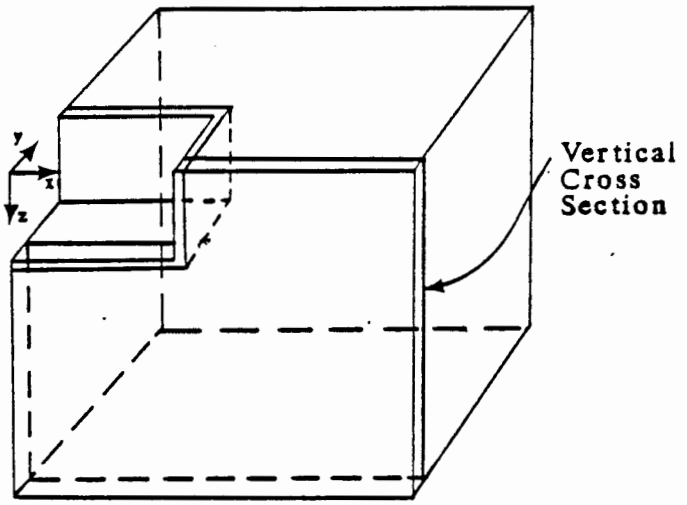

Location of the vertical cross-section in the soil block.

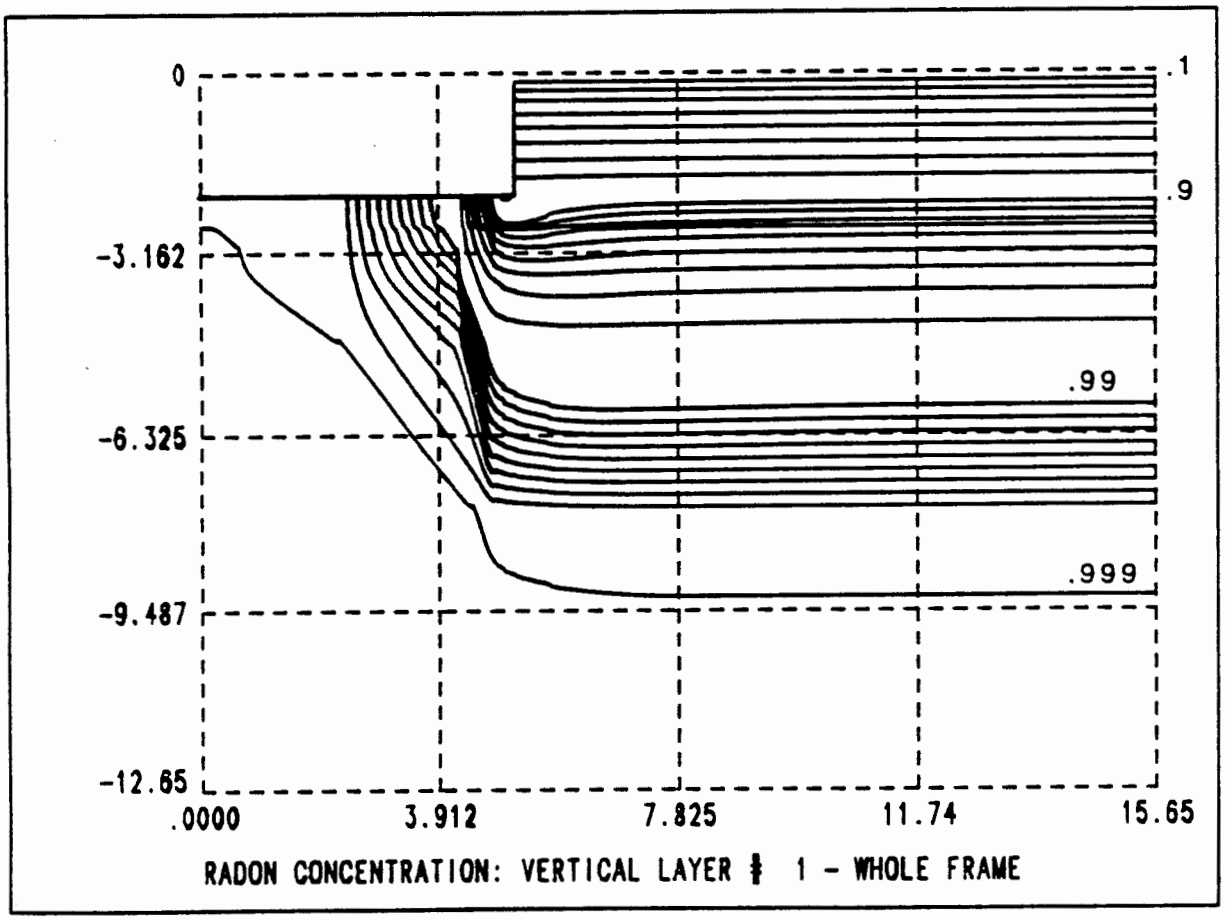

The radon concentration is normalized within the interval $(0, 1)$.

Figure 5.25 — Distribution of radon concentration in soil gas, in a vertical cross-section of the soil block, with soil permeability equal to $1.0\times10^{-12}[m^2]$, and crack width equal to $5.0[mm]$.

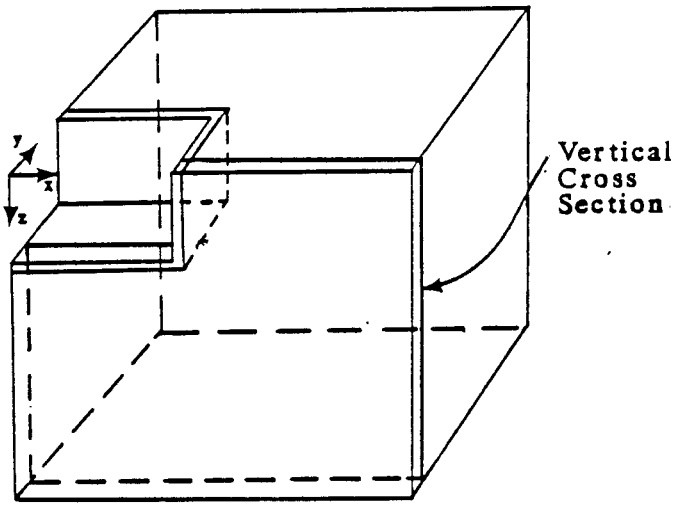

Location of the vertical cross-section in the soil block.

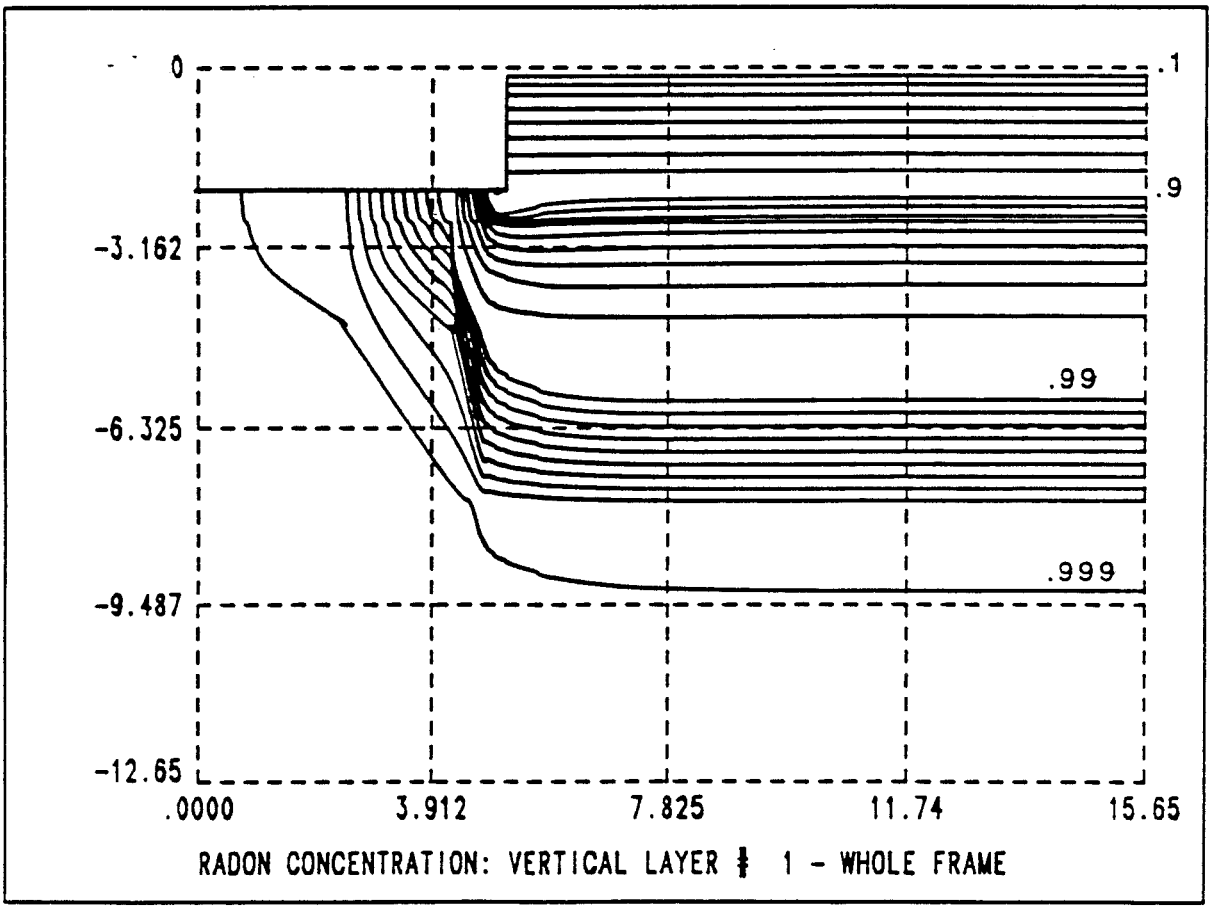

The radon concentration is normalized within the interval $(0, 1)$.

Figure 5.26 — Distribution of radon concentration in soil gas, in a vertical cross-section of the soil block, with soil permeability equal to $1.0\times10^{-11}[m^2]$, and crack width equal to $5.0[mm]$.

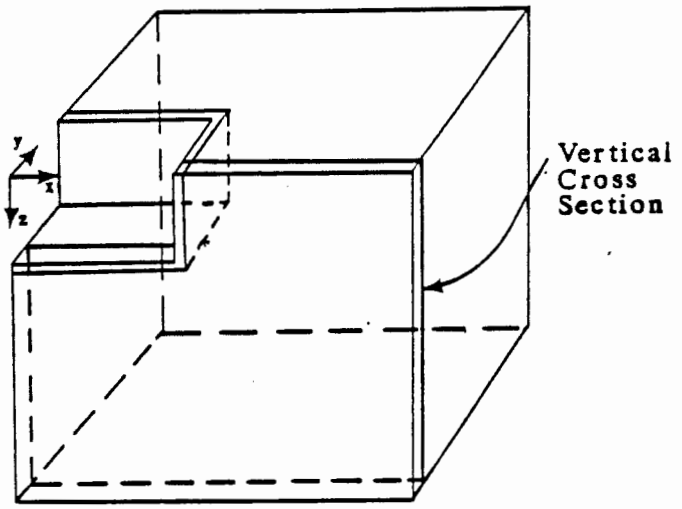

Location of the vertical cross-section in the soil block.

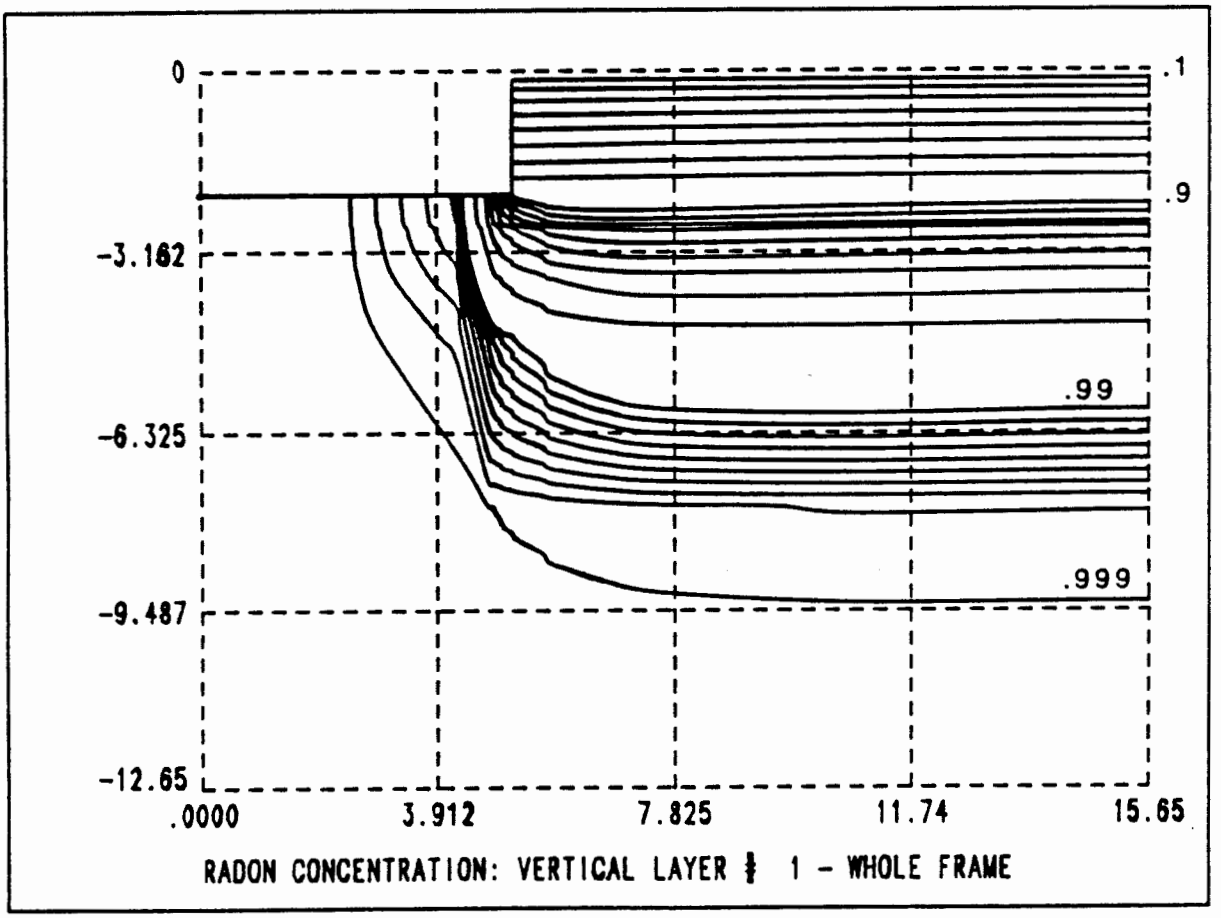

The radon concentration is normalized within the interval $(0, 1)$.

Figure 5.27 — Distribution of radon concentration in soil gas, in a vertical cross-section of the soil block, with soil permeability equal to $1.0 \times 10^{-10}[m^2]$, and crack width equal to $5.0[mm]$.

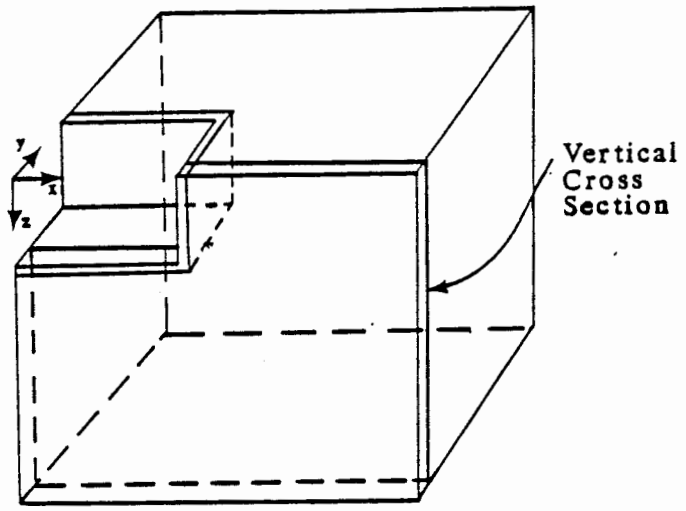

Location of the vertical cross-section in the soil block.

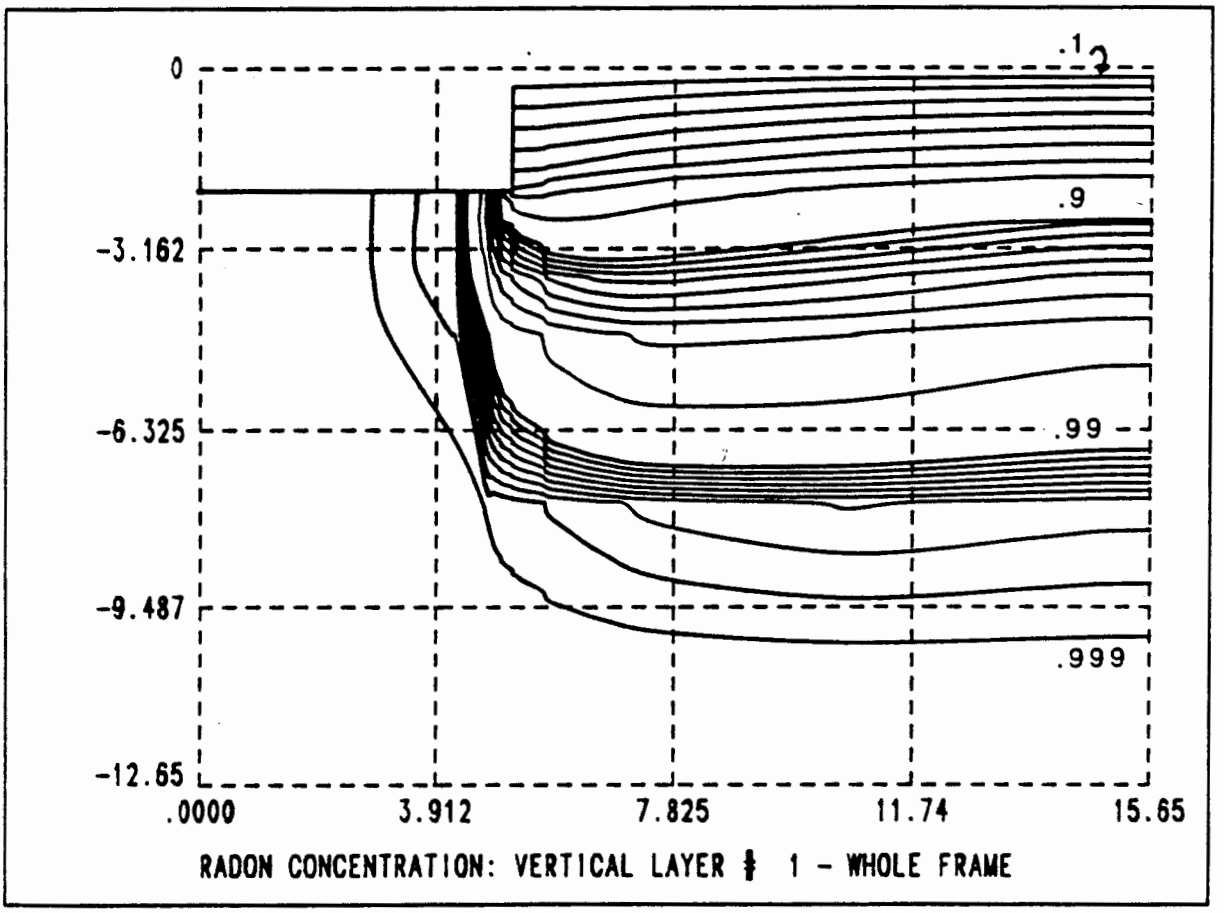

The radon concentration is normalized within the interval $(0, 1)$.

Figure 5.28 — Distribution of radon concentration in soil gas, in a vertical cross-section of the soil block, with soil permeability equal to $1.0\times10^{-9}[m^2]$, and crack width equal to $5.0[mm]$.

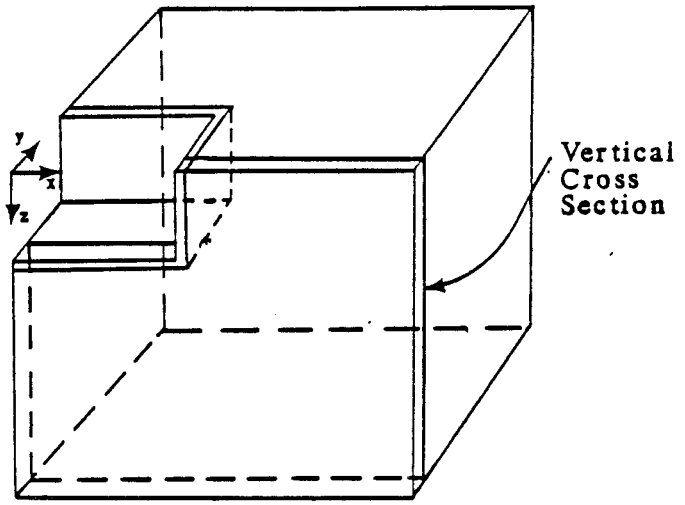

Location of the vertical cross-section in the soil block.

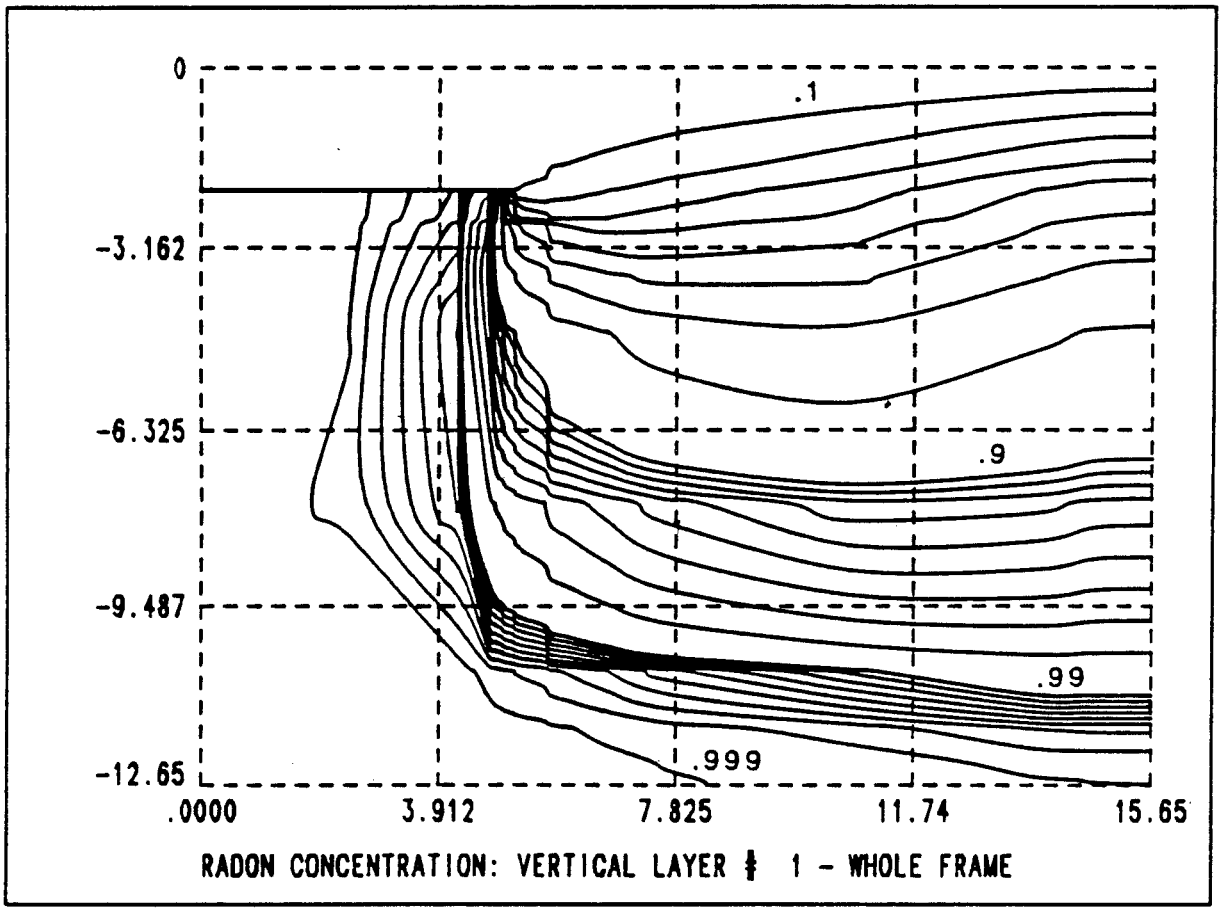

The radon concentration is normalized within the interval $(0, 1)$.

Figure 5.29 — Indoor radon concentration, as a function of the soil permeability, for different values of crack width.

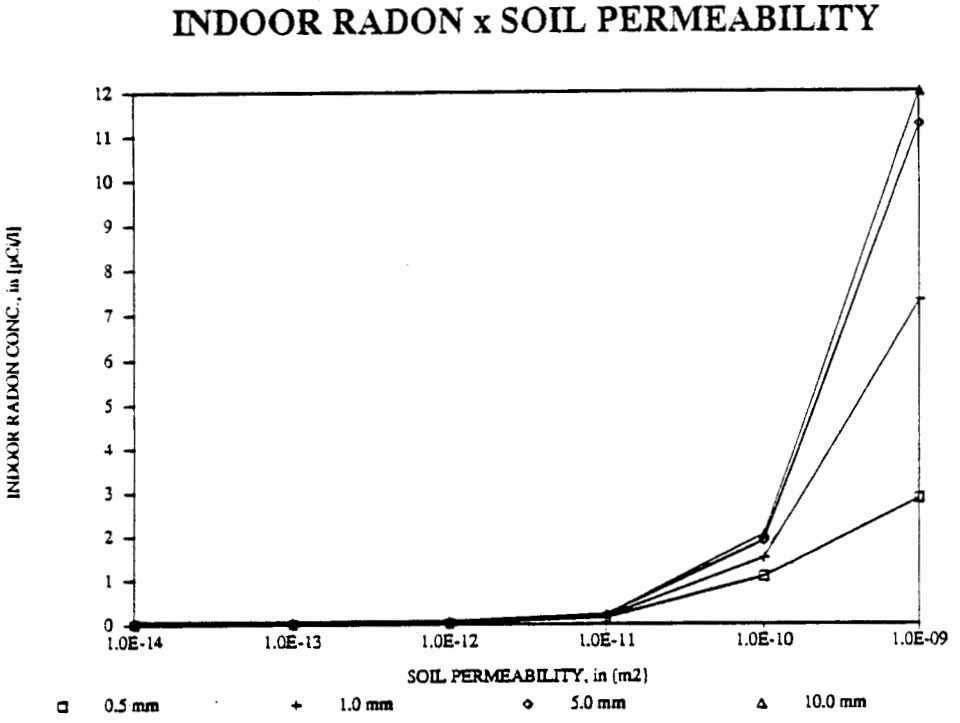

(A) – Version with the indoor radon concentration in a linear scale.

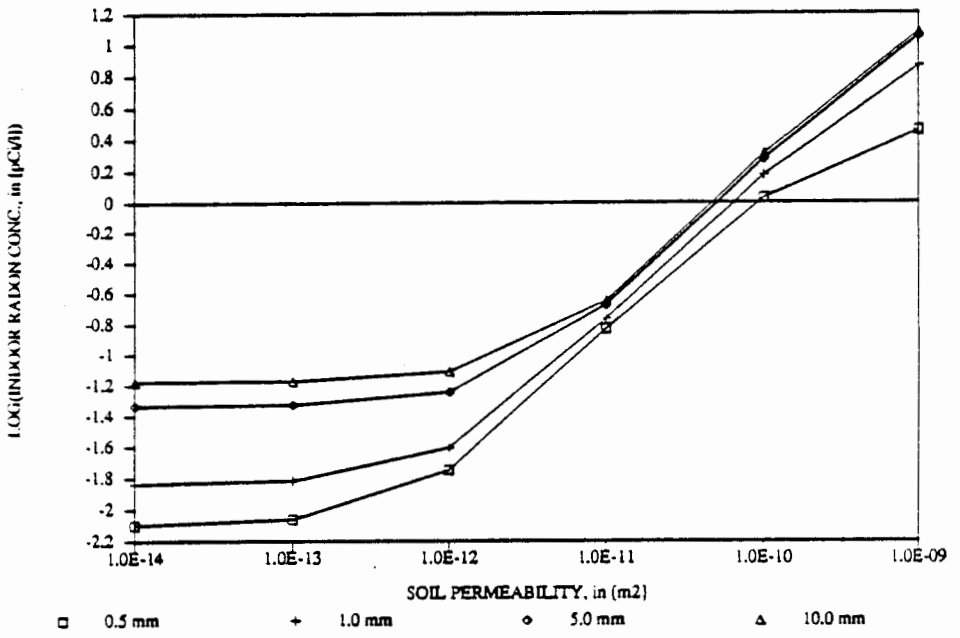

(B) – Version with the indoor radon concentration in a logarithmic scale.

as the distance required for the concentration to be changed by a factor equal to the natural number e. The diffusion length of radon in soil is closely related to its bulk diffusion coefficient. For a small bulk diffusion coefficient, (or a small diffusion length), the radon concentration reaches its limiting value at a shallow depth in the soil. On the other hand, for larger diffusion lengths, the atoms of radon are able to diffuse through longer distances in the soil before being transformed by radioactive decay. Consequently, for those cases, the radon concentration reaches its maximum value at a deeper depth in the soil. Therefore, the distribution of radon concentration with depth in the soil is mainly governed by the bulk diffusion coefficient of radon in soil. The presence of a disturbance pressure distribution in the soil block will tend to alter this natural distribution of radon concentration with depth, the extent of which will depend on the level of the disturbance pressure, as well as the values of some physical parameters of the soil, specially the soil permeability.

The diffusive component of the radon flux from the soil into the house is directly related to the bulk diffusion coefficient of radon in the soil. However, since the convective component of the flux is dependent of the radon distribution in the soil, and since the vertical distribution of radon in the soil is mainly affected by the diffusion length of radon in soil, then the bulk diffusion coefficient of radon in soil may affect both components - diffusive and convective - of the radon flux into the house.

Thus, the purpose of this test is to verify how sensitive the computer model is to variations of the bulk diffusion coefficient of radon in soil, within its anticipated range. In order to perform the test, the program MASTRA was run six times, with the bulk radon diffusion coefficient in soil[8] varying from 0.5 to $5.0 \times 10^{-6}[m^2/s]$. The selected indicators were the average radon flux and the radon concentration at the soil-crack interface, as well as the indoor radon concentration. The results were grouped in Table (5.12), and plotted in Fig.(5.30).

In Fig.(5.30A) we can see that, as the bulk radon diffusion coefficient increased from 0.5×10^{-6} to $1.0\times10^{-6}[m^2/s]$, the absolute value of the radon flux at the crack also increased

[8] Note that the radon diffusion coefficient in free air is equal to $1.2 \times 10\_5[m^2/s]$, [Na85].

Table 5.12 — Sensitivity analysis of the computer programs - Variation of the bulk diffusivity coefficient of radon in soil.

Radon Diff. Coefficient. $[m^2.s^{-1}]$	Indoor Radon Concentration. $[pCi.l^{-1}]$	Average Radon Flux at the Crack Interface $[pCi.m^2.s]$	Average Radon Conc. at the Crack Interface [Dimensionless]
5.0×10^{-7}	2.35×10^{-2}	-49.89	0.7910
1.0×10^{-6}	2.48×10^{-2}	-52.65	0.8356
2.0×10^{-6}	2.47×10^{-2}	-52.33	0.8305
3.0×10^{-6}	2.40×10^{-2}	-50.80	0.8063
4.0×10^{-6}	2.32×10^{-2}	-49.24	0.7815
5.0×10^{-6}	2.26×10^{-2}	-47.81	0.7588

from 49.9 to $52.7[pCi/m^2.s]$. Then, with a further increase of the diffusion coefficient above $1.0\times10^{-6}[m^2/s]$, the variation of the radon flux is reversed, showing an inverse correlation with the radon diffusion coefficient. A similar effect occurs with the radon concentration in soil gas at the soil-crack interface, as well as with the indoor radon concentration, as shown in Table (5.12) and Fig.(5.30). What happens here is that, for a small radon diffusion coefficient in the order of $0.5\times10^{-6}[m^2/s]$, the diffusion length is relatively small, which means that the vertical profile of the radon concentration in the soil block reaches its limit value at a shallow depth. Consequently, at the depth in the soil where the crack is located, the radon concentration is already about its limit value, and therefore the diffusion of radon into the crack is not affected by the presence of the air-soil interface at the upper part of the soil block. In these cases, the concentration of radon at the soil-crack interface increases with the diffusion coefficient, resulting in an increase of both the diffusive and convective components of the radon flux, as we have seen in the first part of the curves in Fig.(5.30). If it were not for the influence of the air-soil interface at the ground level, the radon flux would continually increase as a function of the bulk radon diffusion coefficient in soil. However, as the diffusion length is increased, the vertical profile of the radon concentration in the soil is altered, reducing the concentration at the level where the crack is located. Therefore, in these cases the diffusive component of the flux is increased by the increase of the radon

Figure 5.30 — Sensitivity analysis of the numerical model – Variation of the bulk diffusion coefficient of radon in soil.

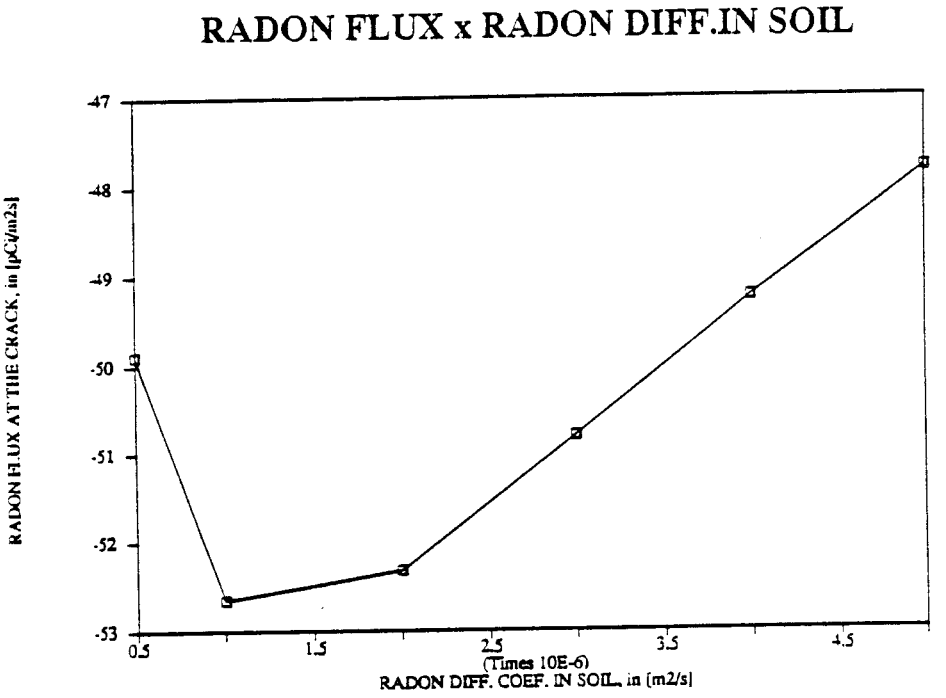

(A) – Average radon flux at the soil-crack interface as a function of the bulk diffusion coefficient in soil.

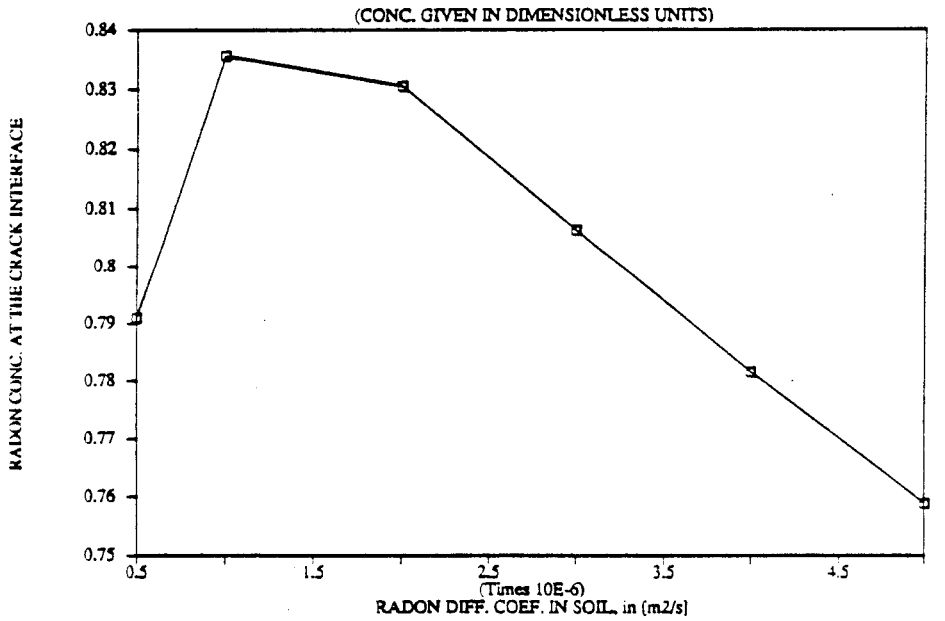

(B) – Average radon concentration in soil gas at the soil-crack interface as a function of the bulk diffusion coefficient in soil.

diffusion coefficient, but the convective component is decreased by the decrease of the radon concentration in the soil around the crack, and consequently the total variation of the net radon flux will be the result of these two distinct tendencies. As we can see in Fig.(5.30), the absolute value of the net radon flux decreased slightly from 52.7 to $52.3[pCi/m^2.s]$, with a doubling of the bulk radon diffusion coefficient from 1 to $2\times10^{-6}[m^2/s]$, but beyond this point the flux decreased rapidly with the increase of the bulk radon diffusion coefficient in soil.

It should be remembered here that, in the basic case for this test, the soil permeability is assumed equal to $1.0\times10^{-12}[m^2]$, and the applied disturbance pressure is equal to $-5[Pa]$, and as it was shown before in Figs. (5.8) and (5.21), for this case, the diffusive and the convective components of the radon flux at the soil-crack interface are of the same order of magnitude. So, for this case, a variation on both components of the flux, as caused by changing the radon diffusion coefficient, will affect the net flux accordingly, depending on the intensity of the variation of each component separately. However, for smaller soil permeabilities, and smaller disturbance pressures, the diffusive component of the flux predominates, and the net flux of radon becomes an increasing function of the bulk diffusion coefficient of radon in soil. On the other hand, for larger soil permeabilities, or larger disturbance pressures, the convective flux predominates, and the net flux of radon is then expected to be: 1) almost invariable with the diffusion coefficient, for values of the diffusion coefficient below $1.0 \times 10^{-6}[m^2/s]$; and 2) inversely related to the bulk diffusion coefficient for the values of the coefficient above $1.0 \times 10^{-6}[m^2/s]$. Yet, these cases were not tested with the model.

Sensitivity Analysis of the Computer Model – Soil Porosity.

According to the model, as expressed by Eq.(3.14), the production rate of radon into the soil pore space is inversely related to the porosity of the soil. In other words, variation of the soil porosity should affect inversely the amount of radon, available within the soil pore space, to be transported into the house. Thus, the purpose of this last test is to verify how the computer model responds to the variation of the soil porosity. In order to perform the

test, the program MASTRA was run five times with the soil porosity varying from 0.2 to 0.6. The model's predictions of the average radon flux at the soil-crack interface, and the indoor radon concentration, as a function of the soil porosity were then grouped in Table (5.13), and plotted in Fig.(5.31).

The results showed that the computer model performed as it was expected to do. They also showed that the model is quite sensitive to variations of soil porosity. For example, the variation of the soil porosity from 0.4 to 0.6, which is the expected range of variation of this parameter, caused a decrease of the radon flux, and the indoor radon concentration, by a factor of two, approximately. It should be remembered though, that in reality the variation of the soil porosity would generally imply a variation of other parameters in the soil, such as the soil permeability, affecting differently the transport of radon through the soil block, as already discussed in the other tests of the model.

Table 5.13 — Sensitivity analysis of the computer model - Variation of the soil porosity.

Soil Porosity. [Dimensionless]	**Average Radon Flux at the Soil-Crack Interface.** $[pCi.m^{-3}.s^{-1}]$	**Indoor Radon Concentration.** $[pCi.l^{-1}]$
.2	-1.92×10^{2}	-9.04×10^{-2}
.3	-1.17×10^{2}	-5.54×10^{-2}
.4	-7.76×10^{1}	-3.66×10^{-2}
.5	-5.27×10^{1}	-2.48×10^{-2}
.6	-3.53×10^{1}	-1.68×10^{-2}

Sensitivity Analysis of the Computer Model - Other Parameters.

The other parameters listed in Table (5.8) – radium concentration in the soil particles; radon emanating fraction; and soil particle density – are all related exclusively to the production rate of radon into the soil pore space, as expressed in Eq.(3.14).

Figure 5.31 — Sensitivity analysis of the numerical model – Variation of the soil porosity.

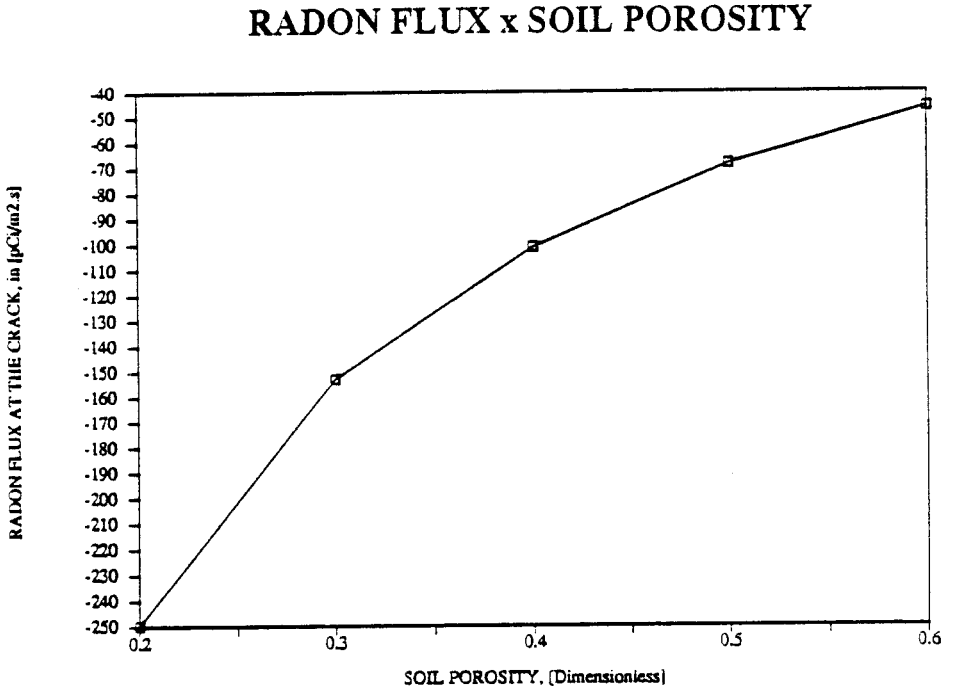

(A) – Average radon flux at the soil-crack interface as a function of the soil porosity.

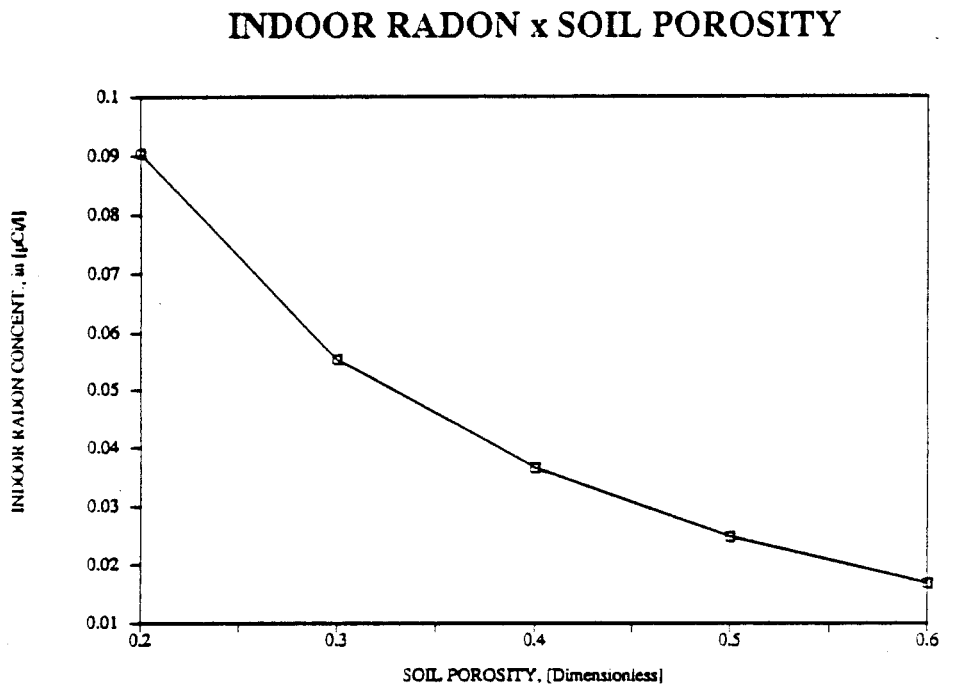

(B) – Average radon concentration in soil gas at the soil-crack interface as a function of the soil porosity.

Predictions of the model in relation to the distribution of radon concentration in the soil, and the radon entry rate into the house, as well as the indoor radon concentration are expected to be directly proportional to the parameter S – the production rate of radon into the soil pore space. Therefore, since the parameters mentioned above are related exclusively to S, and since S is directly proportional to each one of them (see Eq.(3.14)), then the model's predictions on radon concentration are also expected to be directly proportional to each one of these parameters , that is: 1) the radium concentration; 2) the radon emanating fraction; and 3) the soil particle density.

Yet, no actual test was made using these parameters in the computer model. However, based on the considerations above, a few predictions could be made, as it follows. As shown in Table (5.8), concentrations of radium in soil particles vary in a relatively large range (0.2×10^{-9} to $4.0 \times 10^{-9}[Ci/Kg]$), and consequently represent a potentially large source of variation of indoor radon concentration. For example, using the predicted data shown in Table (5.11), for a value of soil permeability of $1.0 \times 10^{-12}[m^2]$, this range of radium concentration would have caused an indoor radon concentration in the range of 1.55×10^{-2} to $3.11 \times 10^{-1}[pCi/l]$. Yet, for a higher soil permeability of $1.0 \times 10^{-9}[m^2]$, the same range of radium concentration would have produced a indoor radon concentration in the range of 2.4 to $48.0[pCi/l]$.

Similarly, for a case of $k = 1.0 \times 10^{-12}[m^2]$, the variation of the radon emanating fraction, in the range of 0.05 to 0.7, would have caused an indoor radon concentration in the range 1.94×10^{-2} to $2.72 \times 10^{-1}[pCi/l]$. And also, for $k = 1.0 \times 10^{-9}[m^2]$, the same range of radon emanating fraction would have produced an indoor radon concentration in the range of 3.0 to $42.0[pCi/l]$.

Variation of the soil particle density occurs in a very small range (from 2.6×10^3 to $2.8 \times 10^3[Kg/m^3]$). Consequently this parameter has little effect on the predictions of the model.

CHAPTER VI

CONCLUSION

Overview.

This thesis was developed from a fundamental hypothesis that soil is the main source of indoor radon. Under this hypothesis, radon in the soil gas enters the house from soil, due to a complex diffusive-convective mechanism, through openings in the basement of the building. The driving forces responsible for this phenomenon are caused by small pressure differences of the order of a few pascals created between the inside and the outside of the building, due to the effects of wind speed, temperature, and any unbalanced mechanical ventilation in the house.

Thus, a mathematical model was developed, based on established principles of diffusion and flow of gas in porous medium, to describe the effect of these phenomena on the indoor radon concentration in a house. The model simulates: 1) the production, decay and the diffusive-convective transport of radon throughout the soil; 2) the diffusive-convective entry rate of radon into houses, through idealized openings in the basement; 3) and the final indoor radon concentration, as a function of the underpressure inside the house. The differential equations of the problem, were then solved by a three-dimensional numerical model, based on a finite-difference approximation, which was implemented by two coupled computer programs: PRESSU and MASTRA. PRESSU was used to calculate the distribution of the

disturbance pressure and the soil-gas velocity field throughout the soil block, as a function of the applied negative pressure in the basement. MASTRA then used the soil-gas velocity field predicted in PRESSU to calculate: 1) the distribution of radon concentration in the soil; 2) the radon entry rate into the house; 3) and the final indoor radon concentration.

The model is restricted to a steady-state condition, and to a physical configuration of a house with basement, containing a well defined crack at the wall-floor joint of the basement. The important input parameters for the model are:

- Applied negative disturbance pressure in the basement;
- Soil permeability;
- Soil porosity;
- Bulk diffusion coefficient of radon in the soil;
- Concentration of radium (Ra-226) in the soil;
- Radon emanating fraction in the soil;
- Geometrical dimensions of the house, including the crack width;
- Air exchange rate in the house.

The computer model was adjusted in relation to its operational parameters in order to assure that: 1) the numerical method was applied correctly; 2) the boundary conditions were satisfied; 3) the iterative process in the computer codes converged to the solution of the algebraic discretization equations; and 4) that the solution of the algebraic discretization equations approximated the solution of the original differential equations of the model.

A parametric sensitivity analysis was then performed to examine the performance of the model, and to describe the phenomenon of radon transport through the soil and into the house under the effect of all important related parameters, within their expected range of variation.

The model developed in this dissertation is expected to be used for the interpretation of experimental results being produced at Lawrence Berkeley Laboratory, as well as in designing new experiments related to the problem of transport of radon from soil into houses.

However, data from the LBL experiments, applicable to the conditions and circumstances assumed in the model, are not readily available yet, and consequently at this present time the model's predictions could not be verified against actually measured data. Therefore, because of the lack of an appropriate set of measured data at the present time, this dissertation will be concluded without a proper validation with real data – a task left to be performed later.

Conclusions.

Results from the adjustment and parametric sensitivity tests showed that the model performs consistently with physical expectations. More importantly, these results also indicated some significant features of the mechanisms and factors which affect the entrance of radon from the soil into the house, leading to the following observations and conclusions:

1). The iterative procedure adopted in PRESSU and MASTRA showed that these programs are effective in solving the algebraic discretization equations representing the differential equations of the problem.

2). Variation of the size of the numerical grid mesh indicated that the results were converging to a fixed value, which is supposedly the solution of the original differential equations of the model. However, increase in the numerical grid beyond 25,000 nodes could not be tried because of the limitations imposed by the computer capacity available.

3). The size of the soil block around the house is important in assuring that the boundary conditions at the external surfaces of the soil block are satisfied. Results of the tests showed then that the soil block size should be at least $10[m]$ beyond the basement walls and floor, in order to assure a proper implementation of the boundary conditions.

4). The value of the turbulent diffusion coefficient of radon in the air inside the basement affects the overall performance of the model – a value of $1.2[m^2/s]$ was necessary to represent a condition of well mixed air in the basement.

5). Selection of the interpolation scheme used for the discretization of the radon transport equation showed very little effect on the model's predictions. However, the parametric tests were performed in cases with low soil permeability, ($k = 1.0 \times 10^{-12}[m^2]$), and a disturbance delta pressure of $-5[Pa]$, where the convective component of the total flux of radon is comparable with, or even smaller than, the diffusive component. For higher soil permeabilities, or higher disturbance delta pressures, a stronger effect of the choice of the interpolation function on the model's predictions would be expected. The power-law discretization scheme has been recommended as the best formulation, and was then adopted as default in the model.

6). Variations of the size of the house, more specifically the area of the basement, have shown very little effect on the performance of the model, which means that the model can be applied reasonably well for houses of varied sizes with no addition of extra errors.

7). Variations of the applied disturbance pressure in the basement have a direct, though not linear, effect on the model's predictions. For a soil permeability of $1.0 \times 10^{-12}[m^2]$, an increase of the delta pressure from almost zero to $-20[Pa]$, caused a 4.8-fold increase in the indoor radon concentration, from 1.45×10^{-2} to $7.0 \times 10^{-2}[pCi/l]$. However, for a higher soil permeability, the same variation of delta pressure would have caused a higher increase in the indoor radon concentration. And vice-versa, for lower soil permeability, the increase in indoor radon concentration would have been lower.

8). The disturbance pressure distribution throughout the soil block is affected by both the crack width and soil permeability. For the presently simulated configuration of the house, with a basement depth of $2.0[m]$, and a basement floor of $0.15[m]$ thick, these effects can be summarized as the following:

- In soil with low permeability, ($k \leq 1.0 \times 10^{-12}[m^2]$), the pressure drop occurs almost entirely within the soil block – an effect that is almost independent of the crack width;
- In soil with high soil permeability, ($k > 1.0 \times 10^{-12}[m^2]$), the pressure drop occurs almost entirely within the soil block, for crack widths larger than $5.0[mm]$, and

is distributed between the crack and the soil block, for crack widths lower than $5.0[mm]$;

- The disturbance pressure distribution within the soil shows an expansion of the isobar lines as the crack width is increased. This general effect occurs at either high or low permeability of the soil;
- For crack widths larger than $5.0[mm]$, the disturbance pressure distribution within the soil is practically unchanged with the soil permeability;
- For crack widths smaller than $5.0[mm]$, the disturbance pressure distribution in the soil is affected by the soil permeability in such a way that increasing the soil permeability causes a contraction of the isobar lines to points closer to the crack.

9). The velocity of the soil gas, as well as the flux of radon at the soil-crack interface, are affected by the crack width and soil permeability in the following ways:

- Except for those configurations of very small crack width ($< 1.0[mm]$), and very high soil permeability ($k \geq 1.0 \times 10^{-9}[m^2]$), the soil gas velocity and the radon flux at the soil-crack interface are inversely related to the crack width;
- Note however that the total flow of radon into the house is always directly related to the crack width and soil permeability;
- For large crack width, ($\geq 5.0[mm]$), the soil gas velocity varies linearly with soil permeability (with a one-by-one slope), within the whole range considered (1.0×10^{-14} to $1.0 \times 10^{-9}[m^2]$). However, for smaller crack widths, ($\leq 1.0[mm]$), the soil-gas velocity varies linearly with the soil permeability, only in a smaller range, from 1.0×10^{-14} to $1.0 \times 10^{-11}[m^2]$. Beyond that, ($k \geq 1.0 \times 10^{-11}[m^2]$), the relationship is less strong than linear;
- Differently from the velocity of the soil gas, the total radon flux at the soil-crack interface does not vary linearly with soil permeability. For soil permeability below $1.0 \times 10^{-12}[m^2]$, the diffusive component of the radon flux predominates, and the total radon flux becomes almost invariable with the soil permeability. However, for soil permeabilities above $1.0 \times 10^{-12}[m^2]$, the convective component of the radon flux predominates and the total radon flux then varies almost linearly with the soil permeability.

10). The radon concentration in the soil gas throughout the soil block is affected by the crack width and soil permeability in the following ways:

- The radon concentration at the soil-crack interface is inversely dependent on the crack width, for any value of soil permeability;
- For low soil permeability, ($k \leq 1.0 \times 10^{-12}[m^2]$), the radon concentration at the soil-crack interface increases very slowly with the soil permeability;
- For larger soil permeability, ($k \geq 1.0 \times 10^{-12}[m^2]$), the radon concentration at the soil-crack interface increases rapidly with soil permeability, until the effect of dilution starts;
- Dilution of the radon concentration at the soil-crack interface, due to mixing with poorer-radon soil gas coming from the upper part of the soil block, begins with soil permeability between 1.0×10^{-11} to $1.0 \times 10^{-10}[m^2]$, and becomes very significant for $k \geq 1.0 \times 10^{-10}[m^2]$. Also, the intensity of the dilution effect is directly related to the crack width;
- Note that the dilution effect is also inversely related to the depth of the basement floor, and directly related to the applied disturbance pressure and the diffusion coefficient of radon in the soil;
- For low permeability, ($k \leq 1.0 \times 10^{-12}[m^2]$), the distribution of radon concentration throughout the soil block is very little affected by variations of the soil permeability. However, for large soil permeabilities, ($k \geq 1.0 \times 10^{-12}[m^2]$), the distribution of radon concentration in the soil block is highly affected by the soil permeability, reflecting the dilution effect in the upper part of the soil block, and a concentration effect in the regions closer to the crack but under the basement.

11). The indoor radon concentration is an increasing function of both the soil permeability and crack width. For soil permeabilities below $1.0 \times 10^{-12}[m^2]$, the radon flux into the house is mainly due to its diffusive component, and the indoor radon concentration varies very slowly with the soil permeability. However, for soil permeabilities above $1.0 \times 10^{-12}[m^2]$, the convective component of the flux predominates, and the variation of the indoor radon concentration becomes strongly dependent on the soil permeability, with an almost linear relationship.

12). The total entrance of radon into the house may be either directly, or inversely, related to variations of the bulk diffusion coefficient of radon in the soil. For bulk diffusion coefficients lower than $1.0 \times 10^{-6}[m^2/s]$, the indoor radon concentration is directly dependent on the diffusion coefficient. However, for bulk diffusion coefficients higher than $1.0 \times 10^{-6}[m^2/s]$, the indoor radon concentration becomes inversely dependent on the diffusion coefficient. It should be noted though that this effect is also dependent on the applied disturbance pressure as well as on the soil permeability. Thus, for a very low soil permeability, or a very low disturbance pressure, the indoor radon concentration is an increasing function of the bulk diffusion coefficient of radon in soil, within its whole range. On the other hand, for a very high soil permeability, or a very high disturbance pressure, the indoor radon concentration becomes: 1) independent of the bulk diffusion coefficient of radon in soil, for values of the diffusion coefficient below $1.0 \times 10^{-6}[m^2/s]$; 2) inversely dependent on the bulk diffusion coefficient of radon in soil for values of the diffusive coefficient above $1.0 \times 10^{-6}[m^2/s]$.

13). The indoor radon concentration is inversely dependent on soil porosity, if this parameter is considered varying separately. However, variations of soil porosity are generally associated with variations of other parameters in the soil, such as the soil permeability, which affects directly the indoor radon concentration. Consequently, the overall effect on the indoor radon concentration is, in fact, the conjugation of the effects caused by the variation on the soil porosity and the associated variation of soil permeability.

Recommendations.

The radon transport model developed in this thesis, despite its simplified assumptions, constitutes an important first-generation step in the modeling effort to characterize the production and transport of radon in soil and its entrance into houses. It provides the basic theoretical framework which can be used to further explore the interrelation of the parameters affecting this phenomenon.

The simulations performed during the sensitivity analysis of the model have provided a great deal of information describing qualitatively and, up to a certain point, quantitatively the basic features of the mechanisms involved in the radon transport in the soil and its entrance into the house. However, much is still left to be done, which will be suggested as it follows.

1). Validation of the model is the most important task to be performed now. Predictions of the model need to be compared with measured results, in order to assure that its performance is quantitatively accurate. The appropriate data for the validation of the model should be collected in houses with basements, and with a well characterized gap at the wall-floor joint, and should be composed of the following measurements: 1) pressure difference between the basement and the ground level outside; 2) air-exchange rate; 3) and indoor radon concentration. These variables should be measured simultaneously, and then averaged over the same periods of time. Information about the physico-chemical properties of the soil should also be provided, such as soil permeability, soil porosity, and concentration of radium (Ra-226), in the soil particles. Other kinds of information, such as the direction and speed of the wind, and the periods of rain or snow, would also be useful in the interpretation of the measured data, and in the validation of the model.

2). After being validated, the model could be used for the investigation of other problems, and in helping design new experiments. For example, it could be used to simulate the effectiveness of employing different materials in the aggregate regions of different thickness around the basement, with the objective of controlling the radon entrance into the house. Results from this simulation could determine the best range of parameters to solve the problem, which could then be verified in an experimental setup.

3). A theoretical question of great importance that could be investigated using the model, at its present stage of development, is related to the concept of the *radon availability* around the house. This question could be stated as: what is the volume of soil contributing its radon to the indoor air of the house, under various configurations of

disturbance delta pressure, soil permeability, and source terms, as well as the geometrical configuration of the house? A better knowledge of the concepts involved in this question would certainly help in the formulation of techniques for the reduction of the radon availability to the house.

4). Improvements of the model could also be suggested. Among the most important are the following:

- The model should be extended to include more flexibility in defining other possible cracks, at different locations, in the building understructure;
- Another region should be defined at the bottom of the soil block, with different physical parameters, to represent the location of the water table;
- The applied disturbance pressure should also be modeled in terms of its generating mechanisms, such as the wind speed and temperature differences from inside to outside of the houses, as well as any unbalanced mechanical ventilation installed in the building. In this approach, the disturbance pressure would be calculated internally in the model, rather than been taken as an input parameter;
- Asymmetrical distribution of the disturbance pressure in the soil around the house, due to the effect of the wind speed and direction, should also be considered. In this case, the numerical model should be developed in the whole soil block, instead of its quarter as it was done in the present version of the model. Furthermore, the boundary condition for the disturbance pressure distribution at the soil-air interface, instead of being fixed equal to zero as it was done here, would be established as a function of the wind speed and direction;
- In this model, the radon entry rate into the house and the air exchange rate were considered as independent processes. However, as it as described in Chapter I, most of the ventilation in the house occurs by uncontrolled infiltration induced by the underpressurization of the house. Consequently, the same forces inducing the entrance of radon from the soil into the basement are also responsible for most of the ventilation of the house. Therefore, as an improvement of this model, the air exchange rate in the house should also be treated as a function of the disturbance

pressure generating mechanisms such as the wind speed, temperature differences, and the unbalanced mechanical ventilation;

- A further improvement would be the development of a time dependent model incorporating the changes suggested above. A dynamical model would be able to account for all the transient effects occurring in the phenomenon of radon transport from soil into houses, expressing it more realistically. However, a three-dimensional time dependent model would be probably very expensive in terms of computer time, requiring for this matter the use of faster machines, such as the new generation of super computers.

APPENDICES

APPENDIX A

DERIVATION OF THE CONTINUITY EQUATION FOR A POROUS MEDIUM.

The purpose of this appendix is to describe the derivation of the continuity equation for a porous medium, which will be used in the formulation of the model for the radon transport in the soil.

Concepts of System and Control-Volume.

SYSTEM.

A system consists of a definite amount of mass distinguished from all other matter called its *surroundings*. The boundaries of a system form a closed surface. This closed surface may vary with time such that the same amount of mass of the system is kept constant. Based on the law of conservation of mass, the mass within a system does not change with time. That means:

$$\frac{dm}{dt} = 0. \tag{A.1}$$

CONTROL-VOLUME.

A control-volume consists of a definite region whose size and shape are arbitrarily defined in the space. The boundaries of a C.V. are called *control-surfaces*.

Figure A.1— Representation of a generic system with identical control-volume at different time steps, t and $t + dt$, in a velocity field $\vec{q}$.

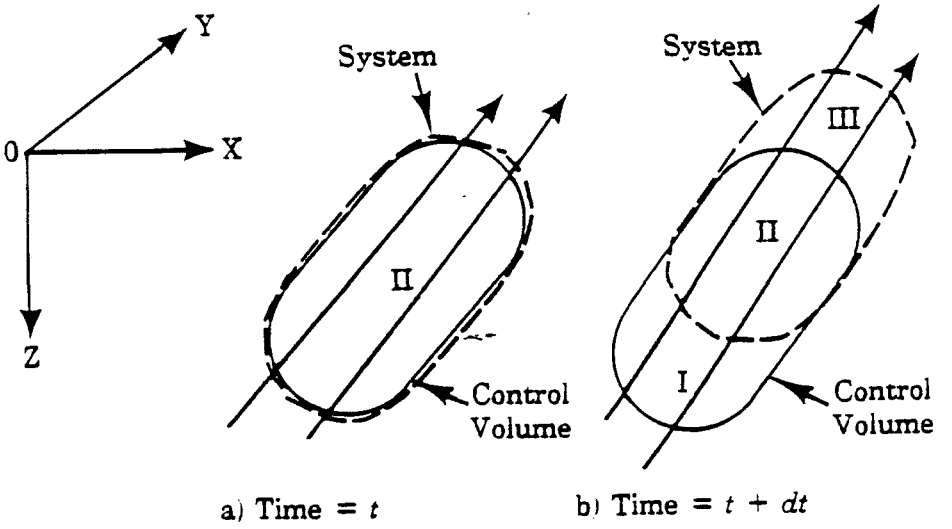

Relation of the System and Control-Volume Concepts in Terms of a General Property of the System.

The objective here is to formulate a general expression relating the concepts of the system and the C.V. in terms of a general property of the system[1].

Figure (A.1) shows a general flow situation, with the fluid moving with a some velocity $\vec{q}$ relative to a fixed system of coordinates. The system is represented by the figure drawn in dotted lines. At certain time t, a control-volume is coincident with the system which contains a certain mass of fluid. At a period of time dt later, the system has moved a little bit, and three regions can now be distinguished: region (I), occupied only by the control volume; region(II), simultaneously occupied by the system and the control-volume; and region (III) occupied only by the system.

[1] This derivation is described in details in the book: Fluid Mechanics, Chapter 3, by Streeter and Wylie, [St85].

Let's now define N as the total amount of some property (mass, energy, momentum, etc) within the system at any specific time; η, the amount of this property per unit of mass throughout the fluid; and ρ as the density of the fluid.

The variation of the property N *in the system* in the time period dt is given by:

$$N_{SYS_{t+dt}} - N_{SYS_t} = \left(\int_{II} \eta\rho dV + \int_{III} \eta\rho dV\right)_{t+dt} - \left(\int_{II} \eta\rho dV\right)_t .$$

Summing and subtracting $\left(\int_I \eta\rho dV\right)_{t+dt}$ to the right, and dividing by dt yields:

$$\begin{aligned}\frac{N_{SYS_{t+dt}} - N_{SYS_t}}{dt} = &\frac{\left(\int_I \eta\rho dV + \int_{II} \eta\rho dV\right)_{t+dt} - \left(\int_{II} \eta\rho dV\right)_t}{dt} + \\ &+ \frac{\left(\int_{III} \eta\rho dV\right)_{t+dt}}{dt} - \frac{\left(\int_I \eta\rho dV\right)_{t+dt}}{dt}.\end{aligned} \tag{A.2}$$

As dt is made infinitesimally small, the left side of the equation above becomes:

$$\frac{N_{SYS_{t+dt}} - N_{SYS_t}}{dt} \rightarrow \frac{dN}{dt}.$$

And the first term of the right side becomes:

$$\frac{\left(\int_I \eta\rho dV + \int_{II} \eta\rho dV\right)_{t+dt} - \left(\int_{II} \eta\rho dV\right)_t}{dt} \rightarrow \frac{\partial}{\partial t}\left(\int_{CV} \eta\rho dV\right).$$

And the last two terms of the right side become:

$$\frac{\left(\int_{III} \eta\rho dV\right)_{t+dt}}{dt} \rightarrow \int_{outflow\ area} \eta\rho\vec{q}\cdot d\vec{A},$$

and,

$$\frac{\left(\int_I \eta\rho dV\right)_{t+dt}}{dt} \rightarrow -\int_{inflow\ area} \eta\rho\vec{q}\cdot d\vec{A}.$$

Therefore, from the two expressions above we get:

$$\frac{\left(\int_{III}\eta\rho dV\right)_{t+dt}-\left(\int_{I}\eta\rho dV\right)_{t+dt}}{dt}\rightarrow\int_{CS}\eta\rho\vec{q}\cdot\vec{dA}.$$

Substituting these terms back into Equation A.2, yields:

$$\frac{dN}{dt}=\frac{\partial}{\partial t}\left(\int_{CV}\eta\rho dV\right)+\int_{CS}\eta\rho\vec{q}\cdot\vec{dA}. \qquad (A.3)$$

The general expression above expresses the fact that the time rate of change of N within a system is equal to the time rate of change of the property N within the control volume (fixed relative to x,y,z), plus the net rate of flux of N across the control-volume surface (control-surface).

Derivation of the continuity equation.

In the Equation A.3 above consider the following:

N = m, the mass of the system;

η = $\frac{m}{m}=1$, the mass per unit of mass.

The continuity equation is then developed from the general principle of conservation of mass, given by:

$$\frac{dm}{dt}=\frac{dN}{dt}=0.$$

Substituting the expression above into Eq.(A.3), we will get the continuity equation in its integral form, expressed as:

$$0=\frac{\partial}{\partial t}\left(\int_{CV}\rho dV\right)+\int_{CS}\rho\vec{q}\cdot\vec{dA}. \qquad (A.4)$$

In words, the continuity equation for a control-volume states that the time rate of increase of mass within a control-volume is equal to the net rate of mass inflow to the control-surface.

Continuity Equation in a Porous Medium.

Consider that the fluid is contained in the void space of the porous medium, and that a control-volume is defined in this porous medium. We also define the porosity of the medium, ϵ, as the ratio of the volume of the void space in the control-volume to the total volume of the control-volume.

Thus, the continuity equation applied to a control-volume of a porous medium states that the time rate of increase of mass *within the void space* of the control-volume is equal to the net rate of mass inflow to the control-surface. Therefore, based on Eq.(A.4), this concept is then expressed as:

$$\frac{\partial}{\partial t}\left(\int_{CV} \epsilon \rho dV\right) + \int_{CS} \rho \vec{q} \cdot \vec{dA} = 0, \tag{A.5}$$

which is the integral form of the continuity equation for the porous medium. In order to derive the differential form of the continuity equation we apply the Gauss Theorem:

$$\int_S \vec{F} \cdot \vec{dS} = \int_V \vec{\nabla} \cdot \vec{F} dV,$$

which in this case becomes,

$$\int_{CS} \rho \vec{q} \cdot \vec{dA} = \int_{CV} \vec{\nabla} \cdot \rho \vec{q} dV. \tag{A.6}$$

Substituting Eq.(A.6) into (A.5), yields:

$$\frac{\partial}{\partial t}\left(\int_{CV} \epsilon \rho dV\right) + \int_{CV} \vec{\nabla} \cdot \rho \vec{q} dV = 0,$$

or,

$$\int_{CV} \frac{\partial}{\partial t}(\epsilon \rho)\, dV + \int_{CV} \vec{\nabla} \cdot \rho \vec{q} dV = 0.$$

The equation above must be valid for any point within the C.V., as well as for the total C.V., therefore the integrand must be zero point-by-point. That means:

$$\frac{\partial}{\partial t}(\epsilon\rho) + \vec{\nabla} \cdot \rho\vec{q} = 0. \qquad (A.7)$$

Equation above is the differential form of the continuity equation in a porous medium. Note that the continuity equation in the porous medium, as expressed by Eq.(A.7) is defined at a point in the medium. However, due to the inhomogeneity of a porous medium at microscopic level, the variables ϵ, ρ, and $\vec{q}$ in Eq.(A.7) are not defined at every point of the medium. Furthermore, the definition of these variables implies in a concept of average over a certain volume of the medium, and consequently they are meaningful only at macroscopic level. Therefore it should be emphasized here that although the continuity equation is defined at a point in the porous medium, its application is only justifiable when the medium is considered in a macroscopic level.

For a rigorous derivation of the continuity equation in a porous medium, and a systematic treatment of averaging techniques for dealing with general multiphase systems, the reader is directed to the book of Jacob Bear, [Be79], and the paper of Hassanizadeh and Gray, [Ha83a].

APPENDIX B

DERIVATION OF THE DIFFERENTIAL FORM OF DARCY'S EQUATION.

Consider the following figure representing Darcy's experiment.[1] Notice that here we set the vertical coordinate (z-axis) oriented downward. Consequently, the final resultant mathematical expressions should reflect this notation.

The result of Darcy's experiment shows that:

$$Q = -KA\left(\frac{h_2 - h_1}{h}\right). \tag{B.1}$$

Where Q is the total volume flow, in $[m^3/s]$; A is the cross section geometric area, in $[m]$; K is a constant in units of $[m/s]$;h, h_1, and h_2 are the heights of the columns, in $[m]$; and the minus sign indicates that the flow is in the opposite direction to increasing h.

The absolute pressure at any point within the column of porous material is equal to:

$$P = P_H + p, \tag{B.2}$$

where P is the absolute pressure, in $[N/m^2]$; P_H is the absolute hydrostatic pressure component, in $[N/m^2]$; and p is the disturbance pressure component due to the flow of the fluid through the column.

The absolute hydrostatic pressures at the points 1 and 2 in the column are:

---

[1] Reference: Scheidegger, A.E., *The Physics of Flow Through Porous Media*, University of Toronto Press, Third Edition, 1974, Chapter 4.

Figure B.1— Schematic of Darcy's Experiment.

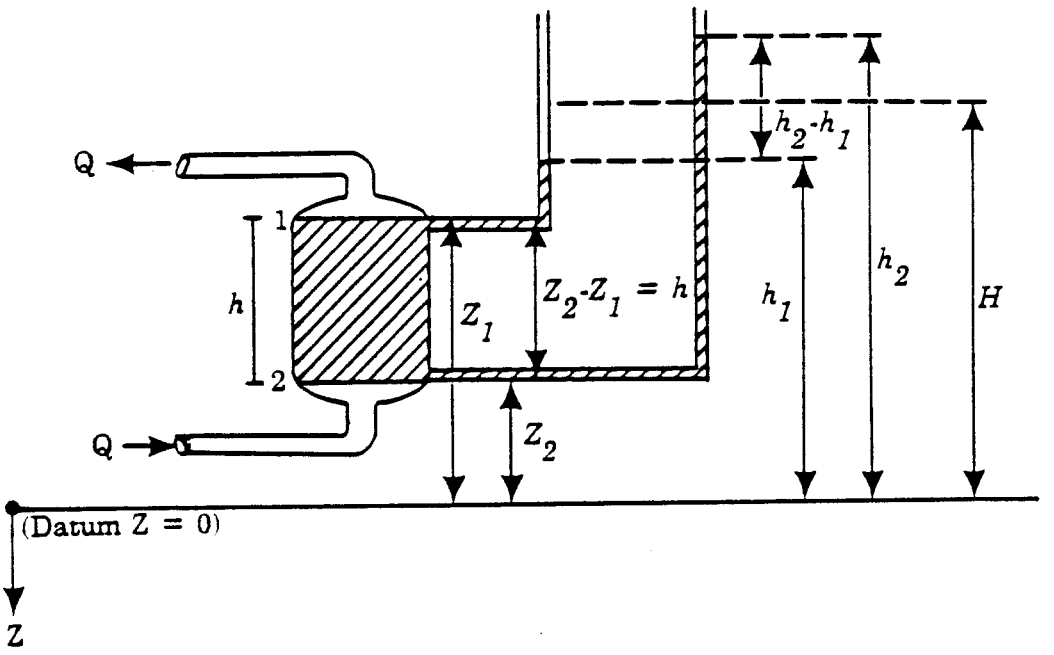

$$P_{H_1} = P_{TOP} + \rho g (H - z_1), \tag{B.3a}$$

$$P_{H_2} = P_{TOP} + \rho g (H - z_2), \tag{B.3b}$$

where P_{TOP} is the absolute pressure at the height H.

The disturbance pressure components at the points 1 and 2 are:

$$p_1 = \rho g (h_1 - H), \tag{B.4a}$$

$$p_2 = \rho g (h_2 - H). \tag{B.4b}$$

Substituting Eqs.(C.4) and (C.3) into Eq.(C.2), yields:

$$P_1 = P_{TOP} + \rho g\,(H - z_1) + \rho g\,(h_1 - H)\,,$$

$$P_2 = P_{TOP} + \rho g\,(H - z_2) + \rho g\,(h_2 - H)\,,$$

or,

$$P_1 = P_{TOP} + \rho g\,(h_1 - z_1)\,, \tag{B.5a}$$

$$P_2 = P_{TOP} + \rho g\,(h_2 - z_2)\,. \tag{B.5b}$$

From the equations above, the value of h_1 and h_2 can be expressed as:

$$h_1 = \left(\frac{P_1 - P_{TOP}}{\rho g}\right) + z_1, \tag{B.6a}$$

$$h_2 = \left(\frac{P_2 - P_{TOP}}{\rho g}\right) + z_2. \tag{B.6b}$$

Substituting these values into Eq.(B.1), yields:

$$Q = -KA\left[\left(\frac{P_2 - P_1}{\rho g h}\right) - 1\right],$$

or,

$$Q = -\frac{K}{\rho g} A\left(\frac{P_2 - P_1}{h} - \rho g\right). \tag{B.7}$$

Now, dividing the equation above by the cross sectional area A, we obtain the seepage velocity q, expressed as:

$$q = \frac{Q}{A} = -K'\left(\frac{P_2 - P_1}{h} - \rho g\right). \tag{B.8}$$

But making,

$$K' = \frac{k}{\mu}, \tag{B.9}$$

where k is defined as the specific permeability of the porous medium, in $[m^2]$; and μ is the dynamic viscosity of the fluid, in $[N \cdot s/m^2]$; and then substituting Eq.(B.9) into (B.8), yields:

$$q = -\frac{k}{\mu}\left(\frac{P_2 - P_1}{h} - \rho g\right). \tag{B.10}$$

We want now to express the equation above in differential form. In this case we would expect that the velocity q becomes a vector $\vec{q}$. We would also expect that the pressure difference should be expressed by the pressure gradient.

However, a priori, there is no unique way of doing this. One possibility of obtaining a differential form for the Darcy's expression is suggested by the equation above, by letting h become infinitesimal [Sc74]. Therefore, assuming the soil as an isotropic[2] porous medium, the differential form of Darcy's law[3] can be expressed as:

$$\vec{q} = -\frac{k}{\mu}\left(\vec{\nabla}P - \rho\vec{g}\right), \tag{B.11}$$

where, $\vec{q}$ is the seepage velocity vector, equal to the volume of soil gas flowing per unit of time per unit geometric area; P is the absolute pressure; and $\vec{g}$ is the vector in the direction of gravity (i.e. downward) and of the magnitude of gravity.

Note that since the adopted system of coordinates has the vertical direction (z-axis) oriented downward, then the gravity vector is always positively oriented.

---

[2] If the soil were considered as an anisotropic porous medium, an expression similar to Eq.(B.11) would have been obtained for the differential form of Darcy's law, except that the soil permeability would have been expressed as $\bar{k}$ – the *permeability tensor* of the soil. (See Scheidegger [Sc74], page 79).

[3] The differential form of Darcy's law can also be derived from examination of the momentum equation, and it has been verified by numerous experiments. [Sc74], [Ha83b].

APPENDIX C

VELOCITY OF THE SOIL GAS THROUGH THE CRACK.

In this appendix I derive an expression for the velocity of the soil gas through the crack, as a function of the crack geometry and the pressure difference between the basement and the crack-soil interface.

The geometry of the crack is approximated by two parallel plates of infinite width, separated by a finite distance and with finite length. The flow regimen of the gas flowing between these parallel plates is assumed to be laminar, incompresssible, and in a steady-state condition.

The flow is analyzed by taking a thin lamina of unit width as a free body, as shown in Fig.(C.1). In steady state, the lamina moves at constant velocity w in the z-direction. But, due to the shear stress, the velocity w is variable in the x-direction, approximating zero near the crack walls, and reaching its maximum at middle distance between the plates.

The sum of all forces applied at this lamina are (at steady-state the sum of the forces is zero):

$$\left[P\delta x - \left(P\delta x + \frac{\partial P}{\partial z}\delta z\delta x\right)\right] + \left[-\tau\delta z + \left(\tau\delta z + \frac{\partial \tau}{\partial x}\delta z\delta x\right)\right] + \gamma\delta z\delta x = 0, \qquad (C.1)$$

where,

P = Absolute pressure, in $[N/m^2]$;

τ = Shear stress, in $[N/m^2]$;

γ = Specific weight, in $[N/m^3]$.

Figure C.1— Representation of all forces applied to a thin lamina of unit width, moving in a laminar, incompressible, steady flow between parallel plates of infinite width.

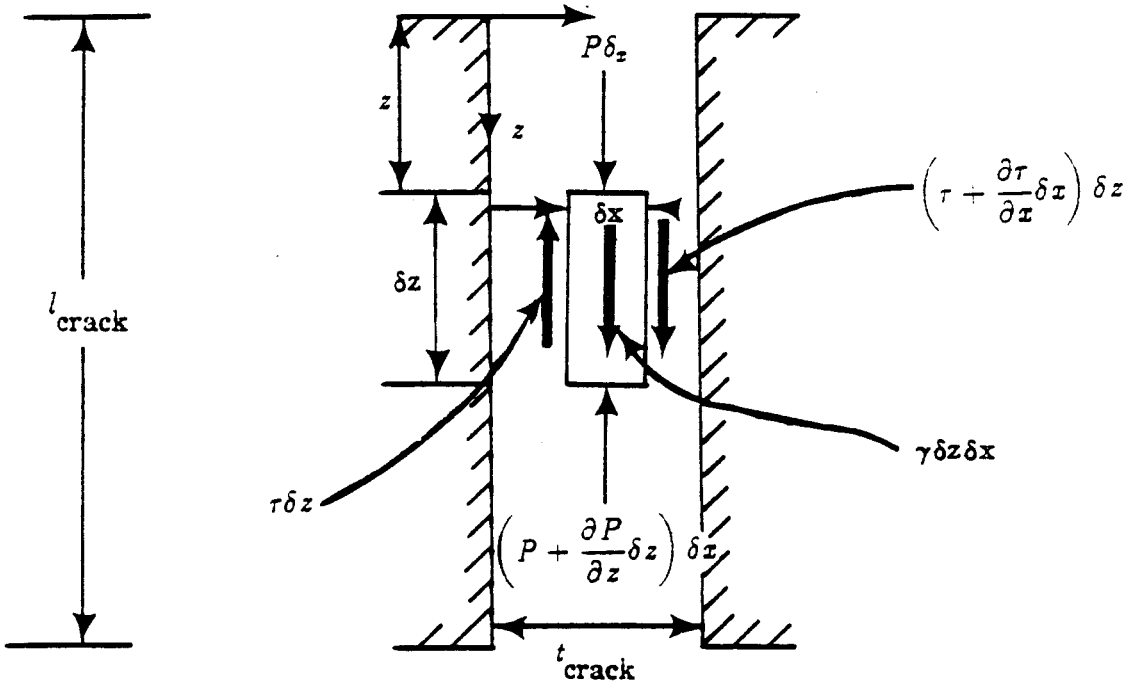

Dividing the equation above by the volume of the lamina element (equal to $dxdy$, and simplifying, yields:

$$-\frac{\partial P}{\partial z} + \frac{\partial \tau}{\partial x} + \gamma = 0,$$

or,

$$\frac{\partial \tau}{\partial x} = \frac{\partial P}{\partial z} - \gamma. \qquad (C.2)$$

Note that the shear stress τ is independent of z, and is only a function of x. Then the partial derivative can be transformed in the following:

$$\frac{\partial \tau}{\partial x} = \frac{d\tau}{dx}.$$

Also note that the pressure P is uniform at any section normal to the direction of the

flow (z-direction), and that $\frac{\partial P}{\partial z}$ is constant for any such section and can only vary in the z-direction. Consequently, the partial derivative of the pressure can also be transformed in:

$$\frac{\partial P}{\partial z} = \frac{dP}{dz}.$$

The specific weight is assumed to be invariable and can then be expressed as:

$$\gamma = \frac{d}{dz}(\gamma z).$$

Making these substitutions into Eq.(C.2) yields:

$$\frac{d\tau}{dx} = \frac{d}{dz}(P - \gamma z).$$

But from the Newton's Law of Viscosity, the shear stress τ can be expressed as:

$$\tau = \mu \frac{dw}{dx},$$

where μ is the soil gas dynamic viscosity, given in $[Ns/m^2]$. Now, from the two equations above, the derivative of the shear stress τ can also be expressed as:

$$\frac{d\tau}{dx} = \mu \frac{d^2 w}{dx^2} = \frac{d}{dz}(P - \gamma z),$$

or,

$$\mu \frac{d^2 w}{dx^2} = \frac{d}{dz}(P - \gamma z). \qquad (C.3)$$

Now, if in Equation (C.3) each side is a function of a separate distinct variable, then it results that each side is always equal to the same constant. Let's call this constant β, and substitute it into Equation (C.3). Then:

$$\mu \frac{d^2 w}{dx^2} = \beta, \qquad (C.4a)$$

and,

$$\frac{d}{dz}\left(P-\gamma z\right)=\beta. \tag{C.4b}$$

Let's now solve Eq.(C.4a) for the velocity w. Integrating it twice:

$$w=\frac{\beta}{\mu}\left(\frac{x^2}{2}+C_1x+C_2\right). \tag{C.5}$$

The two constants $C1$ and $C2$ can be obtained with the following boundary conditions:

$$\begin{aligned} x=0 \quad &\rightarrow w=0; \\ x=t_{crack} &\rightarrow w=0. \end{aligned} \tag{C.6}$$

Then,

$$C_2=0, \tag{C.7a}$$

and,

$$C_1=-\frac{t_{crack}}{2}. \tag{C.7b}$$

So, Equation (C.5) becomes:

$$w=\frac{\beta}{\mu}\left(\frac{x^2}{2}-\frac{xt_{track}}{2}\right),$$

or,

$$w=\frac{\beta}{2\mu}\left(x^2-xt_{track}\right),$$

or,

$$w = -\frac{\beta}{2\mu}\left(x t_{crack} - x^2\right) \qquad (C.8).$$

We now want to express β, the separation constant, in terms of the flow q, per unit of length of the crack.[1]

Thus, making:

$$\begin{aligned} q = \int_0^{t_{crack}} w\,dx &= \int_0^{t_{crack}} -\frac{\beta}{2\mu}\left(x t_{crack} - x^2\right) dx \\ &= -\frac{\beta}{2\mu}\left[\frac{x^2 t_{crack}}{2} - \frac{x^3}{3}\right]_0^{t_{crack}} \\ &= -\frac{\beta}{2\mu}\left[\frac{t_{crack}^3}{2} - \frac{t_{crack}^3}{3}\right], \end{aligned}$$

the flow q could then be expressed as:

$$q = -\frac{\beta t_{crack}^3}{12\mu}. \qquad (C.9)$$

Then, solving for the separation constant β, yields:

$$\beta = -\frac{12\mu q}{t_{crack}^3}. \qquad (C.10)$$

The next step now is to find the variation of the pressure, $(P - \gamma z)$, along the z-direction. Thus, substituting Eq.(C.10) into Eq.(C.4b), yields:

$$\frac{d}{dz}(P - \gamma z) = -\frac{12\mu q}{t_{crack}^3}.$$

Integrating from position 1 (where $P = P_1$, and $z = z_1$) to position 2 (where $P = P_2$, and $z = z_2$), along the whole depth l_{crack} of the crack, the equation above becomes:

---

[1] Note that q is the flow per unit of length of the crack, and is given in units of $[m^3/sm = m^2/s]$.

$$[(P_2 - \gamma z_2) - (P_1 - \gamma z_1)] = -\frac{12\mu q}{t_{crack}^3}(z_2 - z_1).$$

But, $z_2 - z_1 = l_{crack}$, then:

$$P_2 - P_1 - \gamma(z_2 - z_1) = -\frac{12\mu q}{t_{crack}^3}(z_2 - z_1),$$

or,

$$P_2 - P_1 - \gamma l_{crack} = -12\mu q \frac{l_{crack}}{t_{crack}^3}. \qquad (C.11)$$

Solving Eq.(C.11) for the flow q yields:

$$q = -\left(\frac{t_{crack}^3}{12\mu l_{crack}}\right)\left[(P_2 - P_1) - \gamma l_{crack}\right]. \qquad (C.12)$$

Now, I want to find the average velocity $\bar{w}$ causing the flow q, according to the following expression:

$$q = \bar{w}A, \qquad (C.13)$$

where,

$\bar{w}$ = Average gas velocity through the crack, in $[m/s]$;

A = Cross-sectional area per unit of width of the crack, in $[m2/m = m]$.

But the cross sectional area per unit of length of the crack is equal to:

$$A = t_{crack}. \qquad (C.14)$$

Consequently, the flow q can be expressed as:

$$q = \bar{w}t_{crack} \rightarrow \bar{w} = \frac{q}{t_{crack}}. \qquad (C.15)$$

Substituting Eq.(C.12) into Eq.(C.15), yields:

$$\bar{w} = -\left(\frac{t_{crack}^2}{12\mu l_{crack}}\right)\left[(P_2 - P_1) - \gamma l_{crack}\right]. \qquad (C.16)$$

Now, renaming the variables: $\bar{w} = w_{crack}$; $P_1 = P_{bas}$; and $P_2 = P_{crack}$, and substituting them into Eq.(C.16), yields:

$$w_{crack} = -\left(\frac{t_{crack}^2}{12\mu l_{crack}}\right)\left[(P_{crack} - P_{bas}) - \rho g l_{crack}\right]. \qquad (C.17)$$

Note:

- Equation above expresses the average gas velocity through the crack channel;
- The system of coordinates adopted here has the vertical direction oriented downward;
- A negative value of w_{crack} means an upward direction of flow.

APPENDIX D

RADON MASS-BALANCE EQUATION IN A POROUS MEDIUM.

In this appendix I present a very simplified derivation of the radon mass-balance equation applied in a porous medium.

Assumptions and Definitions.

Consider the soil (porous medium) with the following characteristics:

Porosity, ϵ, equal to the ratio of void to bulk volume;

Radon source term, S, equal to the number of radon atoms produced into the void volume (pore space) per unit of time, in $[Ci/m^3 s]$;

Radon concentration, C, in the soil pore space (in the soil gas), in $[Ci/m^3]$;

Soil gas seepage velocity, $\vec{q}$, equal to the ratio of the volume flow by the geometrical cross sectional area, in $[m/s]$;

Total (bulk) flux of radon through the soil, $\vec{J}$, equal to the number of radon atoms crossing a geometrical cross sectional area per unit of time, in $[Ci/m^2 s]$;

Bulk diffusivity constant of radon in the soil, D, equal to the ratio of the diffusive component

of the total flux across a geometrical area, to the gradient of the interstitial concentration (soil gas concentration) of radon, in $[m^2/s]$.

Mass-Balance Principle.

Consider a generic control-volume surrounding a porous medium, as represented in Figure (D.1). Radon atoms are produced in the solid particles within the control-volume, with part of them reaching the soil pore space and mixing with the soil gas. Then, these atoms either decay inside the control-volume, or flow out through the control-volume external surface. The whole control-volume is supposed to be immersed in an external flow field.

Figure D.1— A generic control-volume defined within a porous medium immersed in a flow field.

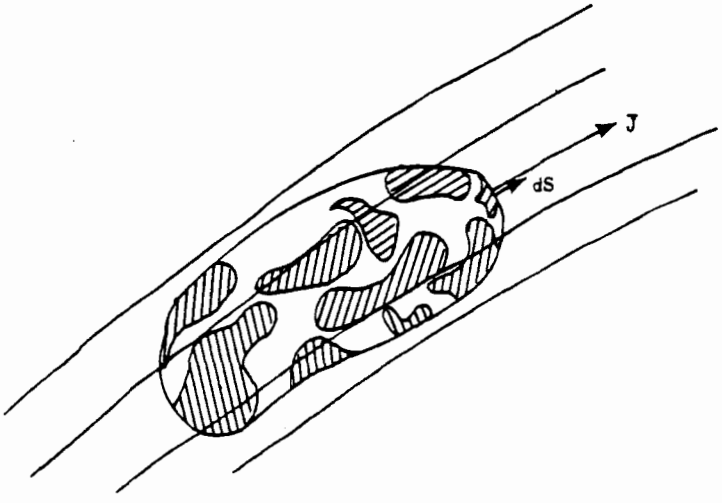

At any instant in time, the total amount of radon atoms present *within the pore space* of the control-volume is given by integrating the elementary amount of radon, $C\epsilon dV$, in the elementary volume of void space ϵdV, over the whole void space of the control-volume. It can be expressed as:

$$M = \int_{CV} C\epsilon dV.$$

Also, the total amount of radon being produced and decaying inside the void space of the control-volume is given respectively by:

$$\int_{CV} S\epsilon dV,$$

and,

$$\int_{CV} \lambda_{Rn} C\epsilon dV.$$

Finally, the total amount of radon crossing the external surface of the control-volume per unit of time is given by:

$$\int_{CS} \vec{J} \cdot \vec{ds}.$$

Now, due to the conservation of mass within the control-volume, the net variation of the amount of radon per unit of time, $\frac{\partial M}{\partial t}$, in the pore space is given by the sum of the terms listed above, such that:

$$\frac{\partial M}{\partial t} = \frac{\partial}{\partial t}\int_{CV} C\epsilon dV = \int_{CV} S\epsilon dV - \int_{CV} \lambda_{Rn} C\epsilon dV - \int_{CS} \vec{J} \cdot \vec{dS}. \qquad (D.1)$$

Using the divergence theorem, the surface integral representing the net flow through the external surface of the control-volume can be transformed in a volume integral, and Eq.(D.1) becomes:

$$\frac{\partial}{\partial t}\int_{CV} C\epsilon dV = \int_{CV} S\epsilon dV - \int_{CV} \lambda_{Rn} C\epsilon dV - \int_{CV} \vec{\nabla} \cdot \vec{J} dV.$$

Now, equating the integrands, it yields:

$$\frac{\partial}{\partial t}(C\epsilon) = S\epsilon - \lambda_{Rn} C\epsilon - \vec{\nabla} \cdot \vec{J}. \qquad (D.2)$$

Equation above represents the general mass-balance principle applied to any point in the medium. At steady-state, $\frac{\partial}{\partial t}(C\epsilon)$ is zero, and the mass-balance is expressed as:

$$\vec{\nabla} \cdot \vec{J} = \epsilon (S - \lambda_{Rn} C) . \qquad (D.3)$$

Now, substituting the total flux, $\vec{J}$, by its convective and diffusive components, $\vec{q}C$ and $-D\vec{\nabla}C$ respectively, the mass-balance equation is expressed as:

$$\vec{\nabla} \cdot (\vec{q}C) - \vec{\nabla} \cdot \left(D\vec{\nabla}C \right) = \epsilon (S - \lambda_{Rn} C) , \qquad (D.4)$$

and in one dimensional configuration it becomes:

$$\frac{d}{dx}(uC) - \frac{d}{dx}\left(D\frac{dC}{dx} \right) = \epsilon (S - \lambda_{Rn} C) . \qquad (D.5)$$

Note that the equations above are valid for any form of u, D, S, and ϵ, constant or not. For ϵ constant with space, Eq.(D.3) becomes:

$$\vec{\nabla} \cdot \left(\frac{\vec{J}}{\epsilon} \right) = S - \lambda_{Rn} C, \qquad (D.6a)$$

or,

$$\vec{\nabla} \cdot \vec{J_{eff}} = S - \lambda_{Rn} C, \qquad (D.6b)$$

where $\vec{J_{eff}}$ is the total effective flux, or the total flux per unit of open pore area.

Note that the radon mass-transport equation in the porous medium, as expressed by Eq.(D.4) is defined at a point in the medium. However, due to the inhomogeneity of a porous medium at microscopic level, the variables ϵ, C, S, and $\vec{q}$ in Eq.(A.7) are not defined at every point of the medium. Furthermore, the definition of these variables implies in a concept of average over a certain volume of the medium, and consequently they are meaningful only at macroscopic level. Therefore it should be emphasized here that although

the continuity equation is defined at a point in the porous medium, its application is only justifiable when the medium is considered in a macroscopic level.

For a rigorous derivation of the mass-transport equation in a porous medium, and a systematic treatment of averaging techniques for dealing with general multiphase system, the reader is directed to the book of Jacob Bear, [Be79], and the paper of Hassanizadeh and Gray, [Ha83a].

APPENDIX E

BOUNDARY CONDITIONS AT THE SOIL-CRACK INTERFACE FOR THE SOLUTION OF THE DISTURBANCE PRESSURE FIELD EQUATION.

The objective in this appendix is to describe in details the boundary conditions imposed on the interface between the crack and the soil, for the solution of the disturbance pressure field equation in the soil block. Although all boundary conditions for this problem were already specified in Table (3.1), it is still necessary to formulate the appropriate mathematical equations expressing the boundary conditions at the soil-crack interface.

Thus, consider Figure (E.1), representing the crack defined at the basement floor, as well as the first control-volume in the soil underneath the crack. Also shown is the interface between the crack and the control-volume in the field.

As a boundary condition imposed at this interface, it is assumed that the disturbance pressure and the velocity of the soil gas through the interface are both continuous functions of distance. So, consider a point (IN) located right at the interface. Then, for a point $(IN-)$ located inside the crack but as near as possible to the point (IN), and for the point $(IN+)$ located in the soil, but very close to the point (IN), the boundary conditions are expressed as:

$$p_{(IN-)} = p_{(IN+)} = p_{IN}, \tag{E.1}$$

$$w_{(IN-)} = w_{(IN+)} = w_{IN}, \tag{E.2}$$

where,

$p_{(IN-)}$ = Value of the disturbance pressure within the crack as it gets closer

Figure E.1— Schematic representation of the soil-crack interface.

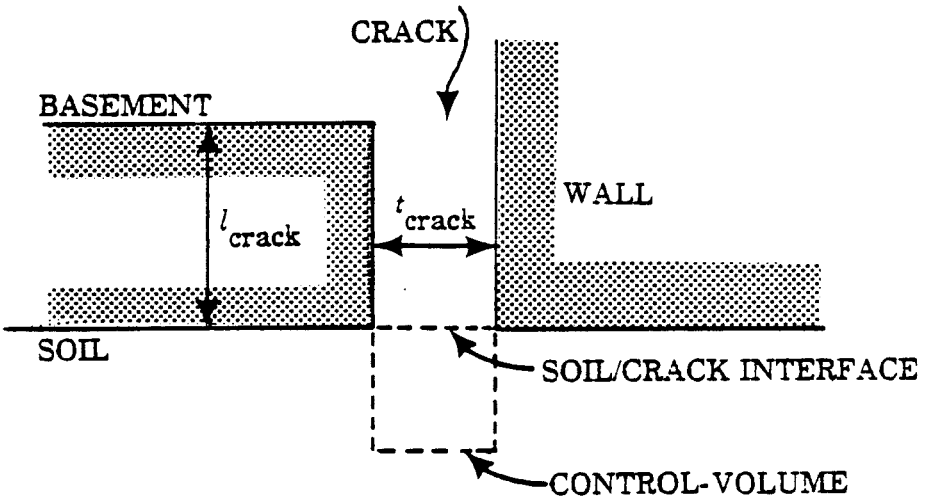

to the interface;

$p_{(IN+)}$ = Value of the disturbance pressure within the control-volume in the soil as it gets closer to the interface;

$w_{(IN-)}$ = Average velocity of the soil gas within the crack at it gets closer to to the interface;

$w_{(IN+)}$ = Average velocity of the soil gas within the control-volume of the soil as it gets closer to the interface.

Here I observe that the disturbance pressure field equation will be solved numerically using an iterative method, in which the value of $p_{(IN-)} = p_{(IN+)} = p_{IN}$ is assumed to be known at each iteration (a first-order boundary condition). The method starts with an arbitrary choice of p_{IN}. Then, the pressure distribution over the whole soil block is calculated. Following this, the values of $w_{(IN-)}$ and $w_{(IN+)}$ are calculated, and compared. If the value of $w_{(IN-)}$ does not match $w_{(IN+)}$ within a tolerance limit, a new value of p_{IN} is assumed, and the whole process is repeated.

Now I proceed with the formulation of the equations expressing the velocity w. I have assumed that the regimen of the flow is at steady-state, and that the walls of the crack are parallel. Therefore, the average velocity of the soil gas flowing through the crack, (w_{crack}), should be constant along the crack length and, consequently, equal to the average velocity of the soil gas crossing the interface. That means: $w_{crack} = w_{(IN-)} =$ constant.

The average velocity of the soil gas through the crack was evaluated in Appendix C, and is expressed as:

$$w_{(IN-)} = w_{crack} = -\left(\frac{t_{crack}^2}{12\mu l_{crack}}\right)\left[(P_{IN} - P_{bas}) - \rho g l_{crack}\right]. \qquad (E.3)$$

I want to represent the equation above in terms of the disturbance pressure p, instead of the absolute pressure P. From Eq.(3.4), the absolute pressure P_{IN}, and the absolute pressure at the basement P_{bas} are given by:

$$P_{IN} = P_A + \rho g(l_z + l_{crack}) + p_{IN}, \qquad (E.4)$$

and,

$$P_{bas} = P_A + \rho g l_z - \Delta P. \qquad (E.5)$$

Then, substituting these equations into Eq.(E.3), yields:

$$w_{crack} = -\left(\frac{t_{crack}^2}{12\mu l_{crack}}\right)\left[P_A + \rho g\,(l_z + l_{crack}) + p_{IN} - P_A - \rho g l_z + \Delta P - \rho g l_{crack}\right],$$

or,

$$w_{crack} = -\left(\frac{t_{crack}^2}{12\mu l_{crack}}\right)(p_{IN} + \Delta P),$$

or,

$$w_{crack} = -K_{crack}\,(p_{IN} + \Delta P)\,, \qquad (E.6a)$$

where,

$$K_{crack} = \frac{t_{crack}^2}{12\mu l_{crack}}. \qquad (E.6b)$$

Equation above gives the average velocity of the soil gas through the whole crack length, in terms of the difference of the disturbance pressure.

Now, I want to formulate an expression for $w_{(IN+)}$, the average velocity of the soil gas as it approaches the interface from the soil. In order to do so, I define a control-volume of very small thickness located in the soil, but as close as possible to the crack-soil interface, in which the disturbance pressure is assumed to be equal to p_{IN}. Figure (E.2) illustrates this configuration.

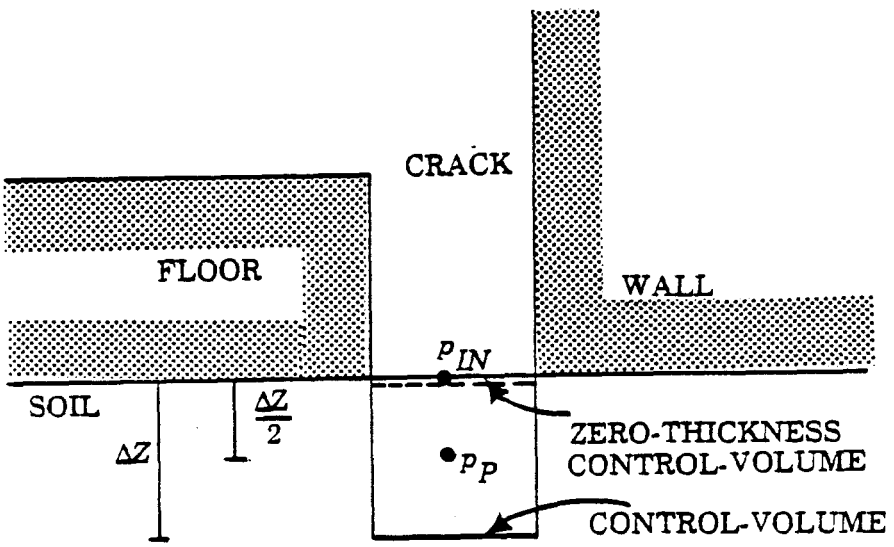

Figure E.2— Configuration at the crack, showing the control-volume defined in the soil underneath the soil-crack interface.

The vertical component of the soil-gas velocity at any point in the soil is given by Darcy's expression (Eq.(3.9a)), and can be expressed as:

$$w_{soil} = -\frac{k}{\mu}\frac{\partial p}{\partial z}. \qquad (E.7)$$

For a point located in the above defined zero-thickness control-volume, the velocity of the soil gas becomes equal to $w_{(IN+)}$, and can be expressed as:

$$[w_{soil}]_{(IN+)} = w_{(IN+)} = -\left(\frac{k}{\mu}\right)_{(IN+)}\left(\frac{\partial p}{\partial z}\right)_{(IN+)}. \qquad (E.8)$$

Note that the point $(IN+)$ is supposed to be inside the soil but infinitesimally close to the interface. Consequently, the value of the permeability k should still be the same as the one considered in the control-volume. Also note that the gradient of the disturbance pressure must be evaluated as close as possible to the interface.

In order to evaluate the pressure gradient at the point $(IN+)$, and to further develop the expression above, I here make the following assumptions:

(1)- The size of the control-volumes underneath the crack interface in the z-direction, Δz, is very small;

(2)- The pressure profile from the center of the control-volume under the crack, to the crack interface, can be approximated by a linear function, such that:

$$\left(\frac{\partial p}{\partial z}\right)_{(IN+)} = \frac{p_P - p_{IN}}{\frac{\Delta z}{2}}. \qquad (E.9)$$

Thus, substituting Eq.(E.9) into Eq.(E.8), yields:

$$w_{(IN+)} = -\left(\frac{k}{\mu}\right)\left(\frac{2}{\Delta z}\right)(p_P - p_{IN}). \qquad (E.10)$$

Equations (E.6) and (E.10) above, expressing $w_{(IN-)}$, and $w_{(IN+)}$ respectively, will be used to implement the boundary conditions at the soil-crack interface, as expressed in Eq.(E.2).

Using the dimensionless variables defined in Chapter III, these equations can be transformed into their dimensionless versions. Thus, substituting Eqs.(3.30) and (3.31) into Eq.(E.6), yields:

$$w^{*}_{crack}\, U_{ch} = -K_{crack}\Delta P\,(p^{*}_{IN} + 1)\,,$$

or,

$$w^{*}_{crack} = -K_C\,(1 + p^{*}_{IN})\,, \qquad (E.11a)$$

where K_C is the dimensionless group given by:

$$K_C = \frac{K_{crack}\Delta P}{U_{ch}} = \left(\frac{t^2_{crack}}{12\mu l_{crack}}\right)\frac{\Delta P}{U_{ch}}. \qquad (E.11b)$$

Also, substituting Eqs. (3.30), (3.31), (3.34), and (3.35) into Eq.(E.10), yields:

$$w^{*}_{soil}\, U_{ch} = -\left(\frac{k^{*}\, k_{ch}}{\mu}\right)\left(\frac{2}{\Delta z^{*} L_{ch}}\right)\Delta P\,(p^{*}_{P} - p^{*}_{IN})\,,$$

or,

$$w^{*}_{soil} = -\left(\frac{k_{ch}\Delta P}{\mu\, U_{ch} L_{ch}}\right)\left(\frac{2k^{*}}{\Delta z^{*}}\right)(p^{*}_{P} - p^{*}_{IN})\,.$$

But from Eqs. (3.28) and (3.29), $U_{ch}L_{ch} = D_{ch}$. So, the equation above becomes:

$$w^{*}_{soil} = -K_S\left(\frac{2k^{*}}{\Delta z^{*}}\right)(p^{*}_{P} - p^{*}_{IN})\,, \qquad (E.12a)$$

where K_S is the dimensionless group given by:

$$K_S = \frac{k_{ch}\Delta P}{\mu D_{ch}}. \qquad (E.12b)$$

APPENDIX F

BOUNDARY CONDITIONS AT THE SOIL-CRACK INTERFACE FOR THE SOLUTION OF THE CONVECTION-DIFFUSION EQUATION.

The objective in this appendix is to propose the boundary conditions at the crack, and at the soil-crack interface, which will then be used for the solution of the radon transport equation in the soil.

Convection-Diffusion of Radon Through the Crack.

Basic Assumptions.

The basic assumptions related to the flow of soil gas within the crack, which will be used later to support the proposed boundary conditions at the soil-crack interface, are the following:

- The flow of radon through the crack is invariable in the x and y directions. Consequently, it can be represented in one dimension (z-direction).
- The air inside the basement (for the whole house, in fact) is well stirred. So it is assumed that:
  - . The diffusion coefficient of radon in the air of the basement is much higher than in the air inside the crack;
  - . As soon as the soil gas leaves the crack and gets into the basement, it becomes homogeneously mixed with the indoor air.

Figure F.1— Representation of the radon concentration, and radon flux at the soil-crack-basement configuration.

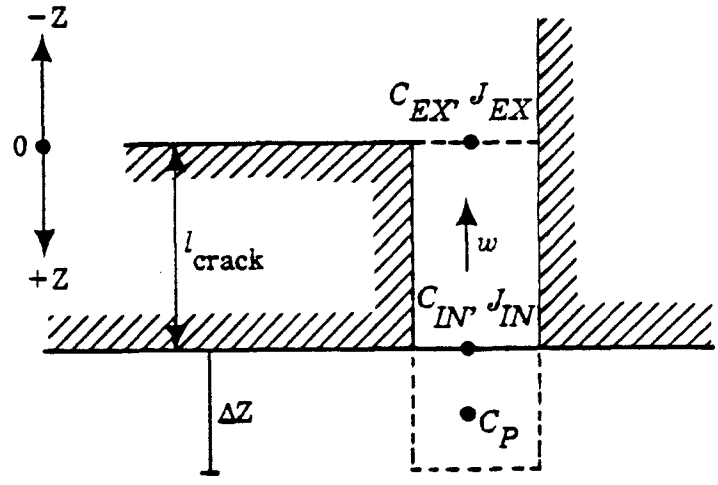

- Concentration of radon inside the house is much smaller than the concentration in the soil gas passing through the crack.
- The flow of radon from the last control-volume in the soil and through the crack, is represented in Figure (F.1), where:[1]

  C_P = Radon concentration at the node P;

  C_{IN} = Radon concentration in the soil, at the crack interface;

  C_{EX} = Radon concentration at the crack exit;

  J_{IN} = Radon flux at the crack-soil interface;

  J_{EX} = Radon flux at the crack exit, into the basement;

  w = Velocity of the soil gas through the crack entrance. (Since we have assumed a constant cross section of the crack, the value of the velocity w is also constant along the crack).

- In the figure above we consider three regions:
  - . Region #a : Control-volume under the crack;
  - . Region #b : Inside the crack;

[1] Note that for the convenience in this appendix only, I have represented the origin of coordinates, for the z-axis, located at the floor of the basement, at the interface between the crack and the indoor air. The coordinate system adopted in the model was defined in Chapter IV, Figs.(4.1) and (4.2).

. Region #c : Inside the basement.

- As an approach for the problem of establishing the boundary condition at the exit of the crack, I have introduced a third region representing the interior of the basement.
- In this approach, I have assumed that the basement (region #c) can also be represented in one-dimension, with a geometry similar to the one representing the crack, but with the following particularities:
  . The length of the 3rd. region extends to infinity;
  . The diffusion coefficient in the 3rd. region is much larger than the one inside the crack;
  . Concentration of radon at the infinity of the 3rd. region tends to zero, due to radioactive decay.

The whole configuration is then represented in Figure (F.2). The diffusion coefficients used in the three defined regions of the soil-crack-basement configuration are the following:

D = Bulk diffusion coefficient of radon in the soil pore space;

D_o = Diffusion coefficient of radon in open air;

D'_o = Diffusion coefficient of radon in a well mixed air, here called the *enhanced radon diffusion coefficient.*

Mathematical Formulation.

The equations for the total radon flux within the regions a, b, and c will be given respectively by:

$$J_a = wC - D\frac{dC}{dz}, \qquad \text{for} \quad l \leq z \leq (l + \Delta z), \tag{F.1}$$

$$J_b = wC - D_o\frac{dC}{dz}, \qquad \text{for} \quad 0 \leq z \leq l, \tag{F.2}$$

$$J_c = wC - D'_o\frac{dC}{dz}, \qquad \text{for} \quad z \leq 0. \tag{F.3}$$

Figure F.2— Simplified representation of the soil-crack-basement configuration, where each defined region is assumed to have the same geometry.

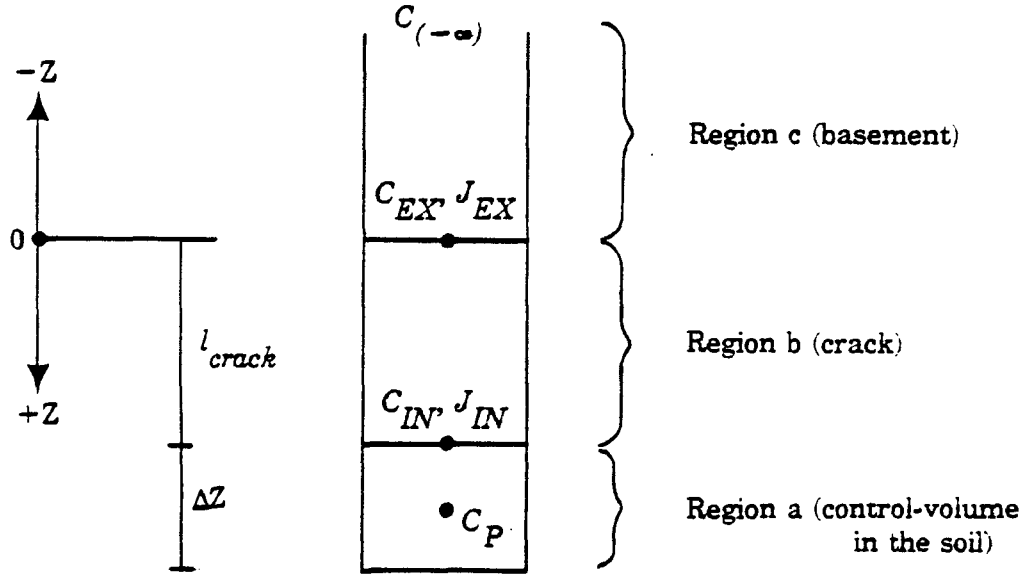

where J is the total flux of radon through a geometric area (or the bulk flux).

Analytical Solution within Regions b and c.

Here we seek an analytical solution for the profile of radon concentration in the regions #b and #c, which will be used to formulate the boundary condition at the soil-crack interface of the region #a, and consequently allowing the solution of the radon transport equation in the whole soil block.

Within regions #b and #c (inside the crack and in the basement), the mass transport equations have the following form:

$$\frac{d^2C}{dz^2} - \frac{w}{D_o}\left(\frac{dC}{dz}\right) - \frac{\lambda_{Rn}}{D_o}C = 0, \qquad \text{for} \quad 0 \leq z \leq l, \tag{F.4}$$

$$\frac{d^2C}{dz^2} - \frac{w}{D'_o}\left(\frac{dC}{dz}\right) - \frac{\lambda_{Rn}}{D'_o}C = 0, \qquad \text{for} \quad z \leq 0. \tag{F.5}$$

Boundary Conditions.

At the boundaries of the regions #b and #c we establish the following conditions:[2]

$$\text{i)} \qquad C_{(z=-\infty)} = 0, \tag{F.6}$$

$$\text{ii)} \qquad C_{(z=0-)} = C(z = 0+), \tag{F.7}$$

$$\text{iii)} \qquad J_{(z=0-)} = J(z = 0+), \tag{F.8}$$

$$\text{iv)} \qquad C_{(z=l_{crack})} = C_{IN}. \tag{F.9}$$

Note that the value of C will be determined iteratively as we make the flux at the interface, calculated from region #b, equal to the flux at the same location but calculated from region #a. (See the item Boundary Condition at the Crack Interface, in this appendix.)

Dimensionless Transformations.

Here we present the dimensionless versions of the equations above, making use of the following change of variables:

$$C^* = \frac{C}{C_{ch}} = \frac{C}{S_{ch}/\lambda_{Rn}}, \tag{F.10}$$

$$z^* = \frac{z}{L_{ch}}, \tag{F.11}$$

[2] Note that this problem is similar to the problem of establishing boundary conditions of flow reactor – See paper of Wehner, [We56].

$$w^* = \frac{w}{U_{ch}}, \tag{F.12}$$

and,

$$D_o^* = \frac{D_o}{D_{ch}}, \tag{F.13a}$$

$$D_o'^* = \frac{D_o'}{D_{ch}}, \tag{F.13b}$$

where, S_{ch}, U_{ch}, L_{ch}, and D_{ch} are the characteristic radon source, soil gas velocity, length, and diffusion coefficient respectively.

However, we have further defined the characteristic length, L_{ch}, and velocity U_{ch} as:

$$L_{ch} = \sqrt{\frac{D_{ch}}{\lambda_{Rn}}}. \tag{F.14}$$

Now, substituting these variables into the mass transport equations, they become:

$$\frac{d^2C^*}{dz^{*2}} - \left(\frac{P_e}{D_o^*}\right)\frac{dC^*}{dz^*} - \left(\frac{1}{D_o^*}\right)C^* = 0, \qquad 0 \le z^* \le l^*, \tag{F.16}$$

$$\frac{d^2C^*}{dz^{*2}} - \left(\frac{P_e}{D_o'^*}\right)\frac{dC^*}{dz^*} - \left(\frac{1}{D_o'^*}\right)C^* = 0, \qquad z^* \le 0. \tag{F.17}$$

Also, the equations for the total radon flux become:

$$J_b^* = P_eC^* - D_o^*\left(\frac{dC^*}{dz^*}\right), \qquad 0 \le z^* \le l^*, \tag{F.18}$$

$$J_c^* = P_eC^* - D_o'^*\left(\frac{dC^*}{dz^*}\right), \qquad z^* \le 0, \tag{F.19}$$

where P_e is the Peclet number, defined as:

$$P_e = \frac{wL_{ch}}{D_{ch}} = \frac{w}{\sqrt{D_{ch}\lambda_{Rn}}} = \frac{w}{U_{ch}} = w^*. \qquad (F.20)$$

Solution of the Mass-Transport Equation.

The general solution of the mass-transport equation within the region #b (Eq. F-16) is given by :

$$C^* = K_1 e^{r_1 z^*} + K_2 e^{r_2 z^*}, \qquad 0 \le z^* \le 0, \qquad (F.21)$$

where r_1, and r_2 are the roots of the auxiliary equation:

$$r^2 - \left(\frac{w^*}{D_o^*}\right) r - \left(\frac{1}{D_o^*}\right) = 0. \qquad (F.22)$$

Then, solving equation above for r_1, and r_2 we will get:

$$r_1 = \left(\frac{w^*}{2D_o^*}\right)\left[(1 + \sqrt{1 + \frac{4D_o^*}{w^{*2}}}\right], \qquad (F.23a)$$

$$r_2 = \left(\frac{w^*}{2D_o^*}\right)\left[1 - \sqrt{1 + \frac{4D_o^*}{w^{*2}}}\right]. \qquad (F.23b)$$

Similarly, the general solution of Eq.(F-17) is given by:

$$C^* = K_3 e^{r_1 z^*} + K_4 e^{r_2 z^*}, \qquad 0 \le z^* \le 0, \qquad (F.24)$$

where,

$$r_3 = \left(\frac{w^*}{2D_o'^*}\right)\left[1 + \sqrt{1 + \frac{4D_o'^*}{w^{*2}}}\right], \qquad (F.25a)$$

$$r_4 = \left(\frac{w^*}{2D_o'^*}\right)\left[1 - \sqrt{1 + \frac{4D_o'^*}{w^{*2}}}\right]. \qquad (F.25b)$$

Determination of the Coefficients K_1, K_2, K_3, and K_4.

These constants will be found from the boundary conditions. Thus, from condition (i) and Eq.(F-24) we will have:

$$\lim_{z^* \to -\infty} C^*(z^*) = \lim_{z^* \to -\infty} \left(K_3 e^{r_3 z^*} K_4 e^{r_4 z^*}\right) = 0.$$

Since $r_3 \leq 0$, and $r_4 \geq 0$ (for all $p_e \leq 0$), then in the equation above we must have:

$$K_3 = 0, \qquad \text{and} \qquad K_4 = 0. \qquad (F.26)$$

Consequently, Eq.(F-24) becomes:

$$C^*(z^*) = K_4 e^{r_4 z^*}, \qquad \text{for} \qquad z^* \leq 0. \qquad (F.27)$$

Using the equation above, as well as its substitution into Eq.(F-19), we can now find :

$$C^*\left(z^* = 0-\right) = K_4, \qquad (F.28)$$

$$J^*\left(z^* = 0-\right) = w^* K_4 - D_o'^* r_4 K_4 = \left(w^* - D_o'^* r_4\right) K_4. \qquad (F.29)$$

Now, from boundary condition (iv), and Eq.(F-21), we will have:

$$C^*\left(z^* = l^*\right) = C_{IN}^* = K_1 e^{r_1 l^*} + K_2 e^{r_2 l^*}, \qquad (F.30)$$

and we also have:

$$C^*(z^* = 0+) = K_1 + K_2, \tag{F.31}$$

$$\begin{aligned} J^*(z^* = 0+) &= w^*(K_1 + K_2) - D_o^*(K_1 r_1 + K_2 r_2), \\ &= (w^* - D_o^* r_1) K_1 + (w^* - D_o^* r_2) K_2. \end{aligned} \tag{F.32}$$

Finally, from boundary conditions (ii) and (iii), and with equations (F-28), (F-29), (F-30), (F-31), and (F-32), we can write the following system of equations for the coefficients K_1 , K_2, and K_4 . Thus:

$$K_4 = K_1 + K_2, \tag{L - 33}$$

$$(w^* - D_o^{l^*} r_4) K_4 = K_1(w^* - D_o^* r_1) + K_2(w^* - D_o^* r_2), \tag{F.34}$$

$$C_{IN}^* = K_1 e^{r_1 l^*} + k_2 e^{r_2 l^*}. \tag{F.35}$$

We now proceed with the solution of the system above. Thus, from Eq. (F-35) we obtain an expression for K_2. That is:

$$K_2 = C_{IN} e^{-r_2 l^*} - K_1 e^{l^*(r_1 - r_2)}. \tag{F.36}$$

Substituting Eq.(F.33) and Eq.(F.36) into (F.34), yields:

$$\begin{aligned} &(w^* - D_o^{l^*} r_4)\left[K_1 + C_{IN} e^{-r_2 l^*} - K_1 e^{l^*(r_1 - r_2)}\right] = \\ &\qquad = (w^* - D_o^* r_1) K_1 + (w^* - D_o^* r_2)\left[C_{IN}^* e^{-r_2 l^*} - K_1 e^{l^*(r_1 - r_2)}\right], \end{aligned}$$

or,

$$K_1\left[w^* - D_o'^* r_4 - \left(w^* - D_o'^* r_4\right) e^{l^*(r_1-r_2)}\right] + C_{IN}^* \left(w^* - D_o'^* r_4\right) e^{-r_2 l^*} =$$

$$= K_1\left[w^* - D_o^* r_1 - \left(w^* - D_o^* r_2\right) e^{l^*(r_1-r_2)}\right] + C_{IN}^* \left(w^* - D_o^* r_2\right) e^{-r_2 l^*},$$

or,

$$K_1\left[\left(D_o^* r_1 - D_o'^* r_4\right) + \left(D_o'^* r_4 - D_o^* r_2\right) e^{l^*(r_1-r_2)}\right] =$$

$$= C_{IN}^* \left(D_o'^* r_4 - D_o^* r_2\right) e^{-r_2 l^*},$$

or,

$$K_1 = \frac{C_{IN}^* \left(D_o'^* r_4 - D_o^* r_2\right)}{\left(D_o'^* r_4 - D_o^* r_2\right) e^{r_1 l^*} - \left(D_o'^* r_4 - D_o^* r_1\right) e^{r_2 l^*}}. \qquad (F.37)$$

Now, from Eqs. (F-37) and (F-36) we will get:

$$K_2 = C_{IN}^*\left[e^{-r_2 l^*} - \frac{\left(D_o'^* r_4 - D_o^* r_2\right) e^{l^*(r_1-r_2)}}{\left(D_o'^* r_4 - D_o^* r_2\right) e^{r_1 l^*} - \left(D_o'^* r_4 - D_o^* r_1\right) e^{r_2 l^*}}\right],$$

or,

$$K_2 = -\frac{C_{IN}^* \left(D_o'^* r_4 - D_o^* r_1\right)}{\left(D_o'^* r_4 - D_o^* r_2\right) e^{r_1 l^*} - \left(D_o'^* r_4 - D_o^* r_1\right) e^{r_2 l^*}}. \qquad (F.38)$$

Finally, from the expression $K_4 = K_1 + K_2$, Eq.(F-33), we can get the expression for K_4. That is:

$$K_4 = -\frac{C_{IN}^* \left(D_o^* r_1 - D_o^* r_2\right)}{\left(D_o'^* r_4 - D_o^* r_2\right) e^{r_1 l^*} - \left(D_o'^* r_4 - D_o^* r_1\right) e^{r_2 l^*}}. \qquad (F.39)$$

Now, with the values of the constants K_1, K_2, and K_4 given by equations (F-37), (F-38) and (F-39), respectively, we can write the solution for the radon profile and the radon flux through regions #b and #c.

Profile of Radon Concentration Throughout the Crack.

The variation of radon concentration within the crack is given by:

$$C^*(z^*) = K_1 e^{r_1 z^*} + K_2 e^{r_2 z^*}, \qquad \text{for} 0 \leq z^* \leq l^*. \tag{F.40}$$

Profile of Radon Flux Inside the Crack.

Substituting Eq.(F-40) into Eq.(F-18) we obtain the expression for the radon flux at any point z^*, inside the crack. That is:

$$J^*(z^*) = w^* \left(K_1 e^{r_1 z^*} + K_2 e^{r_2 z^*} \right) - D_o'^* \left(r_1 K_1 e^{r_1 z^*} + r_2 K_2 e^{r_2 z^*} \right),$$

or,

$$J^*(z^*) = \left(w^* - r_1 D_o'^* \right) K_1 e^{r_1 z^*} + \left(w^* - r_2 D_o'^* \right) K_2 e^{r_2 z^*}, \qquad 0 \leq z^* \leq l^*. \tag{F.41}$$

Flux at the Exit of the Crack into the Basement.

In particular, for $z^* = 0$, the radon flux at the exit of the crack, J_{EX}^* , will be given by:

$$J_{EX}^* = \left(w^* - r_1 D_o^* \right) K_1 + \left(w^* - r_2 D_o^* \right) K_2,$$

or,

$$J_{EX}^* = C_{IN}^* \left[\frac{\left(w^* - r_1 D_o^* \right) \left(D_o'^* r_4 - D_o^* r_2 \right) - \left(w^* - r_2 D_o^* \right) \left(D_o'^* r_4 - D_o^* r_1 \right)}{\left(D_o'^* r_4 - D_o^* r_2 \right) e^{r_1 l^*} - \left(D_o'^* r_4 - D_o^* r_1 \right) e^{r_2 l^*}} \right]. \tag{F.42}$$

Radon Flux at the Crack Interface.

At the crack interface, $z^* = l^*$, and the radon flux, J^*_{IN} is given by:

$$J^*_{IN} = \left(w^* - r_1 D^{\prime *}_o\right) K_1 e^{r_1 l^*} + \left(w^* - r_2 D^{\prime *}_o\right) K_2 e^{r_2 l^*}. \qquad (F.43a)$$

Substituting in the equation above, K_1 and K_2 as given by Eqs. (L-37) and (L-38), yields:

$$J^*_{IN} = M C^*_{IN}, \qquad (F.43b)$$

where,

$$M = \left[\frac{\left(D^{\prime *}_o r_4 - D^*_o r_2\right)\left(w^* - r_1 D^*_o\right) e^{r_1 l^*} - \left(D^{\prime *}_o r_4 - D^*_o r_1\right)\left(w^* - r_2 D^*_o\right) e^{r_2 l^*}}{\left(D^{\prime *}_o r_4 - D^*_o r_2\right) e^{r_1 l^*} - \left(D^{\prime *}_o r_4 - D^*_o r_1\right) e^{r_2 l^*}}\right]. \qquad (F.43c)$$

Notes:

1)- Fluxes given by Eqs. (F-41), (F-42), (F-43) are dimensionless. To find the real value of the flux, these expressions must be multiplied by the characteristic flux, $J_{ch} = S_{ch} L_{ch}$;

2)- Also, the dimensionless radon concentration, C^* , as given by Eq. (F-40) should be multiplied by S_{ch}/λ_{Rn}, in order to find its actual value;

3)- Both the radon concentration and the flux are function of C^*_{IN}, the radon concentration at the crack interface;

4)- C^*_{IN} will be calculated iteratively;

5)- The flux at the entrance, J^*_{IN}, as given by Eq.(F-43), will be used in the convergence criteria. This expression will be compared with another one derived in the next item, for the flux at the crack interface given by the convective-diffusive equation applied at the control-volume just underneath the crack;

6)- The value of C^*_{IN} will be such that makes equal both fluxes calculated at the crack interface;

7)- The flux at the crack exit, as given by Eq.(F-42), will be used to calculate the radon entry rate into the house.

Figure F.3— Configuration at the crack, showing the control-volumes defined in the soil underneath the soil-crack interface.

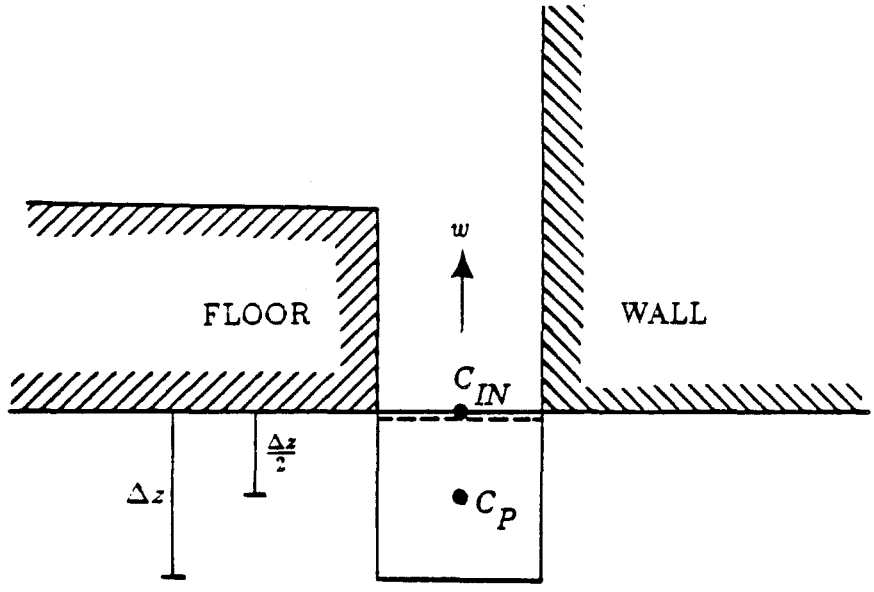

Convection-Diffusion of Radon in the Soil, and into the Crack Through the Interface.

The total flux of radon from the soil and through the interface between the crack and the control-volume can be evaluated by assuming a control-volume of very small thickness at the entrance interface, in which the radon concentration is assumed to be C^*_{IN}. Figure (F.3) illustrates this configuration.

In this figure I define a control-volume of zero thickness around C^*_{IN}, located in the soil but as close as possible to the crack interface. At any point in the soil, and consequently inside the control-volume above, the total radon flux is given by:

$$J^*(z^*) = w^* C^*(z^*) - D^* \frac{dz^*(z^*)}{dz^*}. \qquad (F.44)$$

For a point located in the control-volume, but as close as possible to the interface, the

equation above becomes:

$$J^*_{IN} = (w^*)_{IN}\, C^*_{IN} - (D^*)_{IN} \left(\frac{dC^*}{dz^*} \right)_{IN}. \qquad (F.45)$$

Notes:

1)- The point (IN) referenced in the equation above is supposed to be located inside the control-volume, but infinitesimally close to the interface;

2)- Consequently, the value of the diffusion constant D^* should still be the same as the one considered inside the control-volume;

3)- The idea here is that as the point (IN) gets closer to the exact location of the interface, the flux calculated from Eq.(F-45) above should be the same as the one calculated from Eq.(F-43);

4)- As noted before, the value of C^*_{IN} that makes these fluxes to match will be evaluated iteratively;

5)- Eq.(F.45) above is in dimensionless form. To find the actual value of J_{IN} it is necessary to multiply the dimensionless value, J^*_{IN} by the characteristic flux $J_{ch} = S_{ch} L_{ch}$;

6)- The velocity w^* is already calculated at the interface of the control-volume;

7)- The gradient of the radon concentration should also be evaluated close to the control-volume interface. In order to do this, we make the following assumptions:

. The size of the control-volume in the z-direction (Dz) is very small;

. The actual profile of the radon concentration at points between the center of the C.V. to its interface with the crack could be approximated by a linear function, such that:

$$\left[\frac{dC^*}{dz^*} \right]_{IN} = \frac{C^*_P - C^*_{IN}}{\frac{\Delta z^*}{2}}. \qquad (F.46)$$

Therefore, with the assumptions above, Eq.(F-45) becomes:

$$J^*_{IN} = w^*\, C^*_{IN} - \left(\frac{2D^*}{\Delta z^*} \right) (C^*_P - C^*_{IN}), \qquad (F.47)$$

which can also be written as:

$$J^*_{IN} = \left(w^* + \frac{2D^*}{\Delta z^*}\right) C^*_{IN} - \left(\frac{2D^*}{\Delta z^*}\right) C^*_P. \qquad (F.48)$$

Boundary Condition at the Crack Interface.

As a boundary condition applied at the surface of the crack entrance we consider that due to continuity at the interface we should have:

$$C^*_{(IN-)} = C^*_{(IN+)}, \qquad (F.49a)$$

$$J^*_{(IN-)} = J^*_{(IN+)}, \qquad (F.49b)$$

where,

$C^*_{(IN-)}$ = Dimensionless radon concentration in the crack, as it gets closer to the interface with the soil;

$C^*_{(IN+)}$ = Dimensionless radon concentration in the soil, as it gets closer to the crack interface;

$J^*_{(IN-)} = J^*_{crack}$ = Dimensionless Radon flux, defined in the same way above;

$J^*_{(IN+)} = J^*_{soil}$ = Dimensionless radon flux per unit of geometrical area in the soil matrix, as it gets closer to the crack interface.

Here I notice that both terms $J^*_{(IN-)}$ and $J^*_{(IN+)}$ are defined as the total radon flux per unit of geometrical area. Consequently, it is perfectly justifiable to make $J^*_{(IN-)} = J^*_{(IN+)}$, at points in the interface, as it was done in Eq.(F-49b).

The fluxes J^*_{soil} and J^*_{crack} were already expressed in Eqs. (F-48) and (F-43b), respectively. They are repeated here as:

$$J^*_{soil} = \left(w^* + \frac{2D^*}{\Delta z^*}\right) C^*_{IN} - \left(\frac{2D^*}{\Delta z^*}\right) C^*_P, \qquad (F.50)$$

and,

$$J^*_{crack} = M\, C^*_{IN}, \qquad (F.51a)$$

where,

$$M = \left[\frac{\left(D'^*_o r_4 - D^*_o r_2\right)\left(w^* - r_1 D^*_o\right) e^{r_1 l^*} - \left(D'^*_o r_4 - D^*_o r_1\right)\left(w^* - r_2 D^*_o\right) e^{r_2 l^*}}{\left(D'^*_o r_4 - D^*_o r_2\right) e^{r_1 l^*} - \left(D'^*_o r_4 - D^*_o r_1\right) e^{r_2 l^*}}\right]. \qquad (F.51b)$$

Now, substituting J^*_{soil} and J^*_{crack}, obtained from the equations above, into Eq.(F-49b), we can find the expression for C^*_{IN} which will satisfy the boundary condition. Thus, after some algebraic transformations, we find that:

$$C^*_{IN} = \frac{\left(\frac{2D^*}{\Delta z^*}\right) C^*_P}{\left(\frac{2D^*}{\Delta z^*}\right) + w^* - M}. \qquad (F.52)$$

APPENDIX G

ALGORITHM FOR DISTRIBUTING THE SIZES OF THE CONTROL-VOLUME FACES IN AN SPECIFIED LINEAR SEGMENT OF THE SOIL BLOCK.

I want to divide a segment L in N parts of increasing sizes based on the equation of a quarter of a circle. The method defined here will then be used to generate the numerical grid in the calculation domain of the soil block, where the sizes of the control-volumes within each defined region of the soil have variable values. The idea is to make the sizes of the control-volumes to increase from the extremity of the segment to its center.

So, consider a quarter of a circle of radius L and center at the point (L, L), as shown in Figure (G.1). The variables x and y are defined in the intervals $0 \leq x \leq L$, and $0 \leq y \leq L$ respectively. The circle touches both x and y axis at the distance L.

Now, dividing the segment L in the x-axis into N equal parts, the curve of the circle will then define N subdivisions of increasing sizes in the L segment at the y-axis, with the smaller subsegments near the origin.

The equation representing the quarter of circle, as shown in Fig.(G.1), can be expressed as:

$$\left(\frac{x}{L} - 1\right)^2 + \left(\frac{y}{L} - 1\right)^2 = 1, \qquad \text{for} \quad 0 \leq x \leq L \quad \text{and} \quad 0 \leq y \leq L. \tag{G.1}$$

Now, defining the multiplication factor $K_i = \frac{i}{N}$, where N is the number of parts the segment L will be divided, and i is order of each subsegment, $(0 \leq i \leq N)$, the variable x can be expressed as:

Figure G.1— Division of a segment L in N segments ($N = 4$ in the figure) of increasing size, based on the equation of a circle.

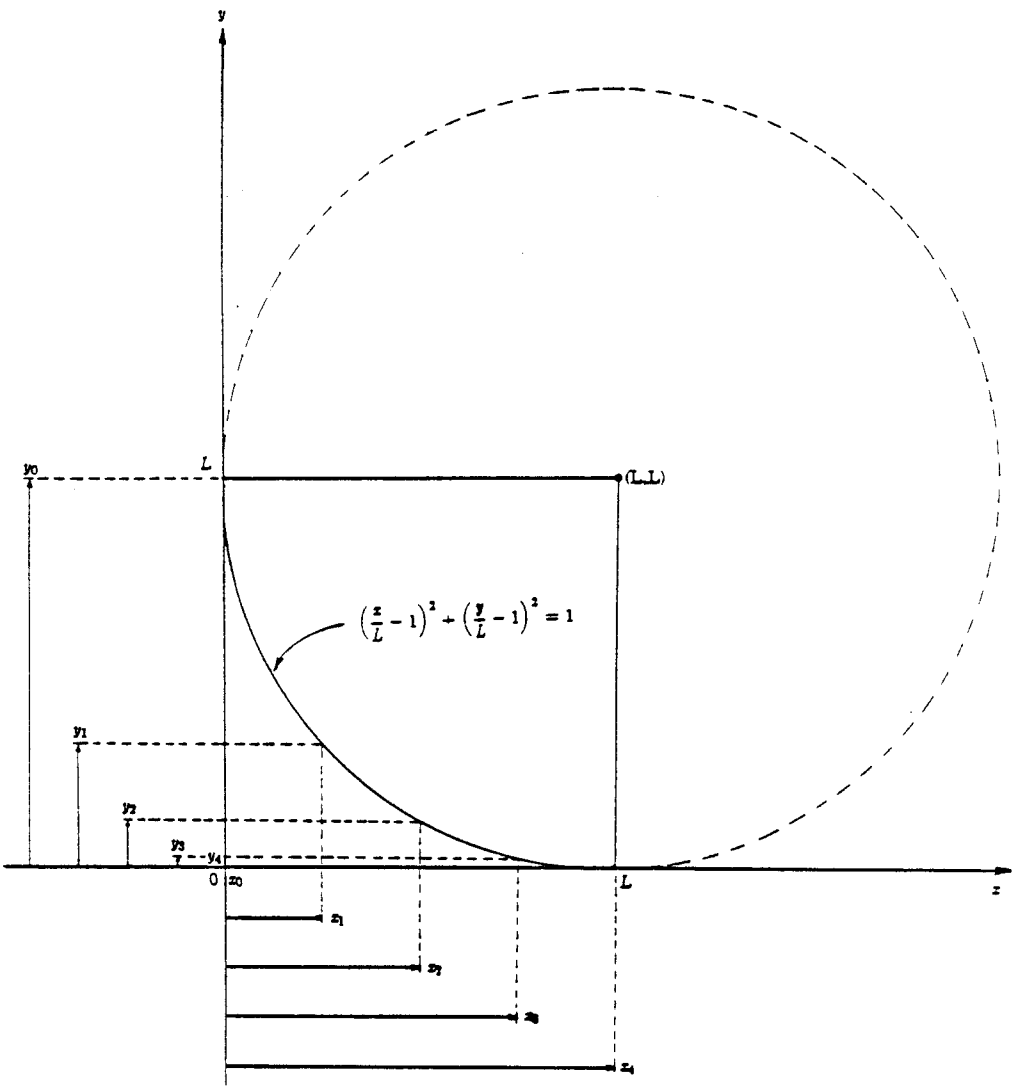

$$x_i = K_i L = \left(\frac{i}{N}\right) L. \qquad (G.2)$$

The objective is to find the resultant multiplication factor J_i that will produce the non-homogeneous and increasing subsegments in the y-axis such that:

$$y_i = J_i L. \qquad (G.3)$$

Therefore, substituting Eqs. (G.2) and (G.3) into Eq.(G.1) yields:

$$(J_i - 1)^2 + \left(\frac{i}{N} - 1\right)^2 = 1,$$

or,

$$J_i = 1 - \left[1 - \left(\frac{i}{N} - 1\right)^2\right]^{\frac{1}{2}}, \qquad \text{for} \quad 0 \leq i \leq N. \tag{G.4}$$

Now, substituting Eq.(G.4) into (G.3), yields:

$$y_i = L\left\{1 - \left[1 - \left(\frac{i}{N} - 1\right)^2\right]^{\frac{1}{2}}\right\}, \qquad \text{for} \quad 0 \leq i \leq N. \tag{G.5}$$

Notes:

1- Eq.(G.5) is used to calculate the sizes of N defined control-volumes within a specified segment of the calculation domain of the soil block;

2- In some segments of the soil block, the sizes of the control-volume increase symmetrically from both extremities of the segment toward to its center. In these cases, the method for dividing the segment, as expressed by Eq.(G.5), is applied at each half of the segment separately.

APPENDIX H

DEFINITION OF THE VALUE OF THE PERMEABILITY AT AN INTERFACE BETWEEN TWO REGIONS OF DIFFERENT PERMEABILITIES.

Consider the following figure representing a generic node P, and its neighbors in the x-direction only. Note that since it is assumed that the nodes are located in the center of the control-volume, the distance between two nodes, $(\delta x)_e$ for example, can be expressed as:

$$(\delta x)_e = \frac{\Delta x_P + \Delta x_E}{2}.$$

Figure H.1— Generic representation of a node cluster in the x-direction.

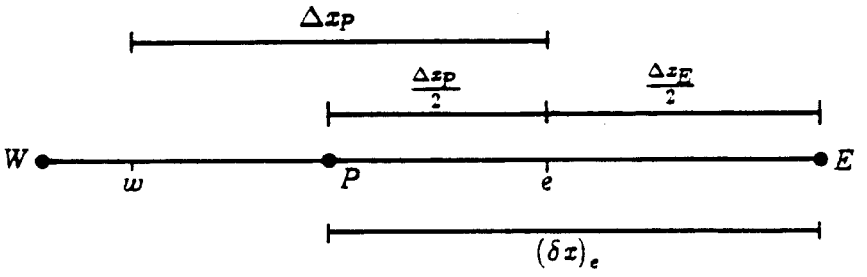

I want to represent the velocity of the flow at the interface e, (or any other), via an expression of the following kind:

$$u_e = -k_e \left[\frac{p_E - p_P}{(\delta x)_e} \right] = - \left[\frac{k_e}{(\delta x)_e} \right] (p_E - p_P) . \qquad (H.1)$$

Yet, I need an expression for k_e, (the permeability at the interface e), that leads to a *correct* value of u_e, when the permeability k has different values at the nodes P and E, as in the case at the boundary of distinct regions in the soil.

Thus, here I assume that:

- The control-volume around P has a permeability k_P;
- The control-volume around E has a permeability k_E.

Then, at the interface e, the velocity u_e would be given by the pressure difference between the two neighbor nodes divided by the sum of the resistivity at each half of the neighbor control-volumes, and can be expressed as:

$$u_e = - \frac{p_E - p_P}{\frac{\Delta x_P/2}{k_P} + \frac{\Delta x_E/2}{k_E}} = - \left(\frac{2 k_P k_E}{\Delta x_P k_E + \Delta x_E k_P} \right) (p_E - p_P) . \qquad (H.3)$$

Comparing these two equations above, yields:

$$\frac{2k_e}{\Delta x_P + \Delta x_E} = \frac{2 k_P k_E}{\Delta x_P k_E + \Delta x_E k_P} ,$$

which can be simplified to:

$$k_e = \frac{k_P k_E}{\frac{\Delta x_P k_E + \Delta x_E k_P}{\Delta x_P + \Delta x_E}} . \qquad (H.4)$$

Note:

- Equation (H.4) above defines the permeability at an interface between regions of distinct permeabilities;
- The same kind of expression is used to define the diffusivity coefficient D_e at the interface e.

APPENDIX I

DERIVATION OF THE DISCRETIZATION EXPRESSIONS FOR THE CONVECTION-DIFFUSION EQUATION.

The objective here is to formulate the algebraic discretization equations[1] for the convection and diffusion differential equation representing the radon concentration field in the soil.

The steady-state mass transfer differential equation expressing the transport of radon throughout the soil block was presented in Chapter 3. Its dimensionless form is repeated here as:[2]

$$\vec{\nabla} \cdot \left(D \vec{\nabla} C \right) - \vec{\nabla} \cdot (D \vec{q} C) + \epsilon (S - C) = 0. \qquad (I.1)$$

The flow field $\vec{q}$ must also satisfy the continuity equation, expressed as:

$$\vec{\nabla} \cdot \vec{q} = 0. \qquad (I.2)$$

These equations can be expressed in cartesian coordinates for a three-dimensional configuration as:

---

[1] Reference: PATANKAR, S.V., 1980, *Numerical Heat Transfer and Fluid Flow*, Chapter Five: Convection and Diffusion, McGraw-Hill Book Company.

[2] In order to simplify the notation in this appendix, I have not used the asterisk in the dimensionless versions of the equations.

$$\left[\frac{\partial}{\partial x}\left(D\frac{\partial C}{\partial x}\right)+\frac{\partial}{\partial y}\left(D\frac{\partial C}{\partial y}\right)+\frac{\partial}{\partial z}\left(D\frac{\partial C}{\partial z}\right)\right]-$$
$$\left[\frac{\partial}{\partial x}(uC)+\frac{\partial}{\partial y}(uC)+\frac{\partial}{\partial z}(uC)\right]+ \qquad (I.3)$$
$$\epsilon(S-C)=0,$$

and,

$$\frac{\partial u}{\partial x}+\frac{\partial v}{\partial y}+\frac{\partial w}{\partial z}=0. \qquad (I.4)$$

Steady One-Dimensional Convection and Diffusion.

Before we attempt to derive the discretization equation for the three-dimensional configuration, with the source and sink terms, let's work with a simpler case where the basic procedures can be established.

The simplest possible case is the steady one dimensional situation with no source or sink terms, which can be represented by (taking the x-direction as example):

- Mass Balance Equation -

$$\frac{d}{dx}\left(D\frac{dC}{dx}\right)-\frac{d}{dx}(uC)=0, \qquad (I.5)$$

- Continuity Equation -

$$\frac{du}{dx}=0. \qquad (I.6)$$

In order to derive the discretization equation, let us consider the grid represented in Figure (I.1).

Note:

Figure I.1— Grid-point cluster for one-dimensional configuration.

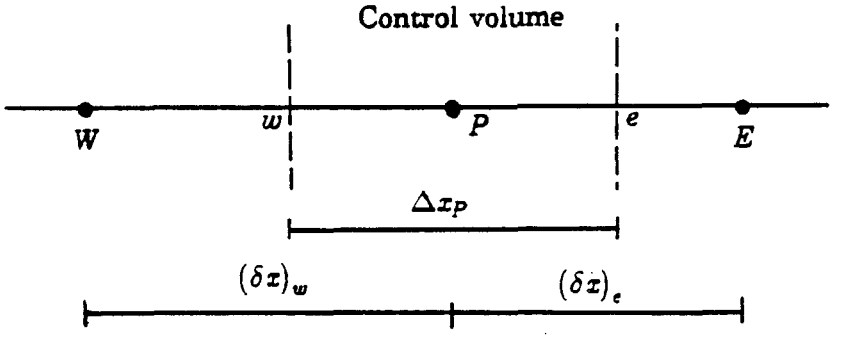

- The node is centered in the control-volume;
- The distances between nodes are given by:

$$(\delta x)_e = \frac{\Delta x_P + \Delta x_E}{2}, \tag{I.7a}$$

and,

$$(\delta x)_w = \frac{\Delta x_P + \Delta x_W}{2}. \tag{I.7b}$$

Now, integrating Eq.(I.5) over the control-volume, we will get:

$$\left(D\frac{dC}{dx}\right)_e - \left(D\frac{dC}{dx}\right)_w = (uC)_e - (uC)_w \tag{I.8}.$$

Equation above constitutes our basic approach for the derivation of the discretization equation. Yet, in order to continue with this derivation, it is important to make some assumptions about the profile of the function C with the distance x. For the simple case of steady one-dimensional configuration, with no source or sink, the profile of C can be found exactly by solving Eq.(I.5) analytically.

Exact Solution for the One-Dimensional Mass-Balance Equation.

Eq.(I.5) can be solved analytically if D is assumed to be constant. We note here that, according to the continuity equation, Eq.(I.6), the velocity u is also constant. Eq.(I.5) can then be written as:

$$\frac{d^2C}{dx^2} = \left(\frac{u}{D}\right)\frac{dC}{dx}. \tag{I.9}$$

A general solution of the equation above is given by the expression:

$$C(x) = K_1 e^{\left(\frac{u}{D}\right)x} + K_2, \tag{I.10}$$

where K_1 and K_2 are constants to be determined from the following boundary conditions.

Boundary Condition for the One-Dimensional Mass-Balance Equation.

$$\text{At, } x = 0, \longrightarrow C(0) = C_0, \tag{I.11}$$

$$\text{At, } x = L, \longrightarrow C(x = L) = C_L.$$

Then, the constants K_1 and K_2 are found as:

$$K_1 = \left(\frac{C_L - C_0}{e^{\frac{uL}{D}} - 1}\right), \tag{I.12a}$$

and,

$$K_2 = C_0 - \left(\frac{C_L - C_0}{e^{\frac{uL}{D}} - 1}\right). \tag{I.12b}$$

Substituting the constants K_1 and K_2 into Eq.(I.10):

$$C(x) = \left(\frac{C_L - C_0}{e^{\frac{uL}{D}} - 1}\right) e^{\left(\frac{u}{D}\right)x} + C_0 - \left(\frac{C_L - C_0}{e^{\frac{uL}{D}} - 1}\right),$$

or,

$$C(x) = C_0 + \left(\frac{C_L - C_0}{e^{\frac{uL}{D}} - 1}\right)\left[e^{\left(\frac{u}{D}\right)x} - 1\right]. \qquad (I.13)$$

The dimensionless term $\frac{uL}{D}$ is now defined as the Peclet Number:

$$P = \frac{uL}{D}. \qquad (I.14)$$

Note:

1)- The Peclet number P represents the ratio of strength between convection and diffusion;

2)- P can be positive or negative, depending on the direction of the velocity u;

3)- In our present case, the Peclet number P was defined for the generic domain $0 \leq x \leq L$, and depends on the value of L, the dimension of the domain;

4)- Later on we will define the *grid Peclet number*, (see Eq.(I.60)), at the interface between two control-volumes. There then, the domain to be considered will be the distance between the neighbor grid nodes, and the velocity, and diffusion coefficient (u, ϵ, and D), should be defined at the interface.

Substituting Eq.(I.14) into Eq.(I.13), yields:

$$C(x) = C_0 + \left(\frac{C_L - C_0}{e^P - 1}\right)\left[e^{\left(\frac{P}{L}\right)x} - 1\right]. \qquad (I.15)$$

The expression above is the exact solution of the problem represented by Eq.(I.5) (Steady one-dimensional situation, with no source or sink, and with constant diffusivity). It represents the actual profile of the concentration $C(x)$ along the domain $0 \leq x \leq L$, as a

Figure I.2— Actual profile of the concentration $C(x)$, along the one-dimensional domain $0 \leq x \leq L$, for several values of the Peclet number P.

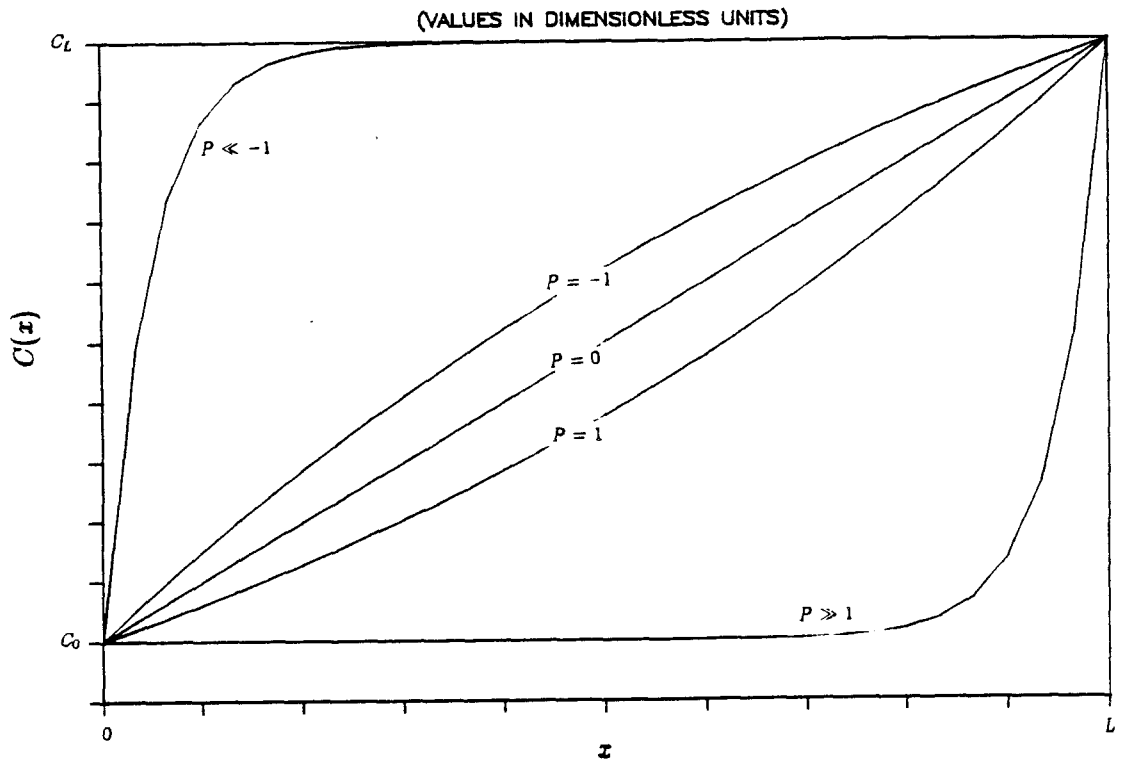

parametric function of the Peclet number P. Figure (I.2) shows the profiles of the concentration $C(x)$, for several Peclet numbers.

Thus, in Fig.(I.2) we can see that when the Peclet number approaches zero, the concentration profiles becomes linear. In other words, for cases with no source or sink, and where the diffusive component of the transport process predominates over the convective component, the variation of the concentration with distance, $C(x)$, converges to a linear function. However, as $|P|$ increases, the concentration profile $C(x)$ deviates more and more from the linear function. For large positive values of the Peclet number, the concentration profile will be unchanged along almost the entire x-domain, increasing suddenly at the end of the segment $(0, L)$. On the other hand, for large negative Peclet numbers, the concentration profile will jump to its maximum value at the beginning of the segment $(0, L)$, keeping that value along almost the entire domain. This could be interpreted in the following way. The large Peclet

number implies that convection predominates over diffusion, which means that the velocity has an important role in the transport process. Thus, with large positive velocities (large P), the concentration $C(x)$ at most of the points along the x-domain will be given by the concentration at the upwind boundary. Consequently the value of C_0 will be unchanged along most of the domain. But then, for large negative velocities, (large negative Peclet numbers), the concentration at the upwind boundary is C_L, which will then predominate along most of the x-domain.

We now return to the derivation of the discretization equation, represented by Eq.(I-8), considering first the exact profile for $C(x)$. The resulting scheme will be called the *Exponential Scheme*. Other discretization schemes, considering different interpolation profiles for $C(x)$, will be presented thereafter..

The Exponential Scheme.

Let us consider the total flux J as composed with the sum of the convective term uC, and the diffusive term $-D\frac{dC}{dx}$, such that:

$$J = uC - D\frac{dC}{dx}. \qquad (I.16)$$

Using this notation, the mass balance expression, Eq.(I.5), can be written as:

$$\frac{dJ}{dx} = 0. \qquad (I.17)$$

Integrating the equation above over the control volume of Fig.(I.1), we will get:

$$J_e - J_w = 0. \qquad (I.18)$$

Now we need to find the value of the total flux J at the interfaces e and w. So, substituting the exact profile of C for the domain $0 \leq x \leq L$, given from Eq.(I.15), into Eq.(I.16), we

will get the actual profile of the total flux J for that specific domain, which can then be expressed as:

$$J = u\left\{ C_0 + \left[\frac{C_L - C_0}{e^P - 1}\right]\left[e^{(\frac{P}{L})x} - 1\right]\right\} - D\left(\frac{C_l - C_0}{e^P - 1}\right)\frac{P}{L}e^{(\frac{P}{L})x}.$$

But $\frac{DP}{L} = u$ (See Eq. J-14). Then, the equation above becomes:

$$J = u\left(C_0 + \frac{C_0 - C_L}{e^P - 1}\right). \qquad (I.19)$$

Note that:

1)- In this case, the total flux J is invariant with the distance x in any specified domain (as it should be expected, since there is no source or sink);

2)- However, since for different domains, the Peclet number P can vary depending on the values of u, D, and L for that specific domain, the total flux J can also vary from a defined domain to the other;

3)- Here we defined a domain as the region between two neighbor nodes. Consequently L is going to be equal to (δx) .

Now let us evaluate the total flux J_e and J_w at the points of the interfaces e and w, in the domains represented by the grid nodes P-E and W-P respectively.

Calculation of J_e, the Flux at the Interface e.

Using the exact profile from Eq.(I.19), and making: $C_o = C_P$, and $C_L = C_E$, and replacing L by the distance between nodes $(\delta x)_e$, we will get:

$$J_e = u_e\left(C_P + \frac{C_P - C_E}{e^{Pe} - 1}\right), \qquad (I.20)$$

where,

$$P_e = \frac{u_e}{D_e}(\delta x)_e, \qquad (I.21)$$

is the Peclet number as defined by Eq.(I.14), and applied at the interface e.

Note that:

1)- J_e does not depend on the location of the interface between points P and E;

2)- The diffusion coefficient D_e, is to be obtained similarly to the way the permeability k_e was obtained, as the weighted average of the diffusion coefficients in the neighbor control-volumes, (See Appendix H);

3)- Although in our derivation so far we have assumed a constant D, here we assume the variability of the diffusion factor D by defining an expression for D_e at the interface e (for example).

The appropriateness of this approach was discussed elsewhere, (see Patankar, [Pa80], footnote at page 87).

Calculation of J_w, the Flux at the Interface w.

Similarly to the procedure above, we can find the expression for J_w as:

$$J_w = u_w\left(C_W + \frac{C_W - C_P}{e^{Pw} - 1}\right). \qquad (I.22)$$

Then, substituting Eq.(I.20) and (I.22) into Eq.(I.18), yields:

$$u_e\left(C_P + \frac{C_P - C_E}{e^{Pe} - 1}\right) - u_w\left(C_W + \frac{C_W - C_P}{e^{Pw} - 1}\right) = 0, \qquad (I.23)$$

or,

$$\left(u_e + \frac{u_e}{e^{Pe} - 1} + \frac{u_w}{e^{Pw} - 1}\right) C_P = \left(\frac{u_e}{e^{Pe} - 1}\right) C_E + \left(u_w + \frac{u_w}{e^{Pw} - 1}\right) C_W.$$

Now, adding $u_w - u_e$ to the expression above, yields:

$$\left(u_e - u_w + \frac{u_e}{e^{Pe} - 1} + u_w + \frac{u_w}{e^{Pw} - 1}\right) C_P = \left(\frac{u_e}{e^{Pe} - 1}\right) C_E + \left(u_w + \frac{u_w}{e^{Pw} - 1}\right) C_W,$$

which can now be written using the standard form for the discretization equation:

$$a_P C_P = a_E C_E + a_W C_W, \qquad (I.24)$$

where,

$$a_E = \frac{u_e}{e^{Pe} - 1}, \qquad (I.25a)$$

$$a_W = u_w + \frac{u_w}{e^{Pw} - 1} = \frac{u_w e^{Pw}}{e^{Pw} - 1}, \qquad (I.25b)$$

$$a_P = a_E + a_W + [u_e - u_w]. \qquad (I.25c)$$

Note that:

1- Equations (I.24) and (I.25) define the exponential scheme;

2- The exponential scheme, when used for the steady one-dimensional problem with no source or sink term produces the exact solution, independent of the Peclet number, and the number of grid nodes;

3- However, this scheme is not exact for two or three-dimensional problems, nonzero sources (and sinks), etc.. Besides, it is important to point out that exponentials are expensive to compute. Consequently, the exponential scheme is not appropriate for multi-dimensional problems;

4- Therefore we need to find an easy-to-compute (and cheap) scheme that can approximate the exponential scheme. Four possible schemes – *central-difference; upwind; hybrid;* and *power law* – will be presented next.

The Central-Difference Scheme.

In the central-difference interpolation scheme, the concentration profile $C(x)$ is assumed to be piecewise-linear between nodes. Therefore, the diffusive component of the flux, $D\frac{dC}{dx}$, and the convective component, uC, can be interpolated linearly at the interfaces e and w, as shown in Fig.(I.1), according to the following expressions:

$$\left(D\frac{dC}{dx}\right)_e = D_e\left[\frac{C_E - C_P}{(\delta x)_e}\right], \tag{I.26a}$$

$$\left(D\frac{dC}{dx}\right)_w = D_w\left[\frac{C_P - C_W}{(\delta x)_w}\right], \tag{I.26b}$$

and,[3]

$$(uC)_e = u_e\left[\frac{\left(\frac{\Delta x_P}{2}\right)C_P + \left(\frac{\Delta x_E}{2}\right)C_E}{\frac{\Delta x_P}{2} + \frac{\Delta x_E}{2}}\right] = u_e\left[\frac{\left(\frac{\Delta x_P}{2}\right)C_P + \left(\frac{\Delta x_E}{2}\right)C_E}{(\delta x)_e}\right], \tag{I.27a}$$

$$(uC)_w = u_w\left[\frac{\left(\frac{\Delta x_W}{2}\right)C_W + \left(\frac{\Delta x_P}{2}\right)C_P}{\frac{\Delta x_W}{2} + \frac{\Delta x_P}{2}}\right] = u_w\left[\frac{\left(\frac{\Delta x_W}{2}\right)C_W + \left(\frac{\Delta x_P}{2}\right)C_P}{(\delta x)_w}\right]. \tag{I.27a}$$

Thus, substituting Eqs. (I.26) and (I.27), into Eq.(I.8), yields:

$$\left[\frac{D_e}{(\delta x)_e}\right]C_E + \left[\frac{D_w}{(\delta x)_w}\right]C_W - \left[\frac{D_e}{(\delta x)_e} + \frac{D_w}{(\delta x)_w}\right]C_P =$$
$$= \left[\frac{u_e}{(\delta x)_e} - \frac{u_w}{(\delta x)_w}\right]\left(\frac{\Delta x_P}{2}\right)C_P + \left[\frac{u_e}{(\delta x)_e}\right]\left(\frac{\Delta x_E}{2}\right)C_E - \left[\frac{u_w}{(\delta x)_w}\right]\left(\frac{\Delta x_W}{2}\right)C_W,$$

or,

$$\left[\frac{D_e}{(\delta x)_e} + \frac{D_w}{(\delta x)_w} + U_e\frac{\Delta x_P}{2(\delta x)_e} - U_w\frac{\Delta x_P}{2(\delta x)_w}\right]C_P =$$
$$= \left[\frac{D_e}{(\delta x)_e} - u_e\frac{\Delta x_E}{2(\delta x)_e}\right]C_E + \left[\frac{D_w}{(\delta x)_w} - u_w\frac{\Delta x_W}{2(\delta x)_w}\right]C_W, \tag{I.28}$$

[3] Note that in Fig.(I.1) the nodes are assumed to be centered in the control-volumes. Therefore, since the control-volumes may have different sizes, the interfaces are not necessarily located midway between nodes.

which can now be expressed in the established standard form for the discretization equation, as:

$$a_P C_P = a_E C_E + a_W C_W, \qquad (I.29a)$$

where,

$$a_E = \frac{D_e}{(\delta x)_e} - u_e \left[\frac{\Delta x_E}{2(\delta x)_e}\right], \qquad (I.29b)$$

$$a_W = \frac{D_w}{(\delta x)_w} + u_w \left[\frac{\Delta x_W}{2(\delta x)_w}\right], \qquad (I.29c)$$

and,

$$a_P = a_E + a_W + (u_e - u_w). \qquad (I.29d)$$

Equation (I.29) represents the central-difference interpolation scheme for the discretization formulation, which is based on the assumption of a piecewise-linear profile of $C(x)$. As it was shown in Fig.(I.2), the concentration profile $C(x)$ could be approximated by a piecewise-linear function, only for values of the Peclet number P close to zero. For large $|P|$, $C(x)$ deviates considerably from the linear function. Therefore, the central-difference interpolation scheme provides a reasonable approximation to the actual profile of $C(x)$, only for the cases of small $|P|$. Since the Peclet number at the grid nodes is given by, $P = \frac{u}{D/\delta}$, it can be decreased, as much as needed, by refining the grid mesh. Consequently, the central-difference scheme can be justified in cases of reduced grid mesh, or when diffusion clearly dominates the transport process. For large convective fluxes, (as compared with the diffusive component), or for a coarse grid mesh, the central-difference scheme is expected to produce unrealistic results.

The Upwind Scheme.

As it was shown in the last item, the weakness of the central-difference scheme occurs at large values of the convective flux, when the assumption of piecewise-linear profile for $C(x)$ is not valid. In essence, the critical issue here is the convective component of the transport process. Thus, in order to solve part of the difficulties found in the central-difference formulation, another interpolation scheme, called *upwind* is presented. In the upwind interpolation scheme, the diffusive component of the flux, $D\frac{dC}{dx}$, is still interpolated linearly at the interfaces between nodes, as it was done in the central-difference scheme. However, the convective component is handled in a different manner. Here, it is assumed that the concentration at the interface, C_e or C_w, is equal to the concentration at the node located at the upwind side of the flow. Thus, the concentrations at the interfaces e and w are expressed, respectively, as:

$$C_e = C_P, \qquad \text{if} \qquad u_e > 0, \tag{I.30a}$$

$$C_e = C_E, \qquad \text{if} \qquad u_e < 0, \tag{I.30b}$$

and,

$$C_w = C_W, \qquad \text{if} \qquad u_w > 0, \tag{I.31a}$$

$$C_w = C_P, \qquad \text{if} \qquad u_w < 0. \tag{I.31b}$$

Therefore, the convective component of the flux at the control-volume interfaces can be expressed as:

$$(uC)_e = u_e C_P, \qquad \text{if} \qquad u_e > 0,$$

$$(uC)_e = u_e C_E, \qquad \text{if} \qquad u_e < 0,$$

and,

$$(uC)_w = u_w C_W, \qquad \text{if} \qquad u_w > 0,$$

$$(uC)_w = u_w C_P, \qquad \text{if} \qquad u_w < 0.$$

The expressions above representing the convective flux can be replaced by a condensed form such as:

$$(uC)_e = C_P \left[\left[u_e, 0\right]\right] - C_E \left[\left[-u_e, 0\right]\right], \tag{I.32a}$$

and,

$$(uC)_w = C_W \left[\left[u_w, 0\right]\right] - C_P \left[\left[-u_w, 0\right]\right]. \tag{I.32b}$$

where the symbol $\left[\left[\ \ \right]\right]$ represents the largest of the quantities within it. Now, substituting Eq.(I.32) into Eq.(I.8), and making a linear interpolation of the diffusive flux, yields:

$$\begin{aligned} &D_e \left[\frac{C_E - C_P}{(\delta x)_e}\right] - D_w \left[\frac{C_P - C_W}{(\delta x)_w}\right] = \\ &= C_P \left[\left[u_e, 0\right]\right] - C_E \left[\left[-u_e, 0\right]\right] - C_W \left[\left[u_w, 0\right]\right] + C_P \left[\left[-u_w, 0\right]\right], \end{aligned} \tag{I.33}$$

or,

$$\begin{aligned} &\left[\frac{D_e}{(\delta x)_e} + \frac{D_w}{(\delta x)_w} + \left[\left[u_e, 0\right]\right] + \left[\left[-u_w, 0\right]\right]\right] C_P = \\ &= \left[\frac{D_e}{(\delta x)_e} + \left[\left[-u_e, 0\right]\right]\right] C_E + \left[\frac{D_w}{(\delta x)_w} + \left[\left[u_w, 0\right]\right]\right] C_W, \end{aligned} \tag{I.34}$$

which can then be expressed in the adopted standard form of the discretization equation as:

$$a_P C_P = a_E C_E + a_W C_W, \qquad (I.35a)$$

where,

$$a_E = \frac{D_e}{(\delta x)_e} + \left[\left[-u_e, 0\right]\right], \qquad (35b)$$

$$a_W = \frac{D_w}{(\delta x)_w} + \left[\left[u_w, 0\right]\right], \qquad (35c)$$

and,

$$a_P = a_E + a_W + (u_e - u_w). \qquad (I.35d)$$

Equation (I.35) above represents the discretization formulation based on the upwind interpolation scheme. Here, a few comments should be made about using the upwind interpolation scheme:

1)- In Fig.(I.2), it can observed that for large values of $|P|$, the concentration profile $C(x)$ between two nodes is nearly constant and equal to the concentration at the node located upstream. This is precisely the assumption in the upwind scheme, which considers the concentration at the interface equal to the concentration at the node located upwind. Therefore, the upwind interpolation scheme can be a satisfactory approximation, for cases with large $|P|$.

2)- For large $|P|$, $C(x)$ is almost constant along most of the segment between nodes, and consequently $\frac{dC}{dx}$ is nearly zero. Therefore, in these cases the diffusive component of the flux is almost absent. However, the upwind scheme always considers diffusion. Thus, for large $|P|$ the upwind scheme is likely to overestimate diffusion.

3)- For small $|P|$ the upwind interpolation scheme is expected to overestimate or underestimate the convective component of the flux, depending on the direction of the flow. If the velocity u is in the direction of the increasing concentration (represented by the cases of $P > 0$ in Fig.(I.2)), then the upwind scheme underestimates the convective

flux. On the other hand, if the velocity u is in the direction of decreasing concentration ($P < 0$ in Fig.(I.2)), the upwind scheme overestimates the convective component of the flux.

4)- As $|P|$ approaches zero, the upwind scheme converges to the exact solution.

The Hybrid Scheme.

In order to define the hybrid scheme and to show its approximation with the exact solution given by the exponential scheme, let us plot the coefficients a_E and a_W as a function of the Peclet numbers P_e and P_w respectively. Here we use, in fact, the dimensionless forms $\frac{a_E}{(D_e/(\delta x)_e)}$ and $\frac{a_W}{(D_w/(\delta x)_w)}$ obtained from Eqs. (I.25a) and (I.25b) such that:

$$\frac{a_E}{(D_e/(\delta x)_e)} = \frac{P_e}{e^{P_e} - 1}, \tag{I.36a}$$

and,

$$\frac{a_W}{(D_w/(\delta x)_w)} = \frac{P_w e^{P_w}}{e^{P_w} - 1}. \tag{I.36b}$$

The variation of a_E and a_W with the Peclet number P, based on Eqs. (I.36a) and (I.36b), is shown in the next Figures (I.3) and (I.4), respectively. In these figures, we represented three straight lines that form an envelope of the exact curve. The hybrid scheme is derived then from these three straight lines. Thus, from Fig.(I.3) we can have:

$$\text{For, } P_e < -2 \longrightarrow \frac{a_E}{(D_e/(\delta x)_e)} = -P_e, \tag{I.37a}$$

$$\text{For, } -2 \leq P_e \leq -2 \longrightarrow \frac{a_E}{(D_e/(\delta x)_e)} = 1 - \frac{P_e}{2}, \tag{I.37b}$$

$$\text{For, } P_e > 2 \longrightarrow \frac{a_E}{(D_e/(\delta x)_e)} = 0. \tag{I.37c}$$

Figure I.3— Variation of the Factor $\frac{a_E}{(D_e/(\delta x)_e)}$ with the Peclet number P_e.

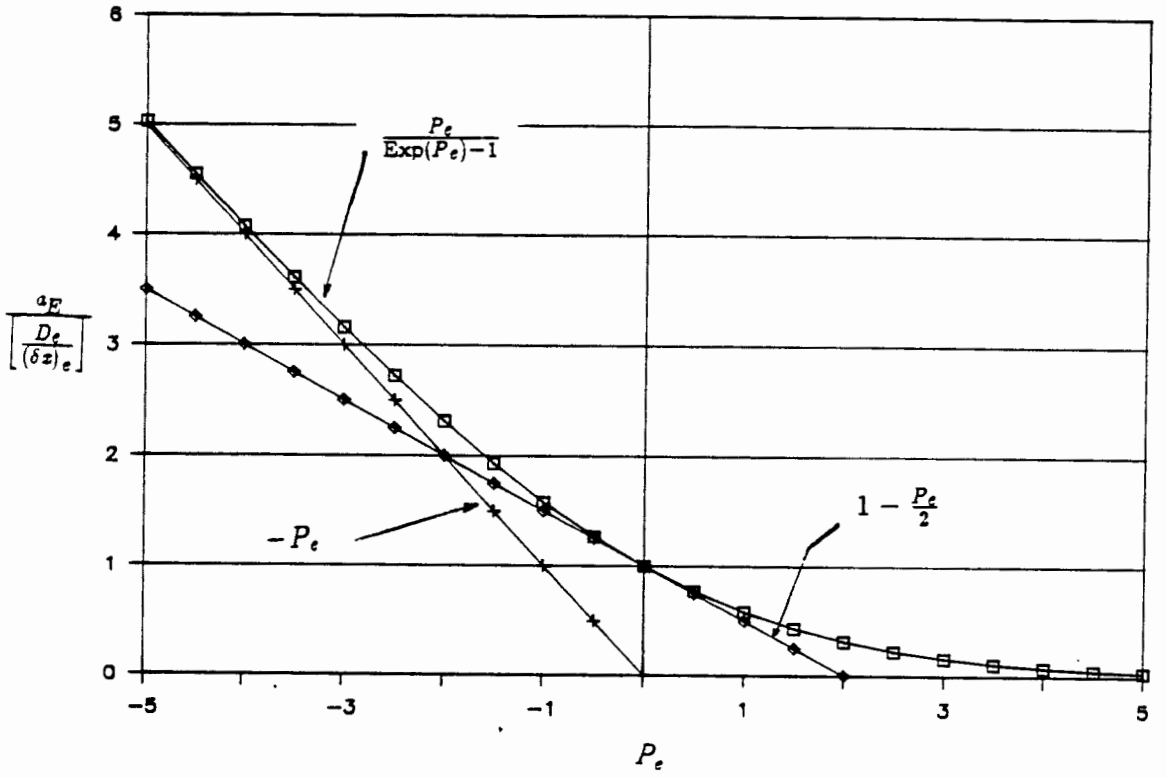

These three expressions can be combined in a condensed formula such as:

$$\frac{a_E}{(D_e/(\delta x)_e)} = \left[\left[-P_e, 1-\frac{P_e}{2}, 0\right]\right], \qquad (I.38a)$$

or,

$$a_E = \frac{D_e}{(\delta x)_e}\left[\left[-P_e, 1-\frac{P_e}{2}, 0\right]\right]. \qquad (I.38b)$$

Similarly, from Fig.(I.4) we can have:

$$\text{For,}\quad P_w < -2 \longrightarrow \frac{a_W}{(D_w/(\delta x)_w)} = 0, \qquad (I.39a)$$

$$\text{For,}\quad -2 \le P_w \le -2 \longrightarrow \frac{a_W}{(D_w/(\delta x)_w)} = 1+\frac{P_w}{2}, \qquad (I.39b)$$

Figure I.4— Variation of the Factor $\frac{a_W}{(D_w/(\delta x)_w)}$ with the Peclet number P_w.

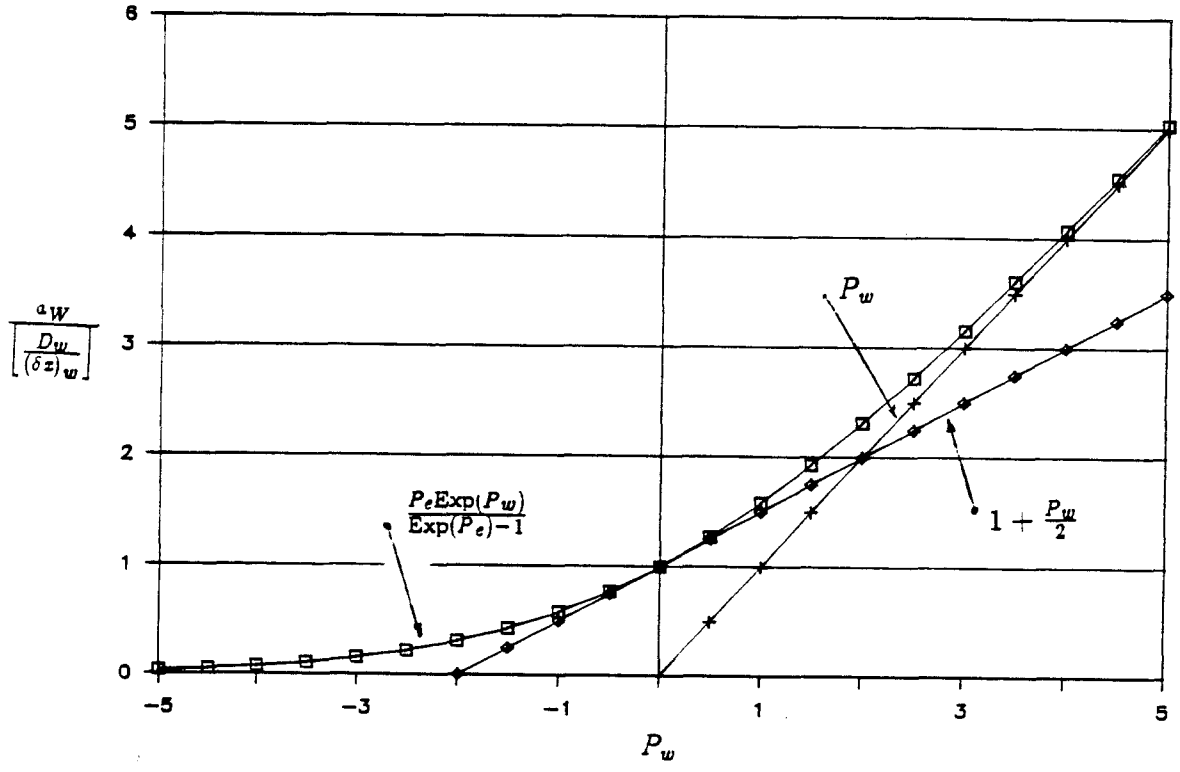

$$\text{For, } P_w > 2 \longrightarrow \frac{a_W}{(D_w/(\delta x)_w)} = P_w, \tag{I.39c}$$

and the condensed expression representing the equation above can be expressed as:

$$a_W = \frac{D_w}{(\delta x)_w}\left[\left[P_w, 1+\frac{P_w}{2}, 0\right]\right]. \tag{I.40}$$

Therefore, substituting Eqs. (I.38) and (I.40) into Eq.(I.24), the *hybrid scheme* for the discretization equation of the steady one-dimensional, no source/sink , convection-diffusion transport equation can then be expressed as:

$$a_P C_P = a_E C_E + a_W C_W, \tag{I.41}$$

where,

$$a_E = \frac{D_e}{(\delta x)_e}\left[\left[-P_e, 1 - \frac{P_e}{2}, 0\right]\right], \tag{I.42a}$$

$$a_W = \frac{D_w}{(\delta x)_w}\left[\left[P_w, 1 + \frac{P_w}{2}, 0\right]\right], \tag{I.42b}$$

$$a_P = a_E + a_W + (u_e - u_w)\,. \tag{I.42c}$$

The Power Law Scheme.

As it was shown in Figs. (I.3) and (I.4), the hybrid scheme has the highest deviation from the exact curve for values of $|P|$ close to 2. A more precise approximation to the exact curve can then be obtained with the following scheme:

Power-law expression for a_E.

$$\text{For,}\quad P_e < -10 \longrightarrow \frac{a_E}{(D_e/(\delta x)_e)} = -P_e, \tag{I.43a}$$

$$\text{For,}\quad -10 \le P_e \le 0 \longrightarrow \frac{a_E}{(D_e/(\delta x)_e)} = (1 + 0.1P_e)^5 - P_e, \tag{I.43b}$$

$$\text{For,}\quad 0 \le P_e \le 10 \longrightarrow \frac{a_E}{(D_e/(\delta x)_e)} = (1 + 0.1P_e)^5, \tag{I.43c}$$

$$\text{For,}\quad P_e > 10 \longrightarrow \frac{a_E}{(D_e/(\delta x)_e)} = 0. \tag{I.43d}$$

The condensed expression for Eq.(I.43) above is then:

$$\frac{a_E}{[D_e/(\delta x)_e]} = \left[\left[0, (1 - 0.1\,|P_e|)^5\right]\right] + \left[\left[0, -P_e\right]\right]. \tag{I.44}$$

Similarly, the power-law expression for a_W is:

$$\text{For, } P_w < -10 \longrightarrow \frac{a_W}{(D_w/(\delta x)_w)} = 0, \tag{I.45a}$$

$$\text{For, } -10 \leq P_w \leq 0 \longrightarrow \frac{a_W}{(D_w/(\delta x)_w)} = (1 + 0.1P_w)^5, \tag{I.45b}$$

$$\text{For, } 0 \leq P_w \leq 10 \longrightarrow \frac{a_W}{(D_w/(\delta x)_w)} = (1 - 0.1P_w)^5 + P_w, \tag{I.45c}$$

$$\text{For, } P_w > 10 \longrightarrow \frac{a_W}{(D_w/(\delta x)_w)} = P_w, \tag{I.45d}$$

with a condensed form expressed as,

$$\frac{a_W}{(D_w/(\delta x)_w)} = \left[\left[0, (1 - 0.1\,|P_w|)^5\right]\right] + \left[\left[0, P_w\right]\right]. \tag{I.46}$$

Therefore, the convection-diffusion discretization equation for the power-law scheme can be written as:

$$a_P C_P = a_E C_E + a_W C_W, \tag{I.47}$$

where,

$$a_E = \frac{D_e}{(\delta x)_e}\left[\left[0, (1 - 0.1\,|P_e|)^5\right]\right] + \frac{D_e}{(\delta x)_e}\left[\left[0, -P_e\right]\right], \tag{I.48a}$$

$$a_W = \frac{D_w}{(\delta x)_w}\left[\left[0, (1 - 0.1\,|P_w|)^5\right]\right] + \frac{D_w}{(\delta x)_w}\left[\left[0, P_w\right]\right], \tag{I.48b}$$

$$a_P = a_E + a_W + (u_e - u_w). \tag{I.48c}$$

A Generalized Formulation.

In this section we look for a generalized formulation for the discretization coefficients that could fit all the discretization schemes so far. Also, this generalized formulation will help us in extending the application of the formulation (derived so far for the one-dimensional, with no source or sink, configuration) to multi-dimensional problems.

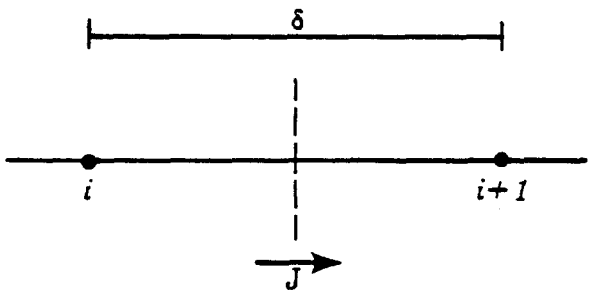

Figure I.5— Grid cluster of two generic neighbor nodes, showing the flux J at the control-volume interface.

Let us consider a simple cluster grid of two nodes represented in Fig.(I.5). The total flux at the interface between these control-volumes is given by Eq.(I.16) and repeated here as:

$$J = uC - D\frac{dC}{dx}.$$

Dividing the equation above by D/δ, where δ is the distance between two generic nodes, and noting that the Peclet number $P = \frac{u}{D/\delta}$, (see Eq.(I-14)), we will get:

$$J' = \frac{J}{(D/\delta)} = PC - \frac{dC}{d(x/\delta)}. \qquad (I.49)$$

Here I make the following observation:

1- The value of the concentration C at the interface between nodes i and $i+1$ will be some weighted average of C_i and C_{i+1};

2- The gradient of the concentration, $\frac{dC}{d(x/\delta)}$, at the interface will be proportional to the difference of the concentrations at the nodes C_i and C_{i+1}.

Therefore, based on these assumptions, we could rewrite Eq.(I.49) substituting the concentration C, and its gradient dC/dx, by the interpolation formulas such that:

$$J' = P\Big[\alpha C_i + (1-\alpha) C_{i+1}\Big] - \beta\Big[C_{i+1} - C_i\Big]. \qquad (I.50)$$

where α and β are functions of the Peclet number P, and represent our proposed relationship of the values of C and $\frac{dC}{dx}$, at the interface, in relation to the values of C at the nodes.

Eq.(I.50) above can also be written as:

$$J' = \Big(P\alpha + \beta\Big) C_i - \Big[P(\alpha - 1) + \beta\Big] C_{i+1}, \qquad (I.51a)$$

or,

$$J' = \mathcal{B}\, C_i - \mathcal{A}\, C_{i+1}, \qquad (I.51b)$$

where,

$$\mathcal{A} = P(\alpha - 1) + \beta, \qquad (I.52a)$$

$$\mathcal{B} = P\alpha + \beta. \qquad (I.52b)$$

The parameters $\mathcal{A}$ and $\mathcal{B}$ are dimensionless coefficients which depend on the value of the Peclet number P.

Now, let us derive some of the properties of these coefficients. From Eq.(I.52) we can get the first property as:

$$\mathcal{B} = \mathcal{A} + P. \qquad (I.53)$$

The second property is of symmetry, and can be obtained from Eq.(I.51b). If we reverse the coordinate axis, P becomes $-P$, and $\mathcal{A}$ and $\mathcal{B}$ will interchange their roles. Consequently we should have:

$$\mathcal{A}(-P) = \mathcal{B}(P), \qquad (I.54a)$$

$$\mathcal{B}(-P) = \mathcal{A}(P). \qquad (I.54b)$$

Also, we will derive the following two expressions relating the coefficients $\mathcal{A}$ and $\mathcal{B}$, with the total flux and the concentration at two neighbor nodes. These expressions will be useful later for the derivation of the discretization equation for the three-dimensional configuration, with source and sink terms.

Thus, combining Eq.(I.53) with Eq.(I.51b) we will get:

$$J' - PC_i = \mathcal{A}(C_i - C_{i+1}), \qquad (I.55a)$$

and,

$$J' - PC_{i+1} = \mathcal{B}(C_i - C_{i+1}). \qquad (I.55b)$$

Equations (I.53) and (I.54) allow us to express both $\mathcal{A}(P)$ and $\mathcal{B}(P)$ in terms of only $\mathcal{A}$ and P, in a compact form. In order to show this transformation, first consider the *negative* values of P.

So, for $P < 0$:

$$\mathcal{A}(P) = \mathcal{B}(P) - P, \qquad \text{from} \quad \text{Eq.(J.53)};$$

$$= \mathcal{A}(-P) - P, \qquad \text{from} \quad \text{Eq.(J.54a)}.$$

But, for $P < 0$, $\mathcal{A}(-P) = \mathcal{A}(|P|)$. Then we will have:

$$\mathcal{A}(P) = \mathcal{A}(|P|) - P. \tag{I.56}$$

Therefore, for all values of P, *positive* and *negative*, the expression above could be written in a condensed form such as:

$$\mathcal{A}(P) = \mathcal{A}(|P|) + \left[\left[-P, 0\right]\right]. \tag{I.57}$$

Similarly, for the coefficient $\mathcal{B}(P)$ we will have:

$$\begin{aligned} \mathcal{B}(P) &= \mathcal{A}(P) + P, \qquad \text{from} \quad \text{Eq.(I.53)}, \\ &= \mathcal{A}(|P|) + \left[\left[-P, 0\right]\right] + P, \quad \text{from} \quad \text{Eq.(I.57)}, \end{aligned}$$

or,

$$\mathcal{B}(P) = \mathcal{A}(|P|) + \left[\left[P, 0\right]\right]. \tag{I.58}$$

With Eqs. (I.57), (I.58) and (I.51b) we can get now a general expression for the total flux between two generic nodes. That is:

$$J' = \left[\mathcal{A}(|P|) + \left[\left[P, 0\right]\right]\right] C_i - \left[\mathcal{A}(|P|) + \left[\left[-P, 0\right]\right]\right] C_{i+1},$$

or,

$$J = \frac{D}{\delta}\left[\mathcal{A}(|P|) + \left[\left[P, 0\right]\right]\right] C_i - \frac{D}{\delta}\left[\mathcal{A}(|P|) + \left[\left[-P, 0\right]\right]\right] C_{i+1}. \tag{I.59}$$

Now, applying the expression above to the interfaces e and w, and considering Eq.(I.18), we will get the following general formulation for the discretization equation of the mass transport equation:

$$J_e = \frac{D_e}{(\delta x)_e}\left[\mathcal{A}(|P_e|) + \left[\left[P_e, 0\right]\right]\right] C_P - \frac{D_e}{(\delta x)_e}\left[\mathcal{A}(|P_e|) + \left[\left[-P_e, 0\right]\right]\right] C_E,$$

and,

$$J_w = \frac{D_w}{(\delta x)_w}\left[\mathcal{A}(|P_w|) + \left[\left[P_w, 0\right]\right]\right] C_W - \frac{D_w}{(\delta x)_w}\left[\mathcal{A}(|P_w|) + \left[\left[-P_w, 0\right]\right]\right] C_P.$$

But since $J_e - J_w = 0$, (see (Eq.I.18)), then we will have:

$$a_P C_P = a_E C_E + a_W C_W, \tag{I.60}$$

where,

$$a_E = \frac{D_e}{(\delta x)_e}\left[\mathcal{A}(|P_e|) + \left[\left[-P_e, 0\right]\right]\right], \tag{I.61a}$$

$$a_W = \frac{D_w}{(\delta x)_w}\left[\mathcal{A}(|P_w|) + \left[\left[P_w, 0\right]\right]\right], \tag{I.61b}$$

$$a_P = a_E + a_W + (u_e - u_w). \tag{I.61c}$$

Note That:

1)- Equations (I.60) and (I.61) represent the general discretization scheme for the convection diffusion equation;

2)- Each specific scheme will result in an specific interpolation function of the kind $\mathcal{A}\left(|P|\right)$;

3)- Expressions for $\mathcal{A}\left(|P|\right)$, related to the discretization schemes presented so far are shown in Table (I.1);

Table I.1 — Interpolation functions of the kind $\mathcal{A}(|P|)$, used in different discretization schemes.

Interpolation Scheme	Formula for $\mathcal{A}(\|P\|)$
Exponential (Exact)	$\frac{\|P\|}{[\exp(\|P\|)-1]}$
Central-Difference	$1 - 0.5\,\|P\|$
Upwind	1
Hybrid	$\left[\left[0, (1 - 0.5\|P\|)\right]\right]$
Power law	$\left[\left[0, (1 - 0.1\|P\|)^5\right]\right]$

Comparison of the Discretization Schemes.

Let us consider, as an example,[4] a one-dimensional grid cluster composed of the nodes W, P, and E, as represented in Fig.(I.1). In this grid, without loss of generality, the grid spacing $(\delta x)_e$ and $(\delta x)_w$ are supposed to be equal to 1. Also, the diffusion constant D is supposed to be constant. The boundary conditions are assumed to be: $C_W = 0$; and $C_E = 1$.

So, in order to compare the performance of the various interpolation schemes presented here, let us calculate the value of C_P, at the node P of the grid cluster described above, using these different discretization schemes. Thus, in Fig.(I.6) I have plotted the values of C_P, as a function of the Peclet number P.[5] As we can see, at $|P| = 0$, the predictions from all schemes converge to the exact solution. The results from the power law scheme are almost coincident with the exact solution, for the whole range of $|P|$. The results from the hybrid scheme also follow very close the exact solution, except for values of $|P|$ around 2. Predictions from the upwind scheme are expected to converge to the exact solution only for large values of $|P|$. The central-difference scheme was the only one to predict unreasonable results. For $|P| > 2$, its predictions were outside of the range imposed by

[4] This example was presented originally by Patankar, [Pa80].

[5] The notation here for the Peclet number P, should not be confused with the subscript P, in C_P, which represents the concentration at the node P.

Figure I.6— Comparison of the predictions of various discretization schemes.

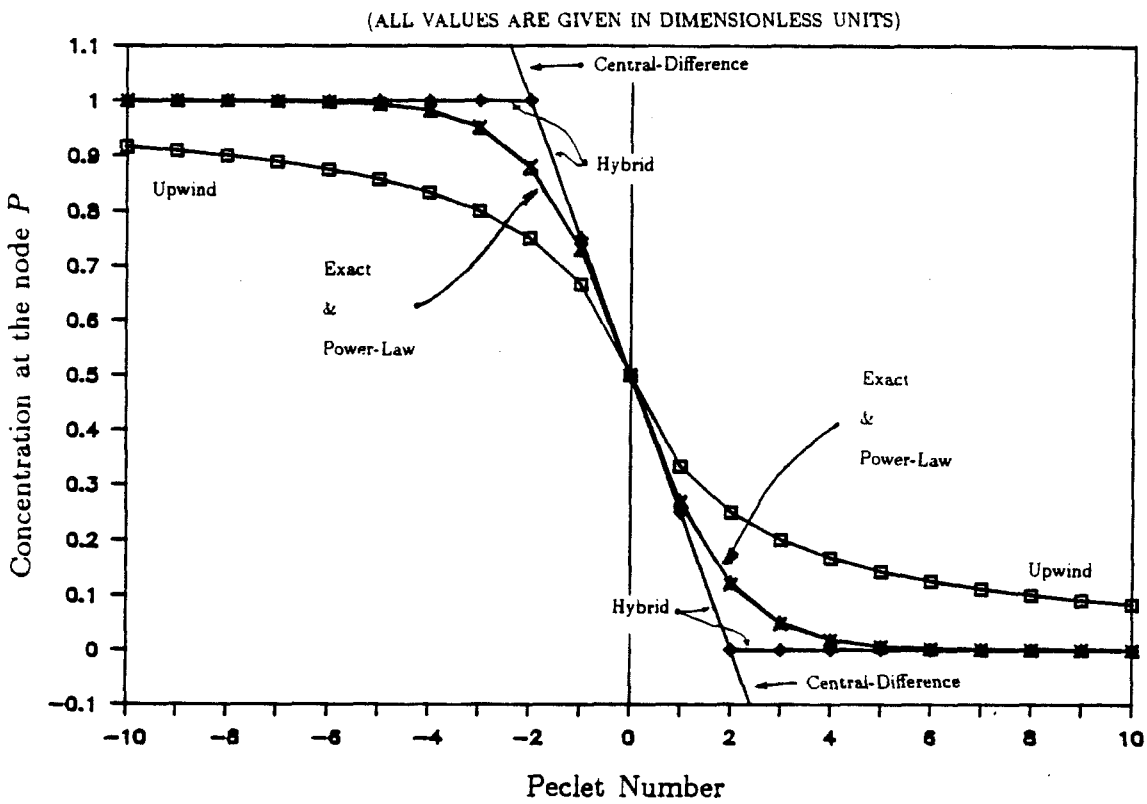

the boundary conditions. However it should be remembered that the central-difference interpolation scheme is strongly dependent on the grid size and, consequently, a reduction of the grid spacing in the example above would have resulted in better predictions from the central-difference scheme.

Therefore, based on the results of this example, we can conclude that the power law discretization scheme is the one that produces the closest approximation to the exact solution, for the whole range of Peclet numbers.

Discretization Equation for Three-Dimensional Configuration.

With the principles and the formulation presented for the one-dimensional case in the first section of this appendix, we can now start writing the discretization equation for the

Figure I.7— Two-dimensional representation of a control-volume, showing the flux defined at the interfaces.

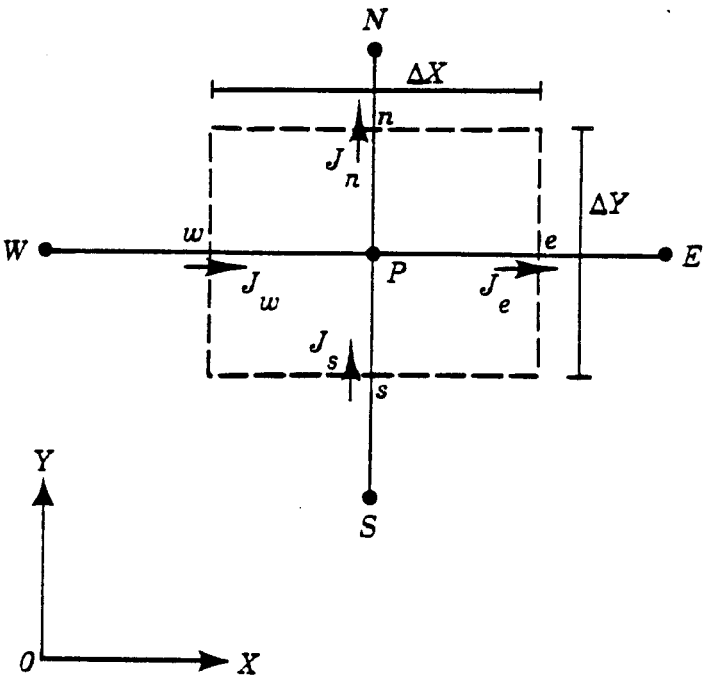

general mass-transport differential equation – Eq.(I.1). Consider then the control-volume represented in Fig.(I.7). (In order to simplify the visualization of the figure, it is represented with only two dimensions).

Note that:

1- The interface b (at the bottom), and t (at the top), are not represented in Fig.(I.7);

2- The practice developed for calculating J_e and J_w in the one-dimensional configuration will be also used here to calculate J_e, J_w,J_n, J_s, J_b and J_t;

3- We assume that the total flux J_i, at a generic interface i, prevails over the entire control-volume face i. For example, the total flux J_e prevails over the entire C.V. face of area $\Delta y \Delta z$.

The general mass balance equation, Eq.(I.1), can be written in terms of the total flux, such that:

$$\frac{\partial J_x}{\partial x} + \frac{\partial J_y}{\partial y} + \frac{\partial J_z}{\partial z} = \epsilon(S - C), \tag{I.62}$$

where,

$$J_x = uC - D\frac{\partial C}{\partial x}, \tag{I.63a}$$

$$J_y = vC - D\frac{\partial C}{\partial y}, \tag{I.63b}$$

$$J_z = wC - D\frac{\partial C}{\partial z}. \tag{I.63c}$$

Integrating Eq.(I.62) over the whole control-volume shown in Fig.(I.7), yields:

$$\int_t^b \int_s^n \int_w^e \frac{\partial J_x}{\partial x} dxdydz + \int_t^b \int_w^e \int_s^n \frac{\partial J_y}{\partial y} dydxdz + \int_s^n \int_w^e \int_t^b \frac{\partial J_z}{\partial z} dzdxdy =$$
$$= \int_t^b \int_s^n \int_w^e \epsilon(S - C) dxdydz,$$

or,

$$\int_t^b \int_s^n (J_{x_e} - J_{x_w})\, dydz + \int_t^b \int_w^e (J_{y_n} - J_{y_s})\, dxdz + \int_s^n \int_w^e (J_{z_b} - J_{z_t})\, dxdy =$$
$$= \int_t^b \int_s^n \int_w^e \epsilon(S - C) dxdydz.$$

Now, assuming that:

1- The values of ϵ, S, and C at the node P, prevail over the entire control-volume;

2- The value of the total flux J, at any interface, prevails over the entire area of that interface;

The equation above then becomes:

$$\left(J_{x_e} - J_{x_w}\right)\Delta y\Delta z + \left(J_{y_n} - J_{y_s}\right)\Delta x\Delta z + \left(J_{z_b} - J_{z_t}\right)\Delta x\Delta y = \epsilon\left(S_P - C_P\right)\Delta x\Delta y\Delta z,$$

or,

$$\left(J_e - J_w\right) + \left(J_n - J_s\right) + \left(J_b - J_t\right) = \epsilon\left(S_P - C_P\right)\Delta x\Delta y\Delta z. \qquad (I.64)$$

where the quantities J_e, J_w, J_n, J_s, J_b and J_t are the integrated total fluxes over the control volume faces, and represent the total mass flow rate through those interfaces. That is:

$$J_e = \left(J_{x_e}\right)\Delta y\Delta z, \qquad (I.65a)$$

$$J_w = \left(J_{x_w}\right)\Delta y\Delta z, \qquad (I.65b)$$

$$J_n = \left(J_{y_n}\right)\Delta x\Delta z, \qquad (I.65c)$$

$$J_s = \left(J_{y_s}\right)\Delta x\Delta z, \qquad (I.65d)$$

$$J_b = \left(J_{z_b}\right)\Delta x\Delta y, \qquad (I.65e)$$

$$J_t = \left(J_{z_t}\right)\Delta x\Delta y. \qquad (I.65f)$$

Similarly, integrating the continuity equation, Eq.(I.4), over the whole control-volume, yields:

$$\int_t^b\int_s^n\int_w^e \frac{\partial u}{\partial x}dxdydz + \int_t^b\int_w^e\int_s^n \frac{\partial v}{\partial y}dxdydz + \int_s^n\int_w^e\int_t^b \frac{\partial w}{\partial z}dxdydz = 0.$$

Also, assuming that the velocity component at any interface prevails over the whole area of that interface, the equation above becomes:

$$\Big(u_e - u_w\Big)\Delta y\Delta z + \Big(v_n - v_s\Big)\Delta x\Delta z + \Big(w_b - w_t\Big)\Delta x\Delta y = 0,$$

or,

$$\big(F_e - F_w\big) + \big(F_n - F_s\big) + \big(F_b - F_t\big) = 0, \tag{I.66}$$

where the quantities F_e, F_w, F_n, F_s, F_b, and F_t are the total volume flow rates defined at the control-volume interfaces, such as:

$$F_e = u_e\Delta y\Delta z, \tag{I.67a}$$

$$F_w = u_w\Delta y\Delta z, \tag{I.67b}$$

$$F_n = v_n\Delta x\Delta z, \tag{I.67c}$$

$$F_s = v_s\Delta x\Delta z, \tag{I.67d}$$

$$F_b = w_b\Delta x\Delta y, \tag{I.67e}$$

$$F_t = w_t\Delta x\Delta y. \tag{I.67f}$$

Multiplying Eq.(I.65) above by C_P, and subtracting it from Eq.(I.64) we will get:

$$\begin{aligned}
&\big(J_e - F_eC_P\big) - \big(J_w - F_wC_P\big) + \\
&\big(J_n - F_nC_P\big) - \big(J_s - F_sC_P\big) + \\
&\big(J_b - F_bC_P\big) - \big(J_t - F_tC_P\big) = \\
&= \epsilon\big(S_P - C_P\big)\Delta x\Delta y\Delta z
\end{aligned} \tag{I.68}$$

Note that:

1- Our assumption of uniformity over the control-volume interfaces allows us to employ the one-dimensional practices for the three-dimensional situation;

2- For the one-dimensional configuration we have already developed an expression to represent the terms like $(J_e - F_e C_P)$ which are found in the equation above.(See Eq.(I.45)).

Before we proceed, we define the variable conductance in the three dimensional configuration as:

$$G_e = \frac{D_e}{(\delta x)_e} \Delta y \Delta z, \qquad (I.69a)$$

$$G_w = \frac{D_w}{(\delta x)_w} \Delta y \Delta z, \qquad (I.69b)$$

$$G_n = \frac{D_n}{(\delta y)_n} \Delta x \Delta z, \qquad (I.69c)$$

$$G_s = \frac{D_s}{(\delta y)_s} \Delta x \Delta z, \qquad (I.69d)$$

$$G_b = \frac{D_b}{(\delta z)_b} \Delta x \Delta y, \qquad (I.69e)$$

$$G_t = \frac{D_t}{(\delta z)_t} \Delta x \Delta y. \qquad (I.69f)$$

Consequently, the *grid Peclet number* at a generic interface i is then defined as:

$$P_i = \frac{F_i}{G_i}. \qquad (I.70)$$

Now we will use Eq.(I.55a) to represent the terms $(J_e - F_e C_P)$, $(J_w - F_w C_P)$, etc. in the three-dimensional configuration, with source and sink terms. Taking the interface e as an example, we multiply Eq.(I.55a) by G_e which will give:

$$G_e\left(J'_e - P_e C_P\right) = G_e \mathcal{A}_e \left(C_P - C_E\right). \qquad (I.71)$$

But, from Eq.(I.49) we know that:

$$J'_e = \frac{J_e}{G_e} \longrightarrow J_e = J'_e G_e.$$

Also we know from Eq.(I.70) that:

$$G_e P_e = F_e.$$

Now, from Eq.(I.57) we can get:

$$G_e \mathcal{A}_e = G_e\left[\mathcal{A}(P_e)\right] = G_e\Big[\mathcal{A}\left(|P_e|\right) + [\![-P_e, 0]\!]\Big],$$

which can also be transformed using Eq.(I.61a) such that:

$$G_e \mathcal{A}_e = \frac{D_e}{(\delta x)_e} \Delta y \Delta z \Big[\mathcal{A}\left(|P_e|\right) + [\![-P_e, 0]\!]\Big] = a_E.$$

Thus, substituting the expressions above into Eq.(I.71) we finally get:

$$J_e - F_e C_P = a_E (C_P - C_E). \qquad (I.72)$$

Similarly for the interface w, we apply Eq.(I.55b) to that interface, and then multiply the result by G_w to get:

$$G_w\left(J'_w - P_w C_P\right) = G_w \mathcal{B}_w \left(C_W - C_P\right). \qquad (I.73)$$

But, from Eq.(I.49) we know that:

$$G_w J'_w = J_w.$$

Also we know from Eq.(I.70) that:

$$G_w P_w = F_w.$$

Now, from Eq.(I.58) we can get:

$$G_w \mathcal{B}_w = G_w\big[\mathcal{B}(P_w)\big] = G_w\Big[\mathcal{A}\big(|P_w|\big) + [\![P_w, 0]\!]\Big],$$

which can also be transformed using Eq.(I.61b) such that:

$$G_w \mathcal{B}_w = \frac{D_w}{(\delta x)_w}\Delta y \Delta z\Big[\mathcal{A}\big(|P_w|\big) + [\![P_w, 0]\!]\Big] = a_W.$$

Thus, substituting the expressions above into Eq.(I.73) we finally get:

$$J_w - F_w C_P = a_W(C_W - C_P). \qquad (I.74)$$

The discretization expressions for the terms $(J - FC)$ at the interfaces n, s, b, and t are obtained similarly to the Eqs. (I.72) and (I.74), for the interfaces e and w respectively. Therefore we have:

$$J_n - F_n C_P = a_N(C_P - C_N), \qquad (I.75a)$$

$$J_s - F_s C_P = a_S(C_S - C_P), \qquad (I.75b)$$

$$J_b - F_b C_P = a_B(C_P - C_B), \qquad (I.75c)$$

$$J_t - F_t C_P = a_T(C_T - C_P). \qquad (I.75d)$$

Finally, substituting Eqs.(I.72), (I.74), and (I.75) into Eq.(I.68) we obtain the following discretization equation:

$$a_P C_P = a_E C_E + a_W C_W + a_N C_N + a_S C_S + a_B C_B + a_T C_T + b, \qquad (I.76)$$

where,

$$a_E = G_e \mathcal{A}\left(|P_e|\right) + \left[\left[-F_e, 0\right]\right], \qquad (I.77a)$$

$$a_W = G_w \mathcal{A}\left(|P_w|\right) + \left[\left[F_w, 0\right]\right], \qquad (I.77b)$$

$$a_N = G_n \mathcal{A}\left(|P_n|\right) + \left[\left[-F_n, 0\right]\right], \qquad (I.77c)$$

$$a_S = G_s \mathcal{A}\left(|P_s|\right) + \left[\left[F_s, 0\right]\right], \qquad (I.77d)$$

$$a_B = G_b \mathcal{A}\left(|P_b|\right) + \left[\left[-F_b, 0\right]\right], \qquad (I.77e)$$

$$a_T = G_t \mathcal{A}\left(|P_t|\right) + \left[\left[F_t, 0\right]\right]. \qquad (I.77f)$$

and,

$$a_P = a_E + a_W + a_N + a_S + a_B + a_T + \epsilon_P \Delta x \Delta y \Delta z, \qquad (I.77g)$$

$$b = \left(\epsilon S \Delta x \Delta y \Delta z\right)_P , \qquad (I.77h)$$

where the flow rates F, and the conductances G are defined as:

$$F_e = u_e \left(\Delta y \Delta z\right)_P \quad ; \quad G_e = \frac{D_e}{\left(\delta x\right)_e} \left(\Delta y \Delta z\right)_P , \qquad (I.78a)$$

$$F_w = u_w \left(\Delta y \Delta z\right)_P \quad ; \quad G_w = \frac{D_w}{\left(\delta x\right)_w} \left(\Delta y \Delta z\right)_P , \qquad (I.78b)$$

$$F_n = v_n(\Delta x \Delta z)_P \quad ; \quad G_n = \frac{D_n}{(\delta y)_n}(\Delta x \Delta z)_P\,, \tag{I.78c}$$

$$F_s = v_s(\Delta x \Delta z)_P \quad ; \quad G_s = \frac{D_s}{(\delta y)_s}(\Delta x \Delta z)_P\,, \tag{I.78d}$$

$$F_b = w_b(\Delta x \Delta y)_P \quad ; \quad G_b = \frac{D_b}{(\delta z)_b}(\Delta x \Delta y)_P\,, \tag{I.78e}$$

$$F_t = w_t(\Delta x \Delta y)_P \quad ; \quad G_t = \frac{D_t}{(\delta z)_t}(\Delta x \Delta y)_P\,, \tag{I.78f}$$

and the Peclet numbers P are defined at each interface as the ratio of F and G such that:

$$P_e = \frac{F_e}{G_e}, \tag{I.79a}$$

$$P_w = \frac{F_w}{G_w}, \tag{I.79b}$$

$$P_n = \frac{F_n}{G_n}, \tag{I.79c}$$

$$P_s = \frac{F_s}{G_s}, \tag{I.79d}$$

$$P_b = \frac{F_b}{G_b}, \tag{I.79e}$$

$$P_t = \frac{F_t}{G_t}. \tag{I.79f}$$

The function $\mathcal{A}(|\ P\ |)$ depends on the discretization scheme adopted, and can be selected from Table (I.1). The *power-law scheme* is the recommended one (see Patankar, [Pa80], pg.100), for which:

$$\mathcal{A}(|P|) = \left[\left[0, (1 - 0.1\,|P|)^5\right]\right]. \tag{I.80}$$

APPENDIX J

CALCULATION OF INDOOR RADON CONCENTRATION.

Radon Entry Rate into the House.

The dimensionless flux of radon leaving the crack and entering the house, *from each control-volume*, can be evaluated from Eq.(F.42) of Appendix F, and expressed as:

$$(J^{*}_{exit})_i = \left(C^{*}_{interface}\right)_i \left[\frac{(P_e - r_1 D^{*}_o)(D'^{*}_o r_4 - D^{*}_o r_2) - (P_e - r_2 D^{*}_o)(D'^{*}_o r_4 - D^{*}_o r_1)}{(D'^{*}_o r_4 - D^{*}_o r_2)e^{r_1 l^{*}} - (D'^{*}_o r_4 - D^{*}_o r_1)e^{r_2 l^{*}}}\right]_i, \qquad (J.1)$$

where, $\left(C^{*}_{interface}\right)_i$ is the radon concentration at the soil-crack interface of each control-volume i.

Now, the dimensionless radon entry rate, $(R^{*})_i$, *from each control-volume* i, can be obtained from Eq.(3.47), and expressed as the product of the radon flux into the house to the area of the control-volume face. That is:

$$(R^{*})_i = (J^{*}_{exit} A^{*}_{crack})_i, \qquad (J.2)$$

where,

$(R^{*})_i$ = Dimensionless radon entry rate, from a control-volume i;

$(A^{*}_{crack})_i$ = Dimensionless cross-sectional area of a control-volume i.

But we have that $(A^*_{crack})_i = (\Delta x^* \Delta y^*)_i$, where Δx^* and Δy^* are the dimensionless size of a control volume i in the x and y directions, respectively. Consequently, the radon entry rate per control volume surface is given by:

$$(R^*)_i = (J^*_{exit} \Delta x^* \Delta y^*)_i . \tag{J.3}$$

Note that the equation above gives the dimensionless value of the radon entry rate. In order to find the actual value we notice that:

$$A^* = \frac{A}{A_{ch}} = \frac{\Delta x}{L_{ch}} \frac{\Delta x}{L_{ch}} = \frac{\Delta x \Delta y}{L^2_{ch}}, \tag{J.4}$$

and,

$$J^* = \frac{J}{S_{ch} L_{ch}}, \tag{J.5}$$

or,

$$J^*_{exit} = \frac{J_{exit}}{S_{ch} L_{ch}}. \tag{J.6}$$

Thus, putting together, these expressions yield:

$$R^* = J^*_{exit} A^*_{crack} = \frac{J_{exit} A_{crack}}{S_{ch} L_{ch} (L_{ch})^2} = \frac{J_{exit} A_{crack}}{S_{ch} L^3_{ch}} = \frac{R}{R_{ch}}, \tag{J.7}$$

where,

$$R_{ch} = S_{ch} L^3_{ch}. \tag{J.8}$$

Therefore, in order to find R we have to multiply its dimensionless form R^* by its characteristic value $S_{ch} L^3_{ch}$, and Eq.(J.3) then becomes:

$$(R)_i = (S_{ch} L^3_{ch}) \, (J^*_{exit} \Delta x^* \Delta y^*)_i . \tag{J.9}$$

The equation above gives the actual value of the radon entry rate from each control volume. In order to find the total radon entry rate, we have to sum the contribution from each control volume along the crack line. That means:

$$R_{total} = \sum_{i=1}^{n} (R)_i, \qquad (J.10)$$

where, i is the order number of a generic control-volume; and n is the total number of control-volumes along the crack line.

Indoor Radon Concentration.

According to Eq.(3.27), the indoor radon concentration is given by:

$$C_{indoor} = \frac{4R_{total}}{V(\lambda + \lambda_V)} + \left(\frac{\lambda}{\lambda + \lambda_V}\right) C_{outdoor}, \qquad (J.11)$$

where,

C_{indoor} = Indoor radon concentration, in $[Ci/m^3]$;

$C_{outdoor}$ = Outdoor radon concentration, in $[Ci/m^3]$;

R_{total} = Total radon entry rate into a quarter of the house volume , in $[Ci/s]$;

V = Total internal volume of the house, in $[m3]$;

λ_{Rn} = Radon decay constant, in $[s^{-1}]$;

λ_V = Indoor air exchange rate (ventilation rate), in $[s^{-1}]$.

In the numerical calculations of the computer model, the outdoor radon concentration - $C_{outdoor}$ - is neglected, and the indoor radon concentration is then expressed as:

$$C_{indoor} = \frac{4R_{total}}{V(\lambda + \lambda_V)}. \qquad (J.12)$$

APPENDIX K

CALCULATION OF THE RADON FLUX TO THE ATMOSPHERE.

The total flux of radon from the soil to the atmosphere, through the soil/air interface can be evaluated by assuming a control volume of zero thickness at the soil/air interface within which the radon concentration is assumed to be $C_{top} = zero$.

Consider the control-volumes defined in the soil near the top of the block (soil-air interface), and represented in Figure (K.1).

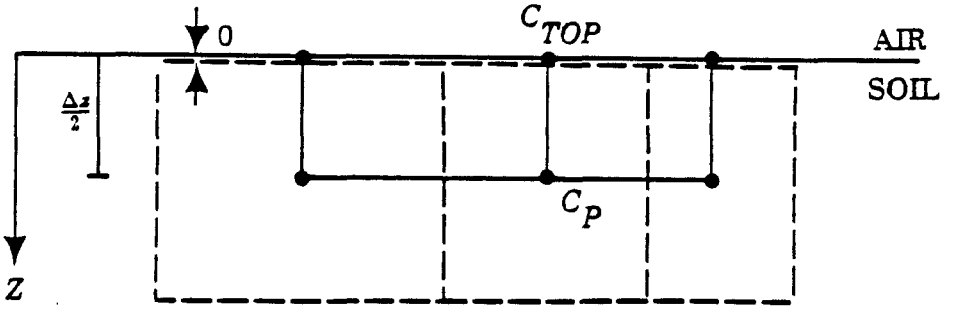

Figure K.1— Cluster of Control-Volumes at the Soil Surface

At any point inside the soil block, and consequently inside the control volume above, the total radon flux in the vertical (z-axis) direction, is given by:

$$J(z) = \omega C(z) - D\frac{dC(z)}{dz}. \qquad (K.1)$$

For a point located inside the control volume, but as close as possible to the interface, the equation above becomes:

$$J_{top} = (\omega)_{top}\, C_{top} - D_{top} \left(\frac{dC}{dz} \right)_{top}, \qquad (K.2)$$

and, since $C_{top} = 0$, the equation above can be written as:

$$J_{top} = -D_{top} \left(\frac{dC}{dz} \right)_{top}. \qquad (K.3)$$

Note that:

1- Equation above gives the flux through a surface of geometric area inside the soil block, but very close to the air/soil interface;

2- The bulk diffusivity coefficient D_{top} should be the one defined inside the block;

3- We assume a linear profile for the radon concentration near that interface. Note however that it is important to make Δz sufficiently small at this first layer of control volumes, in order to assure that this is a reasonable assumption.

Therefore, with the assumption above, the flux in the soil near the soil/air interface could be approximated by:

$$J_{top} = -D \left(\frac{C_P - C_{top}}{\Delta z/2} \right),$$

or,

$$J_{top} = -\frac{2DC_P}{\Delta z}, \qquad (K.4)$$

which in dimensionless form becomes:

$$J^*_{top} = \frac{J_{top}}{S_{ch} L_{ch}} = -\frac{2D^* C^*_P}{\Delta z^*}. \qquad (K.5)$$

Note that:

1- Equation above gives the dimensionless radon flux per unit of geometric cross-sectional area in a surface inside the soil but very close to the soil/air interface;

2- Therefore, the radon flux to the atmosphere is given by:

$$J^*_{atm} = J^*_{top} = -\frac{2D^* C^*_P}{\Delta z^*}. \qquad (K.6)$$

3- In its actual value, the flux to the atmosphere is then expressed as :

$$J_{atm} = (S_{ch} L_{ch}) J^*_{atm} = -(S_{ch} L_{ch}) \left(\frac{2D^* C^*_P}{\Delta z^*} \right), \qquad (K.7)$$

in units of $\left[\frac{Ci}{m^2 \cdot s}\right]$.

APPENDIX L

LISTING OF THE COMPUTER CODE.

The listing of the computer programs PRESSU and MASTRA, with their subroutines, was presented only in the original version of this dissertation, which is available at the Graduate Library of The University of Michigan, in Ann Arbor.

APPENDIX M

LIST OF VARIABLES AND SYMBOLS.

$a =$ Represents the coefficients in the discretization equations of either the pressure field or the mass balance, (a_P, a_E, etc., represent the coefficients for the nodes P, E, etc.);

$A =$ Average cross sectional area per unit of length of the crack line, in $[m^2/m]$;

$A_{crack} =$ Average cross sectional area of the crack in a quarter of the house, in $[m^2]$;

$C_{IN} =$ Concentration of radon at the interface between the crack and the soil, in $[Ci/m^3]$;

$C_{indoor} =$ Indoor radon concentration, in $[Ci/m^3]$;

$C_{outdoor} =$ Outdoor radon concentration, in $[Ci/m^3]$;

$C_{exit} =$ Concentration of radon at the exit of the crack into the basement, in $[Ci/m^3]$;

$D =$ Bulk diffusivity coefficient for Rn-222 in the soil matrix, in $[m^2/s]$;

$D_{ch} =$ Characteristic bulk diffusivity coefficient for Rn-222 in the soil matrix, in $[m^2/s]$;

$D_o =$ Diffusion coefficient of Rn-222 in open air, in $[m^2/s]$;

$D'_o =$ Enhanced radon diffusion coefficient - diffusion coefficient of Rn-222 in a well mixed air, defined in Appendix F - in $[m^2/s]$;

$f =$ Radon emanating fraction from the soil grains into the soil pore space, $[dimensionless]$;

$\vec{g} =$ Gravity accelerator vector, in $[m/s^2]$;

$h =$ Height of the house, in $[m]$;

$\vec{J}_c =$ Convective component of the bulk flux of Rn-222 in the soil matrix, in $[Ci/m^2 s]$;

$\vec{J}_d =$ Diffusive component of the bulk flux of Rn-222 in the soil matrix, in $[Ci/m^2 s]$;

$\vec{J} =$ Total bulk flux of Rn-222, per unit of geometric area in the soil matrix, in $[Ci/m^2 s]$;

$\vec{J}_{eff} =$ Total effective flux of Rn-222, per unit of geometric area in the soil matrix – defined in Appendix D – in $[Ci/m^2 s]$;

$J_{IN} =$ Flux of Rn-222 at the interface between the crack and the soil, in $[Ci/m^2 s]$;

$J_{exit} =$ Flux of Rn-222 at the exit of the crack, entering the house space, in $[Ci/m^2 s]$;

$k =$ Soil permeability, in $[m^2]$;

$k_{ch} =$ Characteristic soil permeability, in $[m^2]$;

$K_C =$ A constant representing the dimensionless group used in the dimensionless form of the equation for the gas velocity inside the crack – defined in Appendix E;

$K_{crack} =$ A constant dependent on the geometry of the crack and on the dynamic viscosity of the soil gas – defined in Appendix E – in $[m^3/Ns]$;

$K_S =$ A constant representing the dimensionless group used in the dimensionless form of Darcy's expression – defined in Chapter III;

$l_{crack} =$ Depth of the crack. Equal to the thickness of the basement floor, in $[m]$;

$L_{ch} =$ Characteristic length, in $[m]$;

$L_x, L_y, L_z =$ Dimensions of one quarter of the soil block, in $[m]$;

$l_x, l_y, l_z =$ Dimensions of one quarter of the basement, in $[m]$;

$M =$ A dimensionless factor used in the calculation of the radon flux at the soil-crack interface – defined in Appendix F;

$P =$ Absolute pressure at a point (x, y, z) in the soil matrix, in $[N/m^2]$;

$p =$ Disturbance pressure component at a point (x, y, z) in the soil matrix, in $[N/m^2]$;

$P_{atm} =$ Atmospheric pressure, in $[N/m^2]$;

$\Delta P =$ Differential pressure disturbance applied to the absolute pressure at the basement floor, in $[N/m^2]$;

$p_{IN} =$ Disturbance pressure in the soil at the entrance of the crack, in $[N/m^2]$;

$P_{bas} =$ Absolute pressure at the basement floor, in $[N/m^2]$;

$P_{IN} =$ Absolute pressure at the entrance of the crack in the soil, in $[N/m^2]$;

$P_e =$ Peclet number, $[dimensionless]$;

$Q_{crack} =$ Average flow of soil gas into the house through the crack line, per unit length of the crack line, in $[m^3/ms]$;

$\vec{q} =$ Seepage velocity vector of the soil gas at the point (x, y, z), in $[m/s]$;

$[Ra] =$ Concentration of Ra-226 in the soil grains, in $[Ci/Kg]$;

$R_{total} =$ Total radon entry rate into a quarter of the house, in $[Ci/s]$;

$S =$ Production rate of Rn-222 into the soil pore space, in $[Ci/m^3s]$;

$S_{ch} =$ Characteristic production rate of Rn-222 into the soil pore space, in $[Ci/m^3s]$;

$t_{crack} =$ Width of the crack opening, in $[m]$;

$u, v, w =$ Components of the seepage velocity vector $\vec{q}$ in the x, y, z directions respectively, in $[m/s]$;

$U_{ch} =$ Characteristic velocity of the soil gas, in $[m/s]$;

$V =$ Total internal volume of the house, in $[m^3]$;

$x, y, z =$ Cartesian coordinates, in $[m]$;

$w_{crack} =$ Average velocity of the flow of soil gas through the crack, in $[m/s]$;

$w_{IN} =$ Average velocity of the soil gas through the soil-crack interface, in $[m/s]$;

Greek Letters.

$\epsilon =$ Soil porosity, $[dimensionless]$;

$\theta =$ Ratio of radon activity to the mass of soil gas, (a relative mass concentration between radon and soil gas), in $[Ci/Kg]$;

$\lambda_{Rn} =$ Radon-222 decay constant, in $[s^{-1}]$;

$\lambda_V =$ Air exchange rate (or ventilation rate), in $[s^{-1}]$;

$\mu =$ Soil gas dynamic viscosity, in $[Ns/m^2]$;

$\rho =$ Soil gas density, in $[Kg/m^3]$;

$\rho_s =$ Density of the soil particles (grains), in $[Kg/m^3]$;

Special Symbols.

$\vec{\nabla} =$ Gradient operator, in $[m^{-1}]$;

$\vec{\nabla}\cdot =$ Divergence operator, in $[m^{-1}]$;

$[\![\ ]\!] =$ This symbol denotes the largest quantity inside it.

BIBLIOGRAPHY

BIBLIOGRAPHY

[Ak84] Åkerblom, G., P. Andersson, B. Clavensjö, *Soil Gas Radon - A Source for Indoor Radon Daughters*, Radiation Protection Dosimetry, Vol. 7, No. 1-4, pp. 49-55, 1984.

[An84] Anderson, D.A., J.C. Tannerhi, and R.H. Pletcher, *Computational Fluid Mechanics and Heat Flow*, McGraw-Hill Book Company, New York, 1984.

[Ba80] Bates, R.C., and J.C. Edwards, *Mathematical Modeling of Time Depending Radon Flux Problems*, in Proceedings of the International Mine Ventilation Congress, New York, Society of Mining Engineers of American Institute of Mining, Metallurgical, and Petroleum Engineers, Inc., pp.412-419, V. 1980.

[Ba81] Bates, R.C., and J.C. Edwards, *The Effectiveness of Overpressure Ventilation: A Mathematical Study*, In Radiation Hazard in Mining: Control, Measurement, and Medical Aspects, Gomes, M. (Ed.), Society of Mining Engineers, New York, NY, pp.149-154, 1981.

[Be79] Bear, J., *Hydraulics of Groundwater*, McGraw-Hill Book Company, New York, 1979.

[Be85] Beier, K.P., *VIEWX-ISOX : Version 3.2 - A Preliminary Documentation*, Department of Naval Architecture and Marine Engineering, College of Engineering, The University of Michigan, Ann Arbor, December 1985.

[Br83] Bruno, R.C., *Sources of Indoor Radon in Houses*, J. Air Pollution Control Association, Vol. 33, pp. 105-109, 1983.

[Bu83] Burkart, W., *Assessment of Radiation Dose and Effects from Radon and its Progeny in Energy-Efficient Homes*, Nuclear Technology, Vol.60, pp. 114-123, January 1983.

[Ca59] Carslaw, H.S., and J.C.Jaeger, *Conduction of Heat in Solids*, Second Edition, Claredon Press-Oxford, 1959, (Reprinted in 1986).

[Cl74a] Clements, W.E., *The Effect of Atmospheric Pressure Variation on the Transport of Rn-222 from the Soil to the Atmosphere*, Ph.D. Dissertation, New Mexico Institute of Mining and Technology, Socorro, NM, February 1974.

[Cl74b] Clements, W.E., and M.H.Wilkening, *Atmospheric Pressure Effects on Rn-222 Transport Across the Earth-Air Interface*, Journal of Geophysical Research, Vol.79, No.33, pp.5025-5029, November 1974.

[Co81] Collé, R., R.J.Rubin, L.T.Knab, and J.M.R. Hutchinson, *Radon Transport Through and Exhalation from Building Materials: A Review and Assessment*, U.S. Department of Commerce, National Bureau of Standards, NBS Technical Note 1139, September 1981.

[Cr75] Crank, J., *The Mathematics of Diffusion*, Second Edition, Claredon Press-Oxford, 1974, (Reprinted in 1985).

[Cu76] Culot, M.V.J., H.G. Olson, and K.J. Schiager, *Effective Diffusion Coefficient of Radon in Concrete, Theory and Method for Field Measurements*, Health Physics, Vol.30, pp. 263-270, March 1976.

[De69] DeWiest, R.J.M., *Flow Through Porous Media*, Academic Press, New York, 1969.

[Do86] D'Ottavio, T.W., and R.N. Dietz, *Radon Trnasport into a Detached One-Story House with a Basement*, Atmospheric Environment, Vol.20, No.5, pp.1065-1069, 1986.

[DS83] DSMA Atcon Ltd., *Review of Existing Instrumentation and Evaluation of Possibilities for Research and Development of Instrumentation to Determine Future Levels od Radon at a Proposed Building Site*, Research Report Info-0096, prepared for the Atomic Energy Control Board, Ottawa, Canada, January 1983.

[DS85] DSMA Atcon Ltd., *A Computer Study of Soil Gas Movement into Basements*, DSMA Atcon Ltd. Report 1389/1333, Department of Health and Welfare, Ottawa, Ontarion Canada, March 1985.

[Ea84] Eaton, R.S., and A.G.Scott, *Understanding Radon Transport into Houses*, Radiation Protection Dosimetry, 7: 251-253, 1984.

[Ed80] Edwards J.C., and R.C. Bates, *Theorectical Evaluation of Radon Emanation Under a Variety of Conditions*, Health Physics, Vol.39, pp.263-274, August 1980.

[Ev69] Evans, R.D., *Engineers' Guide to the Elementary Behavior of Radon Daughters*, Health Physics, Vol.17, pp.229-252, 1969.

[Fa82] Farlow, S.J., *Partial Differential Equations for Scientists and Engineers*, John Wiley and Sons, 1982.

[Fa83] Fahien, R.W., *Fundamentals of Transport Phenomena*, McGraw-Hill Book Company, New York, 1983.

[Ha83a] Hassanizadeh M., and W.G. Gray, *General Conservation Equations for Multi-Phase Systems: 1. Averaging Procedure*, in: Flow Through Porous Medium, George F. Pinder (Ed.), Progress in Engineering Sciences, CLM Publications Ltd., Ashurst Lodge, Ashurst, Southampton, Great Britain, pp.1-14, 1983.

[Ha83b] Hassanizadeh M., and W.G. Gray, *General Conservation Equations for Multi-Phase Systems: 3. Constitutive Theory for Porous Media Flow*, in: Flow Through Porous Medium, George F. Pinder (Ed.), Progress in Engineering Sciences, CLM Publications Ltd., Ashurst Lodge, Ashurst, Southampton, Great Britain, pp.30-45, 1983.

[Ha86] Hart, K.P., D.M. Levins, and A.G. Fane, *Steady-State Radon (Rn-222) Diffusion Through Tailings and Multiple Layers of Covering Materials*, Health Physics, Vol.50, No.3, pp. 369-379, March 1986.

[He84] Hernandes, T.L., J.W. Ring, and H.M. Schs, *The Variation of Basement Radon Concentration with Barometric Pressure*, Health Physics, Vol.46, No.2, pp.440-445, February 1984.

[Hu83] Hurwitz, H.Jr., *The Indoor Radiological Problem in Perspective*, Risk Analysis, Vol.3, No.1. pp. 63-77, 1983.

[IC81] ICRP, *Limits for Inhalation of Radon Daughters by Workers*, ICRP Publication 32, International Commission on Radiological Protection, Pergamon Press, New York, March 1981.

[Ir81] Iribarne, J.V, and W.L. Godson, *Atmospheric Thermodynamic*, D. Reidel Publishing Company, Holland, Second Edition, 1981.

[Je81] Jergling, A., *Air Leakage Through Cracks in Concrete Elements*, 2nd. AIC Conference Proceedings, Air Infiltration Centre, Old Bracknell Lane West, Bracknell, Berkshire, Great Britain, RG12 4AH, 1981.

[Jo75] Jonassen, N., *On the Effect of Atmospheric Pressure Variations on the Radon-222 Concentration in Unventilated Rooms*, Health Physics , Vol.29, pp.216-220, July 1975.

[Ko81] Kocher, D.C., *Radioactive Decay Data Tables*, Technical Information Center, U.S. Department of Energy, DOE/TIC-11026, 1981.

[Kr64] Kraner, H.W., G.L. Schroeder, and R.D.Evans, *Measurements of the Effects of Atmospheric Variables on Radon-222 Flux and Soil-Gas Concentration*, in Natural Radiation Environment, Adams, J.A.S., and W.M. Lowder (Eds.), University of Chicago Press, Chicago, 1964.

[Kr82] Kristiansson, K., and L. Malmqvist, *Evidence for Nondiffusive Transport of Radon-222 in the Ground and a New Physical Model for the Transport*, Geophysics, Vol.47, No. 10, pp.1444-1452, October 1982.

[Lan82] Landman, K.A., *Diffusion of Radon Through Cracks in a Concrete Slab*, Health Physics, Vol.43, No.1, pp.65-71, July 1982.

[Lan83] Landman, K.A., and D.S. Cohen, *Transport of Radon Through Cracks in a Concrete Slab*, Health Physics, Vol.44, No.3, pp. 249-257, March 1983.

[Lap82] Lapidus, L., and G.F. Pinder, *Numerical Solution of Partial Differential Equations in Science and Engineering*, John Wiley and Sons, 1982.

[Mo84] Moed, B.A., W.W. Nazaroff, A.V. Nero, M.B. Schwehr, and A.Van Heuvelen, *Identifying Areas with Potential for High Indoor Radon Levels: Analysis of the National Airborne Radiometric Reconnaissance Data for California and the Pacific Northwest*, LBL-16955, Lawrence Berkeley Laboratory, Berkeley, CA, April 1984.

[Mo86] Mowris, R.J., *Analytical and Numerical Models for Estimating the Effect of Exhaust Ventilation on Radon Entry in Houses with Basements or Crawl Spaces*, M.S. Thesis, LBL-22067, Lawrence Berkeley Laboratory, Berkeley, CA, August 1986.

[My83] Myrick T.E., B.A. Berven, and F.F. Haywood, *Determination of Concentrations of Selected Radionuclides in Surface Soil in the U.S.*, Health Physics, Vol.45, No.3, pp.631-642, September 1983.

[Na84a] Nazaroff, W.W., H. Feustel, A.V. Nero, K.L. Revsan, D.T.Grimsrud, M.A. Essling, and R.E. Toohey, *Radon Transport into a Single-Family House with Basement*, LBL-16572, Lawrence Berkeley Laboratory , Berkeley, CA, January, 1984.

[Na84b] Nazaroff, W.W., and A.V. Nero, *Transport of Radon from Soil into Residences*, LBL-16823, Lawrence Berkeley Laboratory , berkeley, CA, February 1984.

[Na85] Nazaroff, W.W., B.A. Moed, R.G. Sextro, K.L. Revsan, and A.V. Nero, *Factors Influencing Soil as a Source of Indoor Radon: A Framework for Geographically Assessing Radon Source Potentials*, LBL-20645, Lawrence Berkeley Laboratory, Berkeley, CA, 1985.

[Na86] Nazaroff, W.W., S.R. Lewis, S.M. Doyle, B.A. Moed, and A.V. Nero, *Experiments on Pollutant Transport from Soil into Residential Basements by Pressure-Driven Air FLow*, LBL-18374, Lawrence Berkeley Laboratory, Berkeley, CA, January 1986.

[NAS80] National Academy of Sciences, *The Effects on Populations of Exposure to Low Levels of Ionizing Radiation: 1980*, BEIR III Report, Committee on the Biological Effects of Ionizing Radiations, National Academy Press, Washington, D.C., 1980.

[NC84a] NCRP, *Exposures from the Uranium Series with Emphasis on Radon and its Daughters*, National Council on Radiation Protection and Measurements, NCRP Report No. 77, Bethesda, MD, 1984.

[NC84b] NCRP, *Evaluation of Occupational and Environmental Exposures to Radon and Radon Daughters in the United States*, National Council on Radiation Protection and Measurements, NCRP Report No. 78, Bethesda, MD, 1984.

[Ne83a] Nero, A.V., *Indoor Radiation Exposures from Radon-222 and Its Daughters: A View of the Issue*, Health Physics, Vol. 45, No.2, pp. 277-288, August 1983.

[Ne83b] Nero, A.V., *Airborne Radionuclides and Radiation in Buildings: A Review*, Health Physics, Vol.45, No.2, pp. 303-322, August 1983.

[Ne84a] Nero, A.V. and W.W. Nazaroff, *Characterizing the Source of Radon Indoors*, Radiation Protection Dosimetry, Vol.7, No. 1-4, pp.23-29, 1984.

[Ne84b] Nero, A.V., M.B. Schwehr, W.W. Nazaroff, and K.L. Revsan, *Distribution of Airborne Radon-222 Concentrations in U.S. Homes*, LBL-18274, Lawrence Berkeley Laboratory, Berkeley CA, November 1984.

[Ne85] Nero, A.V., *Indoor Concentrations of Radon-222 and its Daughters: Sources, Range and Environmental Influences*, LBL-19346, Lawrence Berkeley Laboratory, Berkeley, CA, April 1985.

[Ne86] Nero, A.V., *The Radon Risk*, LBL Research Review, Lawrence Berkeley Laboratory, University of California, Berkeley, Vol.11, No. 4, Winter 1986.

[NRC80] U.S. Nuclear Regulatory Commission, *Final Environmental Impact Statement on Uranium Milling - Vol. III - Appendices G-V*, Office of Nuclear Material, Safety and Safeguard, U.S.NRC, NUREG-0706, Washington, D.C., 1980.

[NRC83] U.S.NRC, *Radiological Assessment - A Textbook on Environmental Dose Analysis*, U.S. Nuclear Regulatory Commission, NUREG/CR-3332, ORNL-5968, Washington, D.C., September 1983.

[Ot83] Otis, M.D., *Sensitivity and Uncertainty Analysis of the Pathway Radionuclide Transport Model*, Ph.D. Dissertation, Colorado State University, Fort Collins, CO, 1983.

[Pa80] Patankar, S.V., *Numerical Heat Transfer and Fluid Flow*, McGraw-Hill Book Company, New York, 1980.

[Pa84] Paschoa, A.S., M.E. Wrenn, and J.A. Torrey, *A Mathematical Model of Indoor Radon and Daughters*, Radiation Protection Dosimetry, Vol.7, No. 1-4, pp. 139-142, 1984.

[Pe83] Peyret, R., and T.D. Taylor, *Computational Methods for Fluid Flow*, Springer-Verlag New York Inc., 1983.

[Ro81] Rogers, V.C., and K.K. Nielson, *A Handbook for the Determination of Radon Attenuation Through Cover Materials*, U.S. Regulatory Commission, NUREG/CR-2340, December 1981.

[Ro83] Rogers, V.C., K.K. Nielson, G.B. Merrell, and D.R. Kalkwarf, *The Effects of Advection on Radon Transport Through Earthen Materials*, U.S. Nuclear Regulatory Commission, NUREG/CR-3409, October 1983.

[Sc74] Scheidegger, A.D., *The Physics of Flow Through Porous Media*, ISBN 0-8020-1849-1, 3rd. Edition, University of Toronto Press, 1974.

[Sc84] Schiller, G.E., *A Theorectical Convective-Transport Model of Indoor Radon Decay Products*, Ph.D. Dissertation, The University of California, Berkeley, CA, July 1984.

[Sco82] Scott, A.G., *Computer Modeling of Radon Movement*, in EML Indoor Radon Workshop, George, A.C., Lowder, W., Fisenne, I., Knutson, E.O., and Hinchcliffe, L., Eds., Report EML-416, Environmental MEasurements Laboratory, New York, 1982.

[Se66] Servant, J., *Temporal and Spatial Variations of the Concentration of the Short-Lived Decay Products of Radon in the Lower Atmosphere*, Tellus XVIII, 2, pp. 663-670, 1966.

[Se78] Serdyukova, A.S., and Y.T. Kapitanov, *Radon Isotopes and Short-Lived Products of their Disintegration in Nature*, Published originally in Russian, in 1969. English version published for the U.S. Department of the Interior, Bureau of Mines, and the National Science Foundation, Washington, D.C., by the Indian National Scientific Documentation Centre, New Delhi, India, 1978.

[Se85] Sextro, R.G., *Control of Indoor Radon and Radon Progeny Concentration*, LBL-19726, Lawrence Berkeley Laboratory, Berkeley, CA, May 1985.

[Se87] Sextro, R.G., Private communication at the Lawrence Berkeley Laboratory, Berkeley, CA, February 1987.

[Si86] Sinnaeve, J., M. Olast, and J. McLaughlin, *Natural Radiation Exposure Research in the Member States of the European Community- State-of-the-Art and Perspectives*, in Indoor Radon, Proceedings of an APCA International Specialty Conference, Air Pollution Control Association, Phyladelphia, Pennsylvania, February, 1986.

[St80] Stranden, E., and L. Berteig, *Radon in Dwellings and Influencing Factors*, Health Physics, Vol.39, pp.275-284, August 1980.

[St85] Streeter, V.L., and E.B. Wylie, *Fluid Mechanics*, Eighth Edition, McGraw-Hill Book Company, New York, 1983.

[Sw86] Swedjemark, G.A., *Swedish Limitations Schemes to Decrease Rn-Daughters in Indoor Air*, Health Physics, Vol.51, pp. 569-578, November 1986.

[Ta64] Tanner, A.B., *Radon Migration in the Ground: A Review*, in The Natural Radiation Environment, Adams, J.A.S. and Lowder, W.M., Eds., University of Chicago Press, Chicago, 1964.

[Ta80] Tanner, A.B., *Radon Migration in the Ground: A Supplementary Review*, in Proc. Natural Radiation Environment III, Gessel, T.S., and Lowder, W.M., Eds., Conf-780422, U.S. Department of Commerce, National Technical Information Service, Sprongfield, VA, 1980.

[Ta83] Tappan, J.T., *Mitigation Methods for Natural Radioactivity Associated with Energy Efficient Structures*, National Conference on Environmental Engineering, University of Colorado, Boulder, Colorado, July 1983.

[Ta86] Tanner, A.B., *Geological Factors that Influence Radon Availability*, in Indoor Radon, Proceedings of an APVA International Specialty Conference, Phyladelphia, Pennsylvania, Air Pollution Control Association, Pittsburgh, PA, February, 1986.

[Tu86] Turk, B.H., R.J.Prill, W.J. Fisk, D.T. Grimsrud, B.A. Moed, and R.G. Sextro, *Radon and Remedial Action in Spokane River Valley Residences: An Interim Report*, LBL-21399, Lawrence Berkeley Laboratory, CA, March 1986.

[UNS82] UNSCEAR, *Ionizing Radiation: Sources and Biological Effects*, UNSCEAR 1982 Report to the General Assembly, United Nations, New York, 1982.

[Wa84] Wadach, J.B., W.A. Clarke, and I.A.Nitschke, *Testing of Inespensive Radon Mitigation Techniques in New York State Houses*, Twenty-Ninth Annual Meeting of the Health Physics, New Orleans, Luisiana, June 1984.

[Wa85] Wadach, J.B., and C.T. Hess, *Radon-222 Concentration Measurements in Soil Using Liquid Scintilation and Track Etch*, Health Physics, Vol.48, No. 6, pp. 805-808, June 1985.

[We 56] Wehner J.F., and R.H. Wilhelm, *Boundary Conditions of Flow Reactor*, Chemical Engineering Sciences, Vol.6, pp. 89-93, 1956.

[Wi80] Wilkening, M., *Radon Transport Processes below the Earth's Surface*, in Natural Environment III, T.F. Gesell and W.M. Lowder (Eds.), (Proceedings of a meeting held in April, 1978, Houston, Texas), U.S. Department of Energy Report CONF-780422, National Technical Information Service, Sprongfield, Virginia, pp. 90-104, 1980.

[Yo69] Youngquist, G.R., *Diffusion and Flow of Gases in Porous Solids*, in Symposium on Flow Through Porous Media, American Chemical Society Publications, Washington, D.C., pp. 58-69, 1969.